



**National Library
of Canada**

**Bibliothèque nationale
du Canada**

Canadian Theses Service

Service des thèses canadiennes

Ottawa, Canada
K1A 0N4

NOTICE

The quality of this microform is heavily dependent upon the quality of the original thesis submitted for microfilming. Every effort has been made to ensure the highest quality of reproduction possible.

If pages are missing, contact the university which granted the degree.

Some pages may have indistinct print especially if the original pages were typed with a poor typewriter ribbon or if the university sent us an inferior photocopy.

Reproduction in full or in part of this microform is governed by the Canadian Copyright Act, R.S.C. 1970, c. C-30, and subsequent amendments.

AVIS

La qualité de cette microforme dépend grandement de la qualité de la thèse soumise au microfilmage. Nous avons tout fait pour assurer une qualité supérieure de reproduction.

S'il manque des pages, veuillez communiquer avec l'université qui a conféré le grade.

La qualité d'impression de certaines pages peut laisser à désirer, surtout si les pages originales ont été dactylographiées à l'aide d'un ruban usé ou si l'université nous a fait parvenir une photocopie de qualité inférieure.

La reproduction, même partielle, de cette microforme est soumise à la Loi canadienne sur le droit d'auteur, SRC 1970, c. C-30, et ses amendements subséquents.



National Library
of Canada

Bibliothèque nationale
du Canada

Canadian Theses Service Service des thèses canadiennes

Ottawa, Canada
K1A 0N4

The author has granted an irrevocable non-exclusive licence allowing the National Library of Canada to reproduce, loan, distribute or sell copies of his/her thesis by any means and in any form or format, making this thesis available to interested persons.

The author retains ownership of the copyright in his/her thesis. Neither the thesis nor substantial extracts from it may be printed or otherwise reproduced without his/her permission.

L'auteur a accordé une licence irrévocable et non exclusive permettant à la Bibliothèque nationale du Canada de reproduire, prêter, distribuer ou vendre des copies de sa thèse de quelque manière et sous quelque forme que ce soit pour mettre des exemplaires de cette thèse à la disposition des personnes intéressées.

L'auteur conserve la propriété du droit d'auteur qui protège sa thèse. Ni la thèse ni des extraits substantiels de celle-ci ne doivent être imprimés ou autrement reproduits sans son autorisation.

ISBN 0-315-55529-7

Canada

UNIVERSITY OF ALBERTA

GEOTECHNICAL BEHAVIOUR OF DIAPHRAGM WALLS

by

ATTIA M.H. SHALABY

A THESIS

SUBMITTED TO THE FACULTY OF GRADUATE STUDIES AND RESEARCH
IN PARTIAL FULFILMENT OF THE REQUIREMENTS FOR THE DEGREE
OF DOCTOR OF PHILOSOPHY

DEPARTMENT OF CIVIL ENGINEERING

EDMONTON, ALBERTA

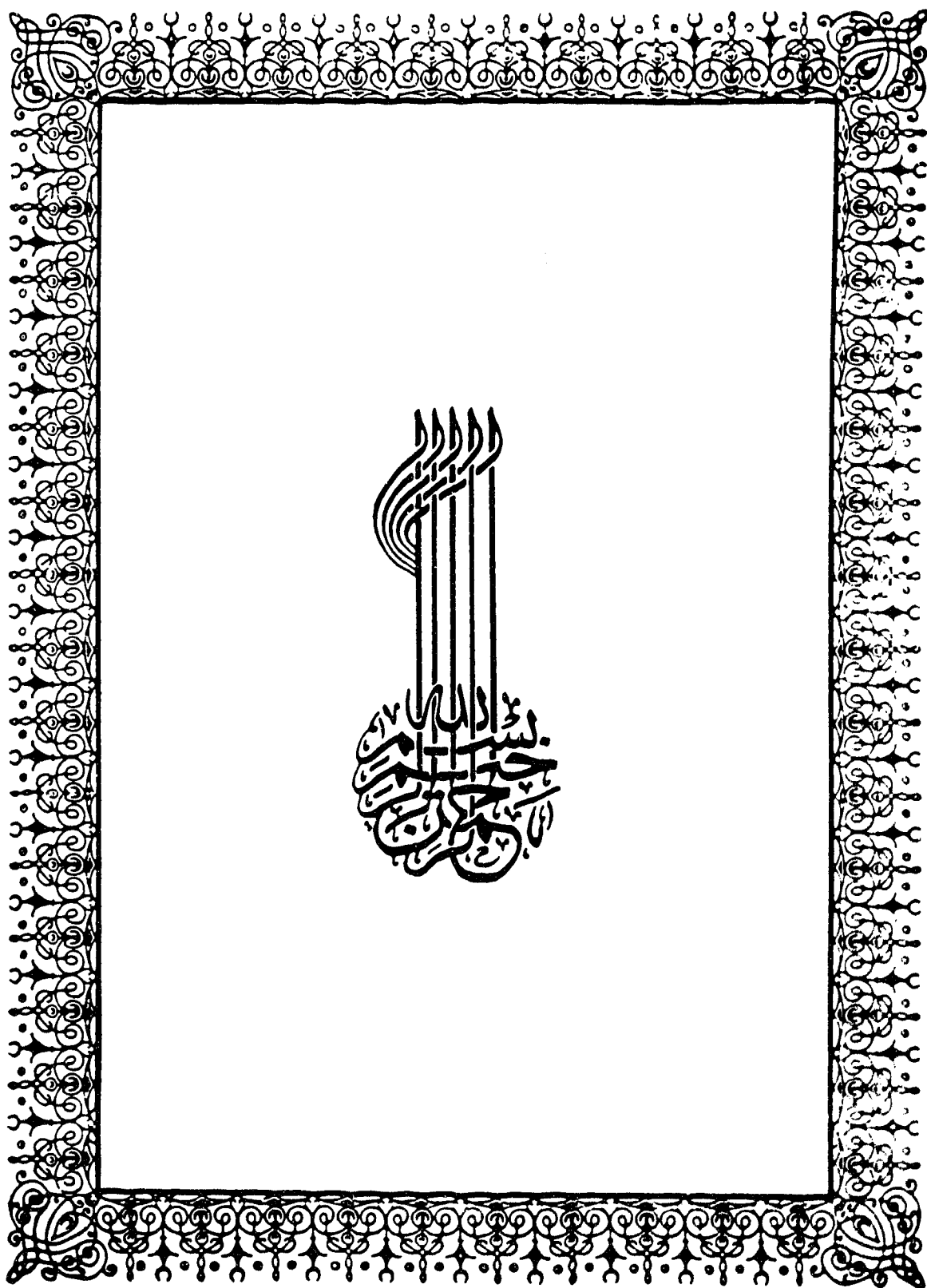
FALL 1989

RELEASE FORM

(S I G N E D)

A. Shalun

DATED July 28th 1989

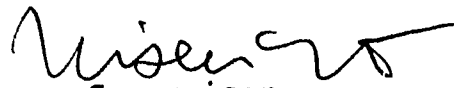


In the name of God , Most Gracious , Most Merciful .

UNIVERSITY OF ALBERTA
FACULTY OF GRADUATE STUDIES AND RESEARCH



The undersigned certify that they have read, and recommend to the Faculty of Graduate Studies and Research, for acceptance, a thesis entitled *Geotechnical Behaviour of Diaphragm Walls* submitted by Attia M.H. Shalaby in partial fulfilment of the requirements for the degree of Doctor of Philosophy.

Z.Eisenstein


Supervisor

A.E. Elwi

W.H. Griffin





J.D. Scott

D.C. Sego



G. Quqing


External Examiner

Date July 28th ,1989

*To the soul of my **father**,
may he rest in peace.*

*To my **mother**,*

*To my **wife** , Nemat (Nani),
and our children:
Ahmed , Jehan , Mona and Noha*

ABSTRACT

To study the geotechnical behaviour of diaphragm walls, the instrumentation of the Greater Cairo Metro project provided the required field measurements. Two test sections were instrumented to observe and record the deformations of the soil, pore water pressures and loads acting on the structural elements (i.e. struts, raft, and roof) due to the excavation and construction method. The first test section was along the running tunnel, an open air excavation using precast panel walls. The second, at a station, was a covered excavation, with cast in situ walls providing lateral support. A finite element analysis was conducted to compute the lateral earth pressures as they can not be measured directly from the field. The use of a simplified plane frame model, run on a microcomputer (such as PFT), to quickly and economically calculate the lateral earth pressures was verified.

The ground reaction characteristics below the groundwater level and a lateral earth pressure concept for diaphragm walls were established. The influence of the construction method, sequence of installation of the temporary and permanent support systems, and the wall thickness were studied for the host material of the Cairo area. As a result, detailed documentation for the Cairo Metro Regional line was provided.

Acknowledgements

The author wishes to express his sincere gratitude to Dr. Z.Eisenstein for his patience, guidance and both technical and moral support throughout the course of this study.

Many thanks go to Drs. D.H.Chan, D.C.Sego and A.E.Elwi for their helpful discussions and input in the finite element analysis section of this thesis.

The enormous help provided by Mr. Richard Wan and Dr. Lal Samarasekera during discussions and their input in various ways, including long endless nights at the computer terminal, are gratefully acknowledged . Oh dear friends, I will certianly miss your company . Richard Wan... , for him it is impossible to find any of the right words !

Special thanks should go to Gerry Cyre, chief technician at the University of Alberta, for his technical support on site and friendship and moral support especially during the difficult times. Also, I thank my Egyptian technical crew in particular: K. Abed ELlatif, Ashraf Hefny and Ayman ELakabawy. The guidance provided by Dr. F. EL-nahhas and Prof. F. EL-kadi from Ain-shams University is appreciated.

General Eng. M. Abdel Salam and Eng. S. EL-Baidawy from the National Authority for Tunnels in Egypt are acknowledged for their support, help, understanding and skills. Special thanks go to his Excellency Eng. S. Metwally, Egyptian

Minister of Transport and Communication for his encouragement and support for this study.

The financial support was provided by Zagazig University in Egypt, the National Authority for Tunnels (NAT) , the International Development Research Centre (IDRC), the University of Alberta and the Natural Sciences and Engineering Research Council of Canada (NSERC) . The author is indebted to the above agencies.

To Tanya Schulz go my sincere appreciation for her effort in editing and skill in typing my thesis.

Without the wonderful help of Eng. M.F. AQLE (my father inlaw) , this work would have never been possible. The debt I owe him is colossal and my gratitude is beyond any imaginable word.

Finally, I do not know how to thank my wife Nemat(*Nani*) for her affection and support over the years I spent on my Ph.D. ... for her love, patience and formidable courage to undertake the sole responsibility for the family during the last year of my thesis I love you . I feel truly humbled . Thank you and may GOD bless us all .

Table of Contents

Chapter	Page
1. INTRODUCTION	1
1.1 Foreword	1
1.2 The Greater Cairo Metro Project	2
1.2.1 The Proposed Network	2
1.2.2 The Regional Line	4
1.3 Aims	7
1.4 Scope of the Thesis	10
2. GENERAL MORPHOLOGIC FEATURES OF EGYPT	12
2.1 Introduction	12
2.2 The Geologic History of the River Nile	15
2.2.1 The Geology of Cairo	15
3. CONSTRUCTION PROCEDURE	18
3.1 Choice of Construction Method	18
3.2 The Cut and Cover Method	19
3.3 Construction Procedure for the Running Tunnel	21
3.4 The Construction Procedure for the Station Section	21
3.5 Grouting Operation	24
3.5.1 Types of Grouting Slurries	24
3.5.2 Sequence of Grouting Operation	27
4. FIELD INSTRUMENTATION PROGRAM	41
4.1 Introduction	41
4.2 The Running Tunnel Test Section	43
4.2.1 Instrumentation	48
4.3 The Orabi Station Test Section	52
4.3.1 Instrumentation of the Orabi Station	55

4.4	Details of the Instrumentation	60
4.4.1	The Settlement Point (SP)	60
4.4.2	The Multipoint Extensometer (ME)	64
4.4.2.1	The Installation Procedure	66
4.4.2.2	Monitoring Procedure	68
4.4.3	The Slope Indicator (SI)	70
4.4.3.1	Installation Procedure	72
4.4.3.2	Monitoring Program	73
4.4.4	Piezometer Lines	74
4.4.4.1	Installation Procedure	77
4.4.4.2	Monitoring Procedure	77
4.4.5	Vibrating Wire Strain Gauges	78
4.4.5.1	Installation Procedure	81
4.4.5.2	The Monitoring Procedure	83
4.5	Laboratory Test Program	83
4.6	Monitoring Routine and Site Condition	85
4.7	Field Measurement of Soil Deformation	89
4.7.1	The Running Tunnel Test Section Measurements	92
4.7.1.1	Vertical Displacement (Settlement)	92
4.7.1.2	Horizontal Displacement (Lateral Deformation)	94
4.7.1.3	Pore Water Pressure Measurements	97
4.7.1.4	Strain Gauge Measurements	100
4.7.2	The Station Test Section Measurements ...	103
4.7.2.1	Horizontal Displacement (Lateral Deformation)	103
4.7.2.2	Strain Gauge Measurements	106

5.	THE NUMERICAL ANALYSIS	109
5.1	Introduction	109
5.2	Material Properties and Parameters used in the Analyses	109
5.3	The Plane Frame Truss (PFT) Program	110
5.4	The Soil Analysis by Finite Element Program (SAFE)	116
5.4.1	Linear Elastic Isotropic Model	117
5.4.2	Non-Linear Elastic Hyperbolic Model	118
5.4.3	Construction and Excavation Simulation for F.E.M. Analysis	120
5.4.4	The Running Tunnel Test Section - Stages of Analysis	121
5.4.4.1	Step (1) - The In Situ Stress Generation	121
5.4.4.2	Step (2) - Slurry Trench and PreCast Panel	124
5.4.4.3	Step (3) - Grouting for the Plug and Dewatering	124
5.4.4.4	Step (4) - Starting the Excavation	125
5.4.4.5	Step (5) - Excavating to Install the Mobile Frame	125
5.4.4.6	Step (6) - Excavating to the Final Level	126
5.4.4.7	Step (7) - The Installation of the Lower Strut	126
5.4.4.8	Step (8) - The Installation of the Upper Strut	126
5.4.4.9	Step (9) - The Removal of the Mobile Frame	126
5.4.4.10	Step (10) - Pouring the Concrete Floor Slab	126
5.4.4.11	Step (11) - Introducing the Sheet Pile Wall	127

5.4.4.12	Step (12) - Introducing the Roof Slab	127
5.4.4.13	Step (13) - The Final Case	127
5.4.5	The Station Test Section - Steps of Analysis	128
5.4.5.1	The Station Test Section Steps of Analysis as an Undercover Excavation	128
5.4.5.2	The Station Test Section - Steps of Analysis as an Open Air Excavation	129
5.5	The Finite Element Analysis Results	129
5.5.1	Finite Element Results of the Running Tunnel Test Section	130
5.5.1.1	The Deformation Analysis	130
5.5.1.2	The Stress Analysis	132
5.5.2	Finite Element Results of the Station Test Section	133
5.5.2.1	The Displacement Analysis as Undercover Excavation	134
5.5.2.2	The Stress Analysis as UnderCover Excavation	135
5.5.2.3	The Displacement Analysis as Open Air Excavation	136
5.5.2.4	The Stress Analysis as Open Air Excavation	137
5.6	The Support System Loading Predictions	138
5.6.1	The Temporary Support System Loading Predictions	138
5.6.2	The Permanent Structural Support Loading	140
6.	ANALYSIS OF THE FIELD AND NUMERICAL RESULTS	143
6.1	Introduction	143
6.2	Soil Profile and Properties	144
6.3	Considerations in the Simulation for F.E.M. Analysis	146

6.4	Horizontal Displacement Analysis	148
6.4.1	Lateral Displacement of the Soil Adjacent to the Wall	148
6.4.2	Lateral Displacement of the Walls	157
6.5	Vertical Displacement of the Soil (Settlement Trough)	160
6.5.1	Vertical Displacement of the Excavation Base	164
6.6	Strut and Normal Loads	167
6.7	Shear Stresses at the Soil-Structure Interaction Zone	170
6.8	Lateral Earth Pressures Acting on the Wall	175
6.9	A Comparison Between SAFE and PFT	198
6.10	The Ground Control Analysis	199
6.11	Summary	209
7.	CONCLUSIONS AND RECOMMENDATIONS	215
	REFERENCES	220
A.	Calculations for Forces from Strain Gauge Readings .	230
B.	Field and Laboratory Tests	233
C.	Determination of Concrete Properties	238
D.	Finite Element Results	243
E.	Input/Output Files for SAFE	292

List of Tables

Table		Page
4.1	Soil and Concrete Properties	84
4.2	Temporary Support Weldable Strain Gauge Readings at the Tunnel Test Section	101
4.3	Embedded Strain Gauge Reading at the Tunnel Test Section	102
4.4	Temporary Support Weldable Strain Gauge Readings at the Station Test Section	107
4.5	Embedded Strain Gauge Reading at the Station Test Section	108
5.1	Linear Elastic Model Parameters	111
5.2	Hyperbolic Model Parameters	112
5.3	Strut Loading as Predicted by F.E.M. and From Field Observation	139
5.4	Structural Elements Normal Loading as Predicted using F.E.M. and from Field Observation	141
C.1	The Results of the Concrete Tests	240
C.2	Moduli of Elasticity for Concrete based on Laboratory Test Results	241

List of Figures

Figure	Page
1.1 The Greater Cairo Metro Project - The Proposed Network	3
1.2 The Regional Line - The Underground Portion	5
2.1 Map of Egypt	13
2.2 The Geological Formation of the Cairo Area	16
3.1 Construction Procedure Steps for the Running Tunnel Test Section	22
3.2 Longitudinal View of the Excavation Procedure Steps for the Running Tunnel Test Section	23
3.3 Details of Excavation and Installation of the Diaphragm Walls for the Running Tunnel Test Section	24
3.4 Details of the Pre-Cast Diaphragm Wall Used for the Running Tunnel Test Section	25
3.5 Construction Procedure Steps for the Station Test Section	32
3.6 Sequence of Construction for the Cast In Situ Panels	34
3.7 The Drilling Details for the Chosen Test Sections	39
4.1 General Layout of Instrumentation at the Tunnel Test Section	44
4.2 The Surface Settlement Point Distribution at the Tunnel Test Section	45
4.3 The Tunnel Test Section - Cross-Sectional View of the Instrumentation	46
4.4 Cross-Section Details of the Tunnel Section and the Soil Profile at this Location	47
4.5 Details of the Multipoint Extensometers at the Tunnel Test Section	49
4.6 The Piezometer Line Details at the Tunnel Test Section	51

Figure	Page
4.7 Orabi Station General Layout	53
4.8 Orabi Station Cross-Section and Soil Stratigraphy at the Test Section	54
4.9 General Layout of the Instrumentation at Orabi Station Test Section	56
4.10 Cross-Section at Orabi Station Test Section	57
4.11 Details of the Multipoint Extensometers at the Orabi Station Test Section	58
4.12 The Piezometer Lines Details at the Orabi Station Test Section	59
4.13 Details of the Settlement Point	61
4.14 Details of the Surveying Rod	63
4.15 Details of the Magnetic Extensometer Point	65
4.16 The Magnetic Fields Around the Magnetic Point	67
4.17 The Extruder used for the Installation of the Magnetic Points	69
4.18 The Slope Indicator Principle	71
4.19 The Basic Principle of the Piezometer	75
4.20 The Pneumatic Piezometer Set-Up	76
4.21 Details of the Strain Gauges	79
4.22 The Observed Settlement Troughs at the Tunnel Test Section	93
4.23 The Subsurface Settlement at the Tunnel Test Section	95
4.24 The Diaphragm Wall Lateral Displacement during Excavation at the Tunnel Test Section (SI2)	96
4.25 The Soil Lateral Displacement during Construction at the Tunnel Test Section	98

Figure	Page
4.26 The Water Pressure Distribution at the Tunnel Test Section During and After Excavation	99
4.27 Soil Lateral Displacements at the Station Test Section	104
5.1 Simplified Geometry for Use in the PFT Program	114
5.2 Lateral Earth Pressure as Predicted by the PFT Program	115
5.3 Running Tunnel Test Section Finite Element Mesh	122
5.4 Station Test Section Finite Element Mesh	123
6.1 Field Measurements and Finite Element Results - Step 4 - Tunnel Section	150
6.2 Field Measurements and Finite Element Results - Step 5 - Tunnel Section	151
6.3 Field Measurements and Finite Element Results - Step 7 - Tunnel Section	152
6.4 Field Measurements and Finite Element Results - Step 9 - Tunnel Section	153
6.5 Field Measurements and Finite Element Results - Step 13 - Tunnel Section	154
6.6 Field Measurements and Finite Element Results - Station Section - Final Case	156
6.7 Settlement Trough and Heave for the Tunnel Section	161
6.8 Settlement Trough and Heave for the Station Section	162
6.9 Settlement trough and Heave for Station Section as Open Air Excavation	163
6.10 Vertical Displacement of the Soil for the Tunnel Section (ME1)	166
6.11 The Predicted Shear Stresses and the Allowable Shear Stress Envelope for the Tunnel Section	171

Figure	Page
6.12 The Predicted Shear Stresses and the Allowable Shear Stress Envelope for the Station (Undercover) Section	172
6.13 The Predicted Shear Stresses and the Allowable Shear Stress Envelope for the Station (Open Air) Section	173
6.14 Final Predicted Lateral Total Earth Pressure for the Tunnel Section	178
6.15 Final Predicted Lateral Total Earth Pressure for the Station Section Excavated Under Cover	179
6.16 Final Predicted Lateral Total Earth Pressure for the Station Section Excavated Open Air	180
6.17 Final Effective Lateral Earth Pressure for the Tunnel Section with Effective Unit Weight for Terzaghi and Peck's Diagrams	182
6.18 Final Effective Lateral Earth Pressure for the Tunnel Section with Total Unit Weight for Terzaghi and Peck's Diagrams	183
6.19 Final Lateral Earth Pressure Diagrams for the Tunnel Section using Effective Unit Weight for Terzaghi and Peck Diagrams	185
6.20 Final Lateral Earth Pressure Diagrams for the Tunnel Section using Total Unit Weight for Terzaghi and Peck Diagrams	186
6.21 Final Lateral Earth Pressure Diagrams for the Station (Undercover) Section using Total Unit Weight for Terzaghi and Peck Diagrams	187
6.22 Final Lateral Earth Pressure Diagrams for the Station (Undercover) Section using Effective Unit Weight for Terzaghi and Peck Diagrams	188
6.23 Final Lateral Earth Pressure Diagrams for the Station (Open Air) Section using Total Unit Weight for Terzaghi and Peck Diagrams	189

Figure	Page
6.24 Final Lateral Earth Pressure Diagrams for the Station (Open Air) Section using Effective Unit Weight for Terzaghi and Peck Diagrams	190
6.25 Final Effective Lateral Earth Pressure Diagrams for the Station (Undercover) Section using Total Unit Weight for Terzaghi and Peck Diagrams	191
6.26 Final Effective Lateral Earth Pressure Diagrams for the Station (Undercover) Section using Effective Unit Weight for Terzaghi and Peck Diagrams	192
6.27 Final Effective Lateral Earth Pressure Diagrams for the Station (Undercover) Section using Total Unit Weight for Terzaghi and Peck Diagrams - Expanded View	194
6.28 Final Effective Lateral Earth Pressure Diagrams for the Station (Undercover) Section using Effective Unit Weight for Terzaghi and Peck Diagrams - Expanded View	195
6.29 The Suggested Pressure Diagrams for Stiff Clays under Similar Construction Procedures	196
6.30 Results of SAFE and PFT programs for the Tunnel Test Section in Terms of Net Pressures	200
6.31 Net Lateral Earth Pressure Diagrams for the Tunnel Section Using the Total Unit Weight for Terzaghi and Peck Diagrams	201
6.32 Net Lateral Earth Pressure Diagrams for the Tunnel Section Using the Effective Unit Weight for Terzaghi and Peck Diagrams	202
6.33 Normalized Settlement Troughs (Suggested by Peck (1969))	204
6.34 Zone I Normalized Settlement Troughs	205
6.35 The Relationship Between Maximum Settlements and Maximum Lateral Wall Movements for Test Sections	207

Figure	Page
6.36 Comparison of volume of Ground Surface Settlement and Lateral Wall Deflection	208
6.37 Maximum Ground Surface Settlement versus Volume of Lateral Wall Deflections	210
B.1 Consolidated Drained Triaxial Test Results for Silty Clay	234
B.2 Consolidated Undrained Triaxial Test Results for Silty clay	235
B.3 Grain Size Distribution of Soils	236
B.4 CPT Results at the Test Sections	237
C.1 Stress-Strain Relationship for Concrete	242
D.1 Displacement Arrows - Tunnel Section - Step (2)	244
D.2 Displacement Arrows - Tunnel Section - Step (3)	245
D.3 Displacement Arrows - Tunnel Section - Step (4)	246
D.4 Displacement Arrows - Tunnel Section - Step (5)	247
D.5 Displacement Arrows - Tunnel Section - Step (6)	248
D.6 Displacement Arrows - Tunnel Section - Step (7)	249
D.7 Displacement Arrows - Tunnel Section - Step (8)	250
D.8 Displacement Arrows - Tunnel Section - Step (9)	251
D.9 Displacement Arrows - Tunnel Section - Step (10)	252
D.10 Displacement Arrows - Tunnel Section - Step (11)	253
D.11 Displacement Arrows - Tunnel Section - Step (12)	254
D.12 Displacement Arrows - Tunnel Section - Step (13)	255

Figure	Page
D.13 Horizontal Displacement - Tunnel Section - Set (1)	256
D.14 Horizontal Displacement - Tunnel Section - Set (2)	257
D.15 Settlement Trough and Excavation Base Heave - Tunnel Section Set (1)	258
D.16 Settlement Trough and Excavation Base Heave - Tunnel Section Set (2)	259
D.17 Lateral Earth Pressure - Tunnel Section Set (1)	260
D.18 Lateral Earth Pressure - Tunnel Section Set (2)	261
D.19 Lateral Earth Pressure - Tunnel Section Set (3)	262
D.20 Shear Stresses - Tunnel Section Set (1)	263
D.21 Shear Stresses - Tunnel Section Set (2)	264
D.22 Shear Stresses - Tunnel Section Set (3)	265
D.23 Displacement Arrows - Station Section Steps (2) and (3)	266
D.24 Displacement Arrows - Station Section - Undercover Step (4)	267
D.25 Displacement Arrows - Station Section - Undercover Step (5)	268
D.26 Displacement Arrows - Station Section - Undercover Step (6)	269
D.27 Displacement Arrows - Station Section - Undercover Step (7)	270
D.28 Displacement Arrows - Station Section - Undercover Step (8)	271
D.29 Displacement Arrows - Station Section - Undercover Step (9)	272
D.30 Settlement Troughs and Excavation Base Heave - Station Section - Undercover	273
D.31 Horizontal Displacement - Station Section - Undercover - Set (1)	274

Figure	Page
D.32 Horizontal Displacement - Station Section - Undercover - Set (2)	275
D.33 Lateral Earth Pressure Station Section - Undercover - Set (1)	276
D.34 Lateral Earth Pressure Station Section - Undercover - Set (2)	277
D.35 Shear Stress - Station Section - Undercover - Set (1)	278
D.36 Shear Stress - Station Section - Undercover - Set (2)	279
D.37 Displacement Arrows - Station Section - Open Air Excavation Step (4)	280
D.38 Displacement Arrows - Station Section - Open Air Excavation Step (5)	281
D.39 Displacement Arrows - Station Section - Open Air Excavation Step (6)	282
D.40 Displacement Arrows - Station Section - Open Air Excavation Step (7)	283
D.41 Displacement Arrows - Station Section - Open Air Excavation Step (8)	284
D.42 Settlement Trough and Excavation Base Heave - Station Section - Open Air Excavation	285
D.43 Horizontal Displacement - Station Section - Open Air - Set (1)	286
D.44 Horizontal Displacement - Station Section - Open Air - Set (2)	287
D.45 Lateral Earth Pressure Station Section - Open Air - Set (1)	288
D.46 Lateral Earth Pressure Station Section - Open Air - Set (2)	289
D.47 Shear Stress - Station Section - Open Air - Set (1)	290
D.48 Shear Stress - Station Section - Open Air - Set (2)	291

List of Plates

Plate	Page
3.1 Prefabrication Factory	20
3.2 The Mobile Frame Mobilization Operation	28
3.3 Details of the Water Tightness Layers at the Base of the Excavation	30
3.4 General View of the Sites During the Grouting Operation	41
4.1 Details of the Installation of the Embedded Strain Gauges	80
4.2 Weldable Strain Gauges Mounted on the Struts	82
4.3 Examples of the Field Obstacles Experienced at the Tunnel Test Section	87
4.4 Damages and Repair Work at the Tunnel Test Section	88
4.5 The Readout Units	90
4.6 The Readout Units	91
4.7 Obstacles Preventing Access to the Instruments at the Station Test Section	105

List of Symbols

c ... cohesion
 c' ... drained shear strength parameter
 CD ... drained shear strength
 CU ... undrained shear strength
 E ... elastic modulus
 E_c ... concrete modulus of elasticity
 f_c ... compressive strength of concrete
 k ... permeability of soil mass
 K ... modulus number
 K_b ... bulk modulus number
 K_A ... active lateral earth pressure coefficient
 K_p ... passive lateral earth pressure coefficient
 K_u ... unloading modulus number
 $L.L$... liquid limit
 m ... bulk modulus exponent
 n ... exponent number
 P_a ... atmospheric pressure
 $P.L$... plastic limit
 R_f ... failure ratio
 S ... stress
 $S.P.T.$... Standard Penetration Test
 S_r ... Degree of Saturation
 w ... water content
 δ ... angle of wall friction
 δ ... displacement

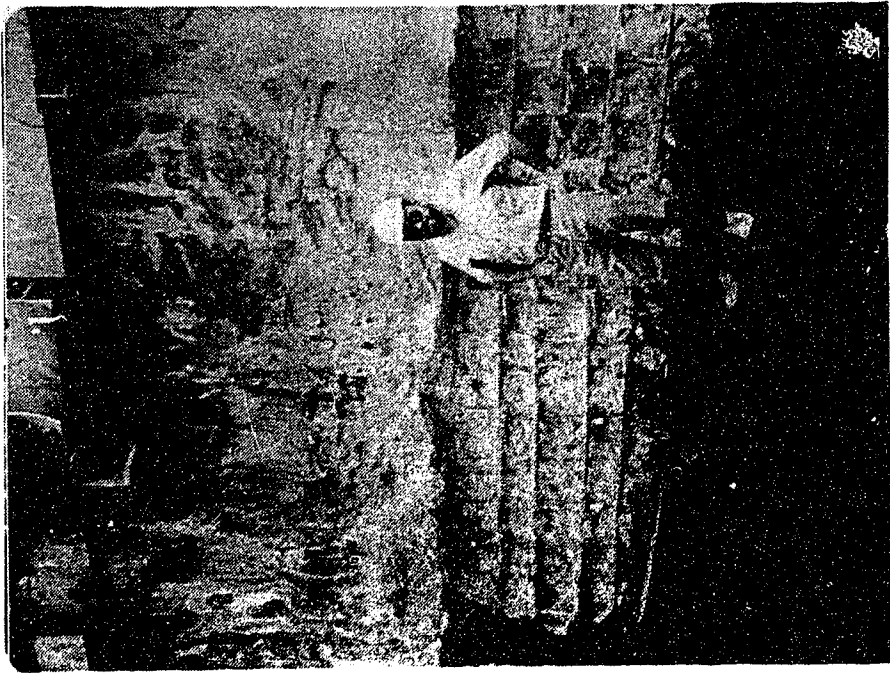
ϵ ... strain
 γ_c ... unit weight of concrete
 γ_{dry} ... dry unit weight
 γ_s ... unit weight
 γ_{sat} ... saturated unit weight
 ν ... Poisson's ratio
 ϕ ... angle of shearing resistance of the soil
 $\sigma_1, \sigma_2, \sigma_3$... total principal stresses
 τ ... shear stress

excavation water tight.

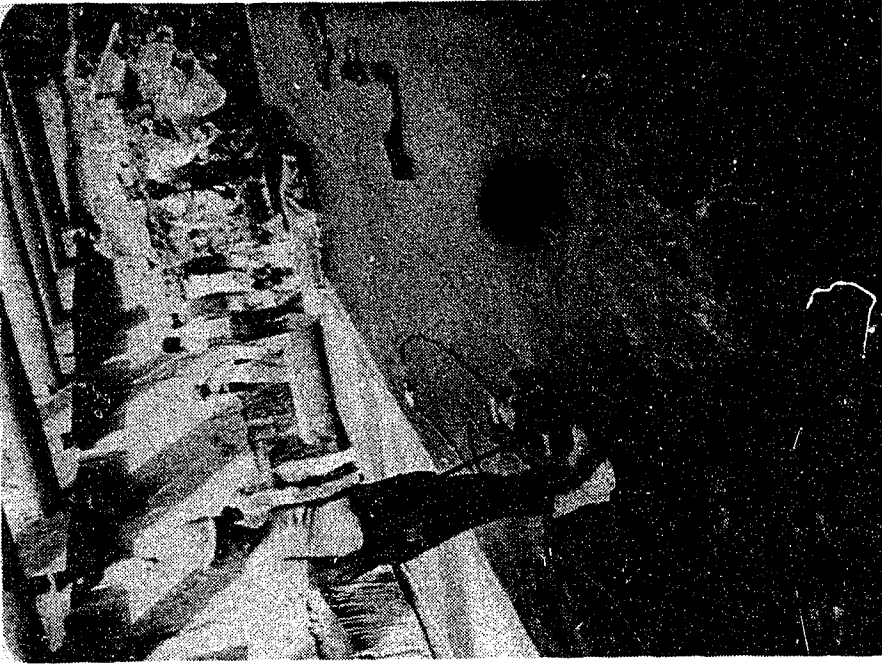
The connection between the precast panel and the raft (floor slab) was then made. The raft thickness was approximately 1.10 m with expansion joints every 35-40 m. The connection between the pre-cast panel and the raft (floor slab) was made by uncovering the connecting steel bars installed previously in the specific zone in the pre-cast panel at the factory. This can be seen in Figure 3.6a. The connecting steel bars form a good connection between the raft reinforcing steel bars and the pre-cast panel reinforcement creating a fixed joint.

Installation of the roof slab constituted the next step. In this procedure, a sheet pile wall approximately 2.5 m long was installed 0.75 to 1.0 m from the walls. This allowed a small trench to be excavated. The sheet pile walls provided space for workers to reach the connection level of the roof slab at the top of the precast panel. As well, it allowed the impervious layer to overlap to the required depth of the wall. The slurry covering the connecting steel bars of the wall was removed and shuttering for the roof slab was installed. The reinforced concrete work was performed as for the raft. A water sealant was applied to the top surface of the roof slab and overlaying was done for the outer side of the wall. The sheet pile walls were removed and the backfilling began.

Two weeks after backfilling had been completed, the temporary supports were removed. At this stage, the



a) The connection between rubber strip of the pre-cast panel and the main layer



b) The main layer installation

plate 3.3 Details of the Water Tightness Layers at the Base of the Excavation

construction of the tunnel section is completed. The rest of the civil work was carried out.

3.4 The Construction Procedure for the Station Section

The station is located in one of the busiest junctions in Cairo. The major factors which influenced the construction method were the traffic conditions and the available work area. The construction procedure had to take into account these conditions despite their high cost. Each working area had to be prepared allowing for traffic diversion, which considerably slowed progress.

Construction of the station began by installing a precast L-shaped section under the street level to form the required guide walls for the slurry trenches. The excavation starts under the support of the bentonite slurry. Steel tubes in both sides of the excavation were inserted for the required construction connection between the adjacent walls. The excavation accommodated two panels, of 5 m width and 20 m depth. Figure 3.5 illustrates the construction sequence. After reaching the final depth of excavation the excavation machine was moved to the next even numbered panel; i.e. an unexcavated area equal to 2 panels between excavations). Steel reinforcement cages were placed in the excavated trench and concrete was cast using two Tremie pipes starting from the bottom of the excavation displacing the slurry. The use of two tremie pipes decreased operation time and ensured that the concrete was poured in equal amounts in both sides

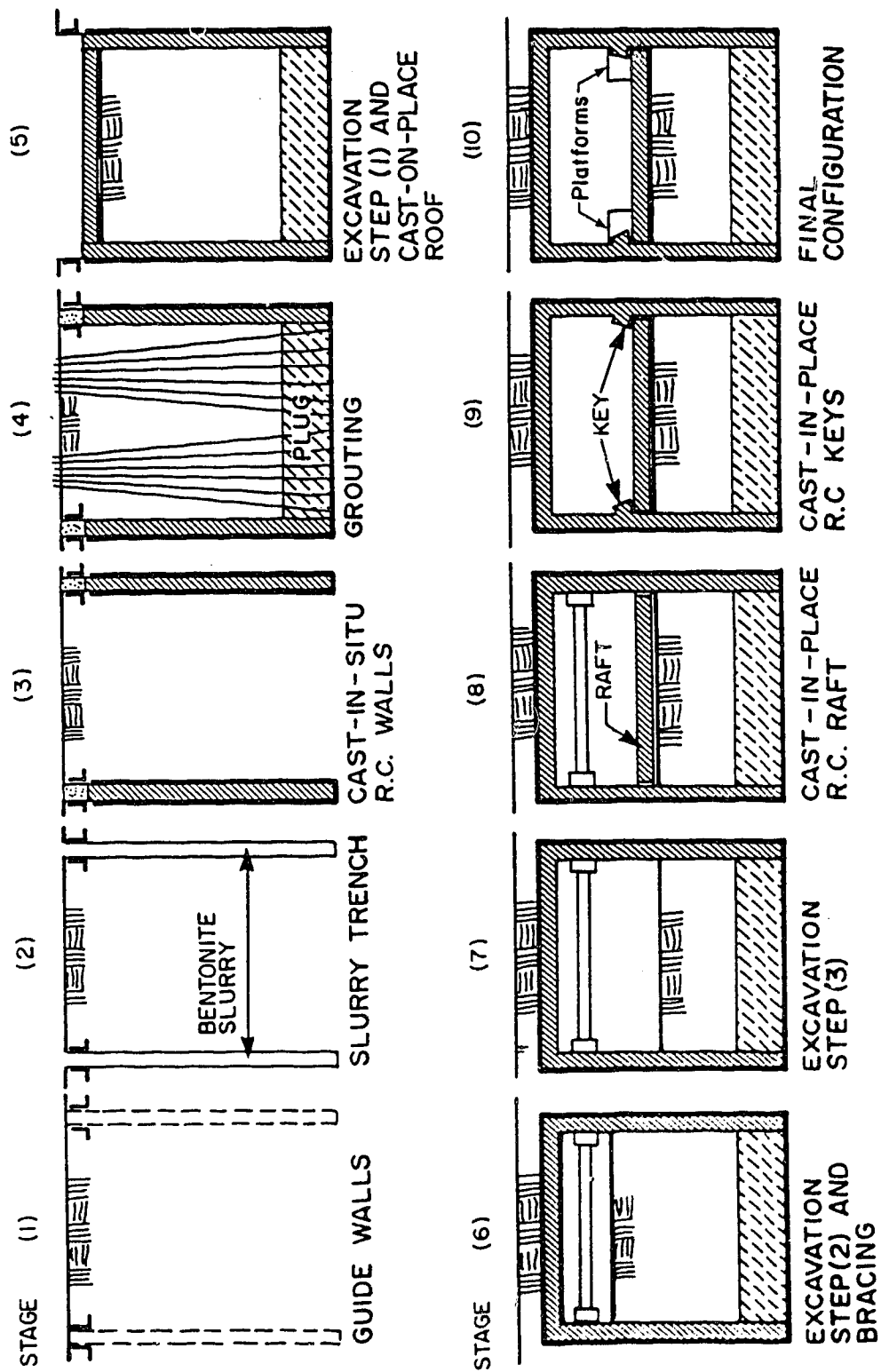
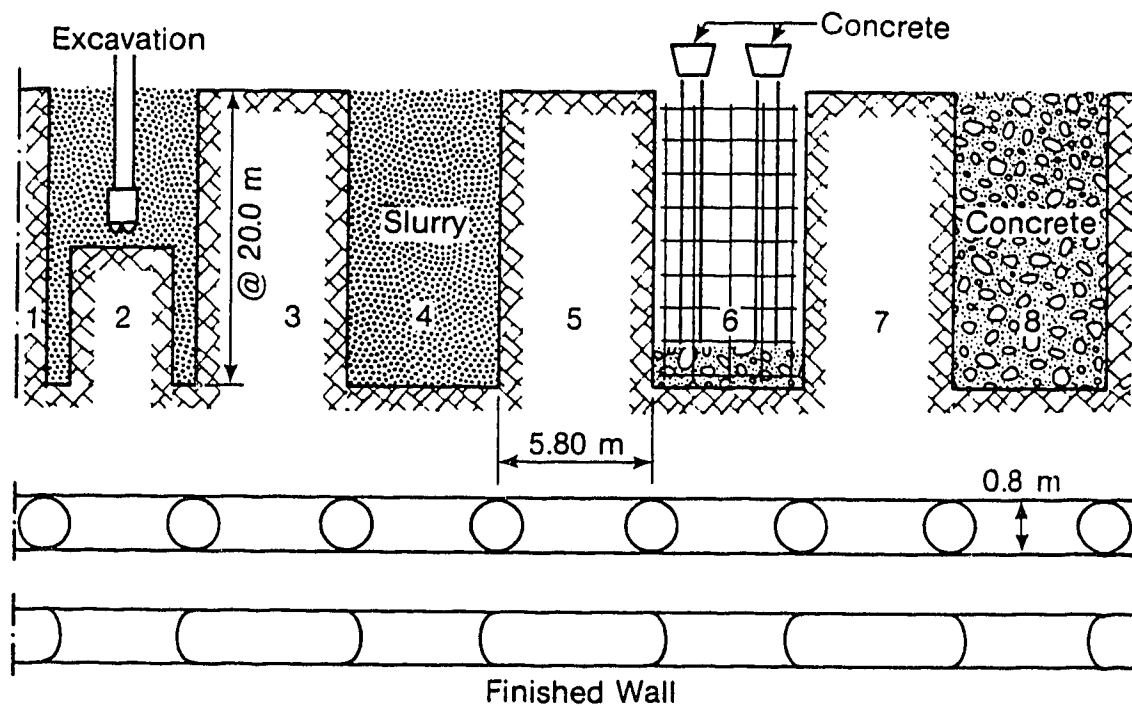


Figure 3.5 Construction Procedure Steps for the Station Test Section

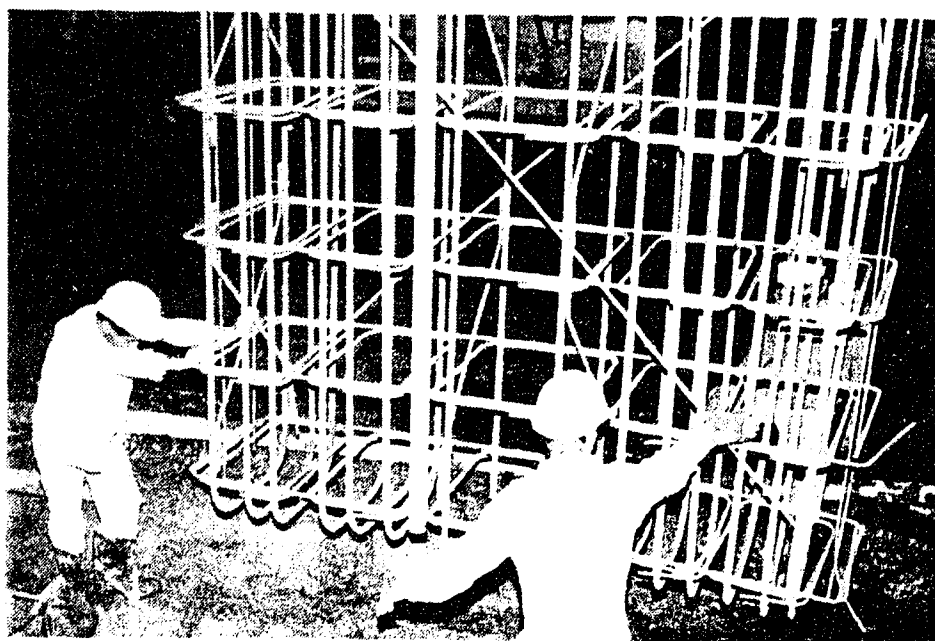
of the trench. The upper 3 m of the wall (measured from street level) was made of weak concrete. This facilitated the uncovering of the connection to the steel reinforced cage to allow the roof slab connections to be made. Figure 3.6 shows in cross-section the sequence of the construction procedure for the cast in situ panels. The street was repaired and the traffic was diverted and the work was moved ahead to another adjacent working area.

In the following step, the plug was constructed as explained in the previous section. The plug had a constant 3 m thickness and its base was at a depth of 20 m. Six weeks were allowed for the grout to set and to reach its maximum strength and impermeability. At this time, the dewatering operation began bring the water level to 0.5 m below the raft base level. The excavation started at a depth of 3 m. A layer of clean sand was spread over the entire excavated site and the shuttering and reinforcement steel work was completed. The reinforcing steel of the diaphragm walls was exposed by removing the upper portion of weak concrete. The connection with the roof slab could then be made. The roof slab was cast in place. One week was allowed for the curing of the concrete. During this period, a moist environment was maintained, by spraying water on the concrete and covering the slab with a specially designed fabric.

After this, L-shaped precast beams were placed on the edges toward the open air excavated area. Backfill material was placed up to the limestone base of the street. The



(a) Sequence of cast-in place walls installation



(b) Steel cage installation at the station test section

Figure 3.6 Sequence of Construction for the Cast In Situ
Panels

excavation started under cover to a depth designed to allow for a single row of temporary support installation. These were similar in design to those in the running tunnel and had a diameter of 800 mm and length of 17 m. Immediately after the installation of the struts, the excavation was continued to its final depth of 10.5 m from street level. The construction of the impervious zone at the base of the excavation was performed in the same sequence as for the running tunnel. Structurally, the raft acted as a simple beam seated in the keys as shown in Figure 3.5. To create the separation between the diaphragm wall and the raft, a 50 mm thick layer of styrofoam was placed at the contact area between the two elements. After placement of the steel, the concrete was cast. Both the roof and raft thickness were 1.0 m. The keys, which act as support for the raft against the uplift forces, were completed and connected to the diaphragm walls similar to the tunnel raft connections. As the final step in the procedure, the structural elements of the platform were constructed. At the completion of this step, the remainder of the civil work was started.

3.5 Grouting Operation

Grouting was used to achieve the required degree of impermeability. The techniques used will be described with reference to the two test sections chosen for this study. Grouting was carried out mainly in the medium and dense sand layers based on the following criteria:

1. Grain size distribution $1.0 \text{ mm} > D_{10} > 0.2 \text{ mm}$
2. Specific surface area $1500 \text{ mm}^{-1} < S < 10000 \text{ mm}^{-1}$
3. Porosity $35\% < n < 45\%$
4. Permeability $10^{-4} \text{ m/s} < k < 10^{-3} \text{ m/s}$

The main aim was to reduce the permeability of the sand zones to less than 10^{-6} m/s by grouting. Pumping tests were carried out after the completion of the grouting work to ensure that the permeability had been reduced to the desired value.

3.5.1 Types of Grouting Slurries

The following types of grouting slurries were used.

1. Bentonite or cement-clay slurries with low cement content. These were for the perforation stage.
2. Bentonite-cement slurry; 250 kg of cement and 37.5 kg of bentonite per cubic meter of mix.
3. Soft silica gels; 140 liters of soda silica and 840 liters of water and 18.5 kg of sodium bicarbonate powder per cubic meter of gel. The initial viscosity of the mix was to be less than 5 centipois. The setting time was adjusted to lie between 40 and 60 minutes. The standard mortar strength was to be 50 kPa after 3 days.
4. Hard-silica gels; the initial viscosity was less than 5 centipois. The setting times were adjusted to between 45 and 70 minutes. The standard mortar strength was approximately 1400 kPa after 6 days (kept sheltered from the air at a temperature of 20°C).

5. Self hardening slurry; used for the slurry trench excavation and to form the sides of the grouted layer.

These slurries were prepared in special mixers permitting permanent automatic monitoring of the dosage of the individual components. The setting times of the various slurries were adjusted in such a way that the total quantity of slurry to be injected into a sleeve was in position before setting starts to prevent blowouts.

3.5.2 Sequence of Grouting Operation

A series of central grouting stations were installed at different locations throughout the project site. Each central station was equipped with mixing, pumping, quality control and communication machines. A network of surface and buried grouting pipes were layed out to provide sources of slurry under pressure at every point of the site. The output of the grouting pumps was designed to vary from 200 to 3200 liters/hour and the pressures may attain 6000 kPa. Most of the grouts were made up by means of the conventional 'rising' method from drillings filled with sleeve tubes. The order of grouting of the drillings was adjusted and the flow restricted in order that the uplift forces on the soil and subsequent movements remained very small. These movements must not be capable of damaging the structures and buildings in the area. The maximum movement beneath the buildings and streets should be 4 mm and 10 mm, respectively. The drilling slurries were recycled and purified through a vibrating

screen, with maximum rate of recycling of 10.

The grouting operation started by perforating a series of holes using a rotary drill rig, combined with circulation of a fluid slurry (type 1). The density of the slurry was sufficient to prevent inward movement of the walls of the hole. The drill rig was capable of drilling a minimum of 7 m of fitted out hole per operating hour with diameters from 76 to 146 mm. The borings for grouts were 90 to 100 mm in diameter. Figure 3.7 shows the details of the boreholes for the running tunnel and station sections. After drilling to the designed depth, a sleeve pipe was inserted into the hole. This pipe is equipped with tubes which allow the flow of the grout slurries in one direction under pressure. The pipe was 38 mm in diameter and the length of the tubes was equal to the grouting area thickness (varied between 3 and 4 m). The next stage was the grouting stage. It was carried out in three steps:

1. Bentonite cement grouting was aimed to fill the eventual open layers and pockets of soft ground and to seal the block to be grouted to the tunnel walls. The grouting rate was 600 to 800 liters/hour under a pressure of 1500 kPa.
2. Soft silica gel was aimed to water seal tight the sand layer. The grouting rate was 500-650 liters/hour under a pressure of 2000 kPa.
3. A second layer of bentonite cement grouting.

The grouting rate was 600-800 liters/hour under a pressure

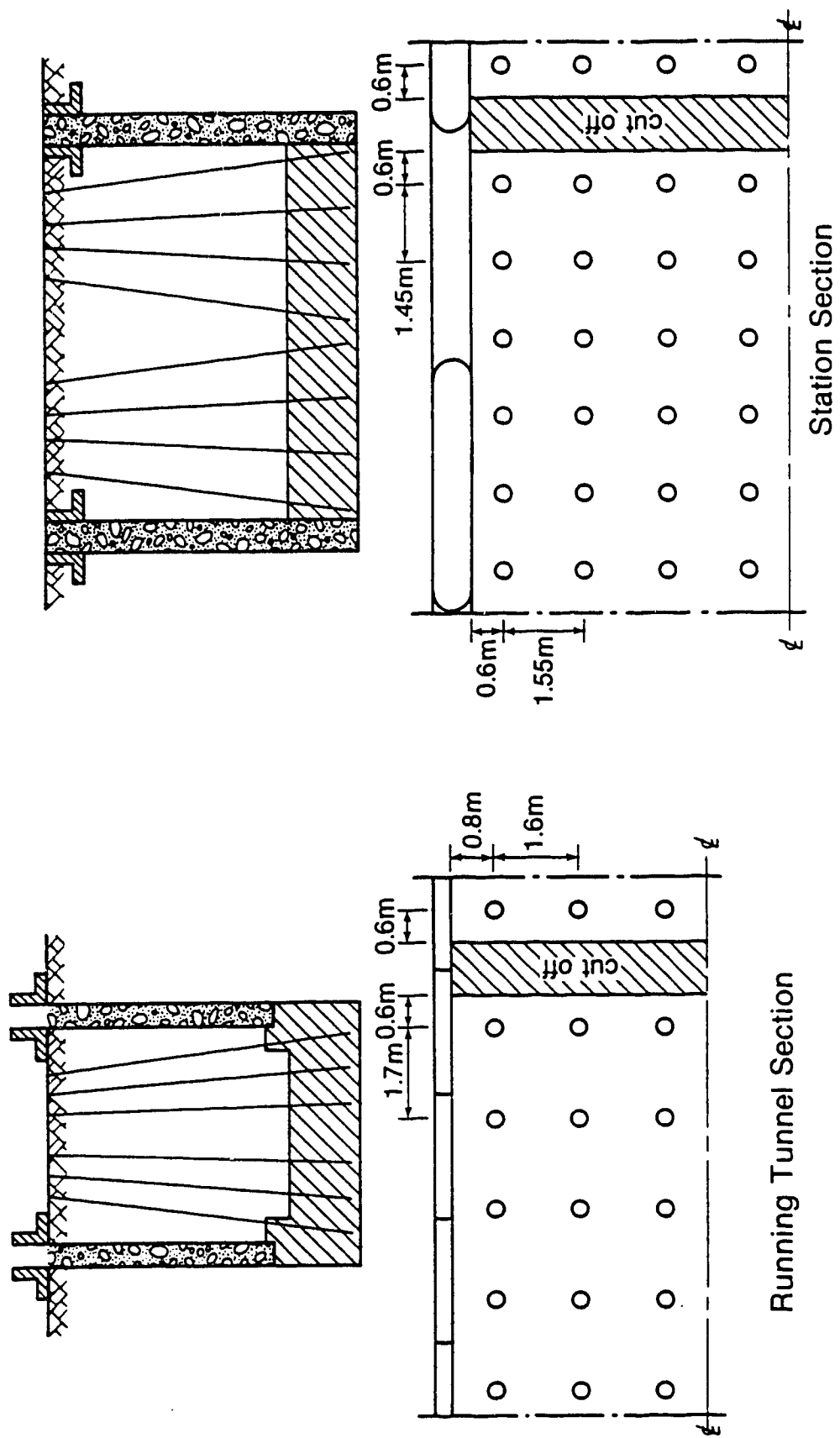


Figure 3.7 The Drilling Details for the Chosen Test Sections

of 2500 kPa. The grouting scheme started from the center lines to the panels (the diaphragm walls). If the pressure was less than 1000 kPa and 20% less than the average, the hole was regouted. Plate 3.4 shows the site during the grouting operation and dewatering of the excavated zone.

A series of permeability tests (pumping tests) were carried out to insure that the permeability of the grouted zone was less than 10^{-6} m/s. Once the results of the pumping tests were satisfactory, the grouting tubes are filled with cement-bentonite slurry as sealant.

In general the grouting operation takes approximately 8 weeks from start to finish, after which the site is ready for excavation. Abdel Salam (1984) discusses the solution for a case of grouting failure in a section of the Cairo metro project. The main source of information about the grouting operation are the project documents and reports dated between 1980 and 1988 . The grouting work was carried out by French/Egyptian Consortium (interinfra Arabco), the sub-contractors are Soletanch-Bachy for the tunnel and EMCC for the Stations.

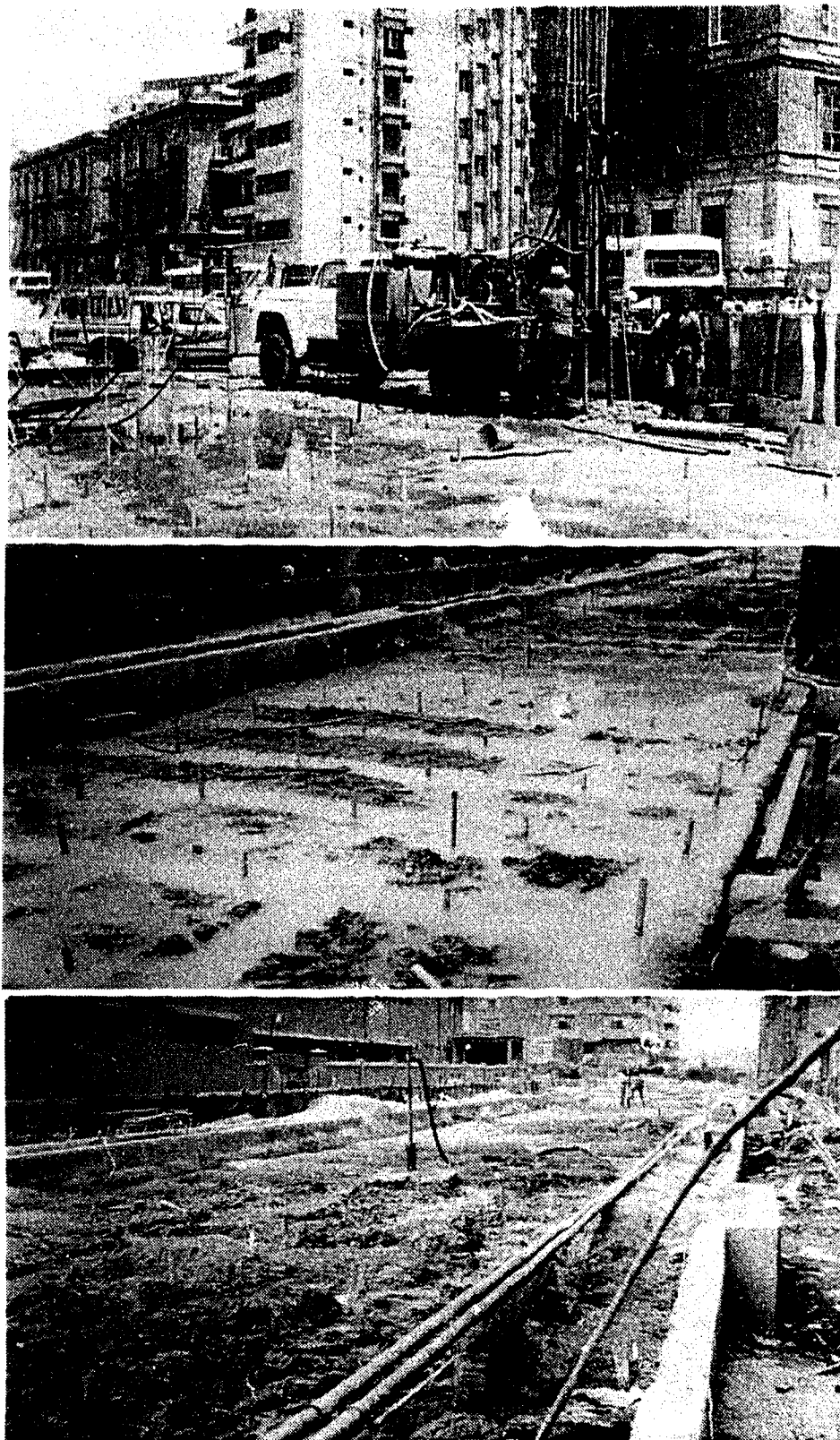


Plate 3.4 General View of the Sites During the Grouting
Operation

4. FIELD INSTRUMENTATION PROGRAM

4.1 Introduction

The primary aim of the instrumentation program was to monitor the deformation of the soil around the tunnel during and after construction. These measurements included

1. horizontal and vertical ground displacements above, beside and below the tunnel
2. pore water pressures around the tunnel
3. loads acting on the structural elements, struts, roof and raft slabs.

In the first line of the Cairo Metro, two typical cross sections were instrumented, one in the normal running tunnel between EL Sayeda Zeinab and Saad Zaghloul Stations and the second at the Orabi Station. This program constituted the first time the observational approach had been used in Egypt.

The criteria governing the choice of instruments was reliability, sensitivity, reproducibility and accuracy. As well, economy had to be considered. This included the cost of the instruments, installation, shipping and the physical monitoring program.

A considerable literature review was performed with the aim of combining the objective and the criteria. From this the decision of the type and quantity of instruments was made. Reports by Cording et.al. (1975) and Schmidt and Dunnicliff (1974) and catalogs published by the

manufacturing companies provided the range of the available instrumentation. This aided in the selection and modification of instruments to suit the site conditions and program requirements.

Details of each instrument, the theory and installation procedure are discussed in later sections.

4.2 The Running Tunnel Test Section

The running tunnel test section was located at the Mansour Street crossing within Safeya Zaghloul Street. Figure 4.1 shows the location and installation pattern of instrumentation in plan view. In Figure 4.2, the distribution of the surface settlement points and benchmarks are shown. A cross-sectional view of the instrumentation installation is presented in Figure 4.3. Dimensions of the tunnel cross-section and details of the soil profile at this location are shown in Figure 4.4.

In cross-section, the tunnel is 6 m high, 8.86 m wide, with precast walls 0.45 m thick. The roof slab is 0.90 m thick while the raft has a variable thickness, 1.10 m at the center increasing to 1.20 m at the walls.

The grouted plug lies approximately 7 m below the raft (base slab). Its thickness varies from 3 m at the centre to 4 m at the edges. The slurry trench wall, 0.60 m wide, in conjunction with the precast wall, acts as an impermeable membrane.

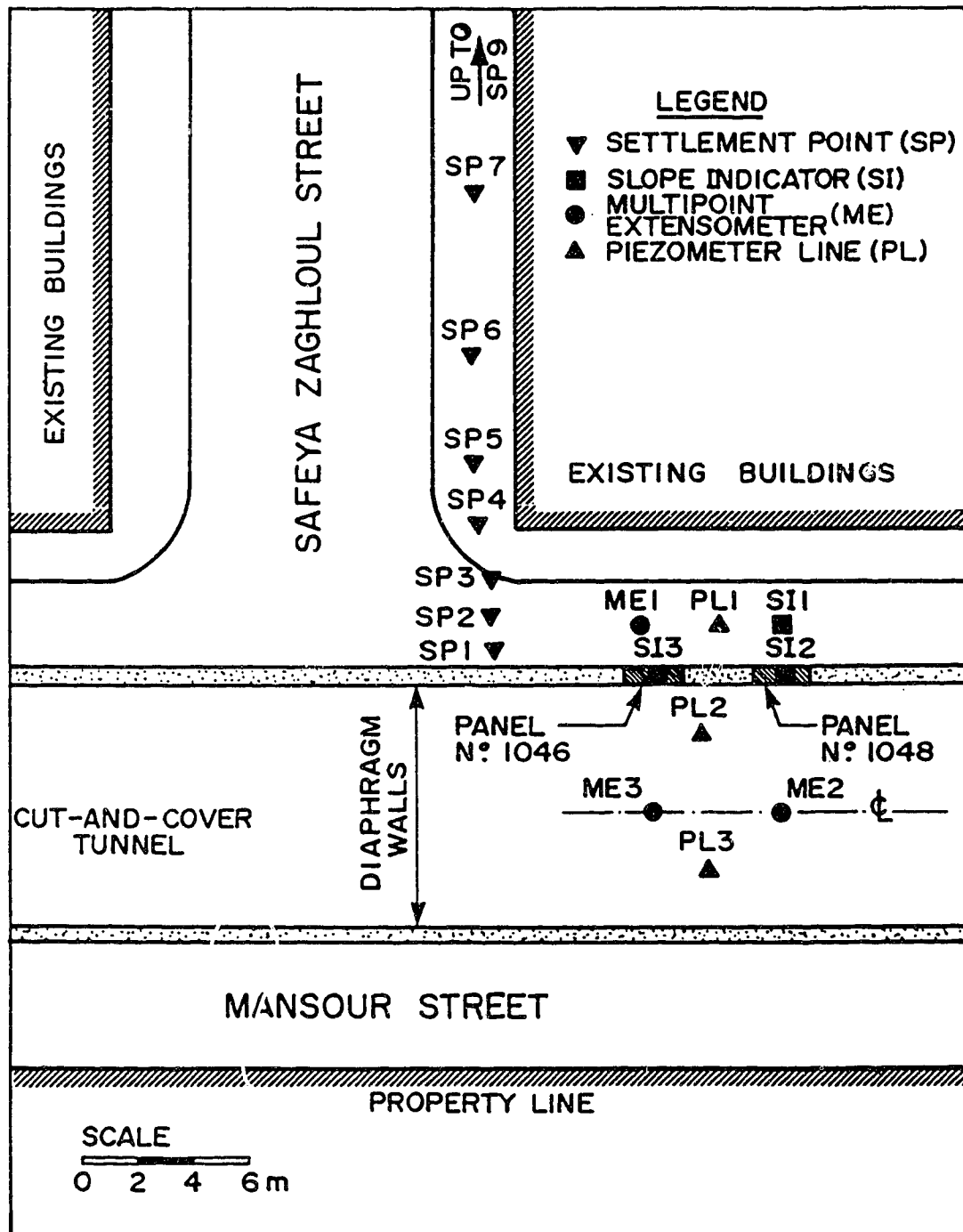


Figure 4.1 General Layout of Instrumentation at the Tunnel
Test Section

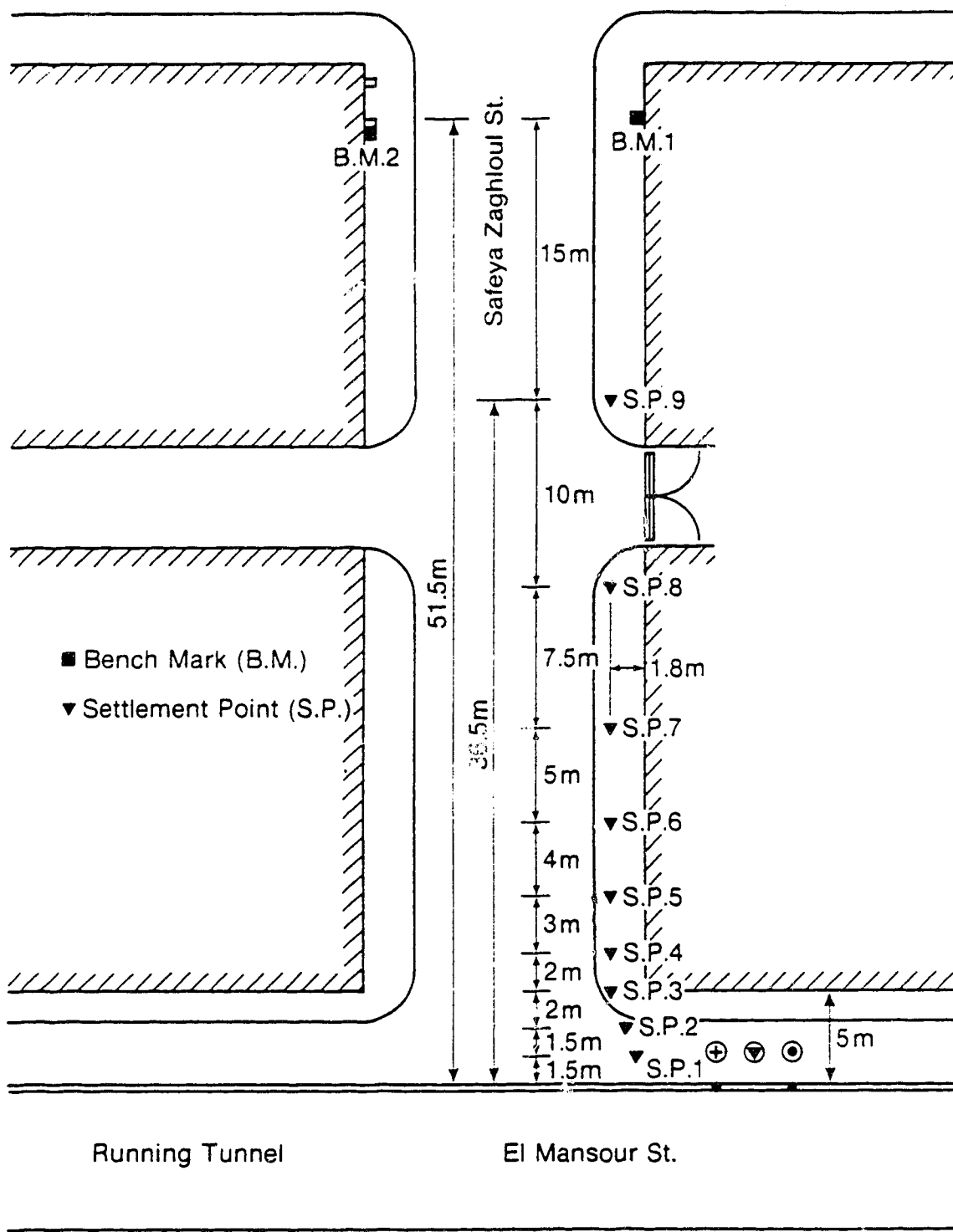


Figure 4.2 The Surface Settlement Point Distribution at the Tunnel Test Section

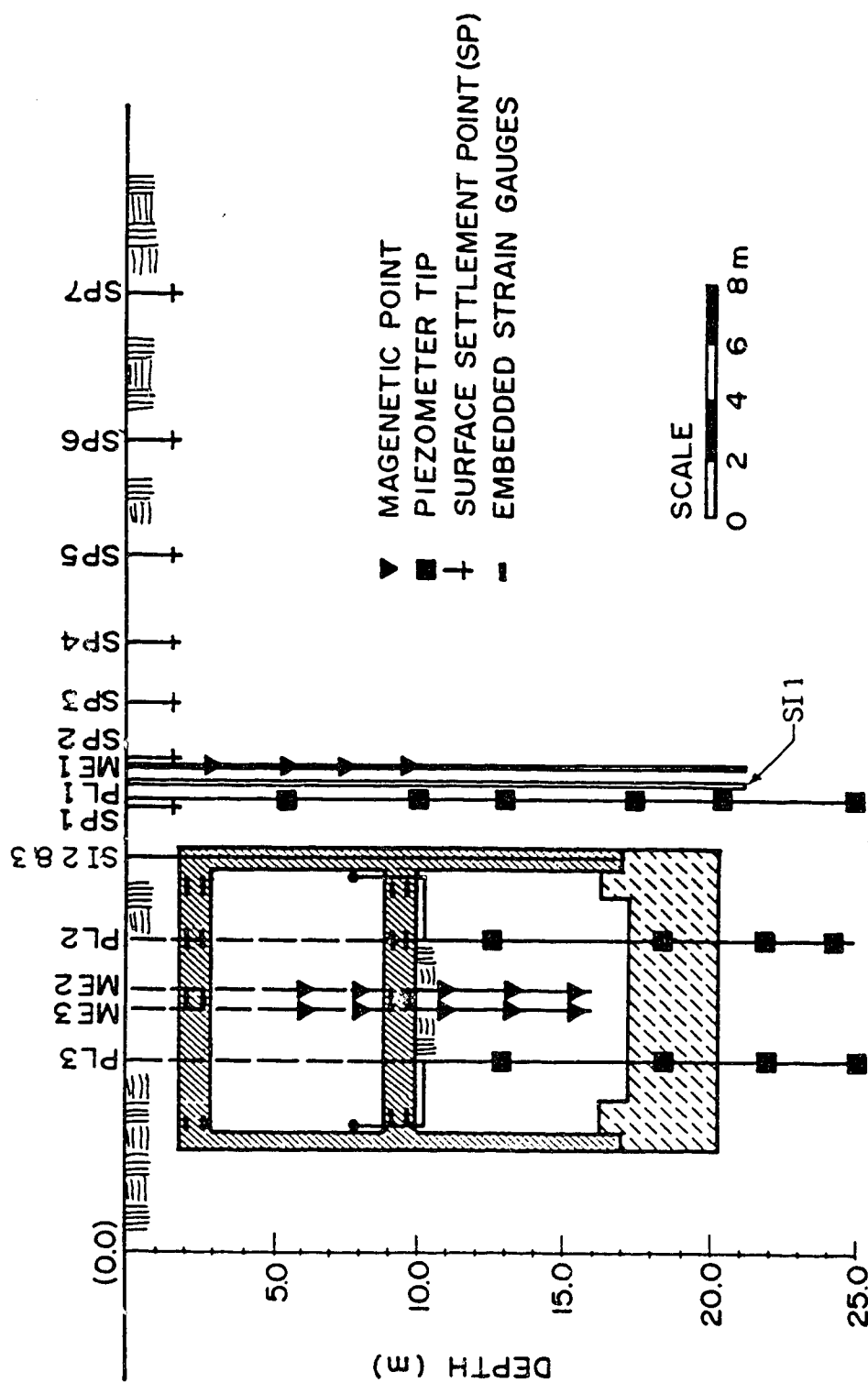


Figure 4.3 The Tunnel Test Section - Cross-Sectional View of the Instrumentation

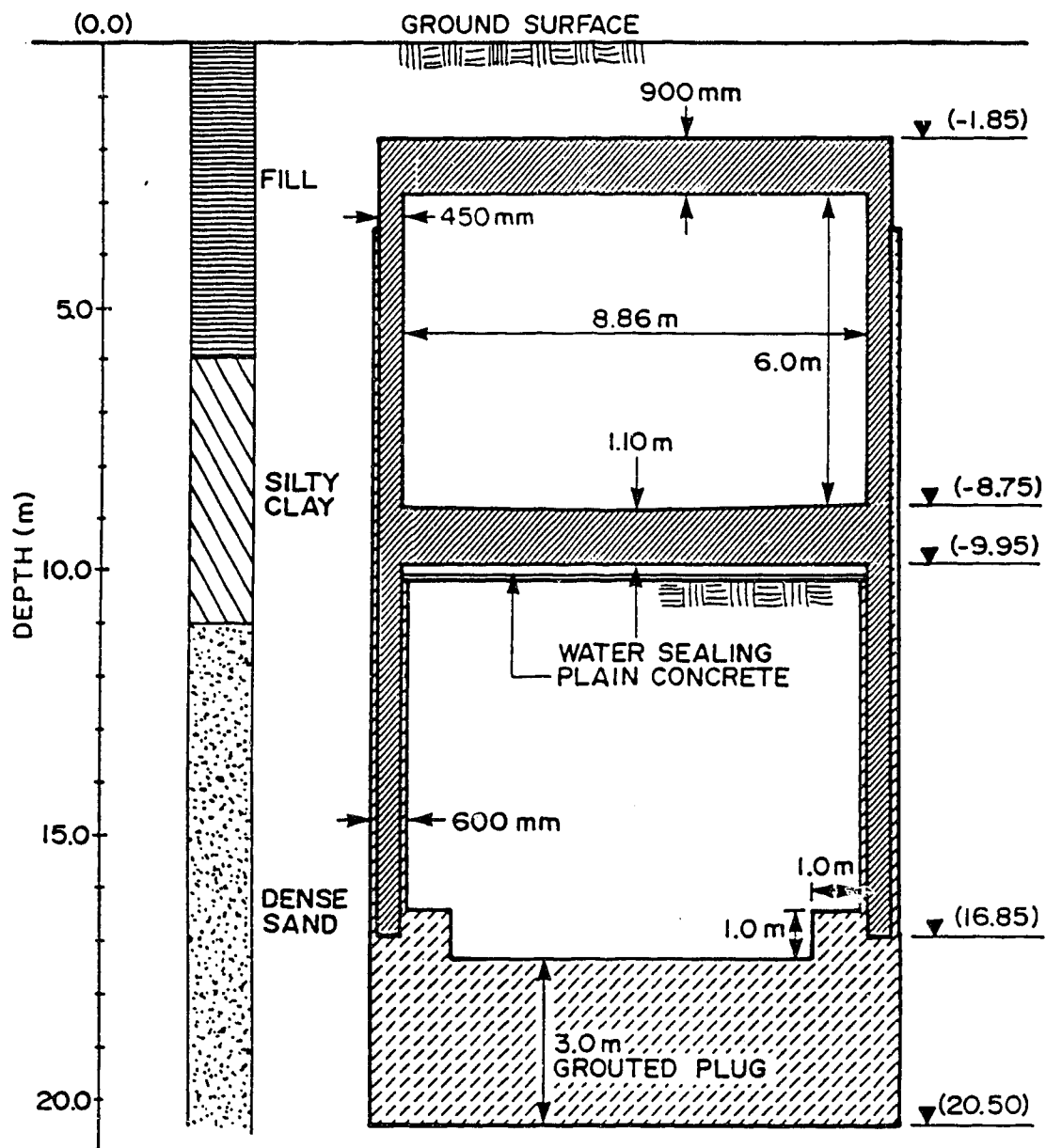


Figure 4.4 Cross-Section Details of the Tunnel Section and the Soil Profile at this Location

4.2.1 Instrumentation

To observe the surficial vertical displacement around the tunnel, 9 surface settlement points were used, and these were referenced to two benchmarks. The settlement points were installed over a lateral distance of 36.5 m measured from the tunnel walls (which is more than 3 times the depth of excavation, 10.50 m). The benchmarks were installed at a depth of 51.50 m to avoid being influence by the excavation.

Three installations of multipoint extensometers (ME) were used to monitor the vertical distribution of displacement near the tunnel and inside the excavation zone. The first string, ME1, consisting of 5 extensometers , was installed 1.5 m from the tunnel walls and to avoid the disturbance caused by construction and removal of the L-shaped guide walls. In Figure 4.5, details of extensometer string, ME1, are shown. The elevations shown in this figure are the final elevations after installation.

After the grouting operation was completed, but prior to dewatering, two strings of multipoint extensometers, ME2 and ME3, were installed inside the tunnel section. The final elevations for each extensometer of ME2 and ME3, are also shown in Figure 4.5.

As the maximum heave was expected at the center of the tunnel, ME2 and ME3, were both located at the centre line, and served to complement each other. Each string consisted of 5 extensometers, and spanned the depth from 6.0 to 15.5 m below street level.

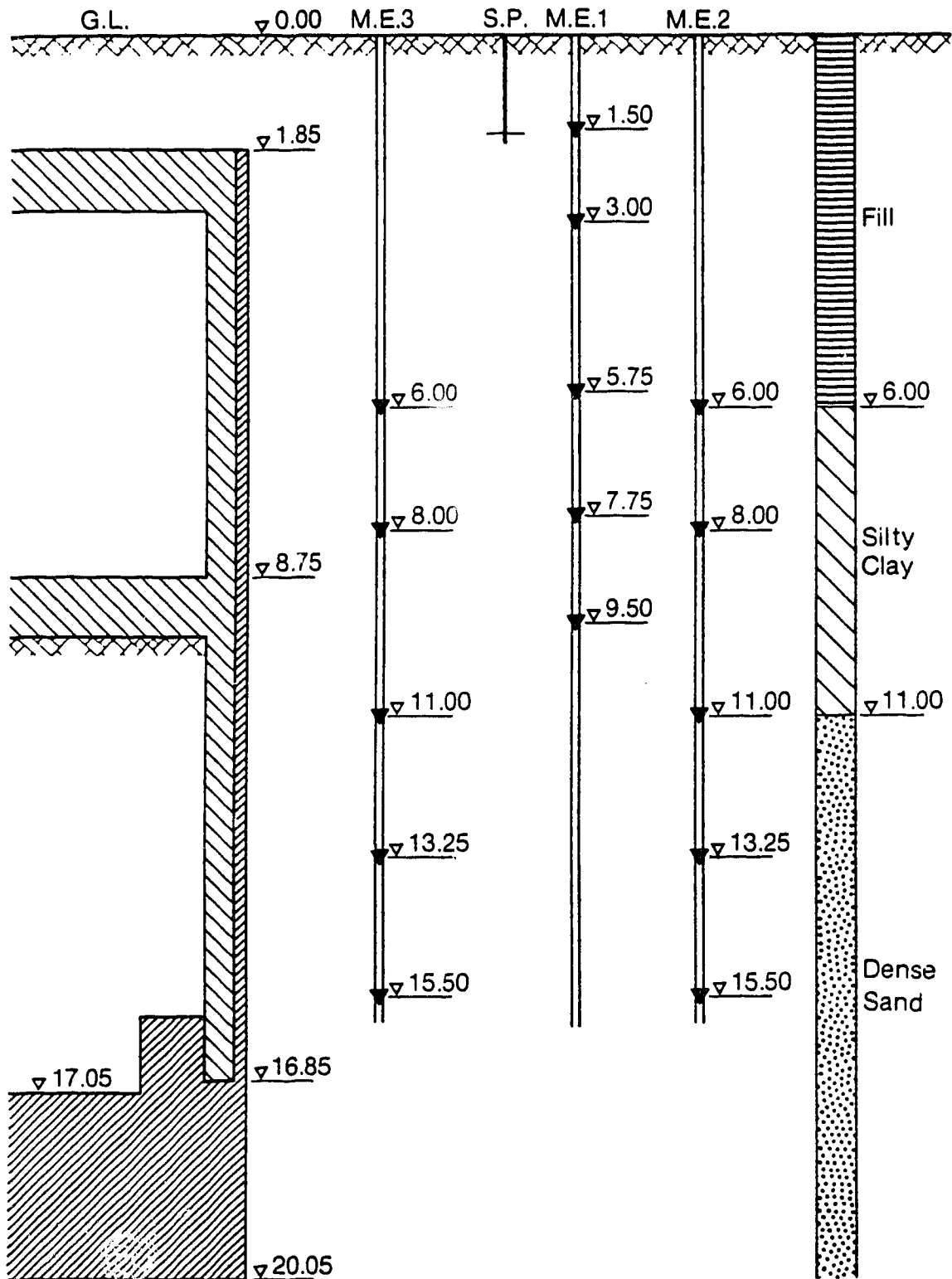


Figure 4.5 Details of the Multipoint Extensometers at the Tunnel Test Section

Three slope indicators (SI) were used to monitor the horizontal displacements of the precast wall and the soil around the tunnel. The first, SI1, was located 1.5 m from the wall at the center line of panel No. 1048, at a depth of 20.5 m. SI2 and SI3 were installed in the center of precast panels No.'s 1046 and 1048. The required panels were prepared in advance at the factory by insertion of 150 mm diameter PVC pipe. These pipes extended 1.5 m above street level. After the panel had been successfully installed, the slope indicator casing was inserted and grouting slurry was pumped to fill the gap between the PVC pipe and the casing. The final depths for SI2 and SI3 were 12 and 11 m, respectively as shown in Figure 4.3.

Three piezometer lines were used to monitor pore water pressures; in the excavation for the short term and in the grouted plug to assess its reliability in the long term (i.e. the determination of the practical age of the plug). The first, PL1, consisted of 6 piezometers and was installed outside the tunnel 1.5 m from the wall. The lower three were electric and the remainder pneumatic. The details of PL1 are shown in Figure 4.6. Line, PL2, with 3 pneumatic and 1 electric piezometer, was located 2.25 m inside the excavation, as measured from the precast wall. The third was installed 2.25 m from the inside face of the opposite precast wall, similar to PL2 (Figure 4.1). These 2 lines are also detailed in Figure 4.6.

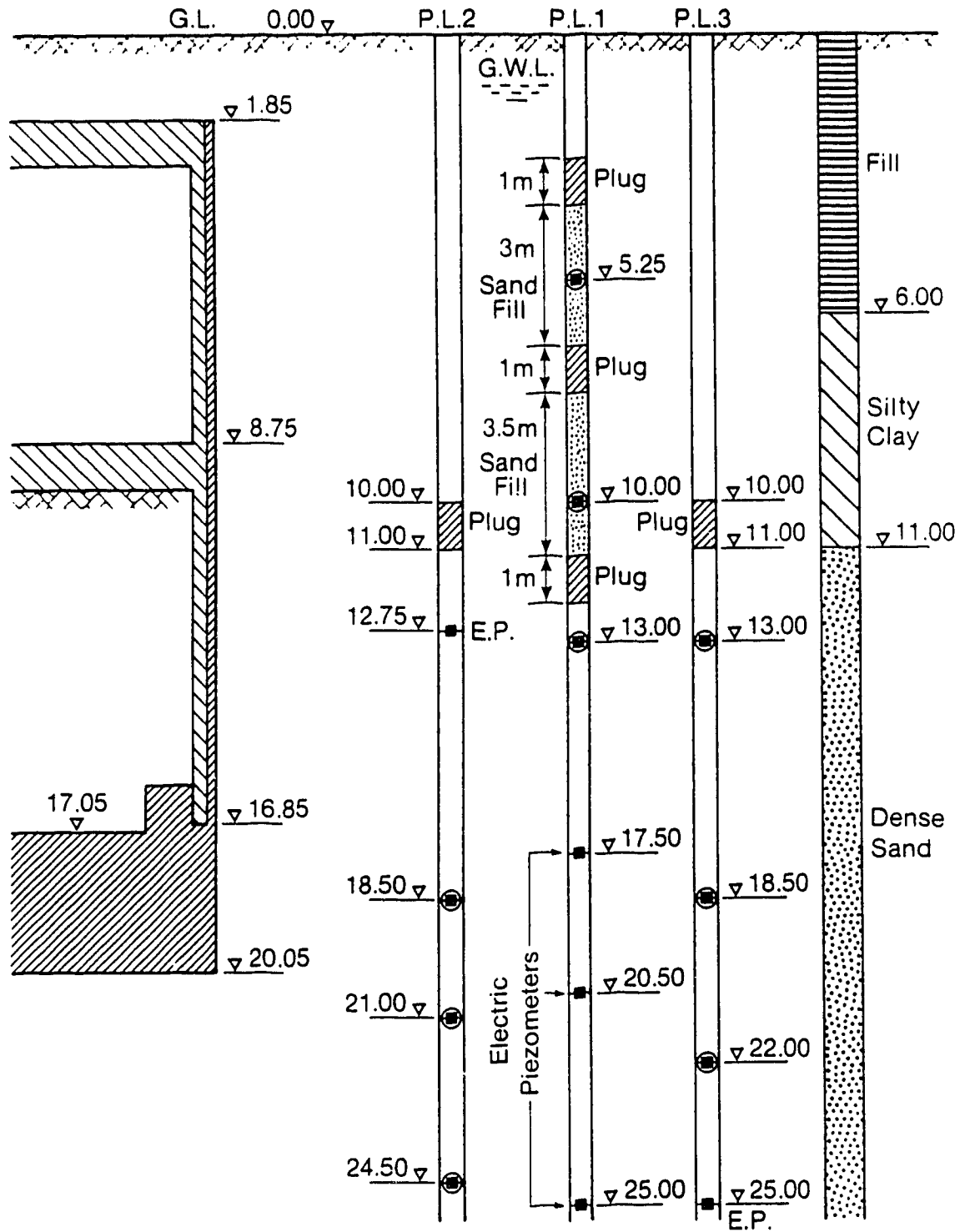


Figure 4.6 The Piezometer Line Details at the Tunnel Test
Section

In the roof and raft slabs, 16 strain gauges were embedded to monitor the normal forces in the structural elements. The distribution of these strain gauges is shown in Figure 4.3. In order to observe the normal forces in the struts, twelve weldable strain gauges were mounted on the upper and lower struts (temporary supports), three in each side of the pipe, with one at the top and the other two at a spacing of 120° .

4.3 The Orabi Station Test Section

As explained previously, the Regional line consists of 5 stations. The Orabi Station at the intersection of Ramsis and Orabi Streets proved to be the most suitable site for instrumentation. In Figure 4.7, the general layout of the station and location of the test section are shown.

In cross-section, the station is 17.17 m wide and 6.2 m high. Cast in situ panels, 800 mm thick and 20 m deep, form the walls. The raft and roof slab have a uniform thickness of 1.0 m. The former is simply supported on a key, which is connected with the walls. The grouted plug lies 6.3 m below the raft and has a thickness of 3.0 m. The station cross-section and soil stratigraphy are provided in Figure 4.8.

Briefly, the soil profile at this site may be described as 3.5 m fill, underlain by 6.5 m of silty clay followed by 5 m of medium density sand. Below this lies a thick layer of dense sand.

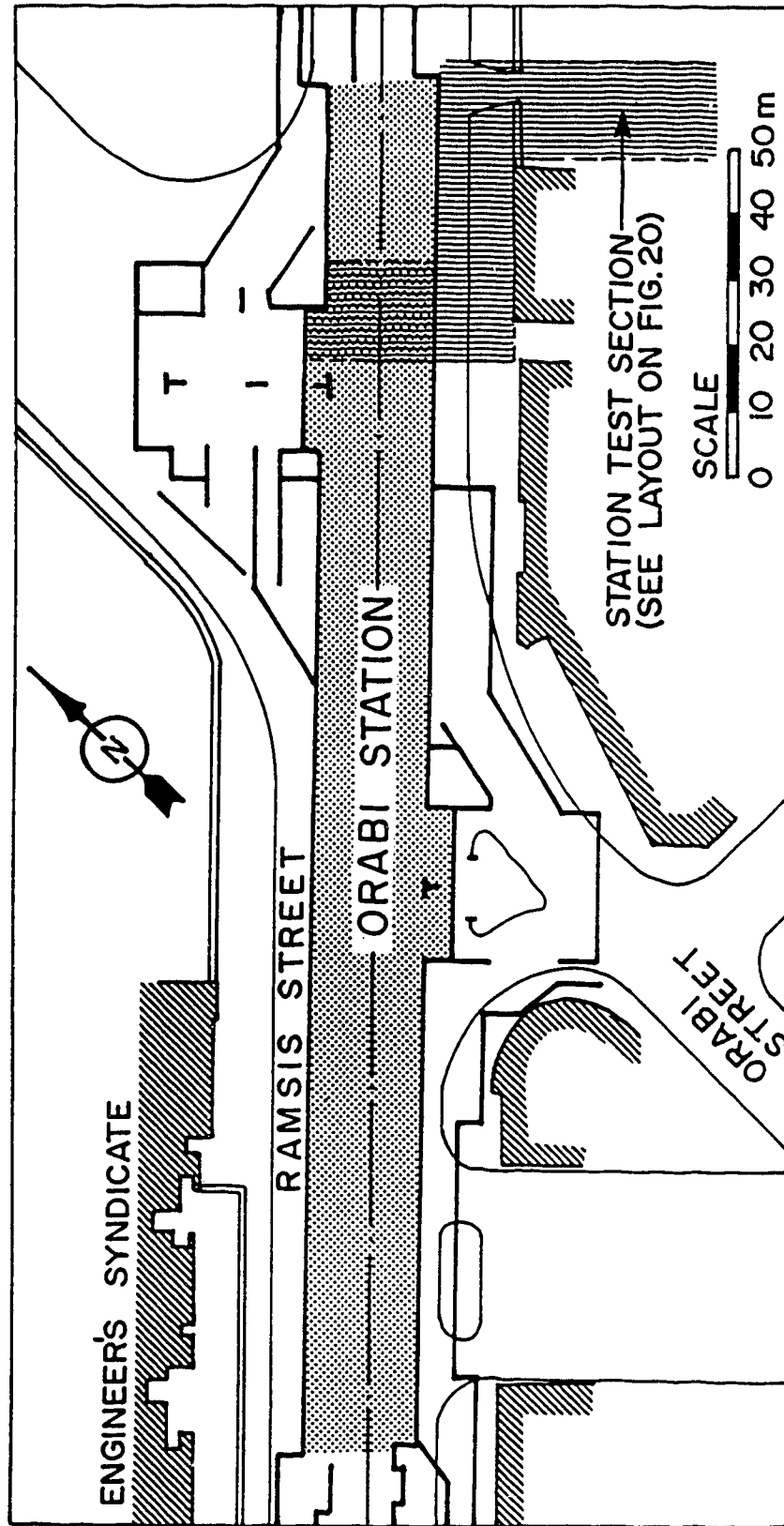


Figure 4.7 Orabi Station General Layout

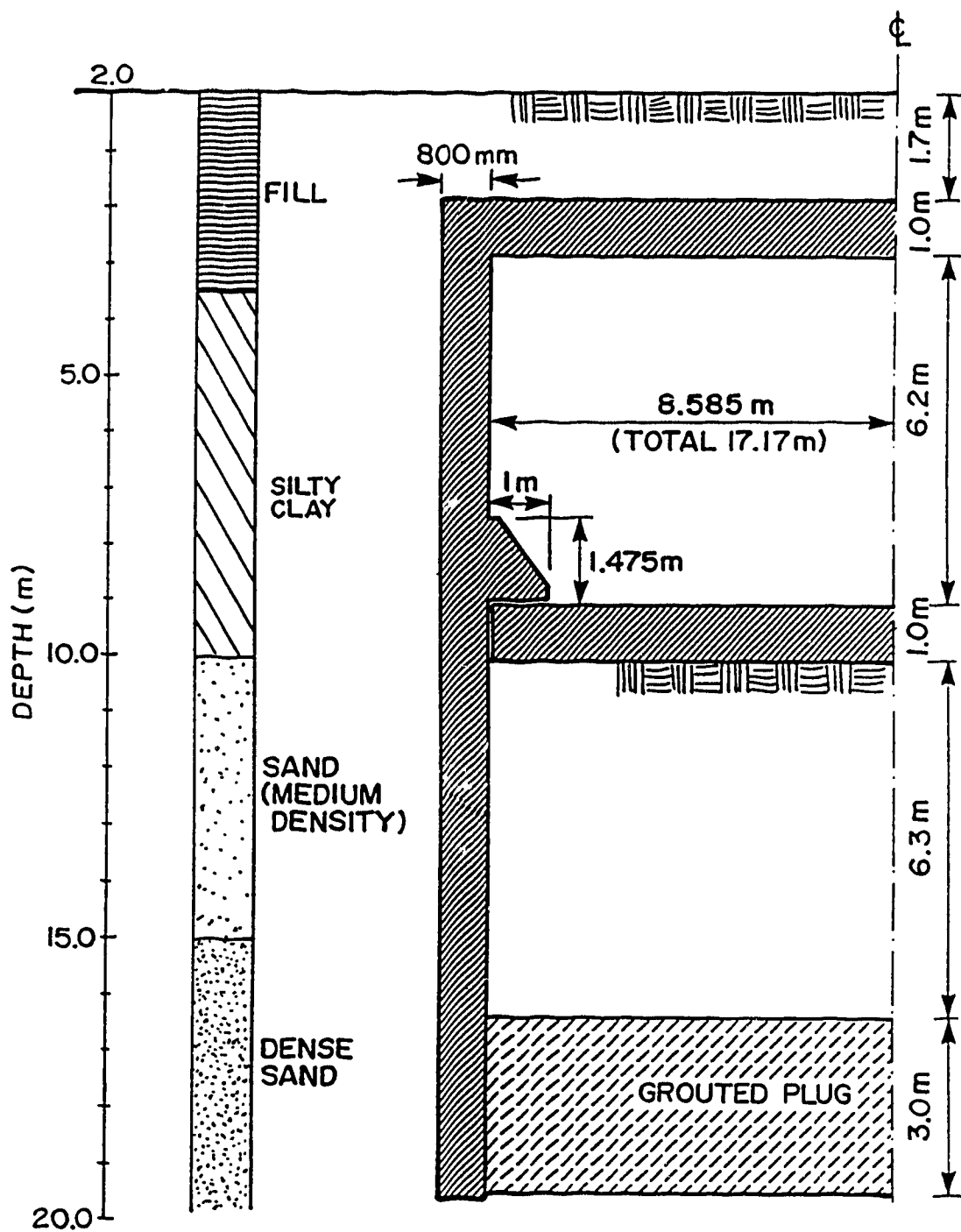


Figure 4.8 Orabi Station Cross-Section and Soil Stratigraphy
at the Test Section

4.3.1 Instrumentation of the Orabi Station

Figures 4.9 and 4.10 show the distribution of the instrumentation at the Orabi station.

Ten settlement points were used to define the settlement trough, and were referenced to 2 benchmarks.

Three strings of multipoint extensometers were installed. ME1, consisting of 6 extensometers, was located 1.5 m from the outside wall. ME2 was installed 4.25 m from the inside wall, and ME3 at the centre line of the cross-section, approximately 8.6 m from the wall. ME2 and ME3 each consisted of 4 extensometers. The locations and elevations are shown in Figure 4.11.

In Figure 4.9, the locations of the three slope indicators (SI) are shown. SI1 was installed 1.5 m from the outside wall, at the center line of Panel No. 55 at a depth of 21 m from the ground surface. SI2 and SI3 were pre-mounted to the steel cages of Panel No.'s 53 and 54. They were installed to a depth of 19 m.

Three piezometer lines were installed, PL1 1.5 m outside the station section, PL2 and PL3 approximately 2.25 m from each side wall inside the excavated area. PL1 consisted of three electric and three pneumatic piezometers. PL2 and PL3 each had 4 piezometers, one electric and three pneumatic. As at the running tunnel section, one piezometer was installed in the grouted plug to assess its effectiveness with time. The piezometers lines are detailed in Figure 4.12.

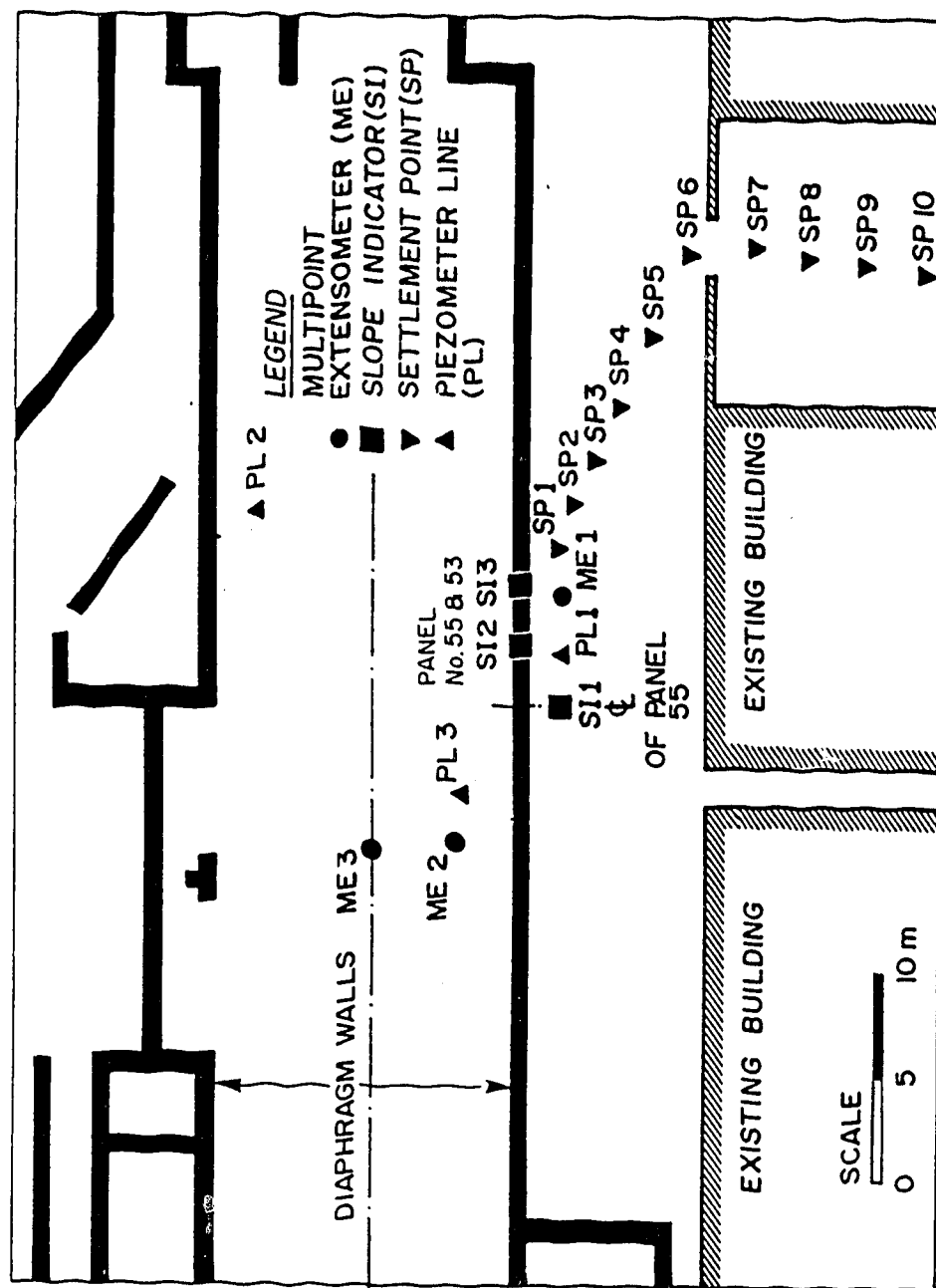


Figure 4.9 General Layout of the Instrumentation at Orabi Station Test Section

1. INTRODUCTION

1.1 Foreword

To study the geotechnical behaviour of diaphragm walls, the Greater Cairo Metro project has been used as a field case history.

The City of Cairo has existed for more than one thousand years and is one of the oldest in the world. It was originally built to accommodate a population of a few hundred thousand. At present, Cairo has an estimated population of 12 million people with an additional influx of three million commuters during the daytime.

Of course, no designer or urban planner could have predicted the rate of growth during this period. As a result of this unexpected development, Cairo suffers from major traffic congestion.

Several studies were conducted by both foreign and local consultants to solve the transportation problems in the Greater Cairo area. The results show that the most appropriate and viable solution is the construction of an underground transit network.

The past and current economic situation in Egypt has led to a delay in confronting and solving this problem, but with the continued high rate of development of the city of Cairo indicates that any further delays in the construction of an underground network may well result in a near blockage of the surface traffic. Feasibility studies have shown that

a high priority must be given to the subway system to avoid the economic problems associated with the congestion that would result.

1.2 The Greater Cairo Metro Project

1.2.1 The Proposed Network

The proposed network consists of three lines, the Regional Line and Urban Lines (1) and (2) as shown in Figure 1.1. The Regional Line is approximately 43.5 kilometers long and passes through several densely populated residential areas and business zones. This line includes an underground portion of 4.5 kilometers, which connects the existing Helwan surface railway line to the south with the EL-Marg surface railway line to the northeast.

Urban Line (1) will connect the northern region of Shoubra EL-Keima with the western district of Boulak EL-Dakrour for a distance of 12 kilometers. It will cross the River Nile between the EL-Galla bridge the EL-Tahrir bridges.

Urban Line (2) will connect the northwestern region of Imbaba to the eastern district of EL-Darasa over a total length of 8.5 kilometers. It will cross the River Nile in two locations; the first near the Zamalik bridge and the second by the Abou-EL-Alla bridge.

In order to integrate the three lines into one system, some of the downtown stations would have to be shared by two

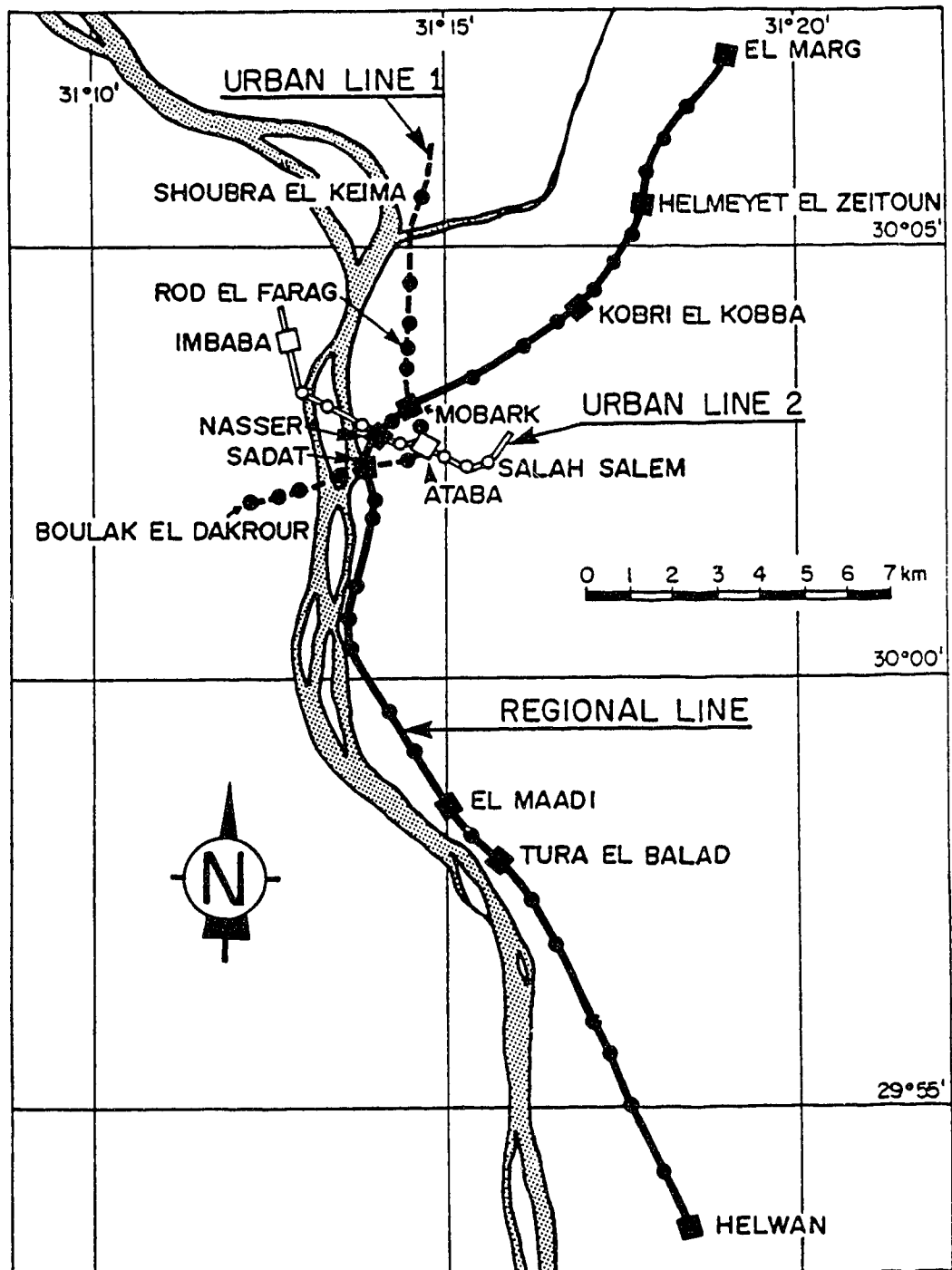


Figure 1.1 The Greater Cairo Metro Project - The Proposed Network

of the three metro lines in the form of double level crossings.

The first priority of construction was given to the Regional Line. For this reason, the Regional Line is discussed in more detail in the following subsection.

1.2.2 The Regional Line

The below surface portion of the Regional Line is approximately 4.5 kilometers in length. It includes five underground stations as shown in Figure 1.2 and one street level station at the entrance. This section must pass through intensely developed areas with buildings and other structures adjacent to the tunnel and deep excavations.

The surficial geology of the region is characterized by highly permeable deposits with the ground water level present at shallow depths of 1.0 to 3.0 m.

These factors made the project technically intricate and economically demanding.

It was necessary to provide good ground control conditions to minimize the disturbance to the adjacent buildings. The most appropriate construction procedure under these circumstances was deemed to be the cut and cover construction method. Details of this approach will be discussed in later sections of this thesis.

Two of the major problems associated with the construction of the Regional line were the diversion of traffic and the diversion and reconstruction of the below

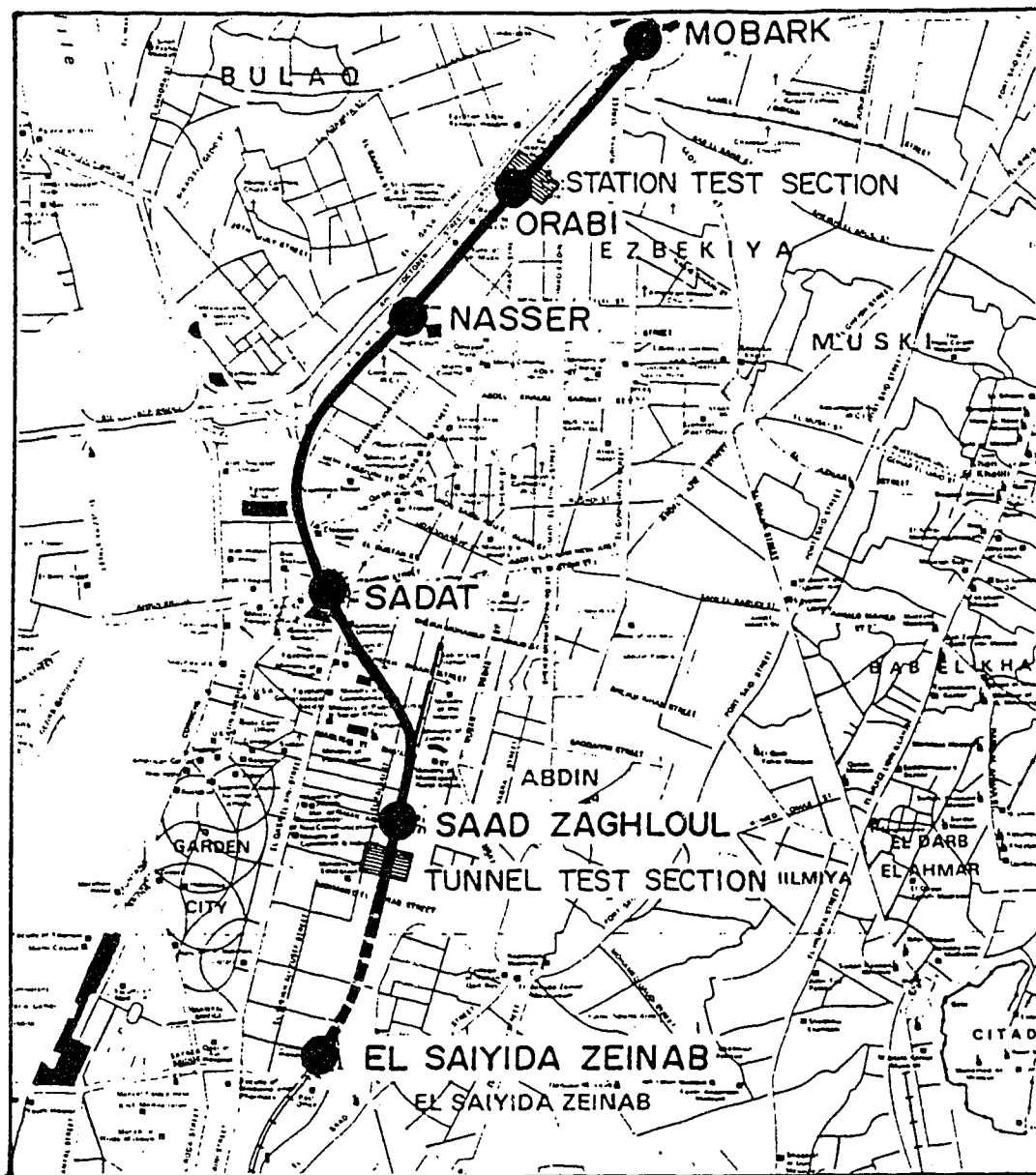


Figure 1.2 The Regional Line - The Underground Portion

surface utilities. Both contributed significantly to the total cost of the project.

The benefits attributed to the construction of the Regional Line outweighed these temporary disruptions. These benefits are summarized below.

1. The Regional Line passes through central Cairo from the remote southwest district to the northeast. This route carries about 30% of the total traffic volume, and therefore would decrease the surface volume by about 30%.
2. It will provide the residential areas of Heliopolice, Shoubra, Roud EL-farag and EL-Sahel with a practical transportation alternative.
3. The construction of the Regional Line in the downtown area will allow the present Tram lines to be removed, which in turn will alleviate one of the major obstacles at surface traffic.
4. The bus service between Ramis and Tahrir Stations, which consists of 54 routes, will be reduced by 50%. The Tahrir station will be reduced to accommodate the Giza and other areas not serviced by the Regional Line.
5. This line is expected to reduce the surface traffic volume allowing more private transportation vehicles to the downtown area as well as alleviating the parking problems. The combined effect is estimated to solve 40% of the traffic problem, particularly in downtown Cairo.
6. The decrease in commuter time should be reflected in the

national economy via improved production levels.

1.3 Aims

The main objectives of this thesis are summarized below.

1. to establish the lateral pressure concept for diaphragm walls and for soils below the ground water level;
2. to establish the ground reaction characteristics of the subsurface materials in the Greater Cairo area;
3. to document the behaviour of the Greater Cairo Metro Regional line to provide data for future geotechnical design .

One of the more difficult engineering tasks associated with this project was and continues to be, the control of the ground water level during excavation. The construction of the first line by the cut and cover method, dealt with this problem by increasing the depth of the concrete side walls and creating an impervious zone, the Plug, between those walls and the excavation bottom. As future underground lines will be located at greater depths, this problem becomes more serious due to the increased water pressure.

Alternate and potentially less expensive methods of ground water control do exist, but ground response to the excavation and ground water lowering is not known with a high degree of certainty.

The determination of ground reaction characteristics to quantitatively describe the development of displacement and stress fields around deep excavations and tunnels, and their relationship to specific construction techniques and progress, is another aspect of the design problem. This information is required to economize the design of the structural elements of the tunnel, and is essential in evaluating the effect of the construction on the adjacent surface structures.

At present, no general corpus of knowledge has been established for the host geological formations present in Cairo.

The most direct way of gathering information to assist in finding a solution to these problems is by field measurements. This approach is referred to as the Observational Method. Instrumentation is installed in the ground and in structural elements used to construct the tunnel line. Monitoring is performed on a frequent basis to yield a relationship between ground and structural response and the excavation process. This then provides information on the adequacy of the design.

Typically, the instrumentation monitors

- a) horizontal and vertical displacements above, beside and below the tunnel structure,
- b) Pore water pressures,
- c) Loads acting on the structural elements,

d) The Soil pressures developing at the contact between the ground and tunnel liner (i.e. the diaphragm walls). The field data is then evaluated by a numerical model simulating the construction procedure using the Finite Element Method as it is not possible to obtain directly a complete set of data such as the lateral earth pressure which can not be measured directly from the field instrumentation.

Two typical cross sections of the Regional Line have been instrumented. The aim of this thesis is to utilize this data, to form a basis for the design of future structures.

The Observational method for design and construction of underground structures is based on information gathered using field instrumentation coupled with criteria based on knowledge of the constitutive behaviour of the ground. The field information will be used to assist in the design of various stages of the project and verification of the numerical model. The Observational Method has not as yet been used in Egypt and there is no local experience with it. At the same time, it is believed that the use of this method on the Cairo Metro project will contribute to more effective and economy design during future phases of the project. The method also has potential for use on other geotechnical projects in Egypt, such as slope stability and foundation problems.

1.4 Scope of the Thesis

Chapter 1, the introduction, is devoted to the aims of the project, its description and problems associated with the construction of The Greater Cairo Metro Project.

In Chapter 2, the geomorphological and geological features of Egypt are discussed with particular reference to the Regional line site.

The construction procedure for both test sections, detailing the excavation, grouting and installation methods, are described in Chapter 3.

The field instrumentation program is described in Chapter 4. It includes the theory of each instrument used and its installation procedure. The general distribution of the instrumentation is detailed. A complete set of field data is also provided.

The procedure used to analysis the instrumented section is detailed in Chapter 5. The computer programs which are used to simulate the behaviour of soil are presented. Also described is the required input for the computer programs, i.e. soil parameters. The finite element results for each test section are shown, while the complete set of results is presented in Appendix D.

A comparison of the field measurements and the results of the finite element analyses are presented in Chapter 6. A detailed discussion of the soil deformation and lateral earth pressure on the diaphragm walls due to stress relief (i.e. excavation), including recommendations, is provided.

The conclusions are presented in Chapter 7, with emphasis placed on the influence of the construction procedure, wall type, wall thickness, predicted lateral earth pressure and corresponding deformation of the soil and structural elements. A lateral earth pressure diagram is proposed for use with diaphragm walls with similar construction methods. Recommendations for further research are also presented.

2. GENERAL MORPHOLOGIC FEATURES OF EGYPT

2.1 Introduction

The country of Egypt lies in the northeastern corner of the African continent. Its shape may be roughly represented by a quadrangle, bounded by Latitudes 22°N and 32°N and Longitudes 25°E and 36°E. With an area of 1 019 600 km², Egypt occupies approximately 3% of the total area of Africa.

Deserts comprise more than 96% of Egypt. The Western and Eastern desert cover 67 and 21% of the total area, respectively. The Sinai occupies approximately 6%. The average rainfall over Egypt is 1 cm/year and along the Mediterranean is approximately 20 cm/year decreasing rapidly inland. A map of Egypt including general morphologic features is illustrated in Figure 2.1.

The Western Desert is characterized by large rocky surfaces. The central limestone plateau slopes northwards, yet its elevation increases sharply to the northeast and the plateau merges into the AL-Qatarani Mountains, which overlook the Faiyum Depression. The plateau is poor in surface water resources which are limited to wells and small reservoirs along the northern coast. The Qattara Depression of the Western Desert is considered to be part of a huge depression in the northern sector. Lateral sand dunes cover approximately 40% of the Western Desert. In appearance, they are similar to a chain of crescentic "barchan" dunes, each approximately 60 km in length, and a few tens of meters in

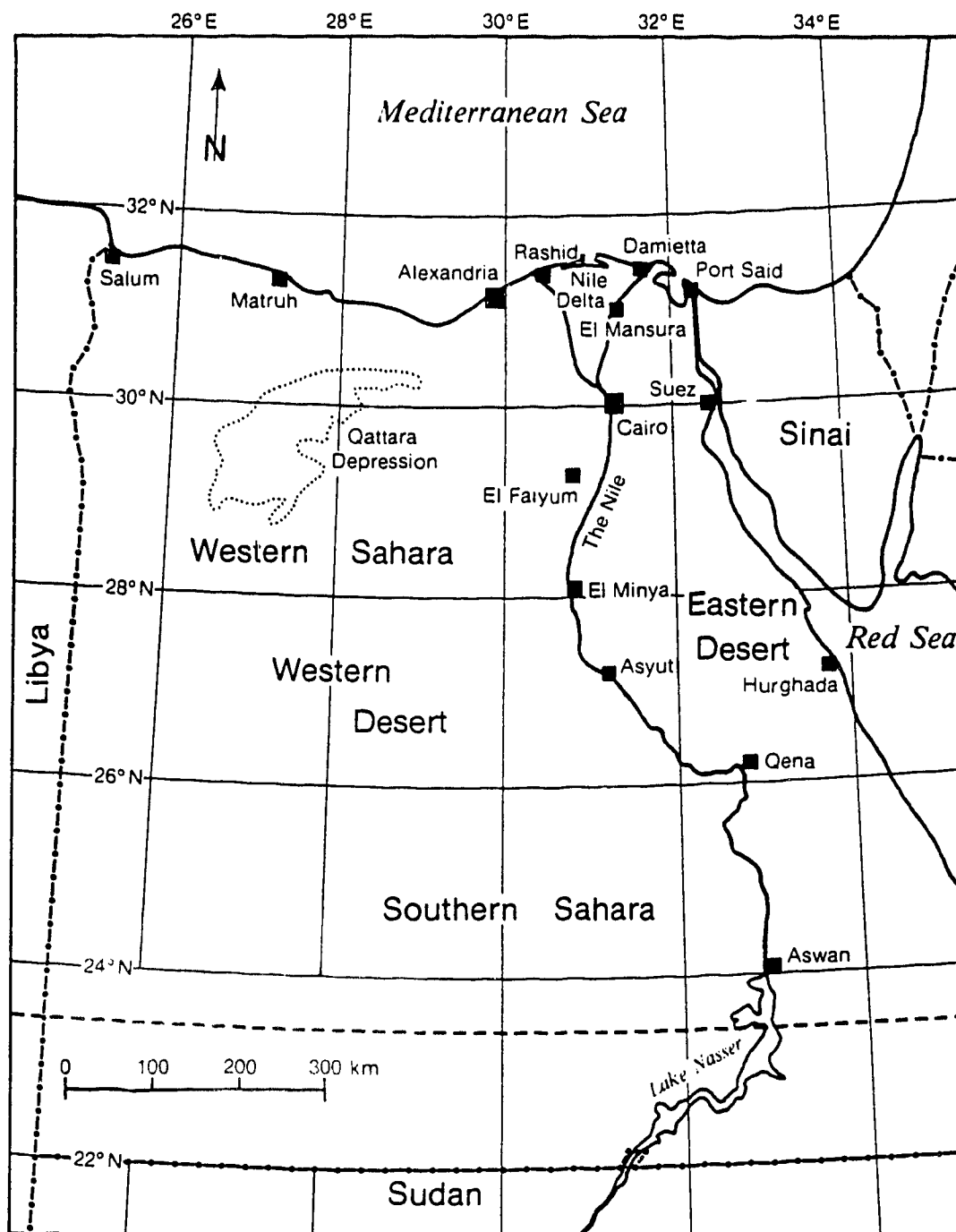


Figure 2.1 Map of Egypt

width. They are constantly in movement due to the aelian effect. This type of landscape is particularly common South of the Qattara depression.

The Eastern Desert consists mainly of the Red Sea Mountain chain, an igneous formation, which runs parallel to the Red Sea. It is separated from the water by a narrow coastal plain.

The southern portion of the Sinai desert is formed by a complex of igneous and metamorphic rocks. The northern two-thirds is dominated by a limestone plateau. The Gabal Katrina, the point of highest elevation in Egypt (2642 m above sea level) is found in the Sinai.

The most predominant feature of Egypt is the River Nile. It enters the country at the Egyptian-Sudanese border and drains into the Mediterranean Sea in the North. For 300 km to the South, the river valley is surrounded by sand ridges with igneous rock formations outcropping at two sites.

The river course is approximately $\frac{3}{4}$ of a kilometer in width and has a flood plain with an average width of 10 kilometres. South of Aswan, the valley is flooded by the man-made lake, Nassar. Twenty kilometers north of Cairo, the River Nile opens into a classic fan shaped delta. The delta has two distributaries, the Rosetta and Damietta branches, each with a length of approximately 242 km. Southwest of the Nile Delta lies the Faiyum Depression.

2.2 The Geologic History of the River Nile

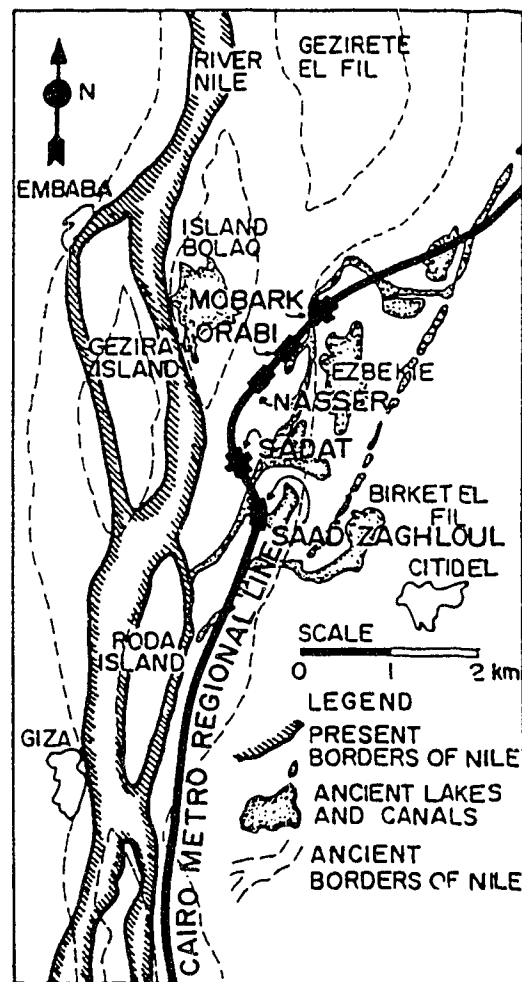
The Nile is one of the best documented rivers in the world (El Makrizi, Willcocks, Hurst, Ball and Awad). Comparatively, it is ranked first in terms of length, fourth by basin area and eighth by drainage volume.

The geologic history of the Nile has been studied by many authors (Ludwig, 1936, Hurst, 1944 and 1966 and Rushdi Said, 1981). Rushdi Said (1981) indicated that the Nile started to incise its course in Egypt in Miocene times and kept deepening its channel through the Eocene and Miocene formations until recent times, when it began to shape its valley. The history of the entire river is beyond the scope of this thesis, therefore emphasis will be given to the Cairo area and the tunnel site location.

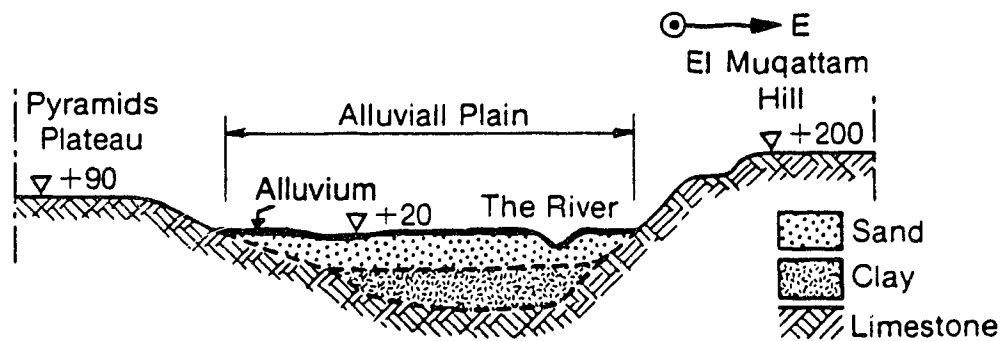
2.2.1 The Geology of Cairo

Cairo is located on the Nile flood plain approximately 20 km south of the apex of the delta. It covers an area of 250 km² and includes the islands of Zamalek and Rowdah in the River Nile. The core of the city is situated on the east bank bounded by the desert hills of the AL Muqattam. Extensive suburbs are found on the West Bank and are bounded by the Pyramids Plateau.

The topography of the city is classified as high and low land as shown in Figure 2.2. The geological formations of the area have been studied by many researchers over the last century; Fourtean, 1897, Cuvilier, 1924, Attia, 1954,



a) Location of ancient lakes, canals and borders of the Nile



b) Section across the Nile valley at centre of Cairo

Figure 2.2 The Geological Formation of the Cairo Area

Said, 1962, Abu AL-Izz, 1971, EL-Ramli, 1985 and El-Sohby and Mazen, 1985, to name but a few.

High land formations that outcrop on the eastern side are Upper Eocene, Middle Eocene, Oligocene, Pliocene and Pleistocene. The fluvial deposits of the low land show that the valley has been filled with deposits ranging from Pliocene to recent river borne deposits. These sediments are classified by their mode of formation into alluvial and diluvial deposits. In Cairo, the observed depth of alluvium is generally 20 m, but in some areas it reaches 60 m. This layer overlies the sands and gravels of the Oligocene Formation. Generally, recent Nile river deposits are silts, clays and fine sands.

Figure 2.2a illustrates that the Nile has significantly changed its course through the Cairo area (Shenouda, 1973). In the 19th century, some of the abandoned branch channels and lakes were filled by man. As a result, a surficial layer of a heterogeneous mixture of silt, clay, sand, bricks, pottery and blocks of limestone is commonly encountered at these locations.

The Regional Line of the Cairo Metro as shown in Figure 1.2, passes through portions of the old river course. The sand deposits alternate in an intricate manner with layers or pockets of silt and/or clay.

3. CONSTRUCTION PROCEDURE

3.1 Choice of Construction Method

The underground portion of the Cairo Metro project passes through areas which are heavily developed and contain many structures of historical interest. Changes in the ground water level, due to construction of the tunnel, could result in excessively large displacements. These in turn could cause major damage to the adjacent structures. Therefore, the primary objective in the selection of a construction method for the tunnel was to maximize ground control.

For the Regional line, the cut and cover method was thought to be the most viable solution. Details of the procedure will be given in the following sections.

Under the classification of the cut and cover procedure, various methods of construction are possible. These are listed below :

1. H-Pile walls,
2. Tangent pile walls,
3. Slurry trench walls (diaphragm walls),
4. Shotcrete walls,
5. Bracing systems, and
6. Anchoring systems

The most effective solution for the Regional line consisted of using a number of these methods.

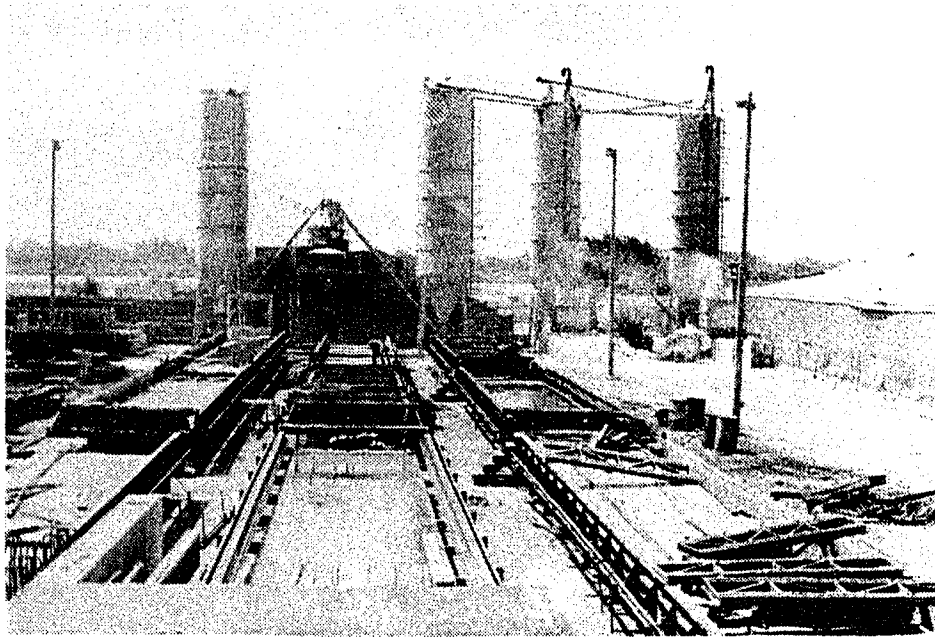
3.2 The Cut and Cover Method

The cut and cover method is widely used in subway construction. In this study, two of the major design considerations were the rerouting of the underground utilities and the diversion of the surface traffic. The resolution of these problems contributed greatly to the total cost of the project.

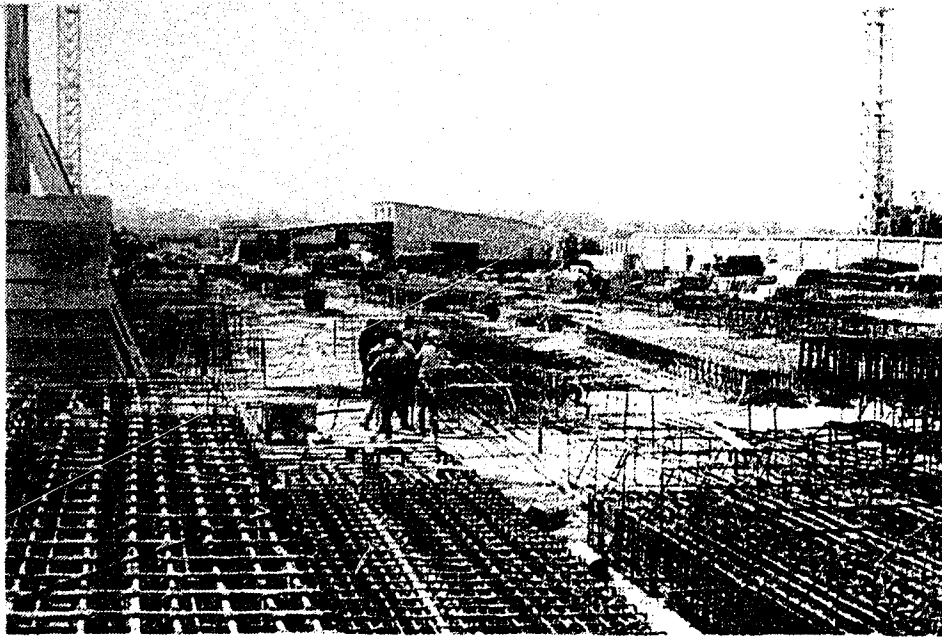
As mentioned previously, the most important aspect of the construction procedure was the control of the ground water. The basic design premise was to create a working area, effectively a box, sealed on the sides and bottom. Diaphragm walls formed an integral part of the structure and served as the longitudinal sides of the box. A grouted plug far below the maximum excavation depth acted as the bottom of the box. Cut-off walls, spaced at approximately 100 m, provided the cross-sides. The sides and bottom of the "box" were assumed to be impermeable. In this manner, the construction of the tunnel had minimal influence on adjacent structures.

For the Regional Line, the running tunnel consisted primarily of pre-fabricated walls. (Plate 3.1a shows the prefabrication factory). Depending on the location, the roof slabs were either prefabricated or cast in situ. The floor slabs were always cast in situ.

For the station, the reinforcing skeleton was assembled in the factory (Plate 3.1b) and transported to the site. The walls were cast in situ.



a) The pre-cast panel cast yard



b) Assembly yard for steel skeletons
of cast in situ station panels

3.3 Construction Procedure for the Running Tunnel

Generally, the running tunnel was constructed using pre-cast structural elements for the diaphragm walls, slabs and beams. Figures 3.1 and 3.2 illustrate in detail the general construction procedure. It is described in stages corresponding to the field method.

The first step was the construction of the guide walls. These L-shaped sections of cast in situ concrete served to guide the excavation of the slurry trenches. The excavation of the 500 mm wide slurry trench wall followed.

The design depth of the excavation varied according to the section and topography of the site, but was usually about 20 meters. Figure 3.3a shows the guide walls and pre cast panels stored on site. In Figure 3.3b details of the excavation for the slurry trench walls are shown. Following in Figure 3.4, the precast panel is detailed.

The connection between the walls consisted of a rubber strip the same length as the panel. Immediately after excavation of the trench, the panel for the particular section was lowered into the trench and kept in position by joining its steel carrying bars to the guide walls. Once the self hardening slurry had set, the panel was at its desired elevation. This sealing system is shown in Plate 3.2.

A special curing process was used at the factory to ensure that the concrete panels were watertight. As well, a sealant coat was applied to the outer surface as the panels were lowered into the trench.

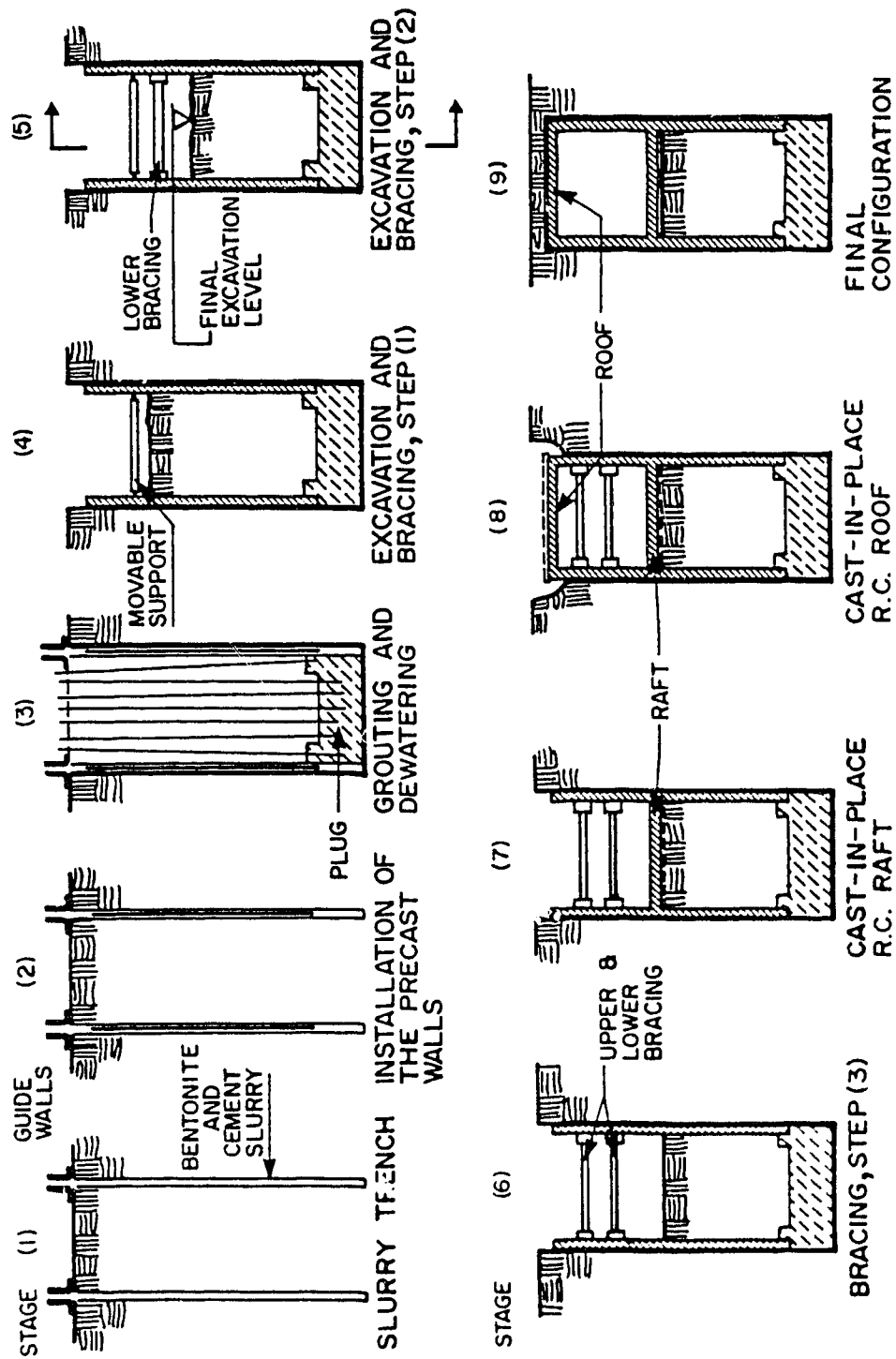


Figure 3.1 Construction Procedure Steps for the Run and Post Section

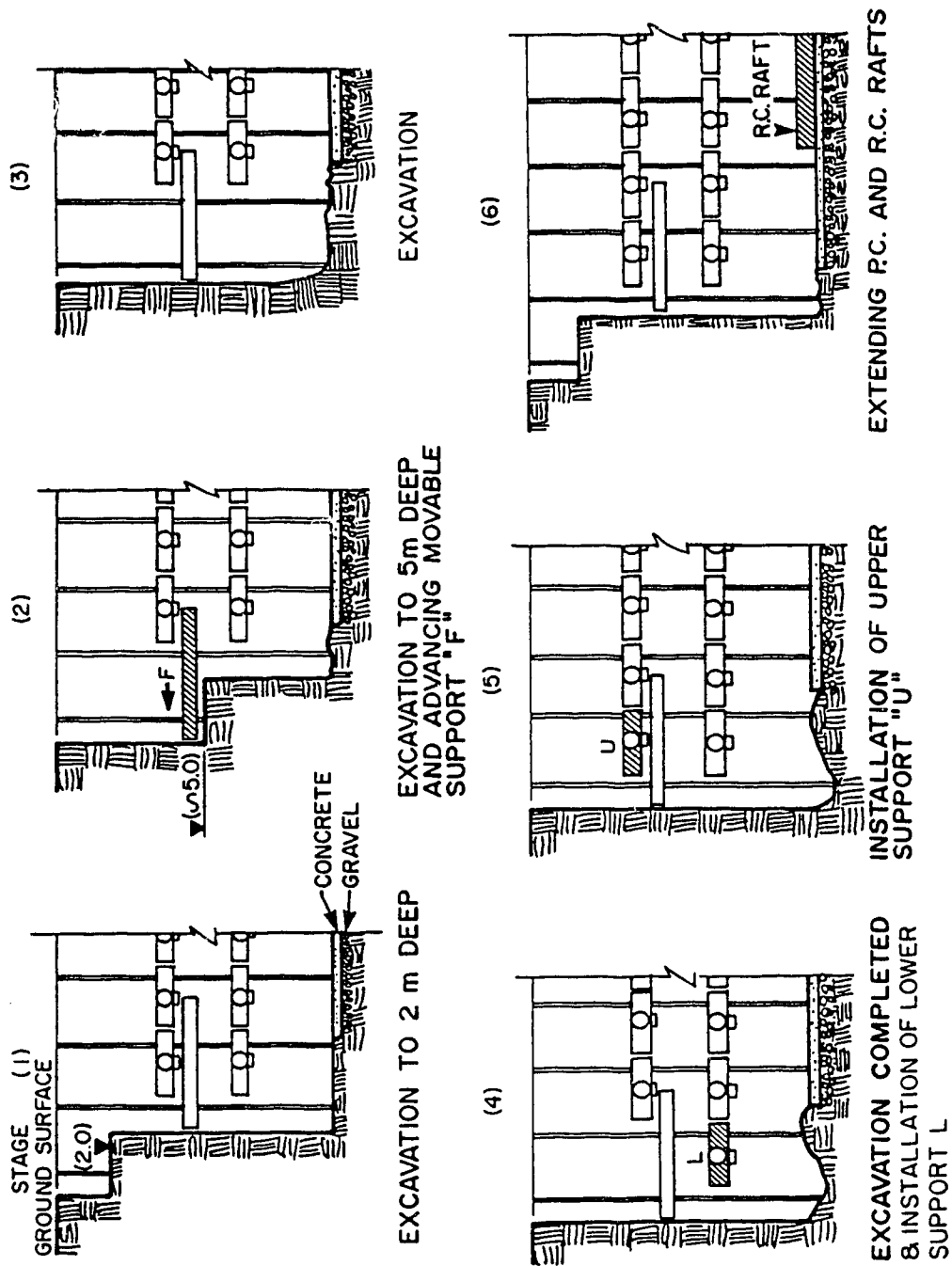
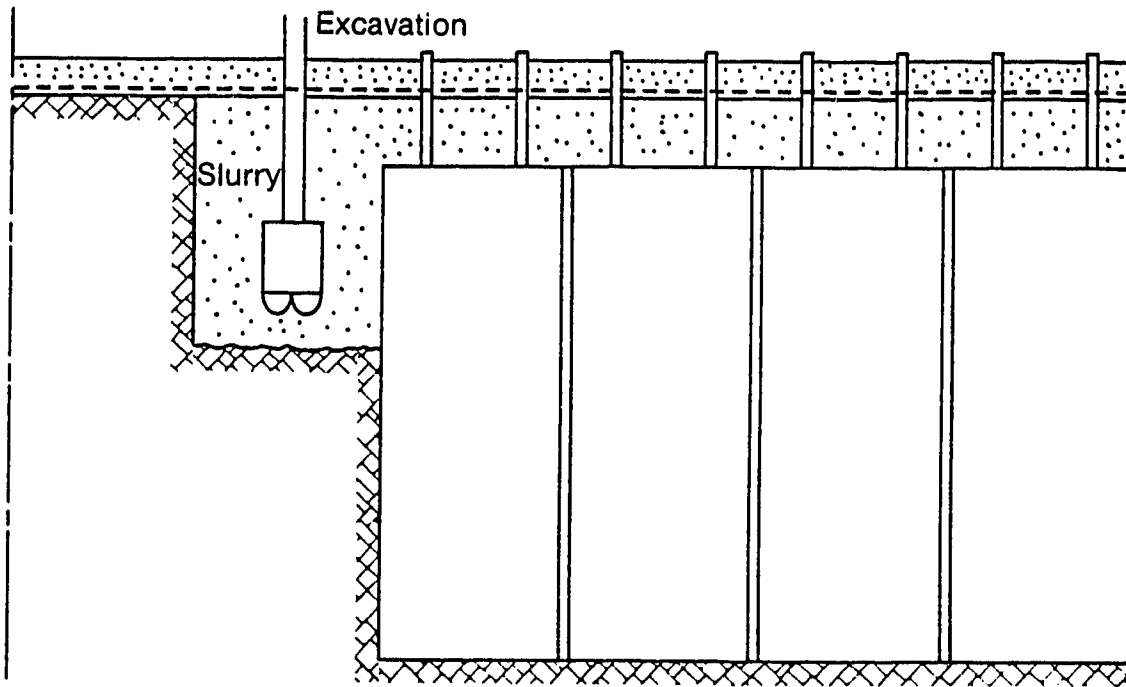
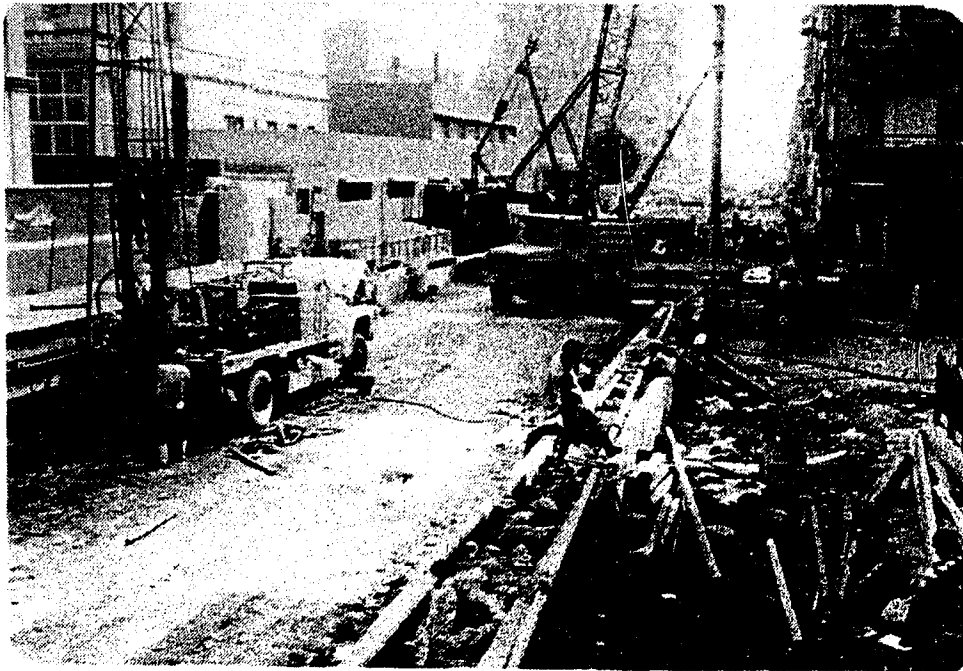


Figure 3.2 Longitudinal View of the Excavation Procedure Steps for the Running Tunnel Test

Section



(a) Details of pre-cast panel installation



(b) Guide walls, excavation

Figure 3.3 Details of Excavation and Installation of the Diaphragm Walls for the Running Tunnel Test Section

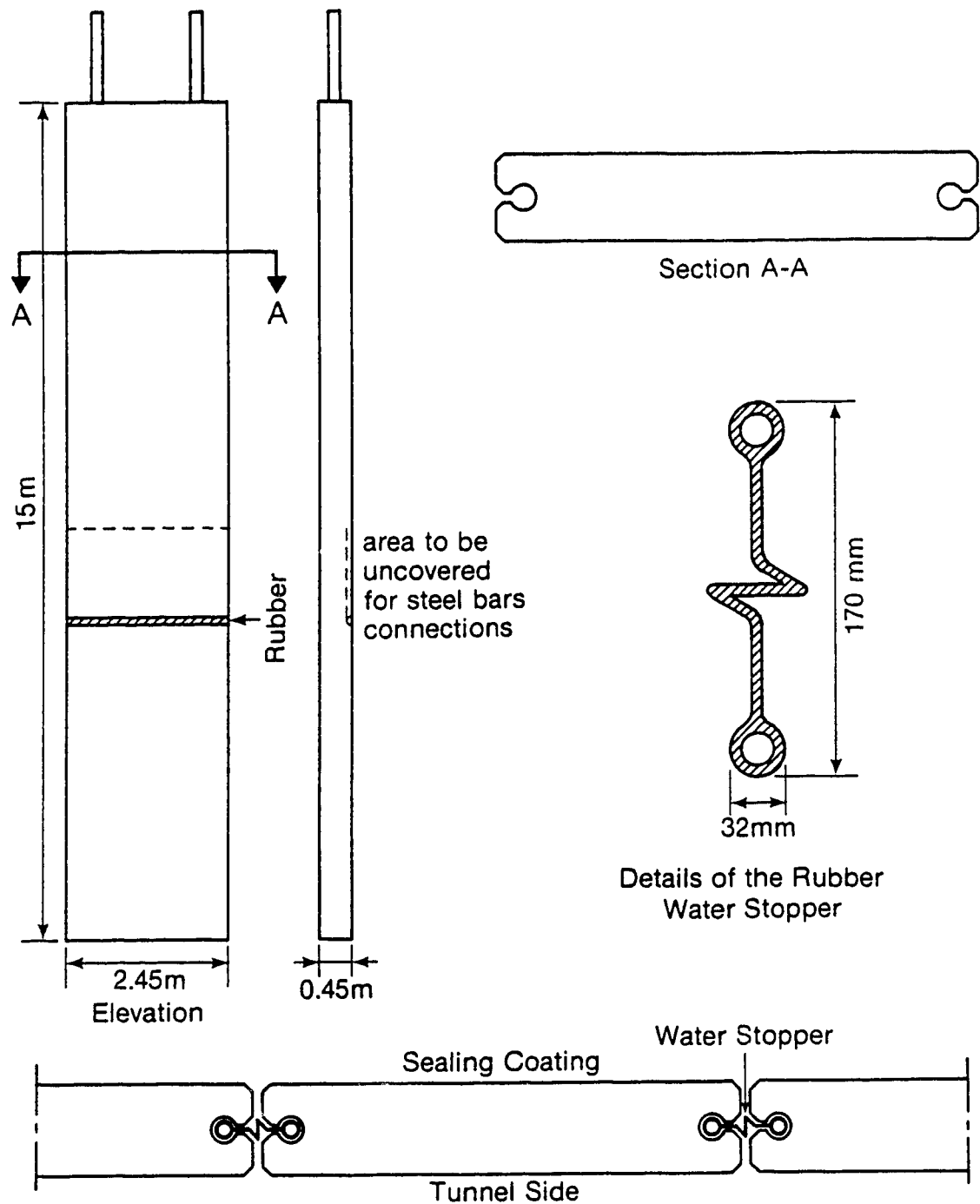


Figure 3.4 Details of the Pre-Cast Diaphragm Wall Used for the Running Tunnel Test Section

To activate the seal between the rubber strips and the panel, the bentonite cement slurry mixture was pumped to fill the pipes at both sides of the rubber water stopper installed between adjacent panels and was allowed to set. As the grout expanded, it created a firm contact between the concrete and the rubber, which prevented water seepage. In the following stage, the grouting of the plug and the cut-off walls was completed. A period of 2 months was allowed for the complete set of the grout.

The grouted zone or plug was constructed during a two month period. It was located at a depth of 20 m and its thickness varied from 3 m in the center to 4 m at the walls (Figure 3.1). The details of the grouting operation will be discussed later in this chapter.

Pumping tests were conducted during the dewatering procedure to determine the permeability inside the excavation and above the plug level. By passing these tests, the site was considered suitable for excavation.

Excavation was performed in stages with a mobile support used to control wall movement until the installation of the two rows of struts. The mobile support was provided by a steel frame 8 m long, 4.5 m wide and 0.40 m high consisting of broad flanges standard I beams. The excavation started by removing a strip about 2.0m deep and 3.0m wide. This provided a safe distance for the excavation machine to work. The mobile frame was hung by chains to the walls and was advanced about 3.0m by the excavation machine. Plate 3.2

shows the mobile frame moving operation. Activation of the frame was accomplished by the insertion of high quality redwood wedges. Sand bags underlying the wedges provided a dismounting tool. These consisted of a rubber hose, 150 mm in diameter, filled with sand, and sealed at both ends. The excavation by machine was continued through the mobile frame.

The lower strut was installed first, by lowering it through the frame. It rested on pre-mounted brackets and was activated using the wood wedges and sand pillows. Three points of contact were made, each with a width of 300 mm, length of 800 mm length and height of 150 mm. The upper strut was installed in the same manner at its design elevation.

The final stage of excavation was performed manually and consisted of levelling the base area. Then, a layer of gravel was spread on the base of the excavation and covered with a plastic sheet. On top of this, plain concrete was poured to a thickness of 200 mm. The concrete formed the base for the primary impervious layer. This operation was performed at approximately 10 m intervals.

The impervious zone consisted of two layers of rubber and a coat of cement mortar. This mortar protected the main layer from damage during installation of the reinforced concrete. The main layer was connected to rubber strips which had been previously installed on the precast panels. Plate 3.3 shows some aspects of the operation to make the

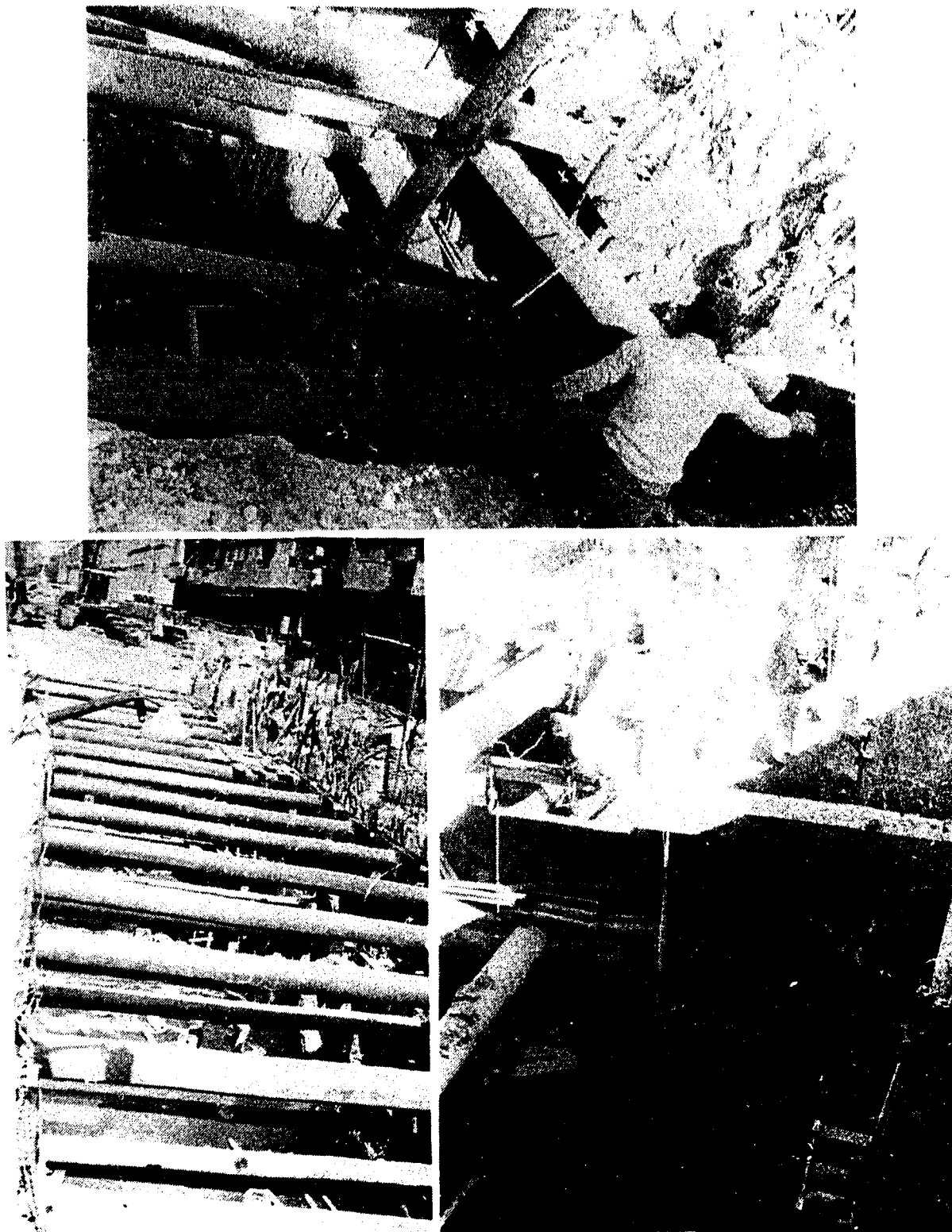


Plate 3.2 The Mobile Frame Mobilization Operation

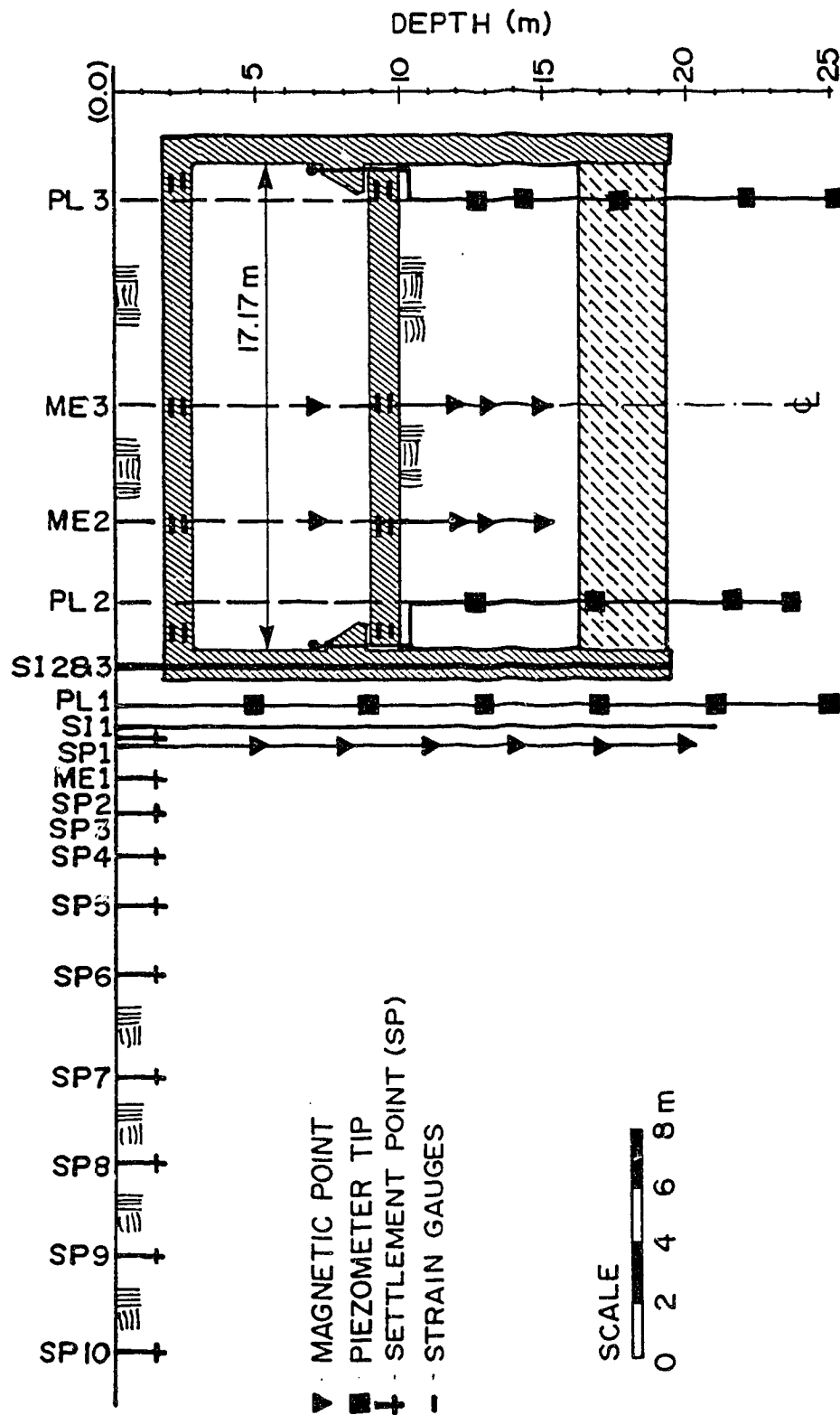


Figure 4.10 Cross-Section at Orabi Station Test Section

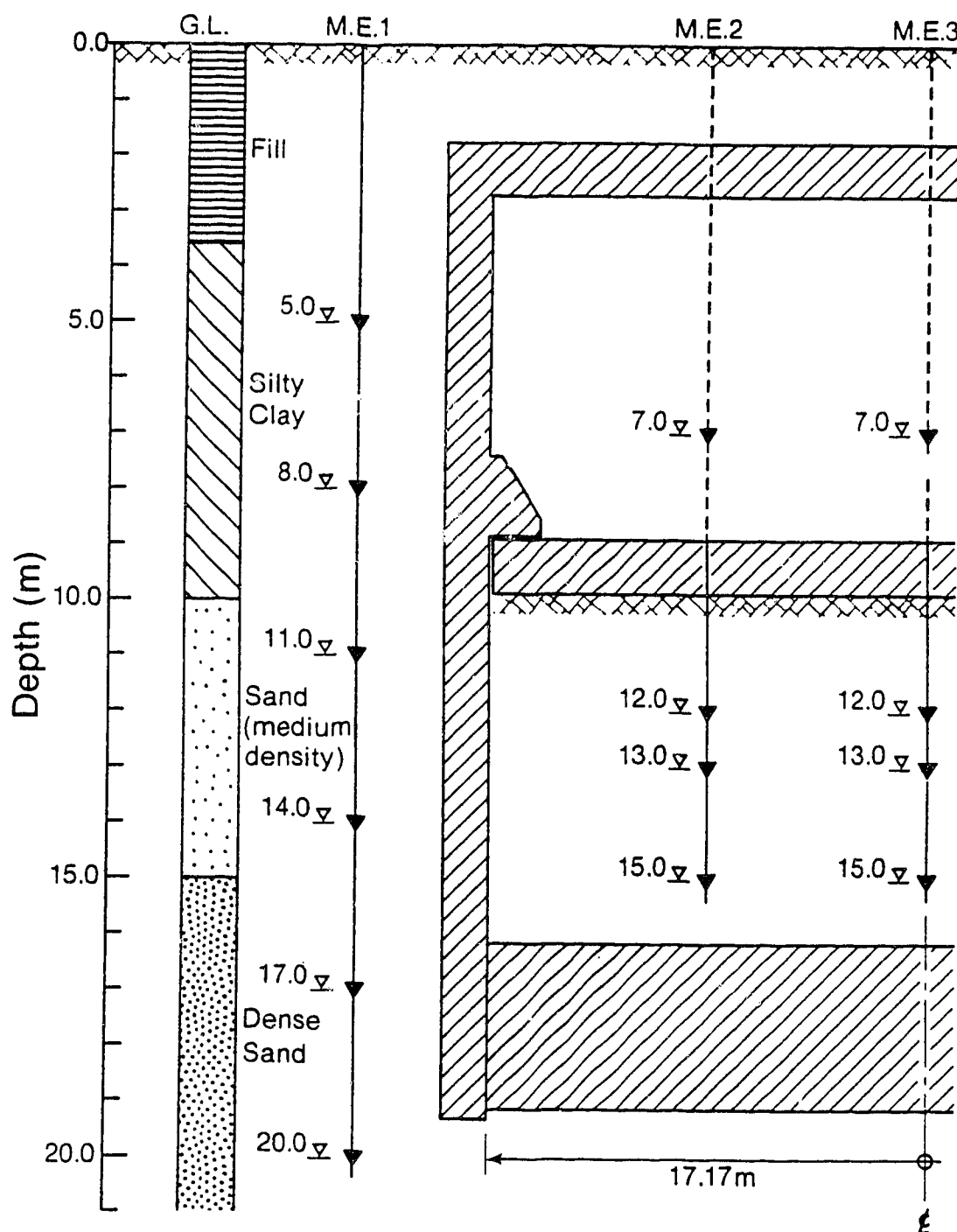


Figure 4.11 Details of the Multipoint Extensometers at the Orabi Station Test Section

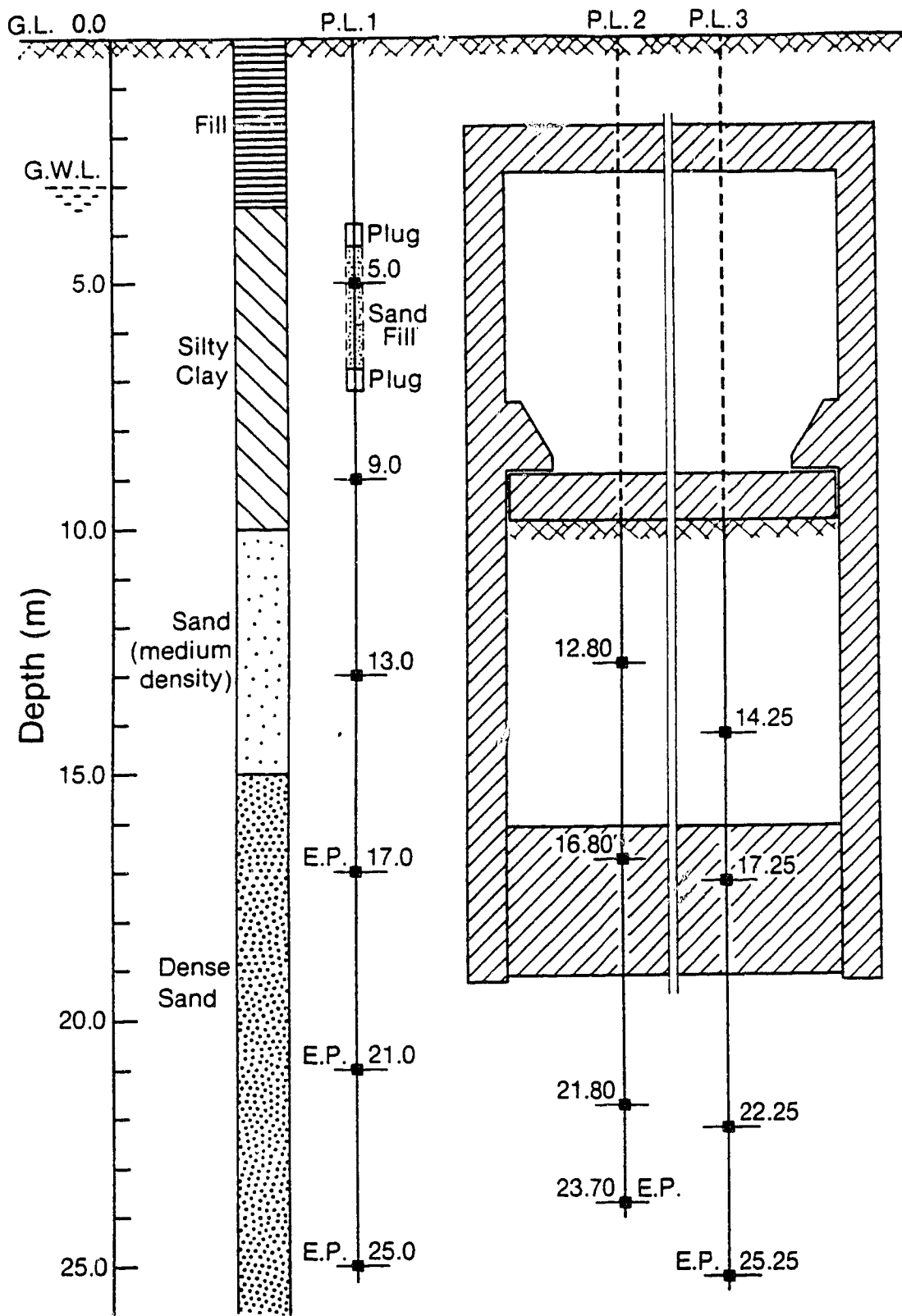


Figure 4.12 The Piezometer Lines Details at the Orabi Station Test Section

The distribution of the 16 embedded strain gauges in the roof and floor slabs is shown in Figure 4.10. A single row of temporary support (struts) was used in the under cover section of this station. Two adjacent struts were instrumented with 12 weldable strain gauges; the placement was the same as at the running tunnel section.

4.4 Details of the Instrumentation

4.4.1 The Settlement Point (SP)

A settlement point is commonly used to measure the vertical displacement of a particular point in a soil mass near the ground surface or at depth. These points are primarily used near surface due to the availability of more economic instruments to measure deformation at depth. A range of designs are given by Bozozuk (1968), Burland and Moore (1973), Marsland (1973), Hansmire (1975), Cording et.al., (1975) and Barratt and Tyler (1976).

Figure 4.13 shows the details of the settlement point employed. It was manufactured locally in Egypt using the available materials and machine shops. Briefly, it consisted of a 1.5 m galvanized steel pipe, 13 mm in diameter, with an drive point mounted at the tip. A 100 mm diameter steel plate was welded 150 mm from the bottom. A grooved steel cap was welded to the top.

A 38 mm diameter PVC pipe acted as a sleeve around the galvanized pipe, and rested on the bottom steel plate. A

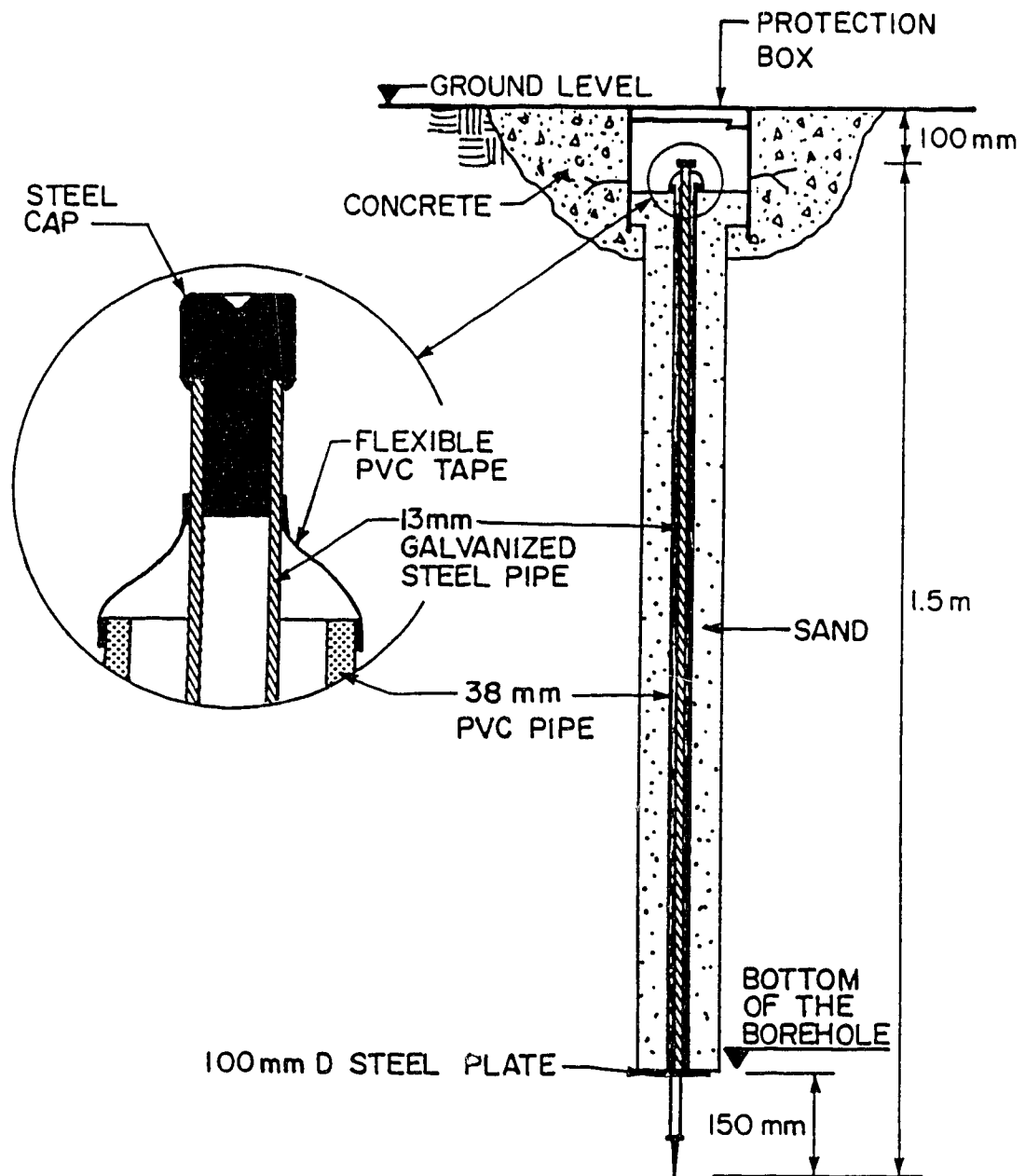


Figure 4.13 Details of the Settlement Point

flexible PVC cap sealed the top to prevent backfill material from entering the sleeve. This sleeve eliminated friction between the steel pipe and the surrounding soil. A specially designed box was used to protect the top of the instrument and was fixed using a large block of plain concrete.

For the settlement point, a 150 mm diameter, 1.35 m deep hole was drilled. The instrument was hammered into position, and the hole backfilled with clean sand. Finally, the protection box was mounted.

The readout procedure was carried out by initially surveying the elevation of each settlement point with respect to the benchmarks. This constituted the zero reading. For each additional reading, a new elevation for each settlement point was calculated and the surface settlement could then be determined. To ensure the highest level of surveying accuracy, a number of techniques were used, i.e., keeping the same survey team, using high quality equipment, etc. Surveying was performed with a N-2 Carlizzes level and a specially designed survey rod. On the back side of the rod was a levelling bubble which insured that the rod was maintained vertical during surveying. One mm graduations were marked on the rod, which allowed reading to the nearest 0.5 mm. Figure 4.14 provides the details of the surveying rod. The accuracy and repeatability of the reading were taken to be within ± 0.5 mm.

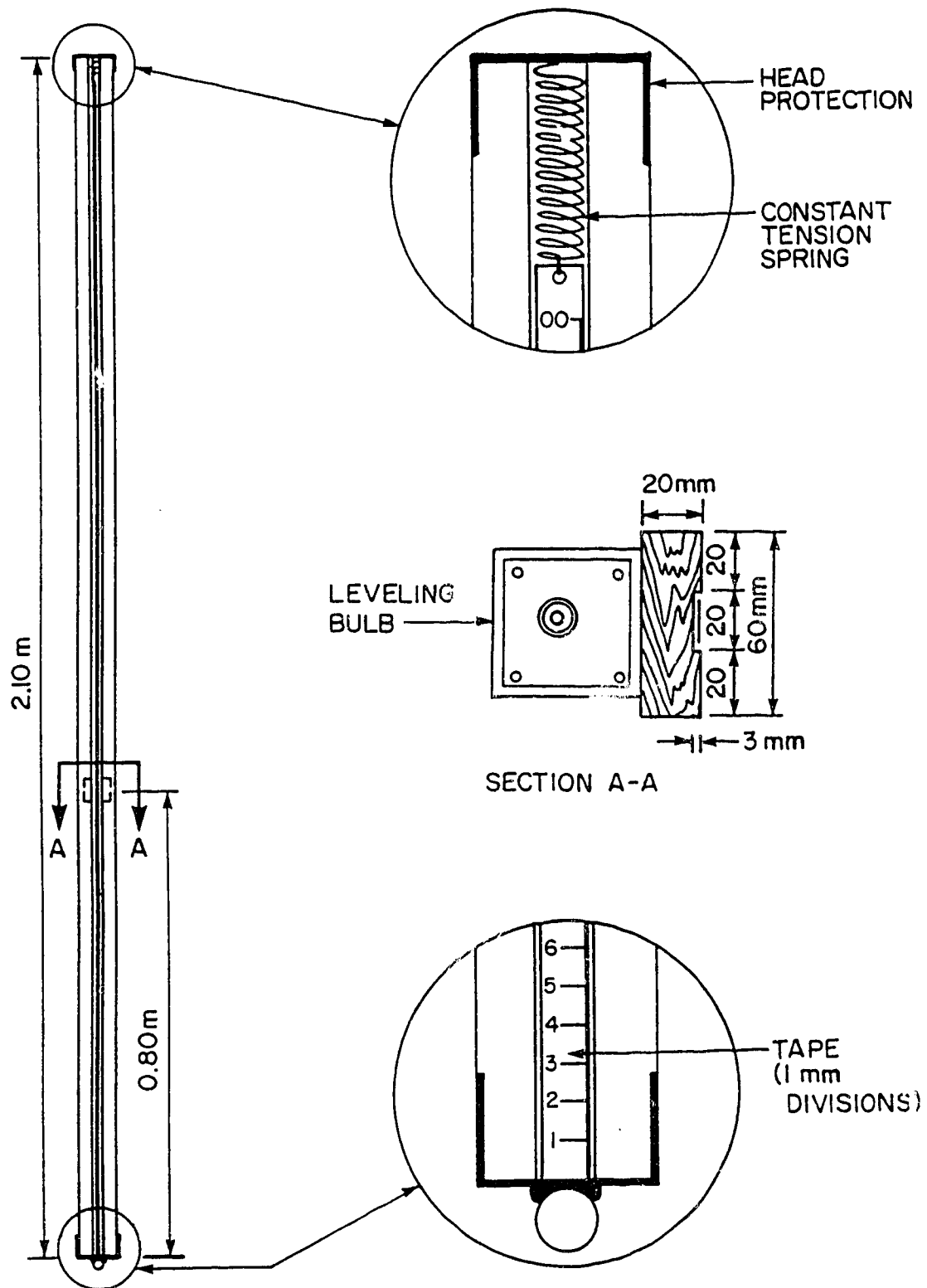


Figure 4.14 Details of the Surveying Rod

4.4.2 The Multipoint Extensometer (ME)

The multipoint extensometer installation was used to provide the vertical deformation distribution with depth. The magnetic multipoint extensometer was designed and developed by the Building Research Establishment, U.K. (Burland, et.al., 1972; Burland and Moore, 1973; Marsland and Quarterman, 1974; and Smith and Burland, 1976). Subsequent work at the University of Alberta has yielded an improved design (Medeiros, 1979).

Details of the magnetic extensometer are shown in Figure 4.15. Its basic components consist of a solid magnetic ring fixed to a rigid PVC housing. The ring has dimensions 70 mm outer diameter, 45 mm inner diameter and 10 mm thickness. The housing was approximately 290 mm in length, with a diameter of 80 mm. The magnetic ring was inserted, fixed and sealed against ground water in the bottom cap of the housing. To fix the extensometer in the borehole, 4 springs shaped with a 30° angle, 540 mm long, were attached at 90° spacing to the main body. In this manner, the vertical deformation of the soil is transferred to the extensometer.

The basic principles for the extensometer are given by Burland et.al. (1972). Some modifications were made to improve the performance of the instrument. The magnetic ring was made of a solid magnet rather than numerous magnetic disks. In this manner a stronger magnetic field was produced, making it easier to detect with the readout

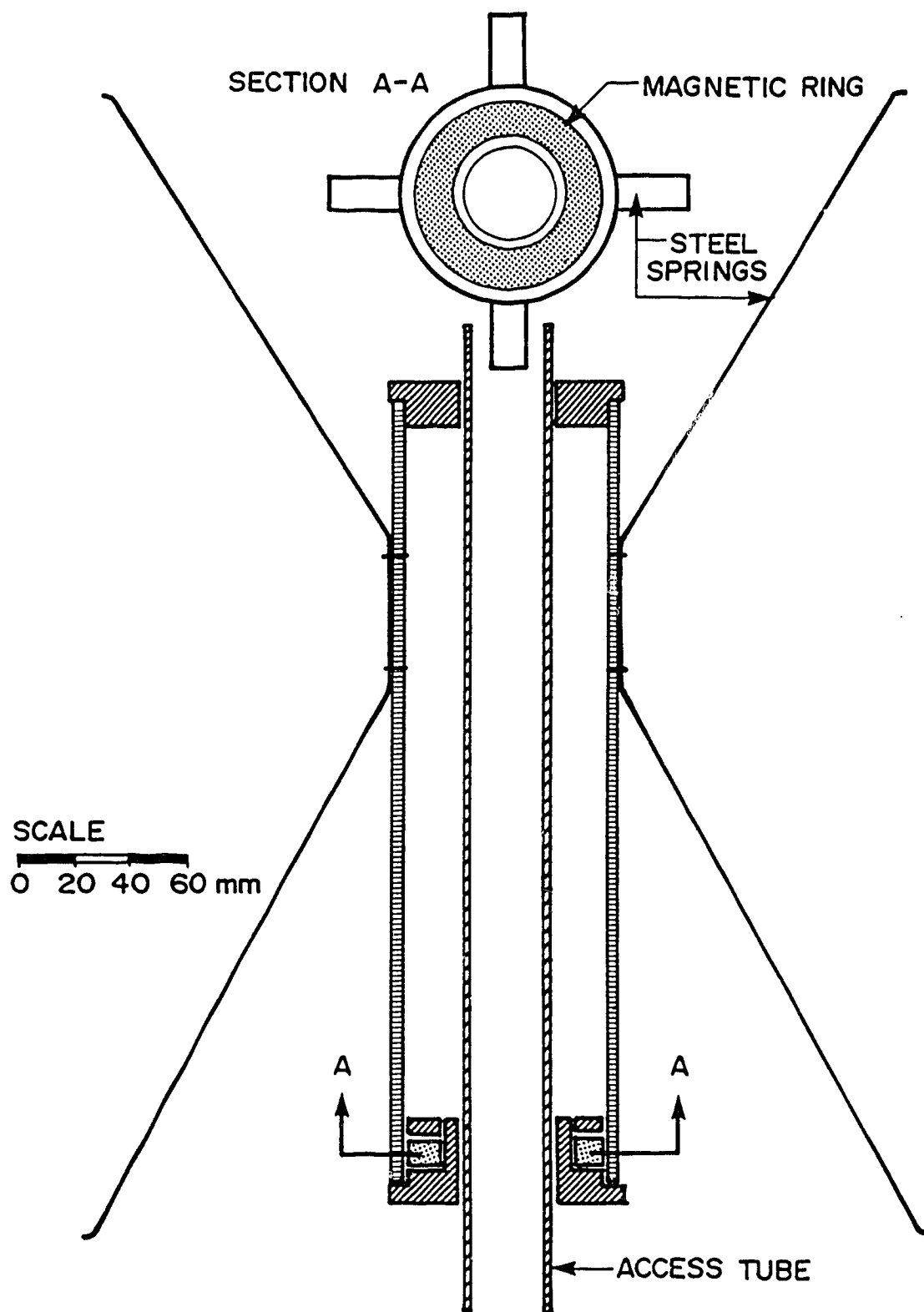


Figure 4.15 Details of the Magnetic Extensometer Point

device. The supporting steel spring design was changed to the shape shown in Figure 4.15. This improved the transfer of the movement from the soil to the magnetic point. As a result, the installation tool (extruder) had to be redesigned. All these improvements were made at the University of Alberta.

Three distinctive magnetic fields are formed as shown in Figure 4.16. The readout unit, supplied by Solinst, consists of a probe attached to a high quality, plastic measuring tape. When the probe is lowered down the access pipe and passes through the magnetic field, two wire ends connect completing an electrical connection. This connection activates a signal, which emits a buzzing sound. The corresponding depth is read from the measuring tape.

El-Nahhas (1980) reported a reproducibility to within 1 mm.

4.4.2.1 The Installation Procedure

For installation of the multipoint extensometer, a hole 150 mm in diameter was drilled using bentonite mud and supported with 150 mm casing. Once the desired elevation was reached, the access pipe was installed. The access pipe was equipped with threaded connections which were also glued to prevent disassembly during installation. The bottom of the pipe was capped, so that the pipe could be filled with water. This aided in overcoming the uplift forces.

It was usually found that the bottom portion of the hole would cave in after a few minutes. This was due to the

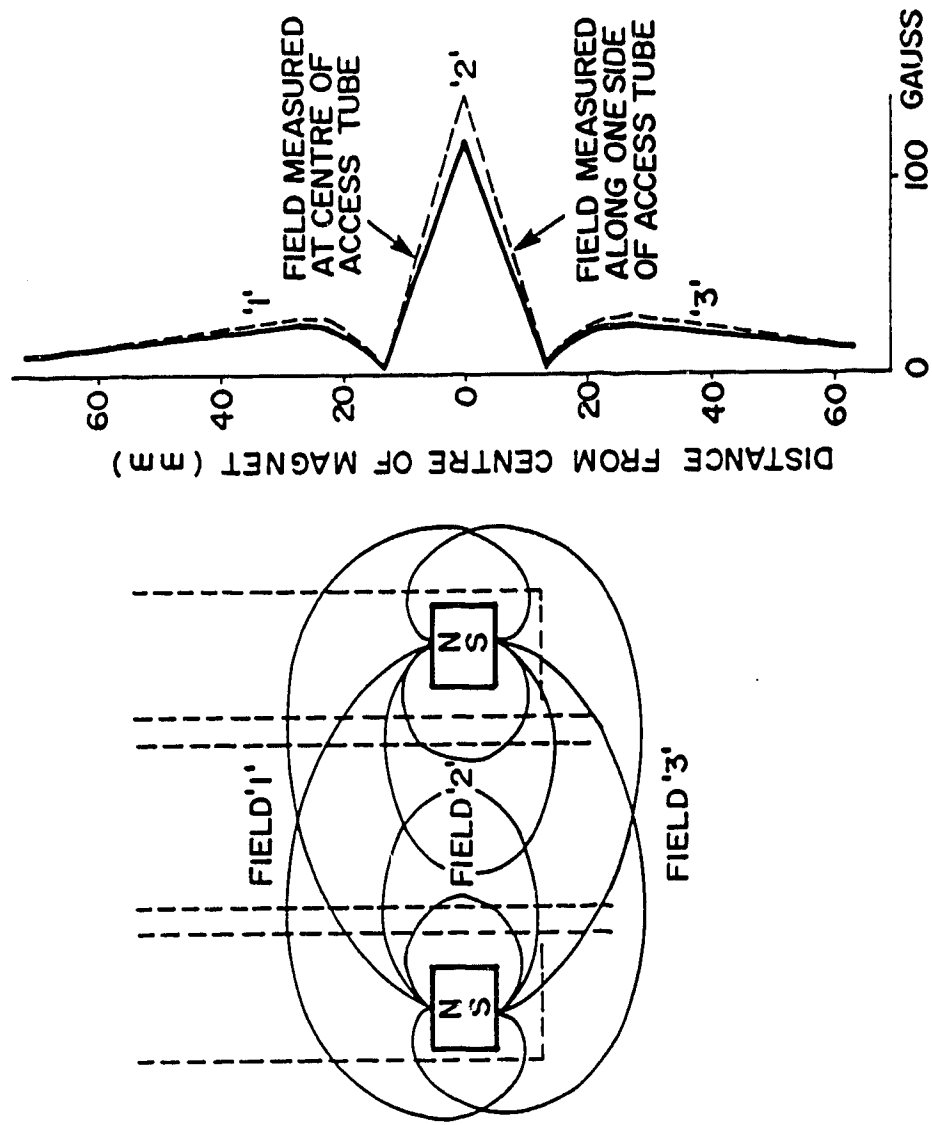


Figure 4.16 The Magnetic Fields Around the Magnetic Point

sand layer and groundwater present at depth, but did not cause any problems; in fact it helped secure the access pipe.

An extensometer was then mounted inside a specially designed extruder as shown in Figure 4.17. The extruder consists of a section 105 mm in diameter and 535 mm in length. At the top end, an annulus with inner diameter slightly greater than the access pipe was fixed and served as a guide. The extruder was attached to the drill rig by a guide wire. At the desired elevation, the extensometer was extruded through reaction of a rod between the drill rig and extensometer. This procedure was repeated until the required number of extensometers were in the borehole. In the clay layer, a bentonitic grout was used.

After installation was completed, initial readings were made to determine the zero positions of each extensometer.

4.4.2.2 Monitoring Procedure

The extensometer probe described in the preceding section, was lowered to the bottom of the hole. The depths of each of the three magnetic fields for each extensometer were recorded to the nearest 0.5 mm. The second reading should be the average of the first and third readings. This was immediately checked to prevent reader error. All data was processed manually.

Survey readings were taken to the top of the access tube and referenced to the benchmarks. This allowed corrections to be made for any movement of the access pipe.

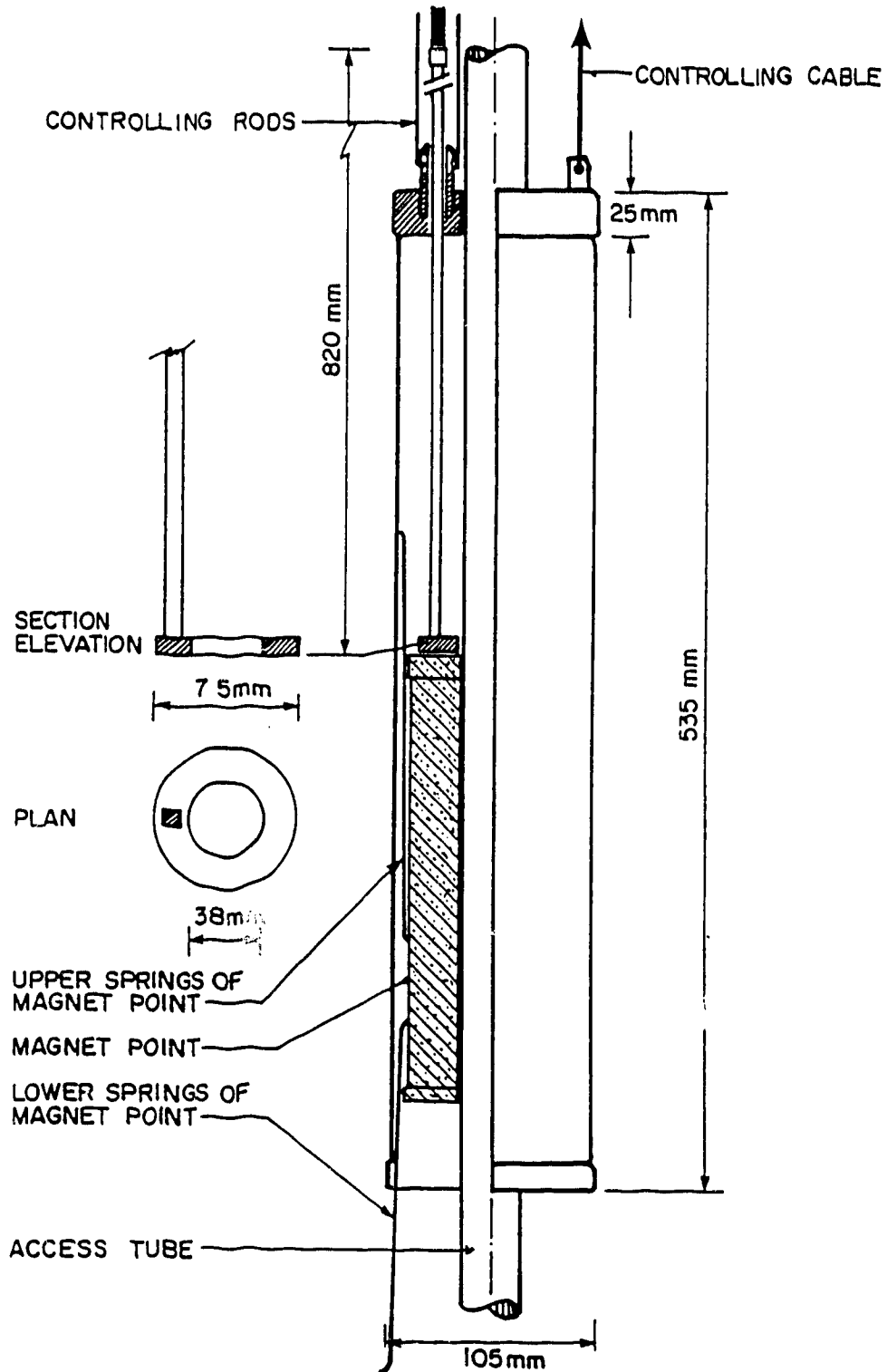


Figure 4.17 The Extruder used for the Installation of the
Magnetic Points

To ensure that operator sensitivity was not a factor, the same 2 man crew was used throughout the monitoring.

4.4.3 The Slope Indicator (SI)

The slope indicator is widely used to measure the horizontal displacement profile in a soil mass. The system consists of 3 primary components; the casing, sensor and readout unit.

The ABS plastic casing was supplied by the SINCO slope indicator company. The inner diameter was 59 mm with 11 mm thickness. Four longitudinal grooves were machined at equal spacing.

The sensor, model 50325 M, contains servo-accelerometers mounted with sensitive axes spaced 90° apart. It is equipped with 4 spring loaded wheels which are compatible with the internal dimensions of the casing. It is suspended by an electrical cable. The probe provides an electrical signal proportional to the angle of inclination from the vertical axis.

The principle of the slope indicator as described by Dunnicliff (1971), Hanna (1973) and SINCO is schematically illustrated in Figure 4.18. Briefly, the servo-accelerometer transforms the tilt into an electrical signal which is transmitted through the electrical cable to the readout unit. The profile is determined in 2 vertical planes, perpendicular to each other, and are usually referred to as the A and B directions. The A direction was chosen to

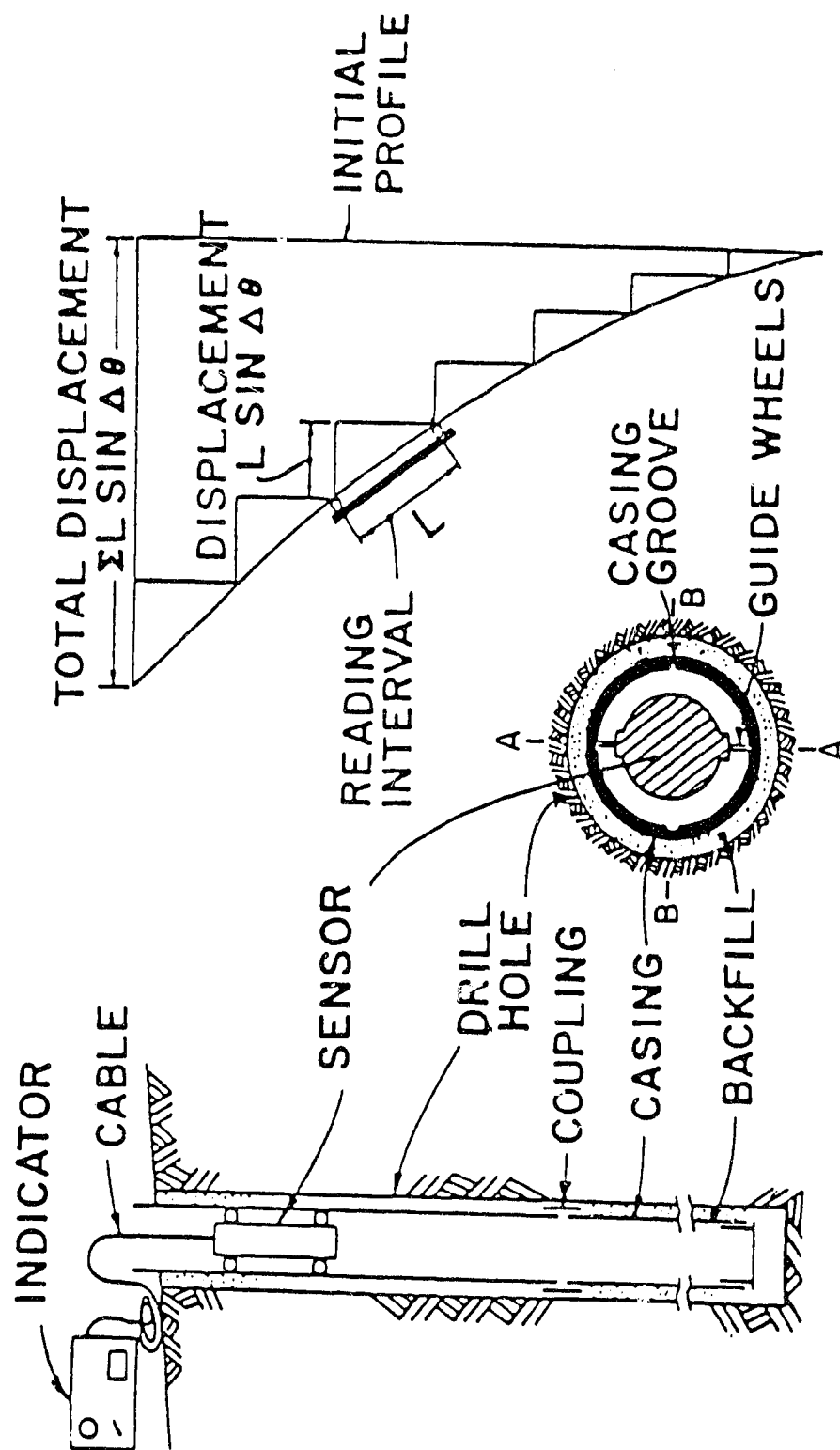


Figure 4.18 The Slope Indicator Principle

represent the direction of principal displacement, i.e. perpendicular to the tunnel centre line.

The portable readout unit, Model 50309, with digital LED display, has a 6 V rechargable battery. It was also supplied by SINCO.

Green (1973), Savigny (1980), El-Nahhas (1980) and Dunnicliff (1988) found that repeatability and accuracy of this instrument was 10 times better than manufacturers specifications.

4.4.3.1 Installation Procedure

A 75 mm diameter hole was drilled to the required depth using a bentonite slurry and casing. The slope indicator casing, capped at the bottom end, was inserted in the hole and filled with water to counteract the uplift forces. A flexible tube was taped to the first joint. Through this, the grout was pumped to replace the mud.

Each joint of the plastic casing was cemented with PVC glue and riveted in place. The orientation was adjusted and the grouting operation began. The grout used was the same as for the slurry trench (self hardening) and was supplied by the contractor.

After grouting, the orientation of the casing was rechecked. The casing was then kept in place by use of a hydraulic jack reacting against the drill rig for a half hour until the grout had set. A box was mounted over the casing at street level for protection of the instrument.

For the precast panels, the pre-fixed PVC pipe was used to install the casing and then the assembly was grouted. For the cast-in-place panels, the casing had been pre-fixed and oriented at the factory. The casing was filled with water to prevent flow of the bentonite slurry into the casing as the steel cage was lowered into the slurry trench.

For the slope indicators in the structural elements, boxes for protection were mounted after the streets were backfilled and paved. Initial readings were taken prior to any excavation.

4.4.3.2 Monitoring Program

The electrical cable was attached to both the sensor and the digital readout, and the power switch activated. The probe was then lowered until the bottom was reached and was allowed to stabilize for 5-10 minutes. Readings were taken at 0.5 m intervals with the probe held at constant elevation by clamping the cable at surface. Both A and B directions are read by simply flipping a switch. The procedure was repeated with the probe rotated 180°.

Again, the data was processed manually and displacement profiles plotted. The slope indicators were read by the same 2 man crew at each stage corresponding to changes in the stress conditions around.

4.4.4 Piezometer Lines

Many types of piezometers are available for monitoring pore pressure in a soil medium. The Pit Slope Manual - Chapter 4 (1977) provides the classification and installation procedures.

For this project, the vibrating wire and pneumatic (mechanical diaphragm) piezometers were used. The cost of the instruments was a major factor in the selection process.

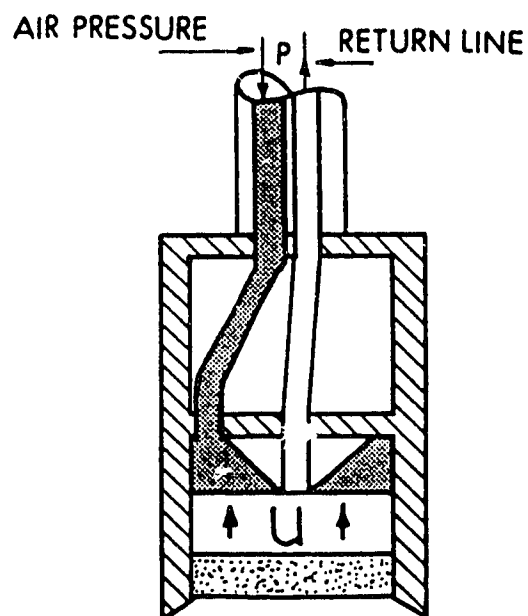
The pneumatic piezometer, which uses compressed air, is very inexpensive compared with the vibrating wire piezometer. Therefore, the number of pneumatic wire piezometers used far outnumbered the electric piezometers.

In the electric piezometer, the change in electrical resistance of a strain transducer mounted on a stiff diaphragm is monitored. The effect of the length of the electrical wire is eliminated. Figure 4.19b presents the details of the electric piezometer. Those used were supplied by IRAD Gauge, Model PWS.PWP (Manual No. 19-2050).

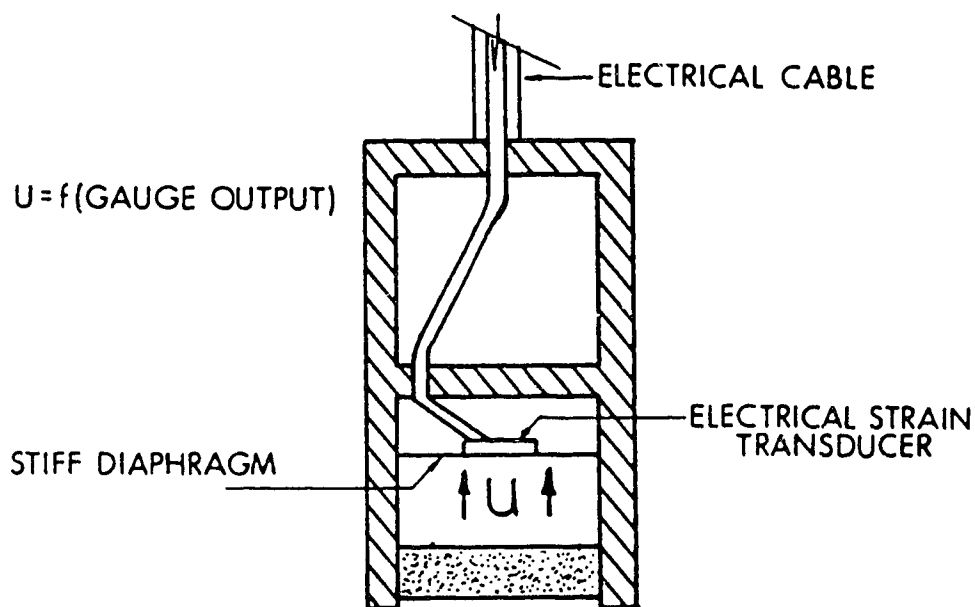
Figure 4.19a presents the basic principle of operation for the pneumatic piezometer. A schematic is shown in Figure 4.20. Basically, compressed air pressure is applied against a sealed, flexible, rubber diaphragm until it equalizes with the hydraulic pressure. A pressure gauge on the compressed air is then read in meters of head.

The pneumatic piezometer and read out device were supplied by Soil Instrumented Ltd. England. (readout Model No. MK III Pneumatic Push Bolton meter).

WATER PRESSURE AGAINST
DIAPHRAGM SEALS OFF OUTLET
P IS INCREASED UNTIL VALVE
OPENS THEN $U = P$



(A) PNEUMATIC PIEZOMETER



(B) ELECTRICAL PIEZOMETER

Figure 4.19 The Basic Principle of the Piezometer

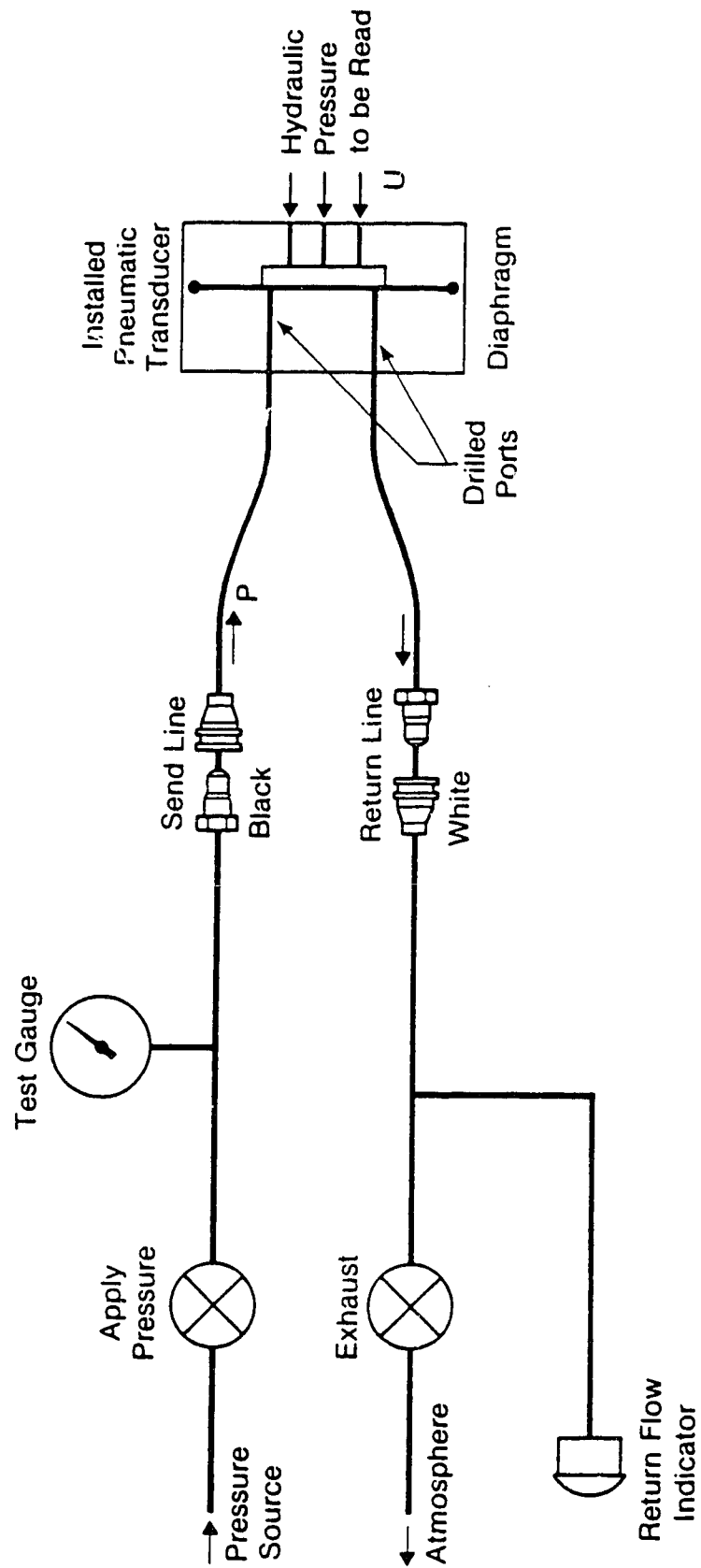


Figure 4.20 The Pneumatic Piezometer Set-Up

4.4.4.1 Installation Procedure

A borehole of 75 mm diameter was drilled using fresh water and was cased to the desired depth. To install a piezometer line consisting of multiple tips, it was found that pre-assembly, including sand filters, was necessary before lowering into the borehole, to avoid jamming problems. This also ensured that each of the tips was at the desired elevation.

The procedure for installation of piezometers in clay layers suggested by Deardorff et.al. (1980) was followed. One meter bentonite plugs were installed between successive tips, and were separated by clean sand as shown in Figures 4.6 and 4.12. Deardorff et.al. (1980) also reported that pneumatic piezometers responded quickly to small changes in water pressure, producing reliable and satisfactory results.

After sealing, backfilling and removal of the casing, the required connections for the pneumatic and electrical piezometers were mounted at the surface. The instrument leads were protected by a box fixed in place with concrete.

4.4.4.2 Monitoring Procedure

For the vibrating wire electrical piezometer, the resistance readings were converted to pore pressure through calibration charts supplied by the manufacturer. Temperature corrections were also made.

The pneumatic piezometers were read 3 times so that an average could be calculated and the readings converted to kPa. Details of the procedure are provided in the

instruction manual supplied by the manufacturing company.

Results show both types of piezometers to be reliable, sensitive to small changes in pore pressure and dependable over the long term.

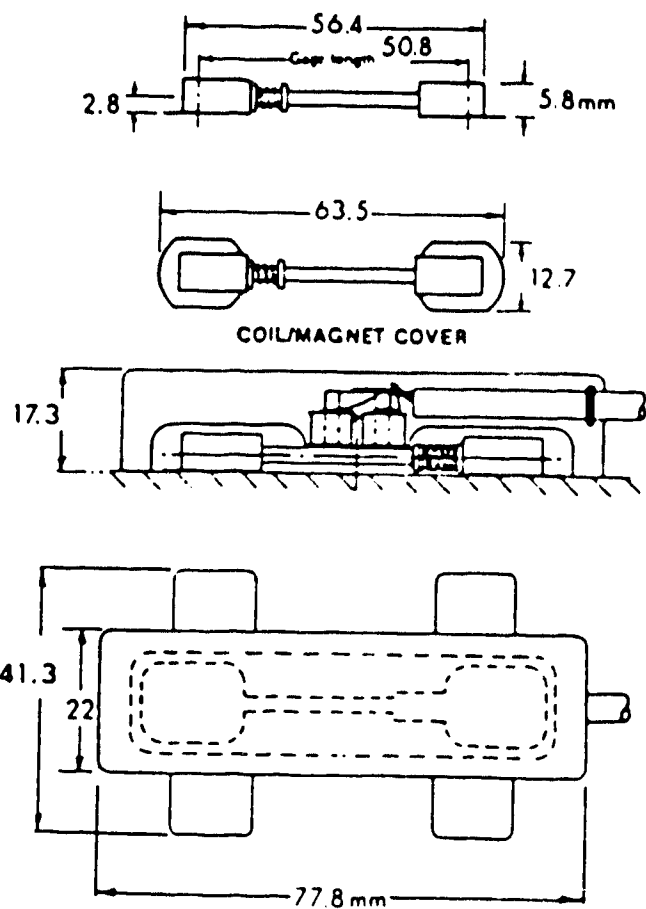
4.4.5 Vibrating Wire Strain Gauges

Vibrating wire strain gauges were selected to measure strains across the structural elements in the temporary support system. These measured strains are used to calculate the normal forces.

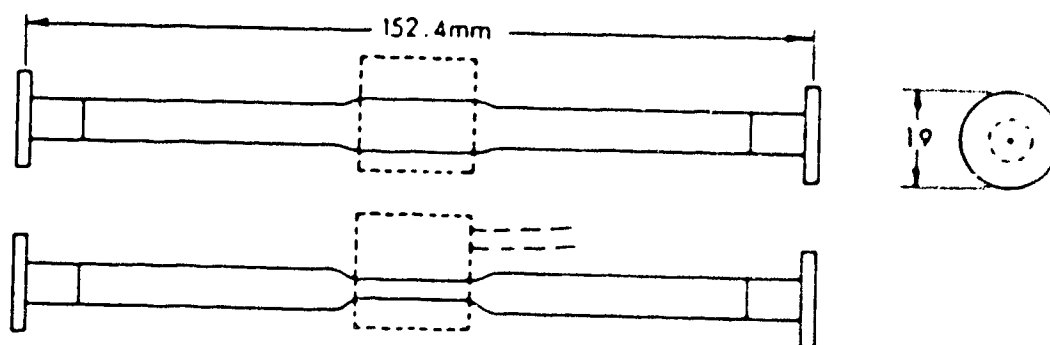
In both the tunnel and braced excavation instrumentation programs, vibrating wire gauges are primarily used due to their ability to resist dusty, humid environments, they have long term reliability and the added advantage of independence of wire length (El-Nahhas, 1980).

The change in the resistance of the vibrating wire element represents the change in a given length. This is explained in detail by the Norwegian Geotechnical Institute (1962) and by Thomas (1965). The strain gauges used in this study are illustrated in Figure 4.21.

Embedded strain gauges were used to determine the normal forces in the roof and raft slabs. As well, the strain gauges were installed in concrete samples used in the laboratory testing program. All the strain gauges, installation equipment and readout devices were supplied by IRAD GAUGE.

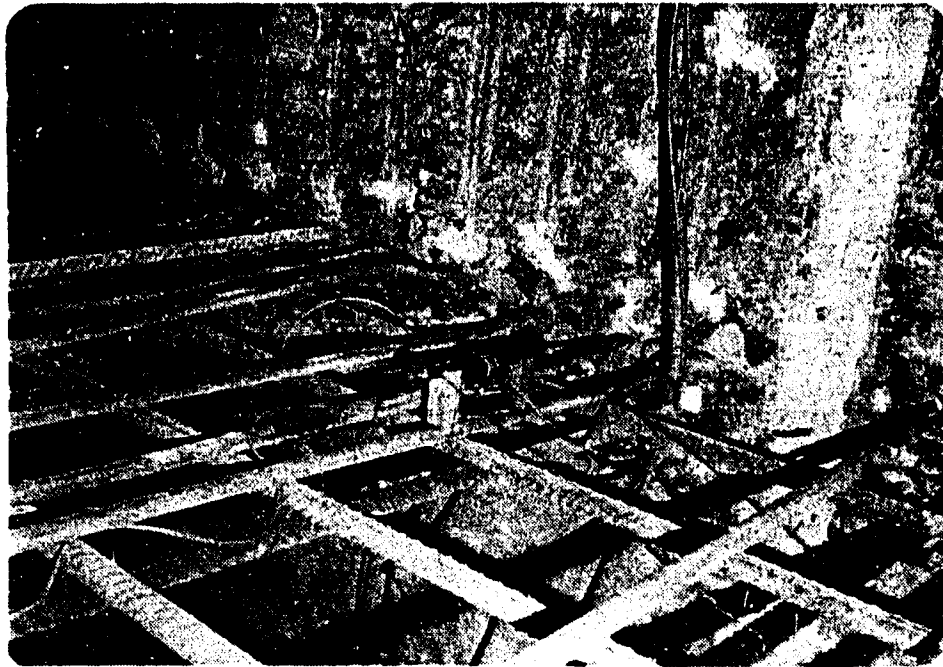


(A) WELDABLE VIBRATING WIRE STRAIN GAUGE



(B) EMBEDDED STRAIN GAUGE

Figure 4.21 Details of the Strain Gauges



a) Embedded strain gauges in the raft



b) Embedded strain gauges in testing cylinder

Plate 4.1 Details of the Installation of the Embedded Strain
Gauges

4.4.5.1 Installation Procedure

The embedded strain gauges were mounted on the reinforced steel bars at a minimum distance of 25 mm from the bars at the desired locations with wooden spacers used to maintain this distance. The gauges were secured in position with thin wire in two directions. The cables for each gauge were directed to two places, one on each side, and fixed to the steel bars until they reached the protection boxes mounted on the walls. A double numbering system was used to avoid any confusion during monitoring. Plate 4.1 details the installation of the embedded strain gauges.

The procedure for mounting the weldable gauges on the temporary supports is explained in the instruction manual IM82.9. Simply, the desired location was ground and cleaned using a disc sander such that a very smooth surface results. Then using the spot welding unit, the gauge was welded to the steel strut and coated with a protective solution. A cover was then welded on for protection. A special pad is mounted above the gauge and a steel protection plate is welded in place to protect the instrument during the installation of the strut and the excavation operation. The cables were mounted on a wood plate at the top of the pre-cast panel or at the side of the cast-in-situ panels. Each cable was marked with respect to its strain gauges. Plate 4.2 shows the gauges mounted on the struts.

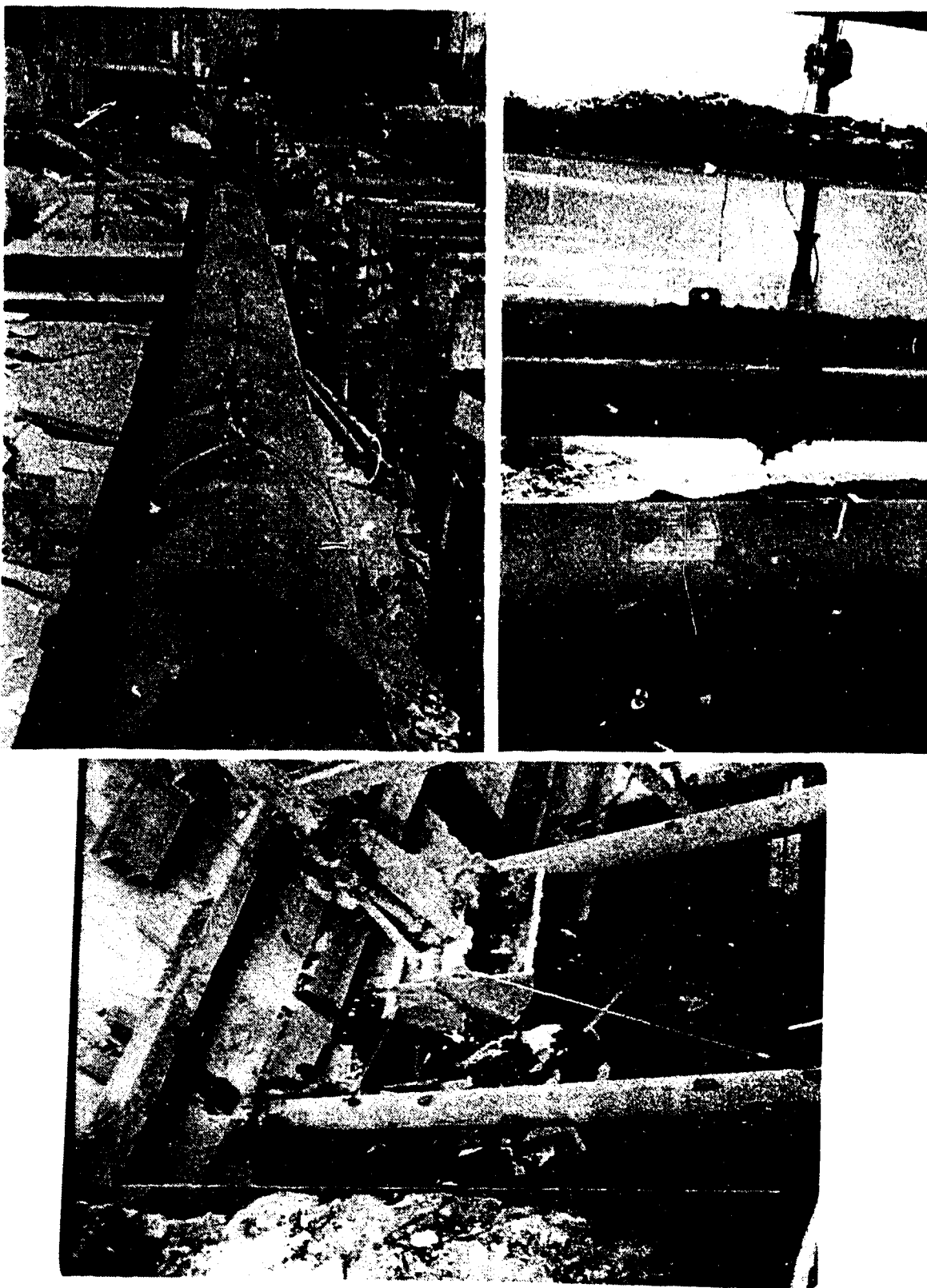


Plate 4.2 Weldable Strain Gauges Mounted on the Struts

4.4.5.2 The Monitoring Procedure

The monitoring procedure was very simple, and is described in detail in the Manufacturers Instruction Manual. Data for each gauge were recorded with corresponding temperatures. Using the tables for temperature correction provided by the manufacturer, the data were processed and the final readings were in microstrains. Appendix A shows a sample calculation for the determination of the normal force in the section.

4.5 Laboratory Test Program

Throughout the construction and excavation procedures, soil and concrete samples were recovered and taken to the Ain Shams University laboratory and Ardman Ace Company to determine the properties of each material. These included sieve analyses, plasticity indices, and consolidated undrained and drained triaxial tests for the soils. The results are summarized in Table 4.1. Several laboratory programs were conducted under the supervision of the NAT. The final report No. 401AAc-000413A (1984) (Project Report) summarizes the geotechnical properties and has been used to compare these data.

In Appendix B, an example of the stress strain volumetric relationship is shown which was needed for the determination of the numerical analysis parameters. Appendix C presents the summary of the concrete tests and test procedures.

Table 4.1 Soil and Concrete Properties

Type of Soil Average Properties	Fill	Clay Silt	Sand	
			Dense	Medium
Saturated unit weight (γ_{sat} kn/m^3)	18	18.3	20	18
Water content (W) %	38	32	*	22
Plastic Limit (P.L) %	30	25		
Liquid Limit (L.L) %	50	60		
Permeability M/S κ	3.5×10^{-8}	10^{-6}	3×10^{-5}	2×10^{-4}
Standard Penetration (S.P.T.) blows/0.3m	7	11	35	20
Degree of Saturation (S_r) %	95	95	95	95
Angle of Shear Resistance ϕ	33	32	30	25
Drained Shear Strength Parameter C' kPa	-	40	-	-
Drained Shear Strength CD kPa	*	60	-	-
Undrained Strength CU kPa	50	60	-	-
% Clay	25	40	0	8
% Silt	30	45	5	15
% Sand	23	15	95	78
% Gravel	22	0	0	0

* Not available

CONCRETE PROPERTIES

Unit Weight kN/m^3	23.750
Compressive Strength MPa	40.0
Modulus of Elasticity MPa	31,250.0

Table 4.1 also shows the average properties for the concrete used in the project. These results have been compared with the data collected for the quality control by the contractor under the supervision of the National Authority for Tunnels (NAT) Egypt. Some concrete test cylinders were instrumented with embedded strain gauges to determine the stress strain characteristics of the concrete. An empirical equation provided by the Canadian Standards Association (CSA, 1984) was used to determine the modulus of elasticity. Good agreement was found between this equation and the laboratory test results. This suggests that in future planning, the equation can be used and the cost of instrumentation can be saved.

4.6 Monitoring Routine and Site Condition

Generally, the instruments have been read continuously since installation. A weekly report containing the recorded data sheets and site activity, was summarized for NAT. The monitoring program was most extensive during the excavation process. At times, excavation proceeded too fast to allow a full complement of instrument readings to be taken. To read the slope indicators took approximately 1.5 hours, and during this time, two excavation steps could take place. Therefore, readings were taken on SI2, the slope indicator in the precast panel, for every step of excavation. If time permitted, SI3 was also read.

For the vertical deformation profile (settlement trough), only the initial and final readings were taken.

In the running tunnel section, the majority of the instruments installed outside the tunnel section were destroyed by the contractor (see Plates 4.3 and 4.4). Some of the instruments originally assigned to the Station section were used to replace the damaged instrumentation at the tunnel section. A new slope indicator was installed in the soil and some surface settlement points were replaced. Difficulty was encountered in clearing the damaged slope indicator casing inside the precast panel. Finally, a drilling crew on site drilled out the casing and the grouting material. The bottom 2 m was filled with small pieces of casing and could not be used.

For the multipoint extensometer outside the tunnel section (ME1), the access pipe had been plugged by small size particles. By pushing the particles to the bottom of the access tube, only the lower two extensometers were lost. The readings were re-initialized taking into account the previously recorded displacement.

The cables and pipes for the piezometer line (PL1) outside the tunnel section were repaired and reconnected. Concrete was poured to remount the protection boxes.

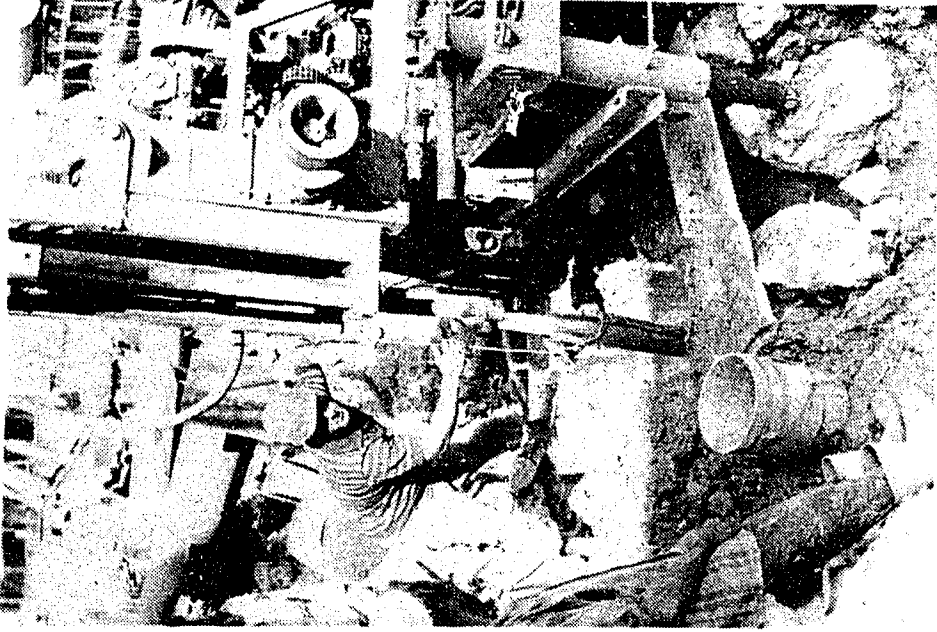
The instrumented section was restored almost to its original condition and monitoring was continued. The instruments performed as expected. The rate of failure due to instrument malfunction was very low except in the case of



Plate 4.3 Examples of the Field Obstacles Experienced at the
Tunnel Test Section



Damage



Repair Work

Plate 4.4 Damages and Repair Work at the Tunnel Test Section

the strain gauges.

The multipoint extensometer inside the tunnel section failed to provide reliable readings due to the rapid excavation and subsequent damage to the access pipe. No time was available to effect the necessary repairs.

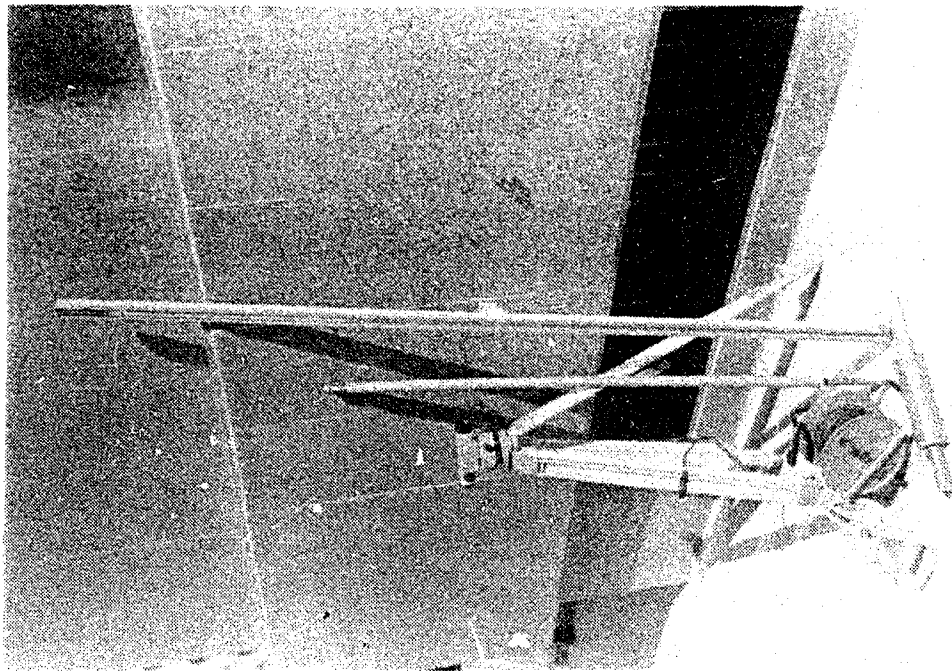
The two piezometer lines (PL2 and PL3) inside the excavation were damaged during excavation but were successfully repaired.

At the station section, major damage to the instruments resulted from the continuous changes to the site plan from the unpredicted utility diversion work. As well, the traffic diversion plan had to be altered on site to ensure adequate traffic flow. As a result of the damage and limited access, only slope indicator, SI1, and the strain gauges in the temporary struts and concrete could be read. It should be stressed that instrument malfunction was not responsible for the apparent lack of success.

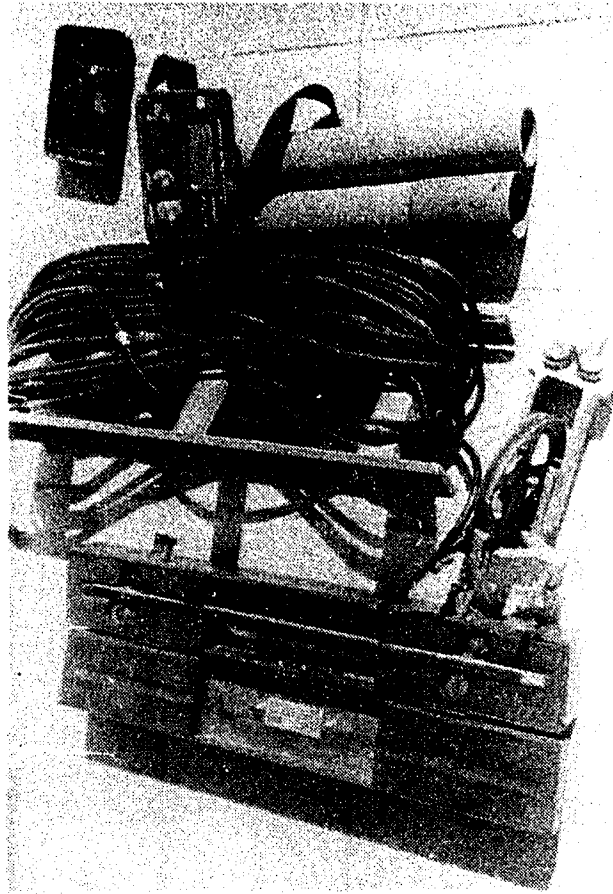
Plates 4.5 and 4.6 show the instrument read out units used in this project. These instruments have been donated to Ain Shams University in Egypt for use in further research work.

4.7 Field Measurement of Soil Deformation

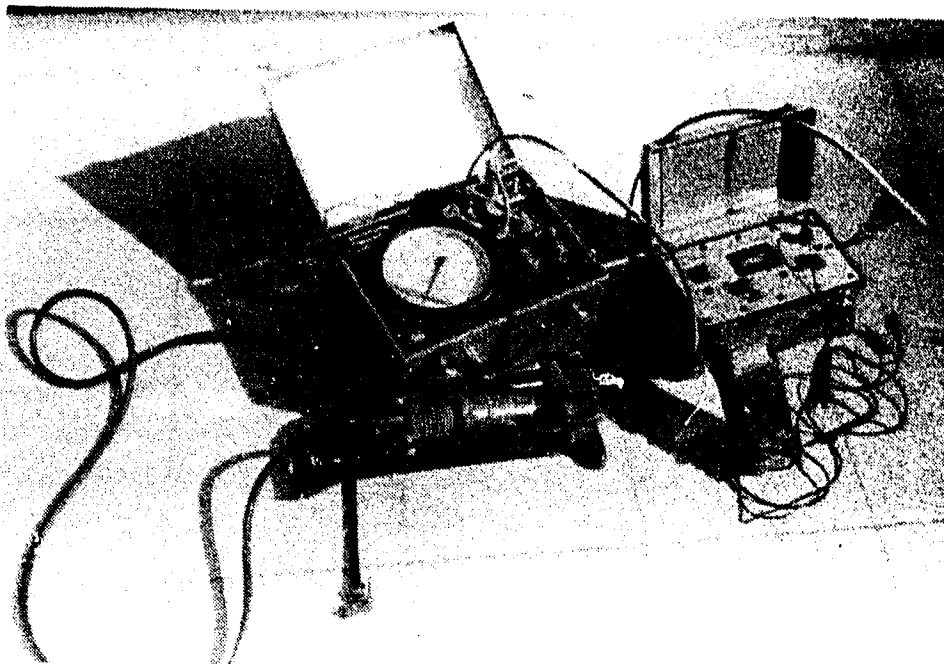
Periodical readings of each instrument were taken during different stages of construction. In particular, more frequent readings were taken during excavation. Monitoring continued until stabilization of the measurement was



Multi extensometers and Settlement points



Slope Indicator



Piezometers and Strain gauges



During instrument read out

obtained or access to the instrument was blocked.

The data was processed and plotted manually after each set of readings. The results have been reported by Eisenstein et.al. (1987) in the final report presented to the International Development Research Center, Ottawa, Canada and the National Authority for Tunnels, Cairo, Egypt. The running tunnel measurements were presented by El-Nahhas et.al. (1988, 1989) to the Tunnels and Water International Congress in Madrid, Spain. The Station results have been reported by EL-Nahhas, Eisenstein and Shalaby (1989).

4.7.1 The Running Tunnel Test Section Measurements

As indicated in Section 4.1, the instrumentation was concentrated at the section close to SAAD Zaghloul Street (project reference at Kielo point 23.914.27). The results from each instrument are presented with respect to measurement type.

4.7.1.1 Vertical Displacement (Settlement)

To determine the settlement trough around the cut-and-cover tunnel, the vertical displacement (the surface settlement) was monitored using the surface settlement points installed in Safeya Zaghloul Street and in the soil adjacent to the tunnel. Figure 4.22 shows the final settlement trough observed after construction and stabilization of the readings. It includes one set of readings during construction. The maximum settlement of 15 mm occurred adjacent to the wall of the tunnel. No

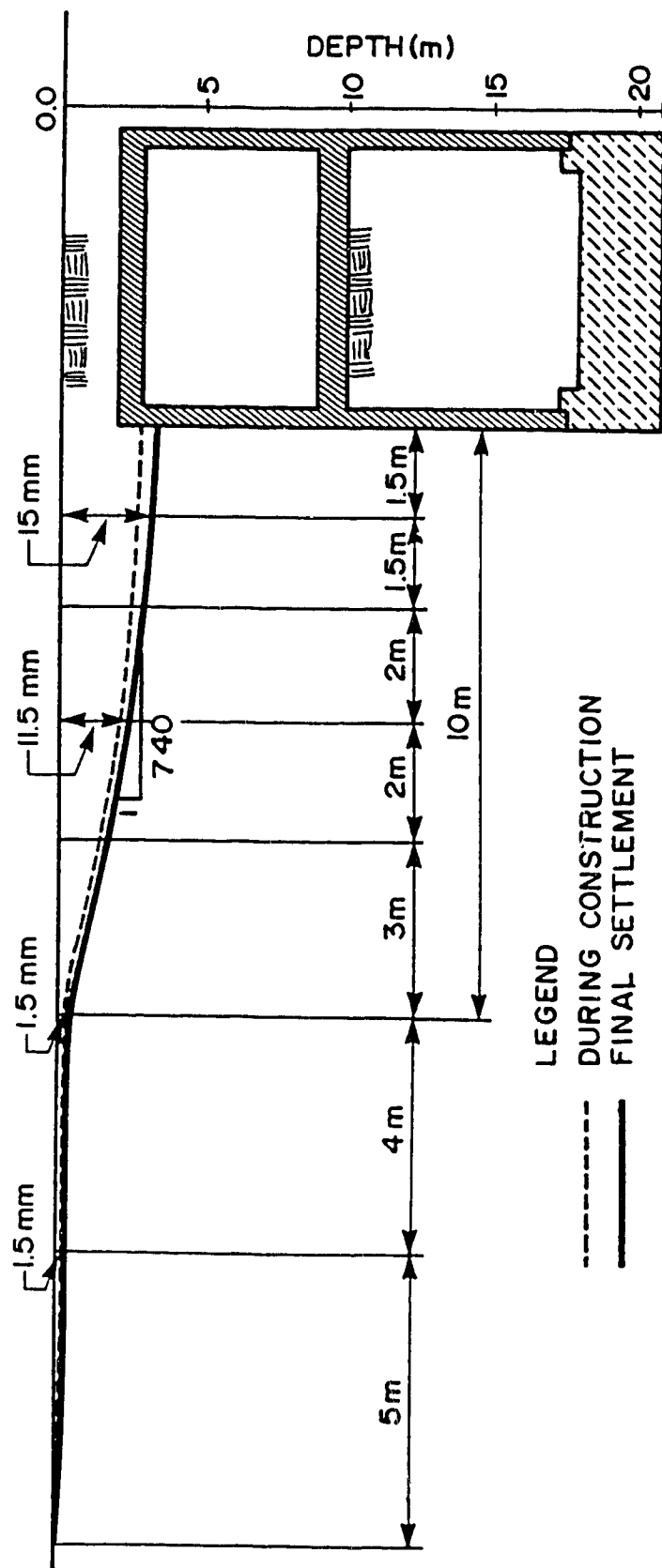


Figure 4.22 The Observed Settlement Troughs at the Tunnel Test Section

settlement was observed during the construction operation at distances more than 20 m from the tunnel walls. The subsurface soil settlement adjacent to the tunnel walls is given in Figure 4.23. These results from installation ME1, show that at 9.0 m depth, the vertical settlement increases with depth. The maximum vertical displacement recorded was 22 mm at elevation -9.0 m. The nearest surface settlement recorded 15 mm at elevation -1.5 m. As a result of the blocked access pipe, the lower two magnetic points were lost.

4.7.1.2 Horizontal Displacement (Lateral Deformation)

The slope indicator was used to monitor the lateral deformation of the diaphragm wall and the soil adjacent to the walls. Figure 4.24 presents a summary of the diaphragm wall deformation during construction and after completion of the tunnel from slope indicator, SI2. The first profile shows the lateral deformation after excavation of 2 m, with a maximum of 8 mm. The second, at 5 m excavation with temporary support in place, shows a maximum of 9-10 mm. The third profile taken when 7 m were excavated and the lower strut installed shows a maximum of 10-11 mm. At the full depth of excavation (10.5 m) and the upper strut installed 19-20 mm were observed at the lower strut level. The last profile represents the final deformed shape of the diaphragm wall with a maximum of 22 mm at the lower strut.

The reading of the slope indicator installed in the soil adjacent to the tunnel walls (SI1) is presented in

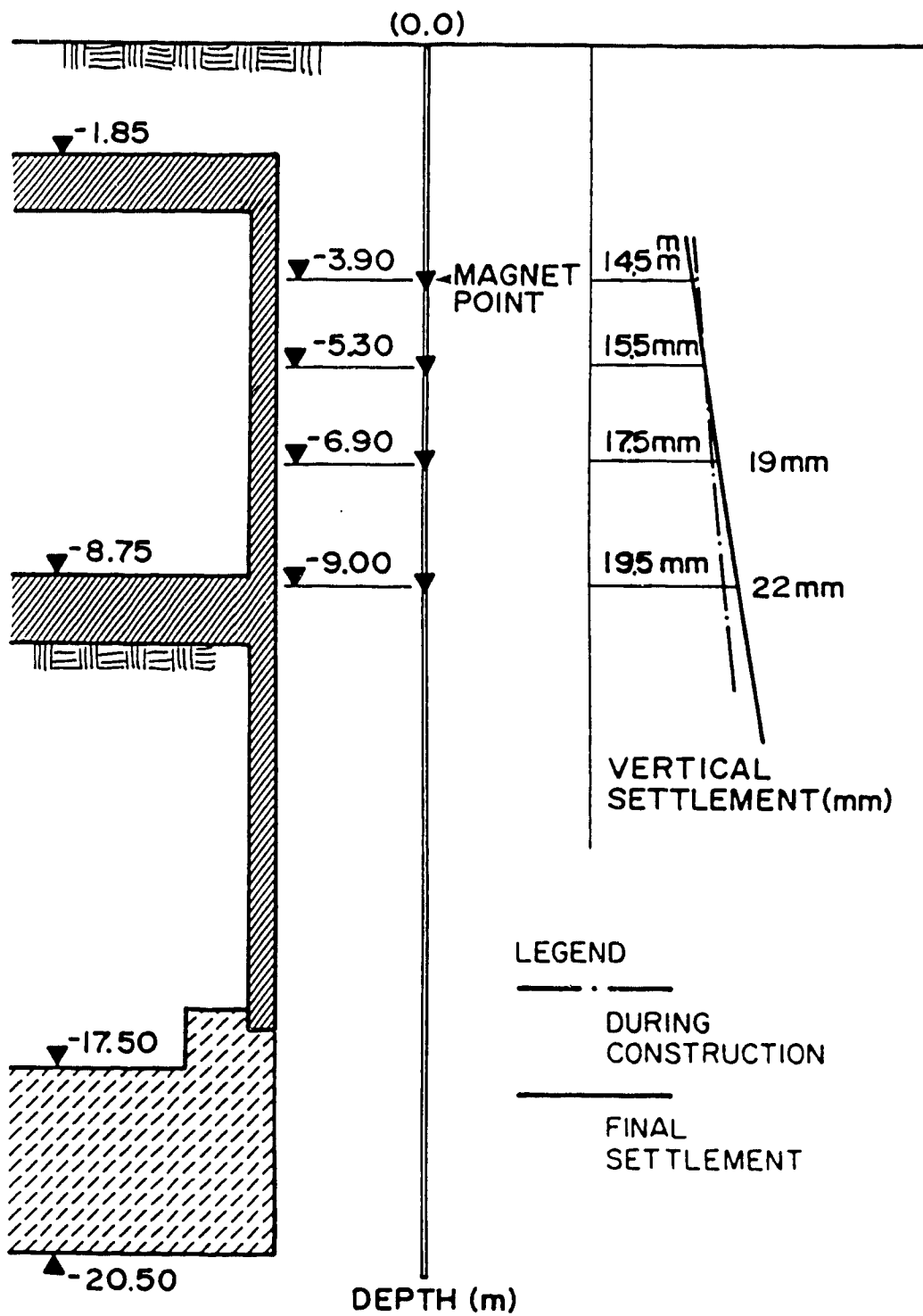


Figure 4.23 The Subsurface Settlement at the Tunnel Test
Section

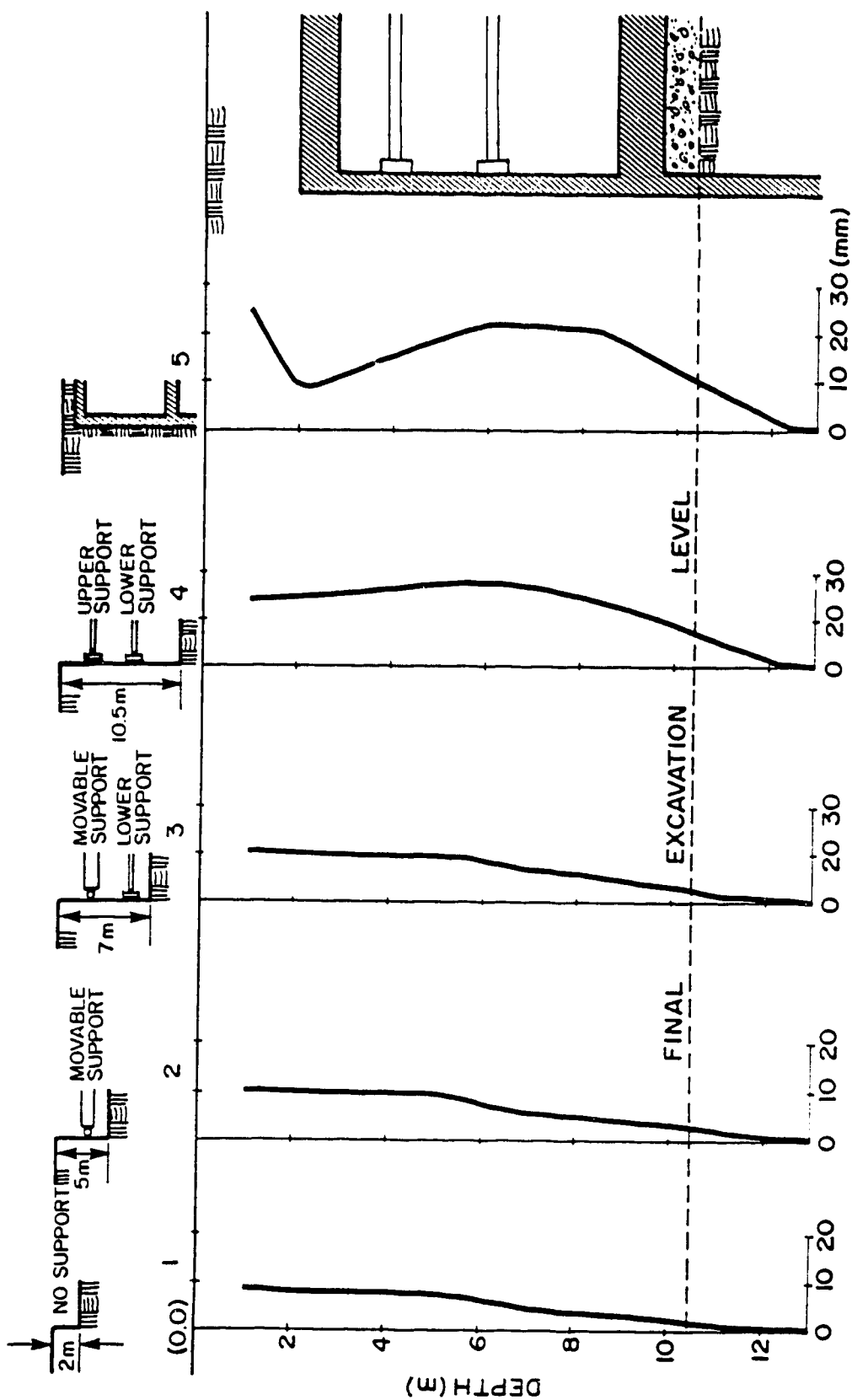


Figure 4.24 The Diaphragm Wall Lateral Displacement during Excavation at the Tunnel Test

Section (SI2)

Figure 4.25. Only four stages of excavation were recorded due to time constraints. The first profile after 2 m excavation inside the tunnel section showed a maximum deformation of 7-8 mm. The second, at the final excavation level, with the lower strut in place and temporary support at the top, recorded a maximum of 18-19 mm. The third set was taken at full excavation level with the support provided by the upper and lower struts. A maximum deformation of 20-21 mm was observed. After completion of the tunnel, 22 mm horizontal displacement was recorded.

4.7.1.3 Pore Water Pressure Measurements

Three piezometer lines were installed in this section as detailed in Section 4.1; one outside the section and two close to the site walls of the tunnel. Figure 4.26 presenting a summary of the recorded data, it shows strong agreement with a hydrostatic pressure distribution. If the piezometers installed inside the tunnel section (within the grouted plug) continue to show a hydrostatic distribution which matches the outer piezometer line, the grouted plug is not functioning.

As the plug was guaranteed for 3 years from installation, the contractor poured an additional concrete layer over the final excavation depth to prevent failure due to uplift forces.

linear elastic model properties.

5.4.4.6 Step (6) - Excavating to the Final Level

The final excavation level of -10.5 m was achieved by deleting the elements up to this level with the support of the mobile frame only. The excavation base upper row of elements was assigned the linear elastic model properties.

5.4.4.7 Step (7) - The Installation of the Lower Strut

The simulation of Step (7) was the same as for Step (5), i.e. installation of the temporary support.

5.4.4.8 Step (8) - The Installation of the Upper Strut

In a manner similar to the previous step, the upper strut was installed.

5.4.4.9 Step (9) - The Removal of the Mobile Frame

The element row of the mobile frame was deleted and the diaphragm wall was supported only by the two rows of struts without any base support.

5.4.4.10 Step (10) - Pouring the Concrete Floor Slab

The concrete floor slab was introduced by rebirthing the corresponding elements with new model properties which were linear elastic model with concrete properties. The soil base row was reassigned as the hyperbolic model in this stage of analysis as the concrete layer provided the required linear elastic surface layer. The diaphragm wall was supported by the floor slab and the two struts.

5.4.4.11 Step (11) - Introducing the Sheet Pile Wall

In this step, excavation of the element column adjacent to the outside of the diaphragm wall and to an elevation of -3.7 m was required. A temporary support system consisting of steel sheet pile walls was installed and the soil was excavated to allow for the required work to be carried out. The best simulation for the sheet pile walls was deletion of the elements without any restriction to the degree of freedom of each node. As well, the upper elements of the diaphragm wall were deleted to allow for the connection between the wall and the roof slab.

5.4.4.12 Step (12) - Introducing the Roof Slab

As explained previously for the floor slab, the roof slab was introduced to the system. The temporary support provided by the two rows of struts was maintained during this stage of analysis.

5.4.4.13 Step (13) - The Final Case

After executing the insulation work (water stoppage) for the exposed side of the diaphragm wall and the surface of the roof slab, the sheet pile walls were removed and backfilling began. The struts were removed and the walls are supported by the floor and roof slabs only. The surface row of elements of the backfill were assigned linear elastic model properties.

5.4.5 The Station Test Section - Steps of Analysis

The construction procedure for the station test section was an undercover excavation. In the original design of the instrumentation installation, the instruments were to be located inside the undercover section. As a result of on site changes to this plan, due to traffic diversion, a shift of the open air excavation zone toward the instrumented section occurred. The slope indicator was located in the open air zone, approximately 3 m from the undercover area.

Due to the multiple problems, two different analyses were used for this section;

1. open air excavation (as in the running tunnel),
2. undercover excavation.

The same procedure followed for the running tunnel test section analysis was used for the station section.

5.4.5.1 The Station Test Section Steps of Analysis as an Undercover Excavation

Step (1) The in situ stress generation

Step (2) The slurry trench and cast in situ diaphragm walls

Step (3) Grouting the plug and dewatering the excavation zone

Step (4) Start excavation to elevation -3.5 m

Step (5) Introduce the roof slab and backfill to street level

Step (6) Excavation undercover to elevation -5.9 m

Step (7) Installation of the strut and excavation to the

final depth of 10.5 m

Step (8) Introduce the floor slab

Step (9) Introduce the key and the final step

5.4.5.2 The Station Test Section - Steps of Analysis as an Open Air Excavation

This analysis continues from Step 4, as the previous three steps are exactly as for the undercover excavation analysis.

Step (4) Excavation to elevation -5.9 m and the installation of the strut

Step (5) Excavation to the final level

Step (6) Introduce the floor slab

Step (7) Introduce the roof slab and backfill to street level

Step (8) Introduce the key and remove the strut (the final case)

5.5 The Finite Element Analysis Results

Convergence was achieved after an average of 15 iterations. Only the result of the non-linear analysis are presented in this chapter. The output contains the vertical and horizontal components of each node displacement and the major stresses and strains at Gaussian points for each element.

As this problem requires special consideration, i.e. choosing the nodes and elements to represent the field instrument locations, the settlement trough, base heave,

horizontal and vertical displacement, lateral earth pressure and shear stresses results were processed manually. The displacement field was presented using the post-processing program to plot the displacement arrows for each step of the analysis for both sections.

5.5.1 Finite Element Results of the Running Tunnel Test Section

5.5.1.1 The Deformation Analysis

The results of the deformation analyses are presented in the form of arrow displacement plotting which concentrated on the major area of interest around the tunnel and up to and below the grouted plug, the settlement trough, base heave, soil vertical displacement and soil and wall horizontal displacements. The results are shown in Appendix D.

The displacement arrow plots (Figures D.1 to D.12) for the running tunnel test section showed that in the early stage of analysis (Steps 2 and 3), the soil tended to move downwards recording the highest displacement values. As the excavation began, a reduction in the magnitude to the displacement was observed. With continued excavation, the walls and surrounding soil moved toward the excavation and the reduction in the surface displacement around the tunnel excavation continued. As the final excavation depth was reached, base heave values began to increase. The horizontal displacement of the wall and surrounding soil increased,

Figures D.13 and D.14, while the vertical displacement decreased. When the floor and roof slabs were introduced, base heave decreased in magnitude. The last step, (13), showed the final displacement pattern.

It was concluded that the grouted plug not only acted as an impervious layer preventing displacements due to ground water level changes, but also reduced the base deformation due to heave.

The settlement trough and heave of the excavation base are presented in Appendix D, Figures D.15 and D.16. The surface settlement generally increased with the progress of excavation and a maximum of 16.77 mm in the final case was predicted. This is considered to be in close agreement with the field measurement of 15 mm at the same point. The maximum base heave predicted occurred at Step (9) of the analysis with a value of 26.3 mm.

The horizontal displacement for the wall and soil are also presented. The results showed that the magnitude of the displacement increased with the progress of the excavation until Step (11). A maximum of 32.47 mm at the top of the wall was recorded. The maximum for the soil was 27.42mm at a depth of 2.75 m in the final step. The general profile can be described by the increase in displacement with the decrease of depth. The soil displacement is almost always less than the wall displacement, by approximately 15%. This 15% difference in deformation profiles for wall and soil , can be attributed to the distance between the two instrument

locations.

5.5.1.2 The Stress Analysis

As mentioned previously, a total stress analysis was performed. The predicted lateral earth pressure was calculated as the average value of the normal stress against the wall in the closest element at the closest Gaussian point. The average was plotted against the elevation of the centre of gravity of the element. For each step of the analysis, the corresponding curve is plotted (Figures D.17 to D.19). In general, the lateral earth pressure increases with increasing depth in a straight line. The plots for the first four steps show an almost typical Rankine's earth pressure distribution. With soil deformation due to excavation, the predicted earth pressure diagrams showed on average a 20% reduction. The predicted passive earth pressure was overestimated at shallow depths, but matched the Rankin's passive earth pressure with an increase in depth (corresponding figures shown in next chapter). At the bottom of the diaphragm wall, the predicted (F.E.M) and calculated (Rankine's) values are in close agreement. It must be noted that the upper portion of the diagram near the ground surface is influenced by the deletion of elements. When the elements have been deleted, the stress is reset to zero which neglects the stress history (i.e. previous steps of analysis).

Figures D.20 to D.22 presented in Appendix D, show the distribution of the shear stresses along the contact area

between the soil and concrete. The first four steps of analysis showed small values and little variation. Negative values were observed as the wall moved downward and the soil upward. In the passive zone, the soil tended to move upward in the contact zone between it and the inside face of the diaphragm wall. The allowable shear stresses depend on the interface surface roughness. For the precast panels in the running tunnel, the surface is relatively smooth and the allowable shear stresses are considerably smaller. In common practice, surface roughness is estimated as one-third the angle of shearing resistance, ϕ . Typically, this value is 10° . This is discussed in the next chapter. In the remaining analyses, the shear stresses were negative, which indicates that the soil is moving downward with the wall. As excavation continued, the inside shear stresses showed a considerable increase. A maximum envelope is defined by the results of the final stage. The predicted shear stresses provide good support for the assumption of non-slip between the wall and soil in this analysis.

5.5.2 Finite Element Results of the Station Test Section

The station test section was analysed in two different ways, first as an undercover excavation and second as an open air excavation. The first two steps of analysis are the same for both methods, so the open air analysis will begin at Step 4. Appendix(E) contains condensed Input and Output computer files for SAFE . Sample of each control card and of

each Output component are presented.

5.5.2.1 The Displacement Analysis as Undercover Excavation

A summary of the results is shown in Figures D.23 to D.29 presented in Appendix D. In Steps 2 and 3, the soil and diaphragm wall are moving downwards, as shown by the displacement arrow plots. As excavation began, the soil inside this zone moved upward reducing the magnitude of displacement. This was in part due to the greater width of the excavated area.

The introduction of the roof slab and backfilling caused the soil to move downward in a similar pattern to the second and third steps with a slight increase in the magnitude to the displacements. With the start of the undercover excavation, a major change in the deformation pattern occurred in the zone between the excavation base and the grouted plug. A large reduction in the lower part and reverse of direction to heave in the upper part. As the final excavation level was reached, the inside zone of the excavation base heaved with a major reduction in the magnitude of displacement as the grouted zone was approached. The presence of the raft slab tended to reduce heave but the same pattern of displacements was observed. In the final step, no significant changes in the displacement pattern were recorded with the removal of the temporary support.

The settlement trough and base heave are shown in Figure D.30 in Appendix D. The greatest vertical displacements occurred during Step (5) with approximately 20 mm at a distance of 1.5 m from the wall. The final value at the same point was 11.5 mm. The base heave reached its peak in Step (7) with a value of 32 mm. A final value of 23.5 mm was recorded at the centre line.

The horizontal displacements for the wall and soil in the initial steps of the analysis were very small (Figures D.31 and D.32), in the order of a few millimeters. At the end of the analysis, maximum values of 2.6 and 2.4 mm, for the wall and soil respectively, were observed at a depth of 9 m. The results showed that the undercover excavation procedure minimizes the horizontal displacement of the wall and soil and generally decreases the soil deformation.

5.5.2.2 The Stress Analysis as UnderCover Excavation

The lateral earth pressure diagrams predicted using the finite element method are shown in Appendix D, Figures D.33 and D.34. The results are in reasonable agreement with the lateral earth pressure calculated using Rankine's theory. The excavation procedure as under cover excavation provides small changes in the pressures during the various steps of the analysis. In the passive pressure zone, it shows a pattern similar to the tunnel test section. The shear stresses in this analysis are positive, Figures D.35 and D.36. As the roughness of the contact surface of the cast in place diaphragm wall was considerably higher than the

precast panels, it was assumed that a surface roughness angle equal to $2/3 \phi$ be used, i.e. 20° . As a result, much higher shear stresses are allowable at the interface surface between the concrete and soil. In the passive zone the shear stress was similar to the active zone and increased with the increase in excavated depth. The results support the assumption of a non-slip surface between the soil and concrete as long as the predicted values did not exceed the allowable stress.

5.5.2.3 The Displacement Analysis as Open Air Excavation

The analysis as open air excavation starts from Step 4 as Steps 2 and 3 are the same as for the undercover excavation. The displacement patterns for each step of this analysis are shown in Appendix D, Figures D.37 to D.41. As a result of the excavation in Step 4, and the installation of the temporary support system, the displacement below the excavation level showed a major reduction as a result of heave. Above the excavation the soil tended to move toward the excavation and just below the base of the excavation a change in direction took place. The strut shows higher displacement. When the final excavation level was reached, all the displacements tended to move toward the excavation area in all directions with higher magnitudes. By introducing the raft slab, the same displacement pattern was observed with the reduction of heave at the base of the excavation. No major change in the displacement pattern was observed as a result of the final steps of the analysis.

The settlement trough (Figure D.42) shows that the result of Step (5) indicates that the surface settlement was upwards, while in Step (6) it was downwards until it reached a maximum in Step (7) of 16.50 mm at a point 1.5 m from the wall. In the final case, Step (8), this value decreased to 14.40 mm. The maximum base heave at the center line of 38.45 mm was reached in Step (5). This continued to decrease to a final value of 19.83 mm. The absolute maximum was 37.89 mm at 5 m from the center line and decreased to 23.05 mm at the end of the analysis. The settlement troughs are shown in Appendix D.

The horizontal displacement of the wall and soil are also presented in Appendix D, Figures D.43 and D.44. The displacement decreases with increasing excavation depth until a maximum of 33 mm at the top of the roof slab was reached. The soil displacement was 29.70 mm. The magnitude of displacement did not show any significant decrease or increase as a result of the excavation process.

The displacement predicted as an open air excavation are the greatest. This may be attributed to the single row of temporary support used during the analysis, while the running tunnel test section was supported by two rows of struts.

5.5.2.4 The Stress Analysis as Open Air Excavation

Lateral earth pressure diagrams as predicted by the F.E.M. as open air excavation are shown in Appendix D, Figures D.45 and D.46. The results showed similar pattern as

for the running tunnel test section and are in close agreement with those calculated using Rankine's earth pressure theory. The surface layer showed tension areas. This may be attributed to the larger horizontal displacement predicted at each corresponding step of analysis. The passive earth pressure was over estimated at the base of the excavation and showed reasonable agreement with Rankine's passive earth pressure with the increase in depth.

The shear stresses at the interface between the wall and the soil are shown in Appendix D, Figures D.47 and D.48. At the active side of the wall, the shear stresses changed from negative to positive indicating change in the soil movement upward or downward with the progress of excavation. The passive side was always negative, but increased with the increase in excavation depth. The allowable shear stresses were in the same order as for the undercover analysis.

5.6 The Support System Loading Predictions

5.6.1 The Temporary Support System Loading Predictions

The forces carried by the temporary support system were predicted for each step of the excavation and construction procedure. The results are shown in Table 5.3. The analysis provided a complete set of values while the field measurement were available for some steps only,. The station analysis as an open air excavation is purely analytical without any field measurements. The results showed that the

Table 5.3 Strut Loading as Predicted by F.E.M. and From Field Observation

Analysis Step No.	Tunnel Section				Station Section			
	Type and Support				Analysis Step No.	Undercover Excavation	Analysis Step No.	Open-air Excavation
	Upper Strut	Lower Strut	Mobile Frame	Total				
5			9.09	9.09	7	36.53	4	74.13
6			30.06	30.06	8	36.44	5	186.84
7		112.47	107.35	219.82			6	193.11
8	19.00	101.84	107.80	228.64			7	184.11
9	37.09	132.705		196.80				
10	42.32	136.14		178.46				
11	38.69	136.07		174.76				
12	17.1	135.93		153.03				
Observed	150	150				60		

Strut loads in kN/m

first support strut installed at the lower level sustains the highest loads throughout the analysis with a reduction in value with the introduction of the permanent support provided by the structural elements. The station section analysed as undercover excavation showed small loads carried by the struts. As an open air excavation analysis, much higher loads were predicted, which suggests the need for two rows of struts to be installed. This, indeed, was the case in some sections of the project.

5.6.2 The Permanent Structural Support Loading

As the structural elements are introduced in the analysis, the normal load on them increases as the temporary support system is removed. The normal force calculated for each step includes the dead load effect. The live load on the structural elements and soil was not taken into account. For the tunnel section, the floor slab introduced in Step (10) carried a load of 161.91 kN/m'. Results are shown in Table 5.4 for every test section analysed. The analysis showed almost no significant change or influence with the floor slab while the normal load on the roof slab nearly doubled when the struts were removed.

For the tunnel section as undercover excavation, an increase in the load on the roof slab with the progress of construction and excavation, with a minimum normal load acting on the floor slab was observed. The open air analysis showed changes in the normal forces with construction and

Table 5.4 Structural Elements Normal Loading as Predicted
using F.E.M. and from Field Observation

Step No.	Tunnel Test Section	
	Floor Slab	Roof Slab
10	161.92	
11	161.7	
12	162.83	68.56
13	164.32	138.225
Observed	-70	80

Loads in kN/m

Step No.	Station Test Section			
	Under Cover Excavation		Open Air Excavation	
	Floor Slab	Roof Slab	Floor Slab	Roof Slab
5		104.5		
6		275	31.8	
7		384.5	-135.63	22.2
8	-5.25	405	-40.87	
9	1.92	414		
Observed	-40	40		

Loads in kN/m

excavation. The influence of the type of support for the floor slab as a simple beam is clear with major increases in the normal loads by the reduction of the tension loading by the removal of struts. The roof slab showed considerably lower values comparing with the values of the undercover analysis.

6. ANALYSIS OF THE FIELD AND NUMERICAL RESULTS

6.1 Introduction

The application of the Observational Method to predict the soil deformation and stresses around an underground structure is considered to be an important tool in the geotechnical practice. Peck (1985) stated that the observational method is one of the most powerful weapons in the geotechnical arsenal, but also warned of its possible misuse. Its main objective is to obtain data through field instrumentation programs, and to utilize these data for modifying and economizing the design throughout the project.

One of the aims of this study was to apply the observational method to the Cairo Metro project, thereby establishing a database on the performance and prediction of soil deformation, lateral pressures and construction methods in such host materials. The finite element method was used to calculate the lateral earth pressures acting on the walls of the tunnel and station as it is not possible at the present time to measure them directly from the field using the available instruments. The soil parameters used in this analysis were based on laboratory tests when field specimens were available, except for the sand parameters which were estimated from the data provided by Duncan et al. (1980). Matching the field deformation with the predicted values of the finite element analysis, yielded the lateral pressures acting on the walls. A detailed analysis of the deformation,

stresses and construction method will be discussed in this chapter. A comparison between lateral pressures obtained in the analysis with the most common theoretical earth pressure theories and empirical pressure diagrams for similar types of soil, is made.

6.2 Soil Profile and Properties

A series of investigations to determine soil properties and profiles throughout the project were conducted. The results of the latest investigation have been used in this study and these were confirmed by laboratory tests. It was summarized in Report No. 401/AAC/00/0413 A (1984) of the project and was also compared to previous investigations. Whenever possible, the stress-strain relationships were obtained for each type of soil.

During instrumentation installation, the soil profiles were confirmed or amended. Samples for geotechnical testing could not be retrieved during this time, but were taken during excavation.

The profile is characterized by a layer of fill, underlain by silty clay, medium density sand and dense sand, respectively. At the tunnel section, the layer of fill was a mixture of sand, silt, clay, pieces of limestone and homra.¹ The fill layer is underlain by a 5 m thick layer of

¹ Homra is a product of crushed red bricks which were the main type used in Egypt. Their use was discontinued in recent years after the construction of the high dam at Aswan. The construction of the dam prevented the clayey particles carried by the Nile during flood periods from reaching the delta. It is this clay which forms a main

silty clay followed by a deep layer of dense sand. As the excavation depth for this section is 10.50 m, the excavation is mainly in clays based on sand. The ground water table was reported to be 1.0 m from the surface. This was confirmed by observation during the project period. It remained constant throughout construction.

The soil profile for the station section shows a 3.5 m fill layer. It was similar in composition to that of the tunnel section. The fill was underlain by a 6.5 m layer of silty clay. Medium density sand, 5 m thick, lay beneath this. At 15 m below the ground surface to the bottom of the borehole, dense sand was found. The groundwater table is 3 m below the surface. It was assumed constant during the construction period. This could not be confirmed as access to the piezometers was blocked during construction, but was based on information provided by the soil investigation reports.

Laboratory tests were conducted to provide the necessary parameters for the finite element analyses. Broms et al. (1986) and Potts and Fourie (1984) concluded that the main limitation in using the finite element method is the evaluation of the soil parameters required for input to the analysis. They also stressed the need for an accurate soil profile and close simulation of the construction sequence.

Consolidated drained tests (CD) and consolidated undrained tests (CU), were conducted and have been used to

'(cont'd) component of the bricks.

determine the required soil parameters. Data from the Cone Penetration Tests (CPT) was converted to equivalent Standard Penetration Test (SPT) values through the method described by Robertson et al. (1983). From these data, the modulus of elasticity was estimated for use in the linear elastic analysis and the PFT program. They were also compared with the initial modulus of elasticity obtained from the stress-strain curves at different confining pressures. Appendix B contains some samples of the laboratory tests and CPT results.

6.3 Considerations in the Simulation for F.E.M. Analysis

SAFE is a computer program developed at the University of Alberta, and has been successfully used in the analysis of many geotechnical problems (Chan, 1986; Chan and Morgenstern, 1987; Kaiser et al., 1987; and Chalaturnyk et al., 1987). It was also used to analyse the performance of SLRT Grandin Station in Edmonton by McRoberts et al. (1988), a case history analytically very similar to the station section in this study.

Lee et al. (1989) conducted a finite element study on a strutted excavation in highly over-consolidated marine clay in Singapore, using the modified cam-clay model. Sheet pile walls were used. Both the struts and the walls were instrumented. The results from the field were compared with those predicted. They concluded that there was a discrepancy, and attributed it the uncertainty of some of

the soil parameters, pore pressure dissipation during excavation, slip between the walls and soil and the limitations in the constitutive model used for the marine clay. No attempt was made to check the lateral earth pressure.

The choice of total stress analysis was based on the fact that the construction method did not allow any changes in the ground water table or any flow or seepage from the surrounding soils into the excavation. With no flow occurring, therefore no change in pore pressure, an undrained analysis was performed. Effective stresses were obtained by subtracting the hydrostatic pressure from the total stress. As explained in the previous section, the results of CD, UD and the tables provided by Duncan et al., (1980) were used to determine the undrained parameters for the hyperbolic model used in the analysis.

The simulation of the construction procedure was based on the sequence of excavation as observed during construction. Multiple steps were used, each simulating the actual steps as explained in Chapter 5. Two different methods of construction were employed in the analysis of the station section, the first - open-air, the second - undercover.

A no slip condition was assumed in the soil-structure interaction zone, based on the results reported by Chan et al., (1986). They compared the calculated shear stresses from the finite element with the allowable shear stresses

and found that no slip occurred as the soil was able to accommodate the shear stress at the interaction zone. This was supported by Schweiger and Hass (1988) who stated that the additional computational effort may not be justified in many cases. The sensitivity of predicting the deformation field depends on the material model used while resulting stresses do not change significantly. Since the finite element program automatically satisfies criteria such as ,compatibility , equilibrium and stability , matching the computed displacements with the ones observed in the field ,secures reasonable accuracy in the stress calculation resulting in a reasonable prediction of lateral earth pressures. The findings of this study will be discussed later on in this chapter.

6.4 Horizontal Displacement Analysis

Field measurements of horizontal displacement were reported in Chapter 4. Predicted and calculated deformations using the finite element method were discussed in Chapter 5 and Appendix D. The lateral movement for soil and wall will be discussed and compared in this section.

6.4.1 Lateral Displacement of the Soil Adjacent to the Wall

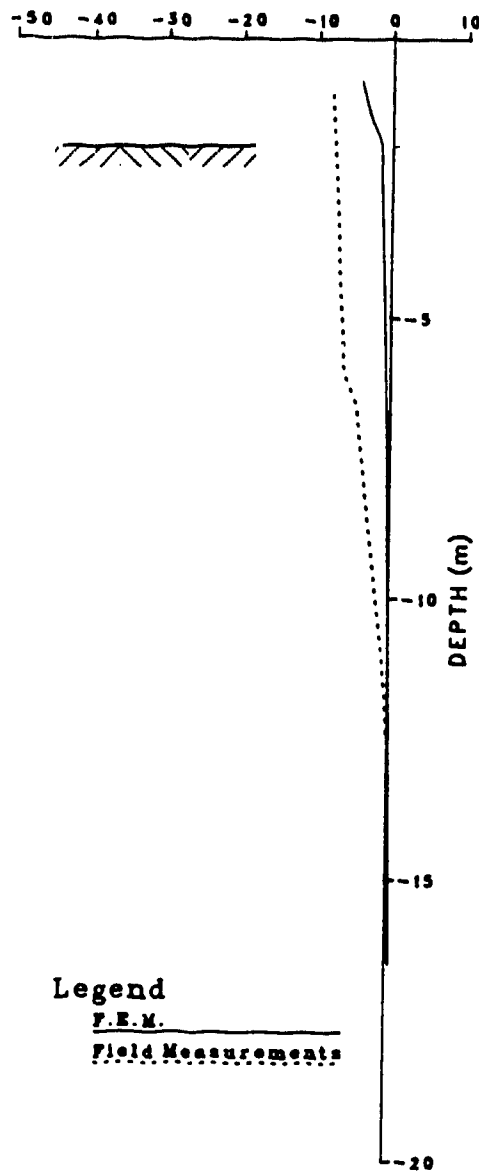
Figures 6.1 to 6.6 present a comparison between the measured and predicted displacement for the tunnel section. In Figure 6.1 the results of Step 4 of the numerical analysis and the field measurements corresponding to 1.85 m

excavation (without support) are shown. The predicted values underestimated the field measurements. This is explained by the fact that the finite element analysis is a plane strain analysis while the field measurements are influenced by the third dimension effect (i.e. in the numerical analysis, the wall and soil are not influenced by the stress relief as a result of excavating previous segments). Therefore it is expected that in the early stages of the finite element analysis, the horizontal soil deformation will be underestimated, with the degree of underestimation decreasing in later stages.

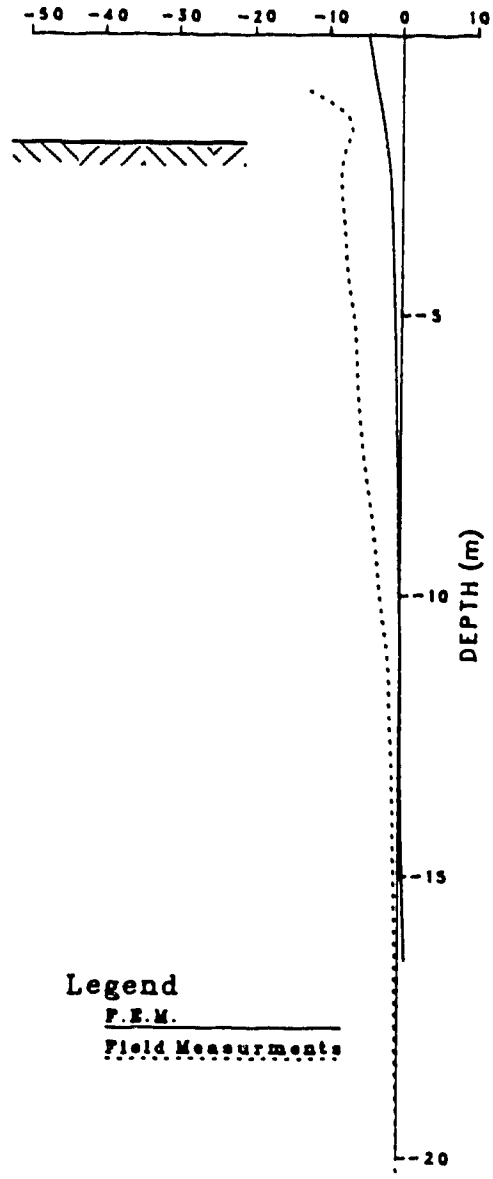
Figure 6.2 presents the results of Step 5 which confirms the 3-D mechanism. Figure 6.3 shows the predicted and measured values in close agreement accounting for the idealized conditions used in the numerical analysis and the actual field soil profile. Figures 6.4 and 6.5 present values for Steps 9 and 13, respectively. In general, the field measurements and the predicted movements are in agreement. The kink in the curve at an approximate elevation of 10 m may be attributed to the change in the soil type from silty clay to dense sand. The reading is constant at 26 mm for the 10 m of fill and silty clay layers. In the final case, a reduction of about 4 mm at the top part is reported while the lower part remained constant from Step 9 to 13. This may be attributed to the forces applied to the top portion of the wall during shuttering and pouring of concrete under pressure, and the use of vibrators at the

HORIZONTAL DISPLACEMENT (mm)
Tunnel Section

HORIZONTAL DISPLACEMENT (mm)
Tunnel Section



WALL DISPLACEMENT

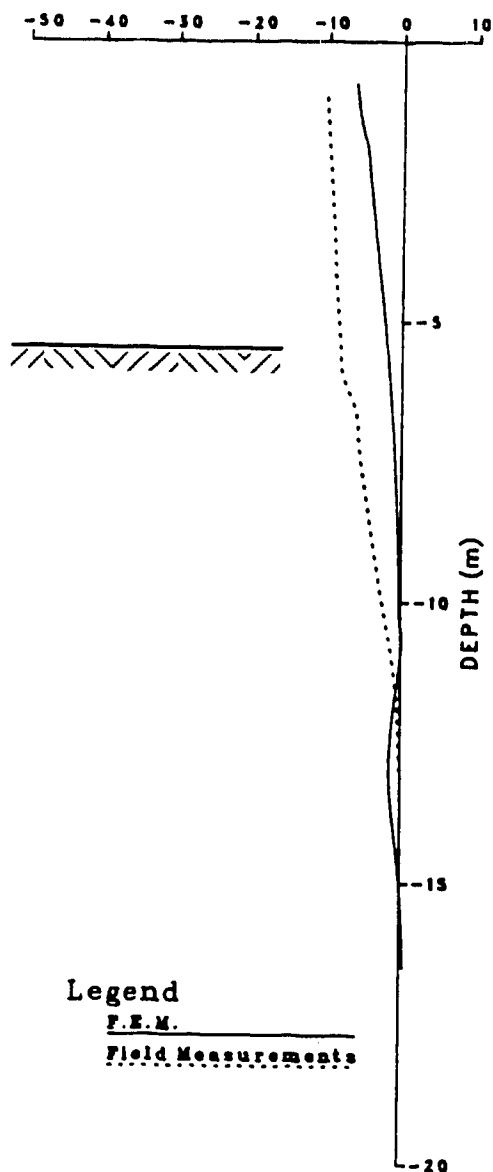


SOIL DISPLACEMENT

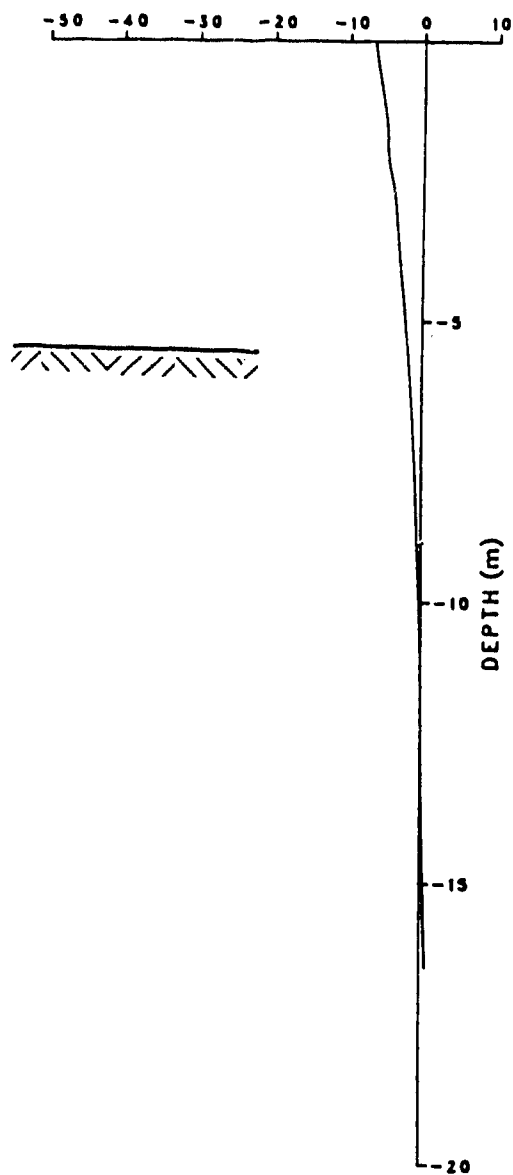
Figure 6.1 Field Measurements and Finite Element Results -
Step 4 - Tunnel Section

HORIZONTAL DISPLACEMENT (mm)
Tunnel Section

HORIZONTAL DISPLACEMENT (mm)
Tunnel Section



WALL DISPLACEMENT

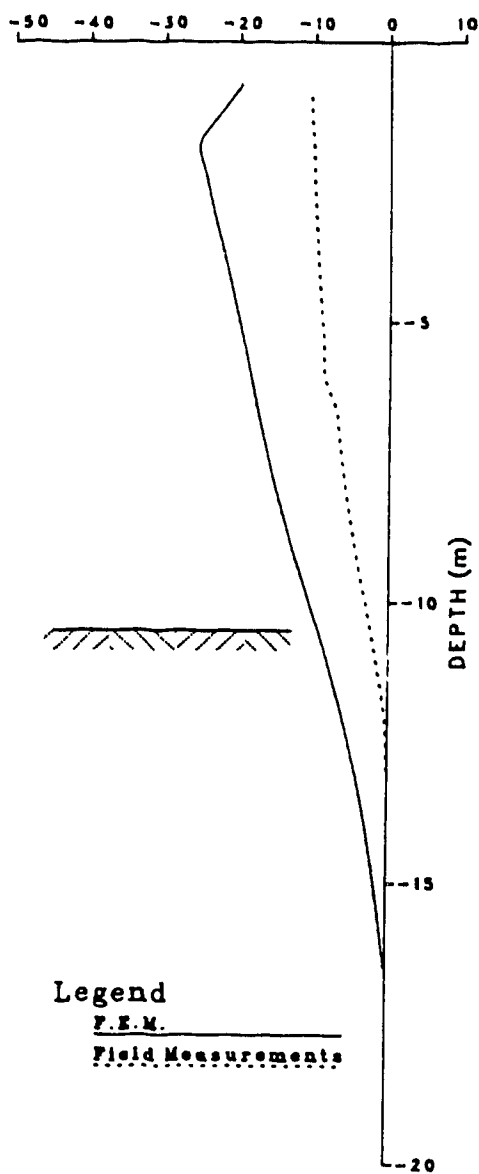


SOIL DISPLACEMENT

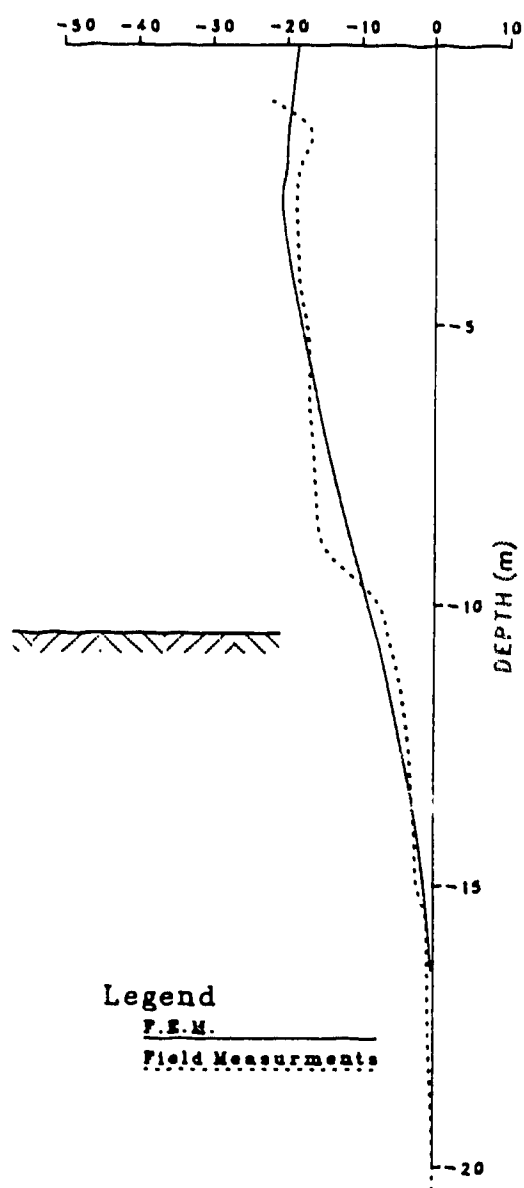
Figure 6.2 Field Measurements and Finite Element Results -
Step 5 - Tunnel Section

HORIZONTAL DISPLACEMENT (mm)
Tunnel Section

HORIZONTAL DISPLACEMENT (mm)
Tunnel Section



WALL DISPLACEMENT

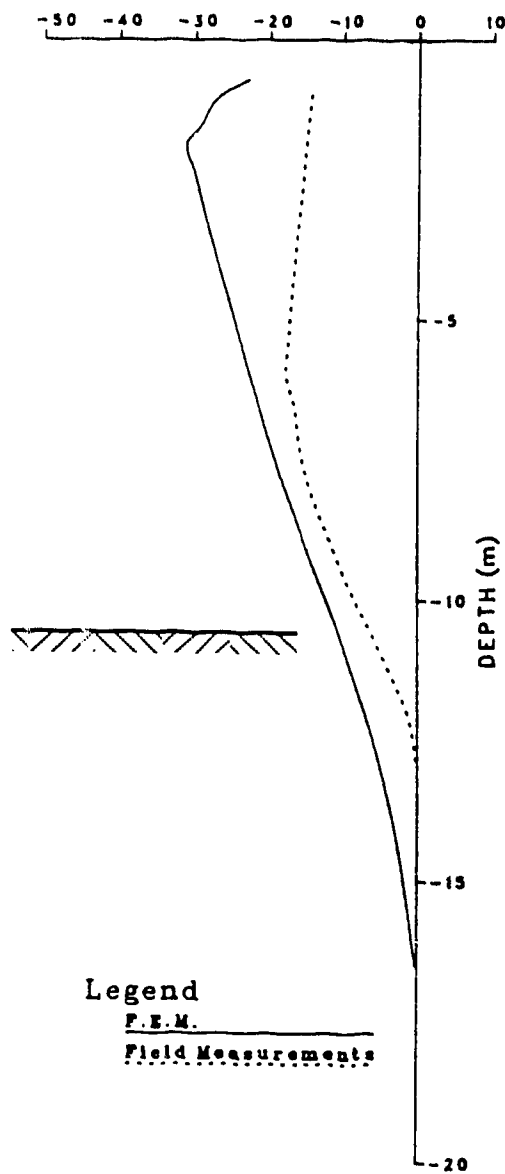


SOIL DISPLACEMENT

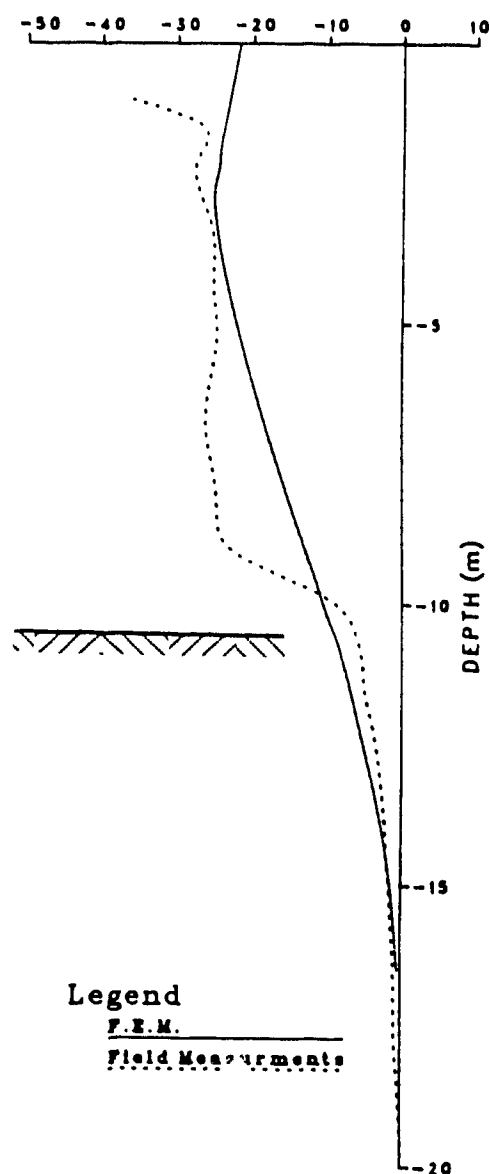
Figure 6.3 Field Measurements and Finite Element Results -
Step 7 - Tunnel Section

HORIZONTAL DISPLACEMENT (mm)
Tunnel Section

HORIZONTAL DISPLACEMENT (mm)
Tunnel Section



WALL DISPLACEMENT



SOIL DISPLACEMENT

Figure 6.4 Field Measurements and Finite Element Results -
Step 9 - Tunnel Section

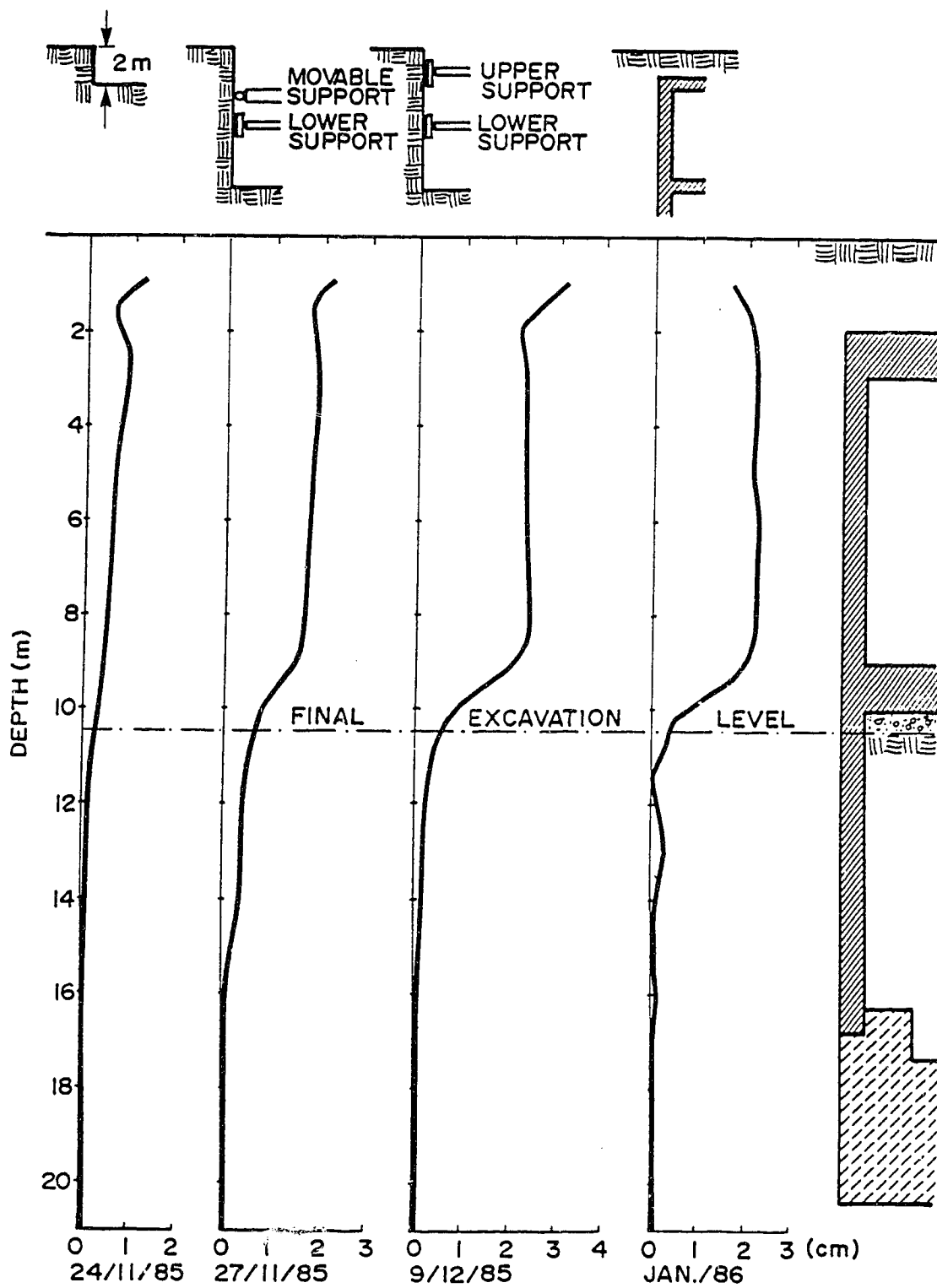


Figure 4.25 The Soil Lateral Displacement during Construction at the Tunnel Test Section

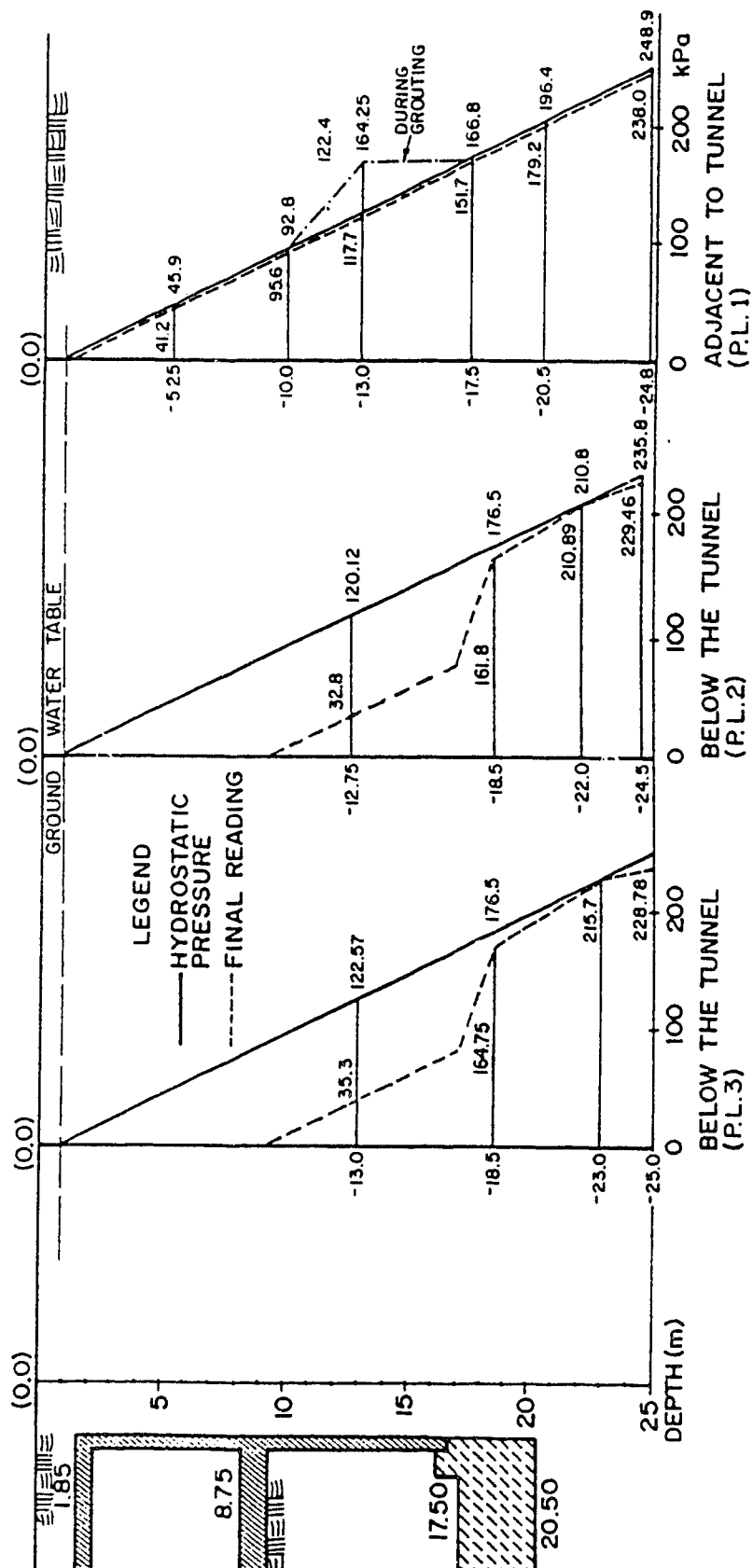


Figure 4.26 The Water Pressure Distribution at the Tunnel Test Section During and After

Excavation

4.7.1.4 Strain Gauge Measurements

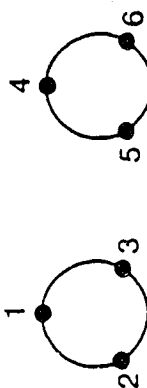
To monitor the normal forces acting on the temporary support system, one strut in each row was instrumented with 6 weldable strain gauges, three in each side as illustrated in the sketch appended to Table 4.2. This table contains the strain gauge readings for the entire project. Table 4.3 presents the readings for the embedded strain gauges in the roof and raft slabs. The calculations yielded an average of 37 tons acting on the upper and lower struts in the critical stage of excavation (i.e. only the struts are supporting the wall, just before introducing the raft and roof slabs). With a strut spacing of 2.5 m, a lineal distribution of 150 kN/m results.

To determine the normal forces acting on the roof and raft slabs, eight embedded strain gauges were installed in each slabs as illustrated in the cross-section appended to Table 4.3. The data yielded a normal force acting on the raft slab of approximately 70 kN/m in compression, while for the roof slab it was in the order of 80 kN/m in tension. These values proved to be two or three times less than the design calculations. The analysis was based on the data collected from strain gauges installed close to the wall (i.e. strain gauges No. 1, 2, 7 and 8) as the other cables were completely destroyed.

Table 4.2 Temporary Support Weldable Strain Gauge Readings at the Tunnel Test Section

Date	23/11/85	28/11	30/11	9/12	29/12	22/1/86	2/21
Gauge No.	Initial	Full load			After raft	After roof	Final
1	2,211	1,782	1,771	1,783	1,842	2,323	2,284
2	1,836	1,969	1,975	1,987	1,998	--	2,204
3	2,022	1,859	1,853	1,851	1,864	2,262	2,297
4	1,824	1,473	1,468	1,470	1,456	2,596	2,585
5	1,939	1,919	1,982	1,986	2,008	2,181	2,197
6	1,929	1,916	1,914	1,922	1,921	2,246	2,266
7	1,945	1,600	1,601	1,617	1,721	2,426	2,413
8	1,859	1,800	1,875	1,876	1,882	2,314	2,307
9	2,480	2,423	2,425	2,426	2,476	1,998	1,994
10	1,857	1,593	1,598	1,607	1,601	2,445	2,431
11	1,975	1,941	1,955	1,962	2,001	2,240	2,235
12	1,979	1,894	1,896	1,899	1,980	2,250	2,250

Upper Strut



Lower Strut

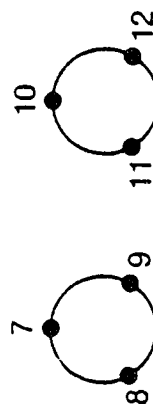
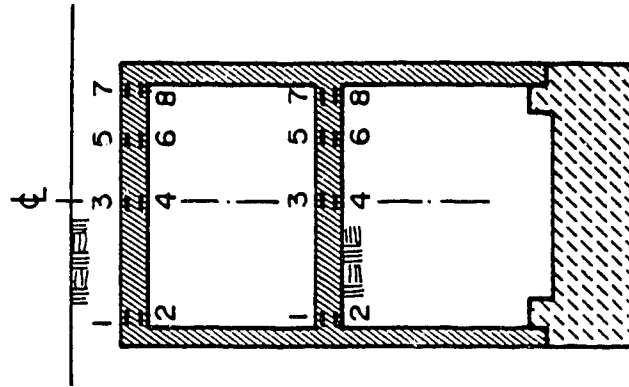
Deformation modulus of the steel used is 206.85×10^6 kPa

Table 4.3 Embedded Strain Gauge Reading at the Tunnel Test Section

Date	Raft			Roof		
	19/12/85	29/12/85	22/1/86	28/12/85	29/12/85	22/1/86
Gauge No.	Initial	After raft	Final	Initial	After raft	Final
1	3,028	2,653	2,649	2,771	2,701	2,662
2	2,511	2,798	2,830	2,682	2,141	2,042
3	2,218	2,134	2,122	2,333	1,905	1,828
4	2,376	2,381	2,387	2,488	2,421	2,292
5	3,255	2,658	2,675	2,352	2,409	2,260
6	2,531	2,878	2,945	2,433	2,822	2,747
7	2,507	2,702	2,735	2,392	23,72	2,390
8	2,279	2,193	2,206	--	2,573	2,522



4.7.2 The Station Test Section Measurements

The instrumentation layout for the station test section was similar to the running tunnel section. All the instruments had been successfully installed according to the schedule. At this Station, located at one of the busiest intersections in downtown Cairo, the traffic diversion design was inadequate for the traffic flow and many on site alterations had to be made. This resulted in a reduced work area for the instrumentation installation. With the destruction of instruments and blocked access (Plate 4.7) only one slope indicator, SI1 and the strain gauges were read.

4.7.2.1 Horizontal Displacement (Lateral Deformation)

The slope indicator, SI1, installed outside the station section adjacent to the cast-in-situ diaphragm panels was accessible despite the risk due to the continuous flow of traffic. Figure 4.27 presents a summary of the measured lateral deformation of the adjacent soil. The excavation was carried out under cover and the first profile reflects the deformation as a result of excavation with the support provided by the strut and the roof slab. The maximum horizontal displacement recorded at the raft level was approximately 11 mm. The second profile taken just after introducing the raft and the removal of the strut, shows a maximum horizontal displacement of 12-13 mm. The third profile presents the final and stabilized lateral deformation with a maximum of 13 mm. As a result of traffic

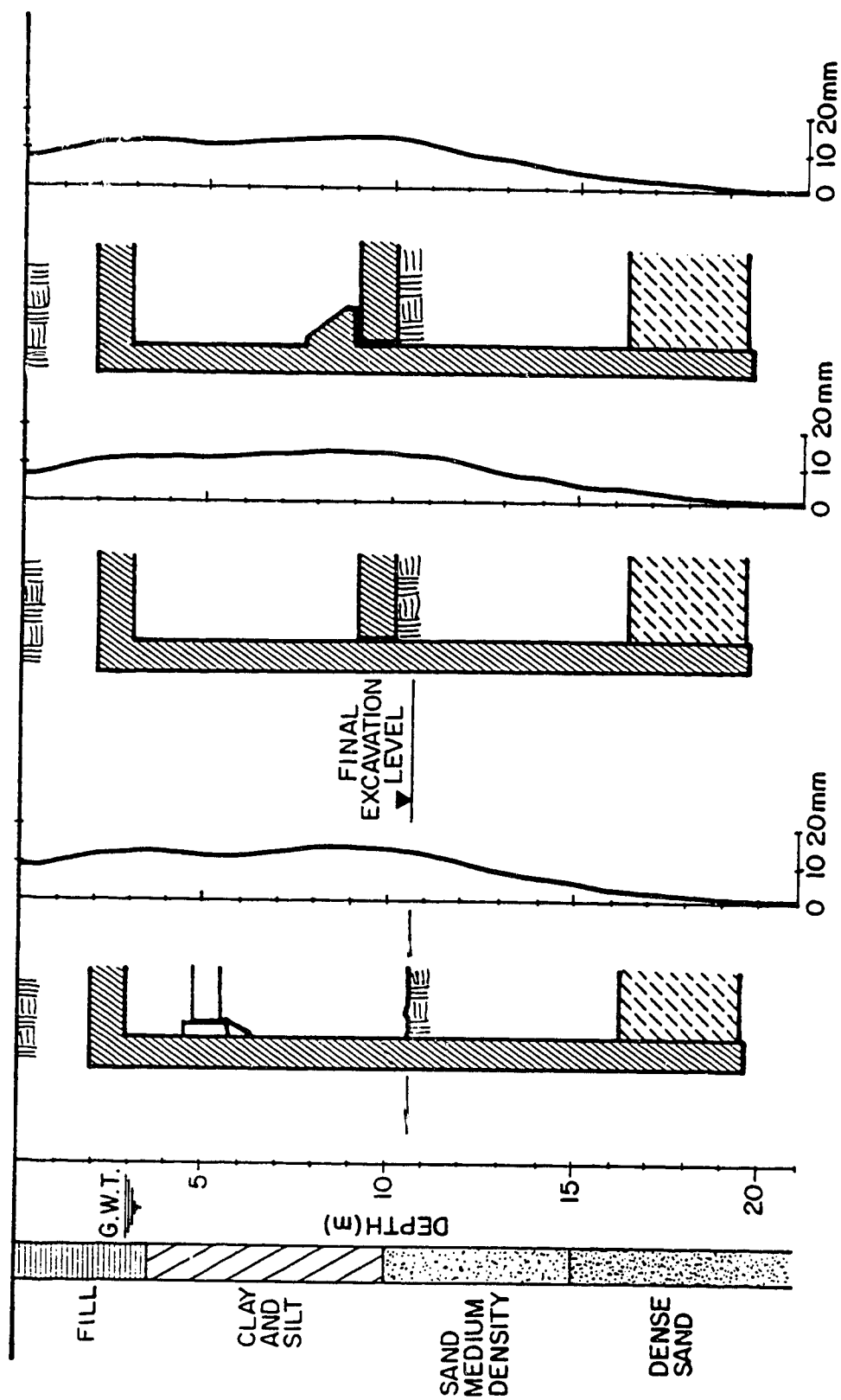


Figure 4.27 Soil Lateral Displacements at the Station Test Section

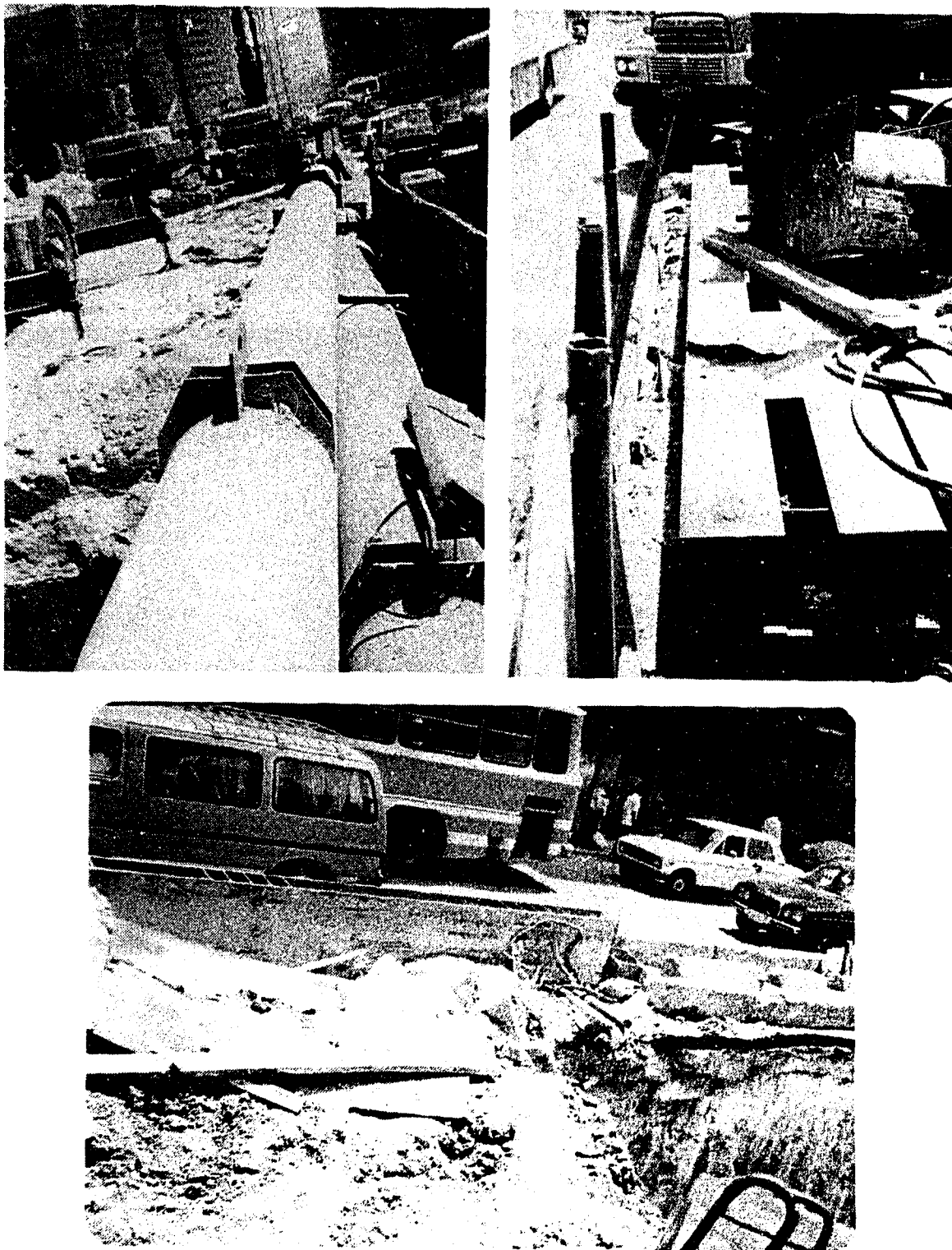


Plate 4.7 Obstacles Preventing Access to the Instruments at
the Station Test Section

diversion work, continued access to the instrument was not possible. The original location of SI1 was designed to be within the under cover excavated area, but changes in the traffic diversion plan resulted in it being placed approximately 3 m from the under cover area. This was accounted for during analysis.

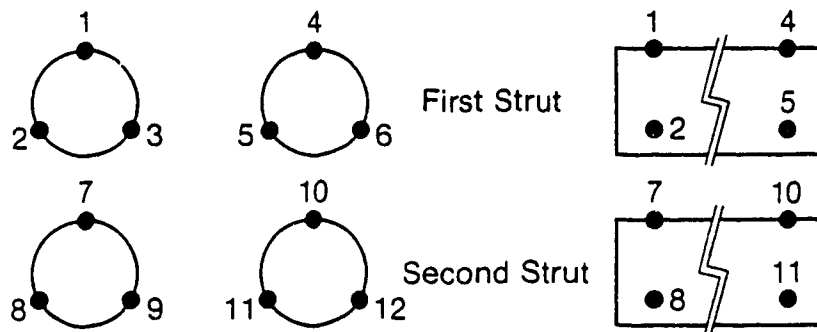
4.7.2.2 Strain Gauge Measurements

Two sets of weldable strain gauges were installed in two adjacent struts in the single row of temporary support. The arrangement is similar to that of the running tunnel section. Results are presented in Table 4.4. Analysis yielded an average normal force of 60 kN/m acting at the strut centre line. The spacing between the center line of each strut was 2.5 m and the total force carried by a single strut was 15 tons.

Embedded strain gauges were installed first in the roof slab and then the raft slab. All the cables were routed through a PVC pipe which led a locked box mounted on the diaphragm walls. The boxes were below the platform level and were accessible through a service manhole. Access to the instrument is still possible if required. Table 4.5 presents the recorded data. Interpolation of the data was difficult due to damages and repairs to the cables. The resulting estimates were 40 kN/m in compression and 40 kN/m in tension for the raft and roof slabs respectively.

**Table 4.5 Temporary Support Weldable Strain Gauge Readings
at the Station Test Section**

Date		25/8/86	28/8/86	7/9/86
Gauge No.		Initial	After Activating	Final
First Strut	1	4,033	3,184	3,186
	2	2,297	2,901	2,902
	3	1,864	2,386	2,387
	4	2,343	2,704	2,117
	5	533	757	759
	6	515	1,628	1,629
Second Strut	7	2,683	4,013	4,013
	8	2,740	1,889	1,809
	9	2,177	9,367	2,370
	10	663	9,657	2,657
	11	1,022	888	889
	12	9,199	1,331	1,334



5. THE NUMERICAL ANALYSIS

5.1 Introduction

The field measurements were evaluated using a three part finite element numerical analysis. It was necessary to use this procedure as it is not viable at the present to obtain direct field measurements for the required input parameters such as the lateral earth pressure. A total stress state was considered. The first step utilized the Plane Frame Truss (PFT) program, in which the problem was simplified modeled as beam and truss members. This initial analysis predicted the lateral earth pressure as a result of prescribed displacements. In the second step, the Soil Analysis by Finite Element Program (SAFE), was used. A linear elastic model represented the soil and each step of construction was simulated. This served as the preliminary analysis. In the final step, the analysis was repeated using a hyperbolic elastic model for the soil.

5.2 Material Properties and Parameters used in the Analyses

Laboratory tests were carried out to evaluate the soil parameters and properties to be used in the analyses. Appendix B provides the stress-strain curves for the soil. These provided the required parameters for the linear and hyperbolic models. Duncan et.al. (1980) describes the procedure used to determine the hyperbolic parameters. Deficiencies in the data were supplemented by data provided

in tables in Duncan et.al. (1980).

Concrete strength tests were conducted to determine its elastic properties. The properties for the steel were provided by the contractors in Report No. 403G AA-00A001C. Equivalent parameters were used in the finite element analyses. Wood properties were taken from the Timber Design Manual (1980).

In Tables 5.1 and 5.2, a summary of the properties of the materials used in the analyses are presented.

5.3 The Plane Frame Truss (PFT) Program

The PFT program was prepared by Dr. S. Simmonds (1981) at the University of Alberta. It is available through the Civil Engineering Computing Library at the University of Alberta.

The program is a two-dimensional analysis using the direct stiffness method and a linear elastic model. The simplified simulation of the geotechnical aspects and the geometry of the problem are the most important facets of this analysis.

In this study, the diaphragm wall was simulated by a beam, fixed at depth and supported by rollers at the roof and raft elevations. The soil was represented by a series of horizontal linked members. These varied in length, with the length increasing with increasing depth. The displacement is varied according to field measurements taken from the slope indicator installed inside the precast panel. The force

Table 5.1 Linear Elastic Model Parameters

Parameter/Material	γ_{sat} kN/m ³	γ_{dry} kN/m ³	σ_t kpa	E Mpa	ν
Fill	18.0	13.04		15,000.0	0.4
Silty Clay	18.3	13.04		20,000.0	0.4
Medium Density Sand	18.0			20,000.0	0.4
Dense Sand	20.0			22,000.0	0.4
Grouted Dense Sand	22.0		1,200.0	200,000.0	0.4
Concrete		25.0	3,350.0	31.25E7	0.2
Steel*		1.91	36,000.0	5.034E7	0.4
Wood*		0.6		10,000.0	0.4

* = equivalent or fictitious parameters

γ_{dry} = dry unit weight

E = elastic modulus

γ_{sat} = saturated unit weight

σ_t = tensile strength

ν = Poisson's ratio

Table 5.2 Hyperbolic Model Parameters

Parameter Material	K	K_u	n	R	C kPa	ϕ°	K_b	m
Dry fill	200	450	0.79	0.69	60	33	120	0.37
Wet fill	225	450	0.79	0.69	60	33	120	0.37
Dry silty clay	225	450	0.45	0.7	60	32	120	0.37
Wet silty clay	225	450	0.45	0.7	60	32	140	0.37
Medium density sand	250	450	0.4	0.7	-	25	140	0.2
Dense sand	300	500	0.4	0.7	-	30	150	0.2

P_a = Atmospheric pressure = 101.33 kPa

k = Modulus number

R_f = Failure ratio

ϕ = Angle of shear resistance

m = bulk modulus exponent

K_u = Unloading modulus number

n = Exponent number

C = Cohesion

K_b = Bulk modulus number

required to cause the strain increases as the length of the member decreases. The simplified geometry for the case of the running tunnel is presented in Figure 5.1.

The properties of the precast panel were assigned to the beam and soil properties were assigned to the linked members. The linked members are assumed to be hinged at the wall and at a point located away from the zone of influence. This zone is represented by a 45° line drawn from the fixed end of the wall as shown in Figure 5.1. This ensured that the free end of the linked members was not influenced by the deformation of the soil. The measured horizontal displacements were prescribed to the two roller supports and a point midway between them.

The program calculated the forces in each link member and the resulting horizontal displacements were compared with the measured ones. Figure 5.2 presents the computed net lateral earth pressure diagram. These results will be compared with the output from the SAFE program which uses a hyperbolic soil model. This will allow an evaluation of the simpler model. The advantage of the PFT program are its simplicity, economy and speed. This program may be run on a microcomputer which lends itself to on site use. The lateral earth pressure may be calculated within minutes of the deformation readings being taken. Site problems may be evaluated without running a highly sophisticated, time consuming finite element program.

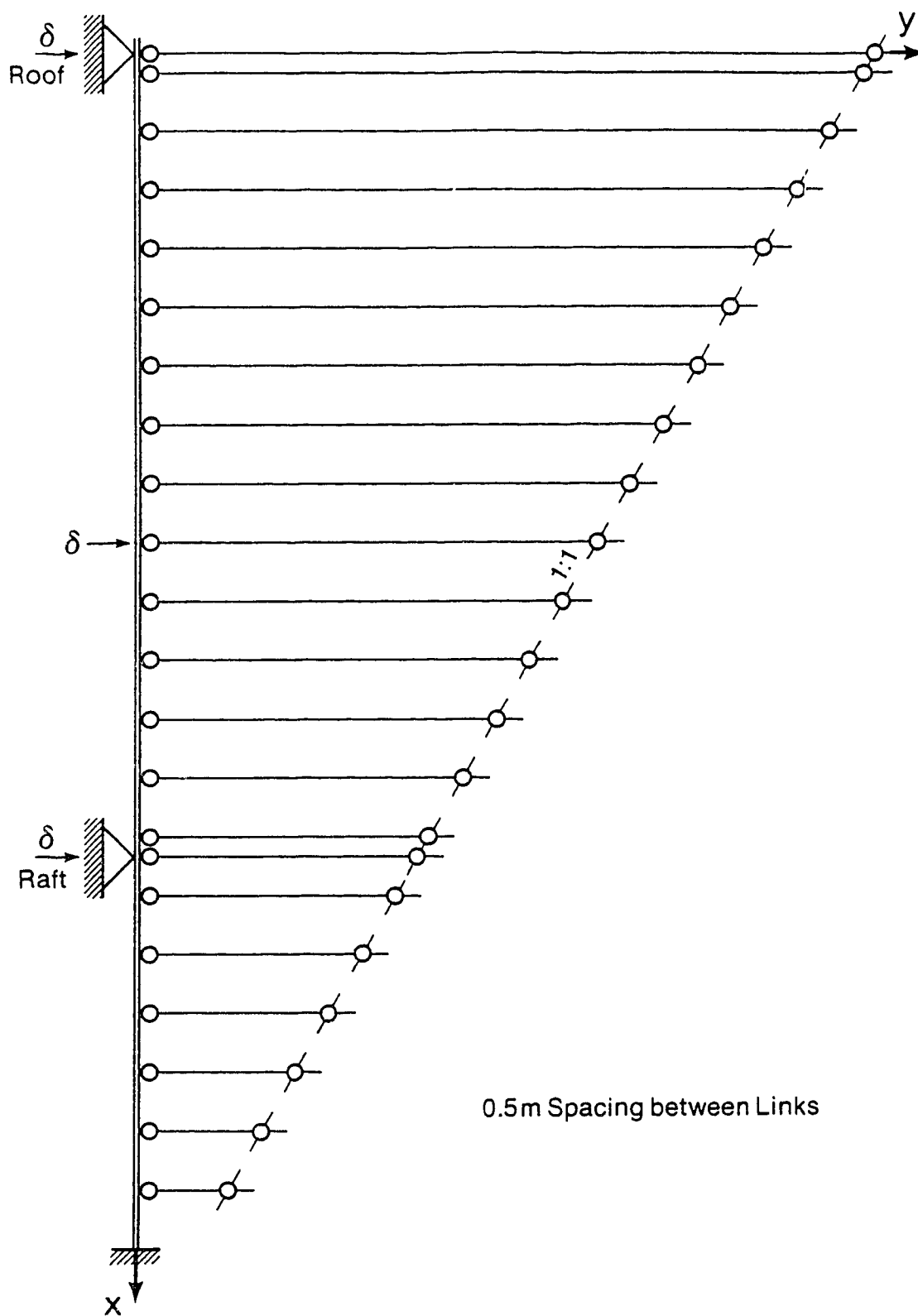


Figure 5.1 Simplified Geometry for Use in the PFT Program

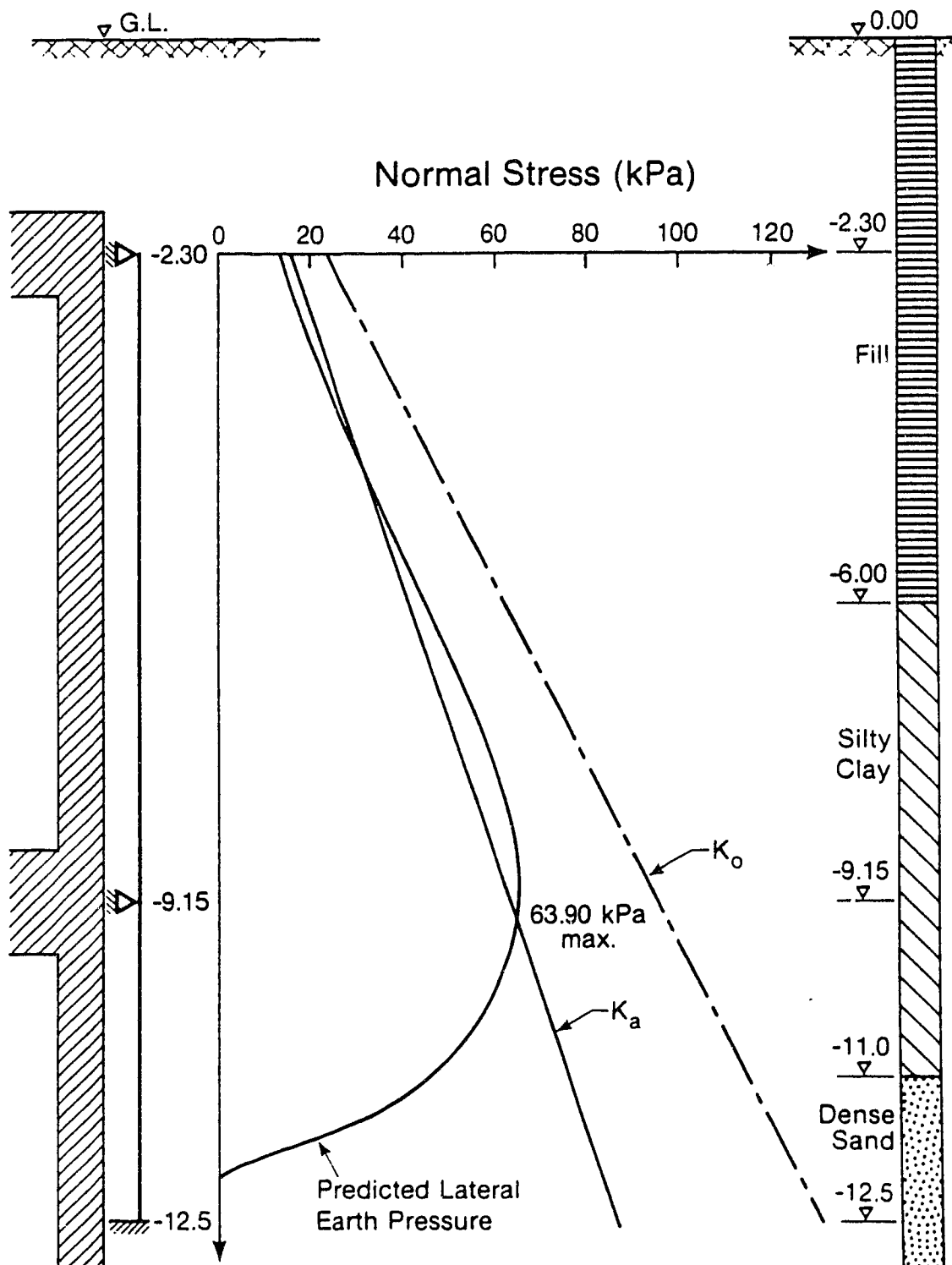


Figure 5.2 Net Lateral Earth Pressure as Predicted by the PFT Program

The program has been successfully used by Evison (1988) in the analysis of a ring and spring model for tunnel liner design. A comparison of the PFT program with a complicated finite element program was performed by Simmonds (1988) and the conclusion was in favour of the PFT program due to the time and cost savings.

5.4 The Soil Analysis by Finite Element Program (SAFE)

The finite element program chosen for this study was SAFE, "Soil Analysis by Finite Element". It was developed by Chan (1986) at the University of Alberta. A user manual Chan (op.cit) and Chan and Chan (1988) is provided by the Civil Engineering Department.

The program uses isoparametric elements with six or eight nodes. It is capable of conducting one, two or three dimensional linear or non-linear elastic and elastic-plastic analyses, including various yield criteria. The analyses may be performed either in terms of total or effective stresses. SAFE includes supplementary programs for mesh generation, plotting and developing contour lines.

The program has been used in analysing different types of geotechnical problems. It is capable of handling complex geotechnical behaviour. SAFE was used in the deformation study of the LRT Government Station, Edmonton, Alberta (Chan et.al., 1987).

In order to gain a basic understanding of the behaviour of the soil around the structure, a series of linear elastic

analyses were performed. The excavation was represented in multiple stages to simulate a more realistic situation.

The non-linear analyses using the hyperbolic model represents the stress-strain behaviour of each material in a more realistic manner. The hyperbolic model, introduced by Duncan and Chang (1970) has been used because of its simplicity. The parameters for the model can be determined from triaxial test results. As a result of the stress path dependence of material behaviour, a realistic unloading sequence (i.e. excavation) is a fundamental requirement in order to obtain correct and representative results.

5.4.1 Linear Elastic Isotropic Model

In general, the stress strain relationship of a material can be described using the following expression:

$$\sigma_{ij} = C_{ijkl} \epsilon_{kl} \quad [5.1]$$

where C_{ijkl} is the constitutive tensor. It is a function of 81 parameters. These can be reduced to two parameters by assuming the symmetry of the stress and strain tensors and the existence of elastic potential and isotropy. Thus, the constitutive tensor may be expressed as:

$$C_{ijkl} = \frac{E\nu\delta_{ij}\delta_{kl}}{(1+\nu)(1+2\nu)} + \frac{E\delta_{ik}\delta_{jl}}{1+\nu} \quad [5.2]$$

where E is the elastic modulus

ν = poisson's ratio

δ_{ij} = the kronecker delta = $\delta_{ij} = 1$ if $i=j$ and

$\delta_{ij} = 0$ if i not equal to j .

The elastic modulus and Poisson's ratio are related to the bulk modulus, B , by

$$B = \frac{E}{3(1-2\nu)}$$

and to the shear modulus, G , as

$$G = \frac{E}{2(1+\nu)}$$

5.4.2 Non-Linear Elastic Hyperbolic Model

The proposed hyperbolic model by Duncan and Chang (1970) has been used for its simplicity and its wide application. The required parameters are determined using triaxial test results. The initial modulus E_i for the hyperbolic model is dependent on the confining pressure, σ_3 . Janbu (1963) suggests that

$$E_i = K P_a \left(\frac{\sigma_3}{P_a} \right)^n \quad [5.3]$$

where σ_3 = minor principal stress

P_a = atmospheric pressure

K = modulus number

n = exponent number

The hyperbolic relationship may be written as:

$$(\sigma_1 - \sigma_3) = \epsilon / \left[\frac{1}{E} + \frac{\epsilon R_f}{(\sigma_1 - \sigma_3)_f} \right]$$

where ϵ = axial strain

σ_1 = major principle stress

$(\sigma_1 - \sigma_3)_f$ = deviator stress at failure

R_f = the failure ratio

As the non-linear analysis is performed in steps, it is necessary to determine the incremental stiffnesses of the material. The tangent modulus can be expressed as:

$$E_t = \left[1 - \frac{R_f(\sigma_1 - \sigma_3)(1 - \sin\phi)}{2c \cos\phi + 2\sigma_3 \sin\phi} \right]^2 K P_a \left(\frac{\sigma_3}{P_a} \right)^n \quad [5.4]$$

where ϕ = angle of shearing resistance

c = cohesion

For the case of unloading, a higher modulus E_{ur} is used and may be expressed as:

$$E_{ur} = K_{ur} P_a \left(\frac{\sigma_3}{P_a} \right)^n$$

where K_{ur} = unloading modulus = constant.

The unloading modulus, E_{ur} , will vary depending on the confining pressure.

As the tangent bulk modulus is dependent on the confining pressure, it may be expressed as

$$B_t = K_b P_a \left(\frac{\sigma_3}{P_a} \right)^m$$

where K_b = the bulk modulus number

m = the bulk modulus exponent

More details are found in the SAFE user manual and Duncan and Chang (1980). It should be noted that one of the major limitations of this model is its inability to sustain tension. To circumvent this, the elements which are susceptible to tension are made linear elastic. Also, some numerical problems may occur during unloading. To overcome these, SAFE always performs an elastic analysis using the unloading modulus in the first iteration of every loading step.

The improved Euler scheme was selected for the stress calculation to achieve better results and optimize the use of computer time. The number of integration points was 2×2 . To obtain greater accuracy, the strain increments were subdivided into intervals in calculating stresses; a typical value of 10 was found to be satisfactory.

5.4.3 Construction and Excavation Simulation for F.E.M.

Analysis

After establishing the parameters required for the numerical analysis, a finite element mesh was constructed for each test section. As the final depth of excavation was 10.5 m from the ground surface for the running tunnel test section, a mesh of 40 m by 40 m was found to be adequate for the analysis. This satisfied the ratio of four times the height and 3 times the depth as suggested by Desai and

Christian (1977). The mesh used for the linear and non-linear analysis is shown in Figure 5.3. It is composed of 300 quadrilateral isoparametric elements with 8 nodes for a total of 981 nodes.

The excavation is simulated in the finite element method by deleting the elements within the excavated zone and the soil support is simulated by changing the element properties to represent the structural support.

The mesh used for the station test section was 60X50 m as the station span is almost double that of the tunnel section. It is composed of 299 quadrilateral isoparametric elements with 8 nodes for a total of 975 nodes, as shown in Figure 5.4.

5.4.4 The Running Tunnel Test Section - Stages of Analysis

The construction and excavation procedure was simulated in the analysis in several stages, with each stage representing one step of the procedure. A total of 13 stages were used.

5.4.4.1 Step (1) - The In Situ Stress Generation

A linear elastic two dimensional plane strain analysis was used in this step. The initial in situ stress field was generated using the switch-on-gravity process. The stress were calculated due to the application of gravity forces which are dependent on the unit weight of the material. The vertical stresses were equal to the unit weight multiplied by the depth at any given point. The horizontal stresses

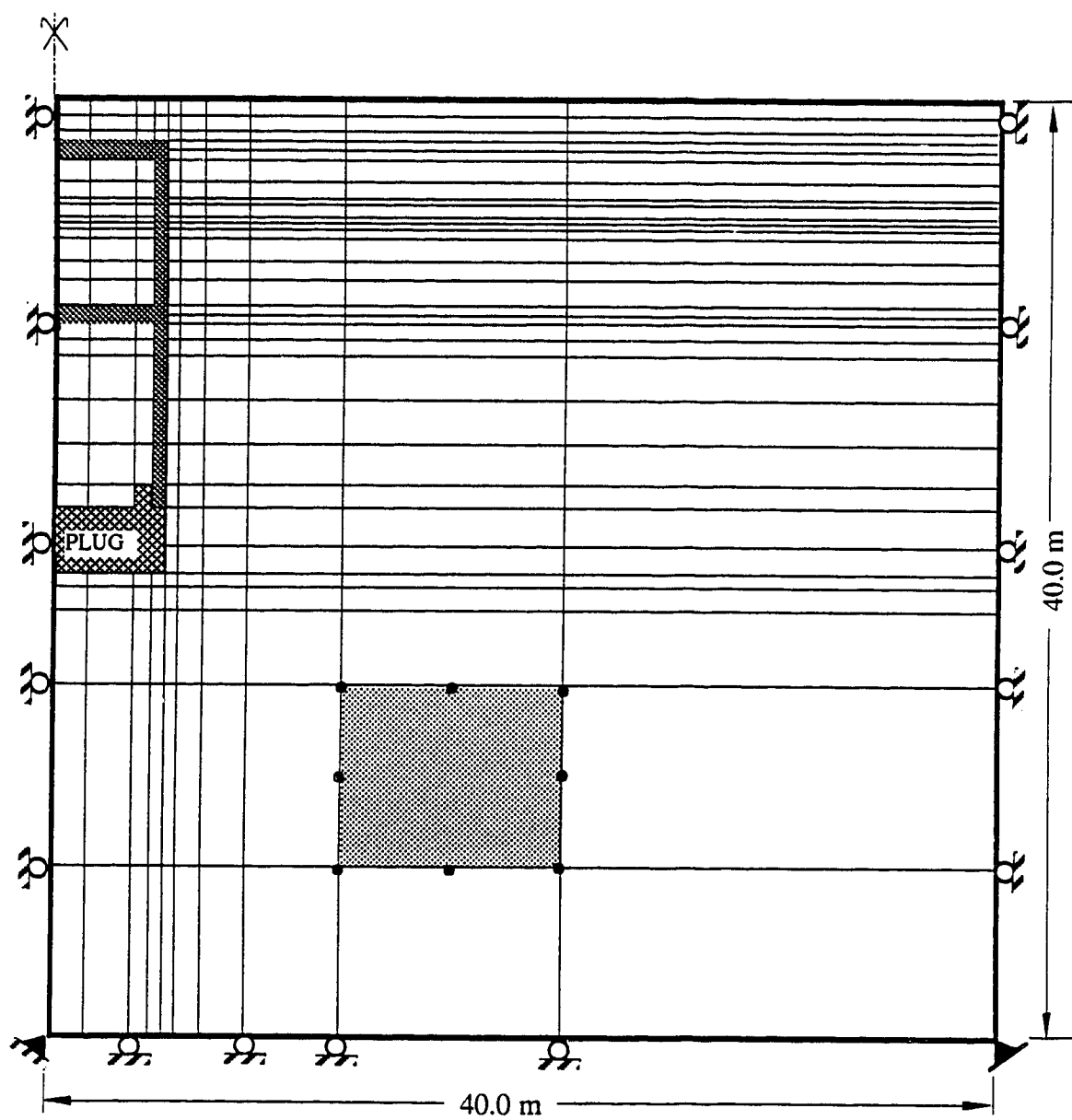


Figure 5.3 Running Tunnel Test Section Finite Element Mesh

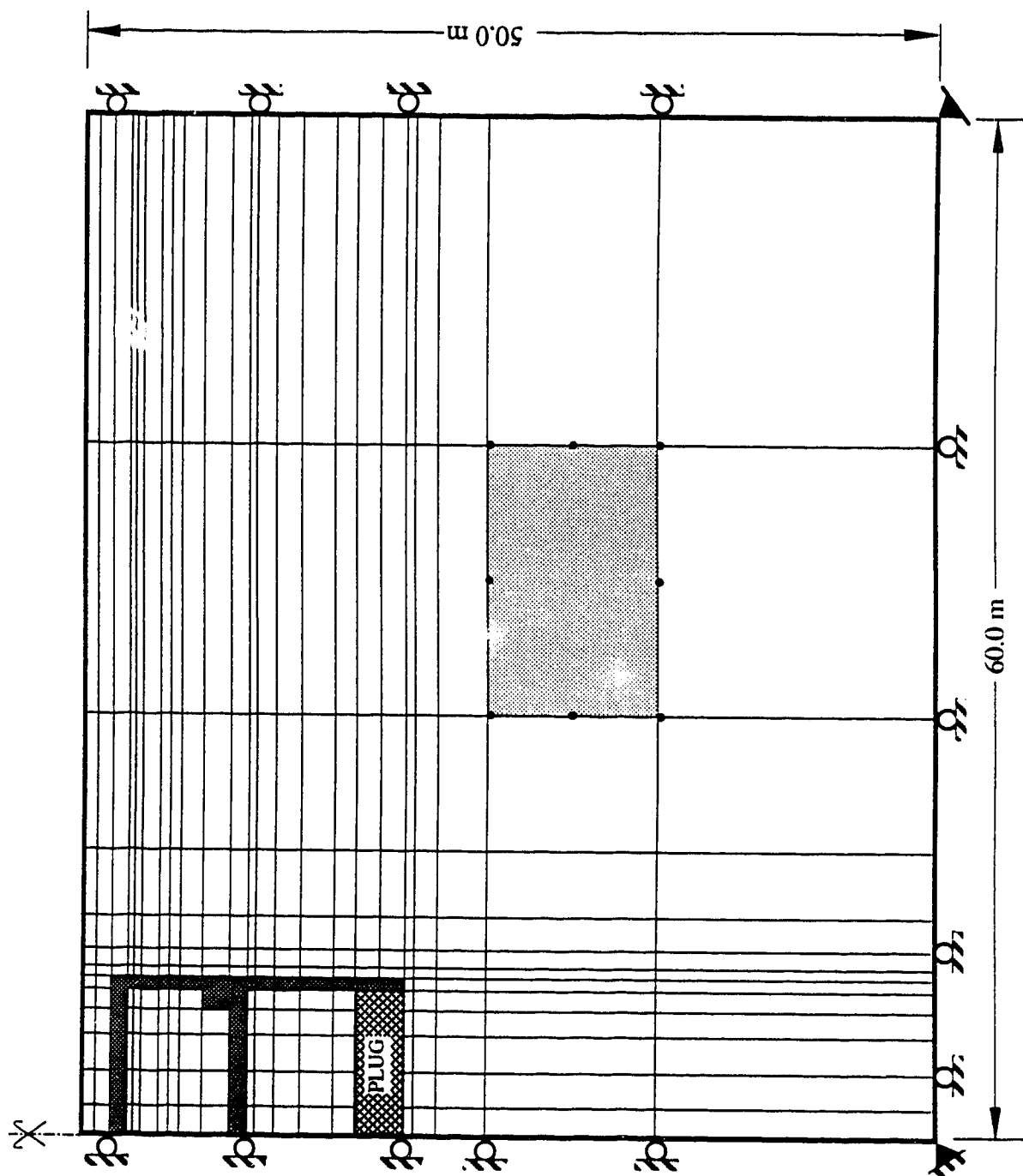


Figure 5.4 Station Test Section Finite Element Mesh

were calculated as a function of Poisson's ratio, ν . For homogeneous, isotropic linear elastic material under the condition of no lateral movement, the coefficient of earth pressure at rest, K_0 is equal to $\nu/(1-\nu)$. From this, the horizontal stress may be calculated. The calculated displacements and strains were reset to zero after this stage of analysis only.

5.4.4.2 Step (2) - Slurry Trench and PreCast Panel

After generation of the in situ stresses and setting the strains and displacements to zero, the material properties were changed from linear elastic to non linear elastic-plastic. A two dimensional plane strain analysis in terms of total stress analysis was performed. This was achieved by changing the material model from linear to hyperbolic elastic model number 11. To avoid the tension problems associated with the use of the hyperbolic model, the upper (surface) row of elements were assigned the linear elastic model properties.

The slurry trench was excavated by deleting the element columns in the finite element mesh. The elements were reintroduced with the material properties for concrete and grout material. This was done in the same step of analysis. Only the soils were assigned hyperbolic model properties.

5.4.4.3 Step (3) - Grouting for the Plug and Dewatering

The grouting operation was simulated in the finite element analysis by changing the plug zone elements to the

grout properties by changing the material number.

The excavated zone was dewatered by pumping the water out through the drain port which had been used to measure the permeability of the grouted zone. The material parameters for this zone was changed to those corresponding to dry soil.

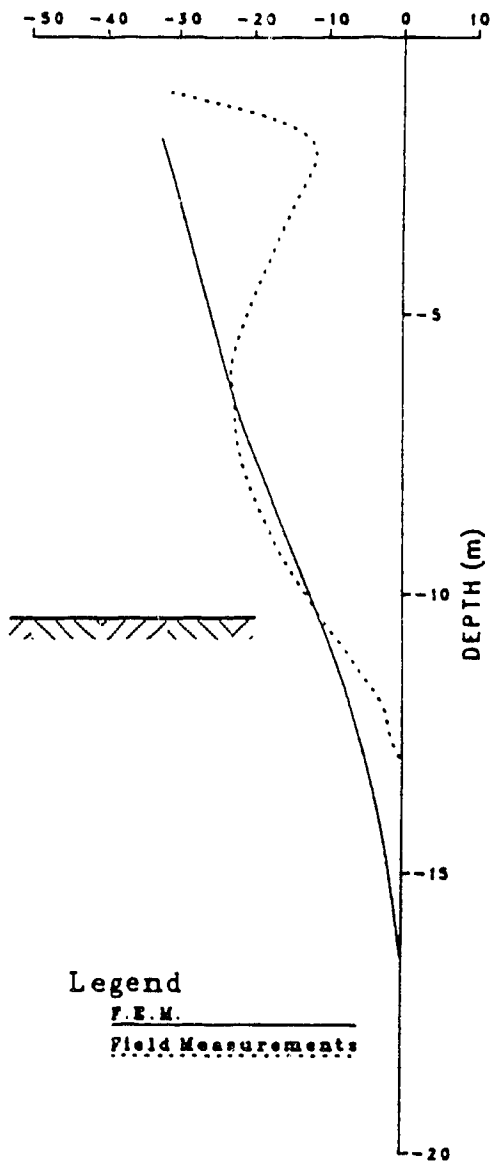
5.4.4.4 Step (4) - Starting the Excavation

The excavation began by excavating to -1.85 m. The first four elements of the first row from the left side, and the first three elements from the second and third row were deleted to simulate the excavation. The exposed row of the hyperbolic model was changed to linear elastic model.

5.4.4.5 Step (5) - Excavating to Install the Mobile Frame

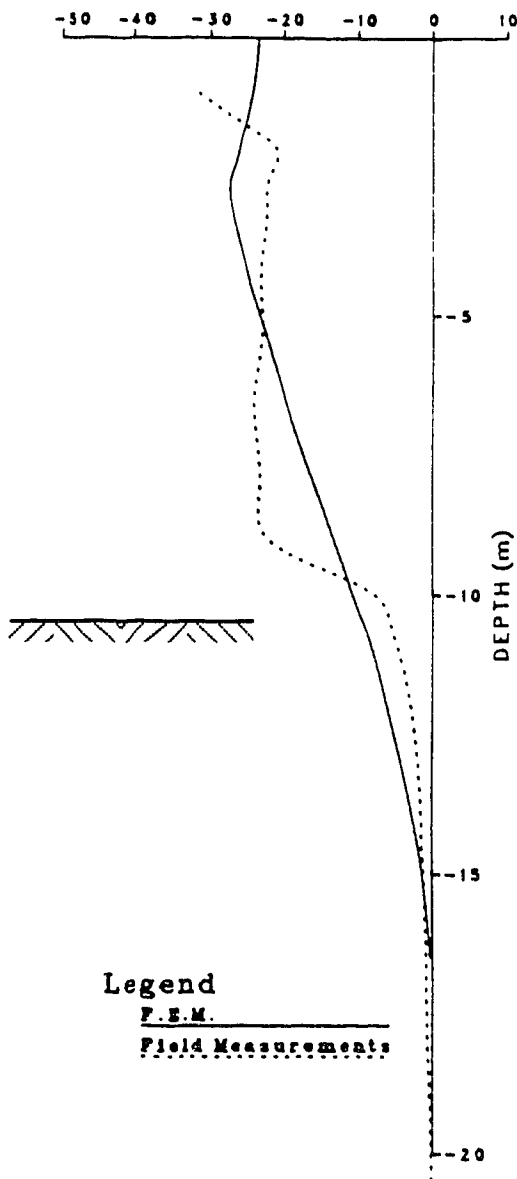
The excavation continued to the appropriate level to allow for the installation of the first temporary support system (mobile frame). As explained above, rows of elements were deleted to just below the frame level. This allowed the mobilization of the support to the precast diaphragm walls during excavation. The support was simulated by reintroducing the corresponding row with new material properties. The element connecting the frame with the diaphragm wall was assigned the wood properties to introduce the effect of the use of the wooden wedge to activate the support system. The effect of the sand pillows was neglected. The first row to the excavation base was assigned

HORIZONTAL DISPLACEMENT (mm)
Tunnel Section



WALL DISPLACEMENT

HORIZONTAL DISPLACEMENT (mm)
Tunnel Section



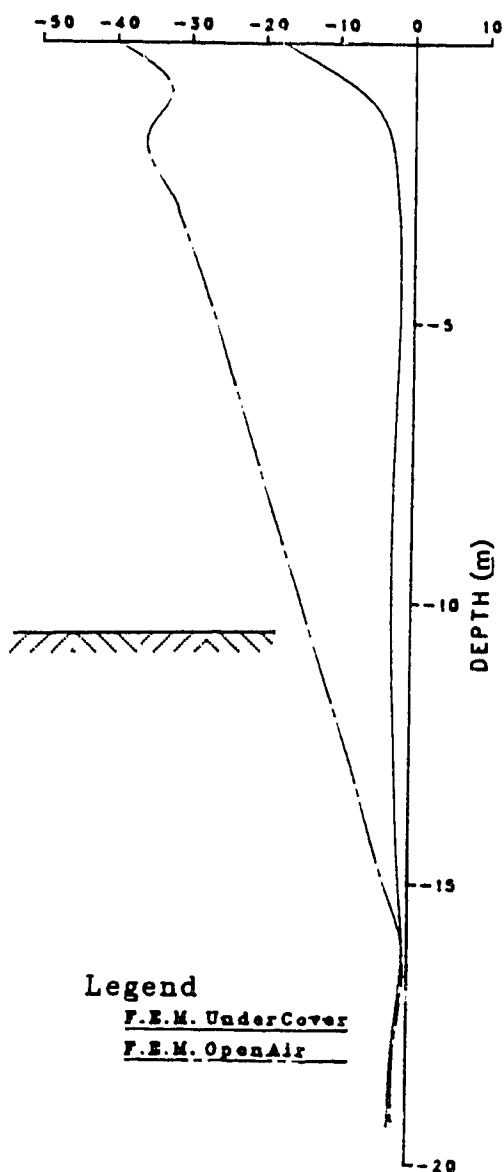
SOIL DISPLACEMENT

Figure 6.5 Field Measurements and Finite Element Results -
Step 13 - Tunnel Section

free end of the cantilever wall.

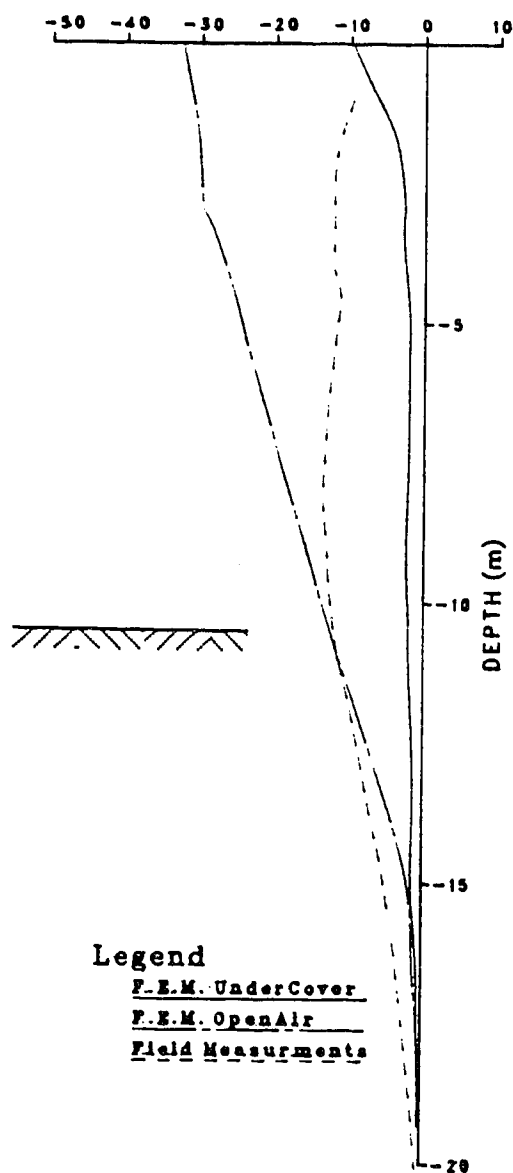
In Figure 6.6, the results for the final case of the station section are presented as an undercover and open air excavation. The field measurements agreed with the portion below 10 m elevation with the open air analysis and shifted toward the undercover results at greater depths. This can be explained as the final location of the slope indicator, No. SI1, was 3 m from the edge of the undercover excavated zone and less than 10.5 m depth, which is the depth of the excavation. The horizontal movement calculated in the undercover analysis was considerably less than the open air analysis. The performance of the open air excavation can be improved by the use of two rows of struts at different elevations instead of the single row used in the analysis. This leads to a reduction in the magnitude of the lateral movement. The results reported by Wood and Perrin (1984) and Tominaga et al. (1985) showed that finite element results are slightly less than field measurements. The same conclusion was reached by other researchers (Konokike and Ono, , and Fang, 1987). Fang analysed a diaphragm wall constructed in Taipei in clays of about 14 m depth excavation. He assumed a lateral earth pressure diagram and used it to predict the strut loads and moments acting on the diaphragm wall. The gap between the measured and predicted values is considerably narrower but usually the measured values form an envelope for the predicted ones. This may be applied to similar site conditions and wall types.

HORIZONTAL DISPLACEMENT (mm)
Station Section



WALL DISPLACEMENT

HORIZONTAL DISPLACEMENT (mm)
Station Section



SOIL DISPLACEMENT

Figure 6.6 Field Measurements and Finite Element Results -
Station Section - Final Case

6.4.2 Lateral Displacement of the Walls

Figures 6.1 to 6.5 show that the field measurement of the lateral displacement of the wall at the start of excavation was greater than the predicted values. As shown in Figure 6.4, at Step 9, the observed values begin to approximate the predicted profile. The final profile is presented in Figure 6.5. There is some deviation between the two profiles in the top section. This is only found in the final case, and occurs between Steps 9 and 13. In Step 11, a short temporary steel sheet pile was hammered in place to allow for the shuttering and water proofing of the roof slab. Finno et al. (1988) stated that driving sheet pile walls into saturated clays to provide temporary support for a braced excavation can lead to excessive pore pressure generation, which appears to be in the same order of magnitude as the applied forces in their study. The lateral extent appears to be greater. They attribute this phenomenon to the difference between the plane strain conditions representative of sheet pile walls and the axisymmetric conditions representative of piles. In this study, the driving force spread to a large extent forming horizontal and lateral hydrostatic forces during the installation operation. This influence was not taken into account in the finite element analysis because of the uncertainty of the magnitude of the driving force and its lateral extent. Generally, the predicted and measured deformation patterns show that the installation sequence of the bracing system

influences the pattern of movement. In Figure 6.6, a comparison between the open air and undercover excavation procedures is presented. The undercover procedure controls and minimizes the lateral deformation of the soil and wall. The open air excavation procedure allows greater lateral movement, but the magnitude is in the order of 10's of millimeters which is considered small compared with sheet pile walls. The maximum lateral movement for the wall was approximately 26 mm which considering the type of temporary support is small. Struts were installed to prevent any additional deformation, as the major part of the deformation occurred before their installation.

For the case of the open air excavation, the lateral movement pattern is similar to the free end cantilever deformation pattern while the undercover pattern is close to a beam supported at the top by the roof slab and fixed at the bottom by the effect of penetration depth into the unexcavated area. Cappellari and Ottaviani (1981) reported similar vertical profiles of horizontal displacements for a precast concrete diaphragm wall in Italy. Their work concentrated on the bending moments acting on the wall inside the excavation. The applied forces are strut loads not lateral earth pressure forces as the wall was excavated from both sides. Small deformations were recorded even though the finite element analysis was linear elastic for the cemented sand. They stated the diaphragm wall, especially the precast panels, were very promising and would

be recommended for future subway construction using the cut-and-cover method. They also reported that the simulation of earth pressure using hydraulic jacks was not satisfactory but was correct for the bending moments in the panel. Rott and Veder (1980) reported a similar wall deformation profile for a cast-in-place diaphragm wall in Vienna. The excavation depth was approximately the same as the open air excavation analysis, with the struts installed about 1 m below the street level. It was similar to the undercover excavation in that the roof slab acted as a permanent strut. Rott and Verder (op.cit.) used slope indicators to observe the deformation, and calculated the bending moments. The reliability of this method of calculation for the bending moments has been questioned. Wolosick and Feldman (1987) proved that it only gives reasonable results if it is used with flexible steel structures such as sheet piles as the deflections in this case are large and the moment of inertia can be reliably determined at each section of calculation. The observed maximum lateral displacement was in the order of 5 mm compared with 3 mm predicted for the station analysed as an undercover excavation. Figures 6.5 and 6.6 show that the predicted lateral displacement for the tunnel and station sections are in close agreement regardless of the differences in wall stiffness for wall thicknesses from 450 mm to 800 mm. This leads to the conclusion that the wall stiffness does not significantly influence the lateral deformation of the wall. Peck (1969) reported that the

stiffness of ordinary soldier piles and steel sheet piling, including the heavy sections, is not a significant factor affecting the magnitude of the lateral movement of the wall. This study showed that Peck's remarks extend to the performance of the diaphragm wall. It must be noted that the tunnel section has two rows of struts while the station section was analysed with one row of struts to allow the analysis to be conducted using the same finite element mesh for two different excavation procedures.

6.5 Vertical Displacement of the Soil (Settlement Trough)

The vertical displacement of the surrounding soil was observed in the field by means of settlement points and mulitpoint extensometers. Figure 6.7 presents the corresponding settlement trough for each step of the analysis and the final field measured settlement trough. There was close agreement between the predicted and observed values. The predicted troughs showed deformation to a distance of 40 m from the excavation, whereas the field measurements showed no effect at a distance of 10-15 m from the wall. It must be noted that the field measurements were accurate to ± 0.5 mm and that the values predicted by the finite element were less than this. The general trend of the settlement troughs showed reasonable agreement with the results reported by Medeiros (1979) and Shi et al. (1987). A maximum of 15 mm was recorded in the field while the maximum predicted was 16.75 mm.

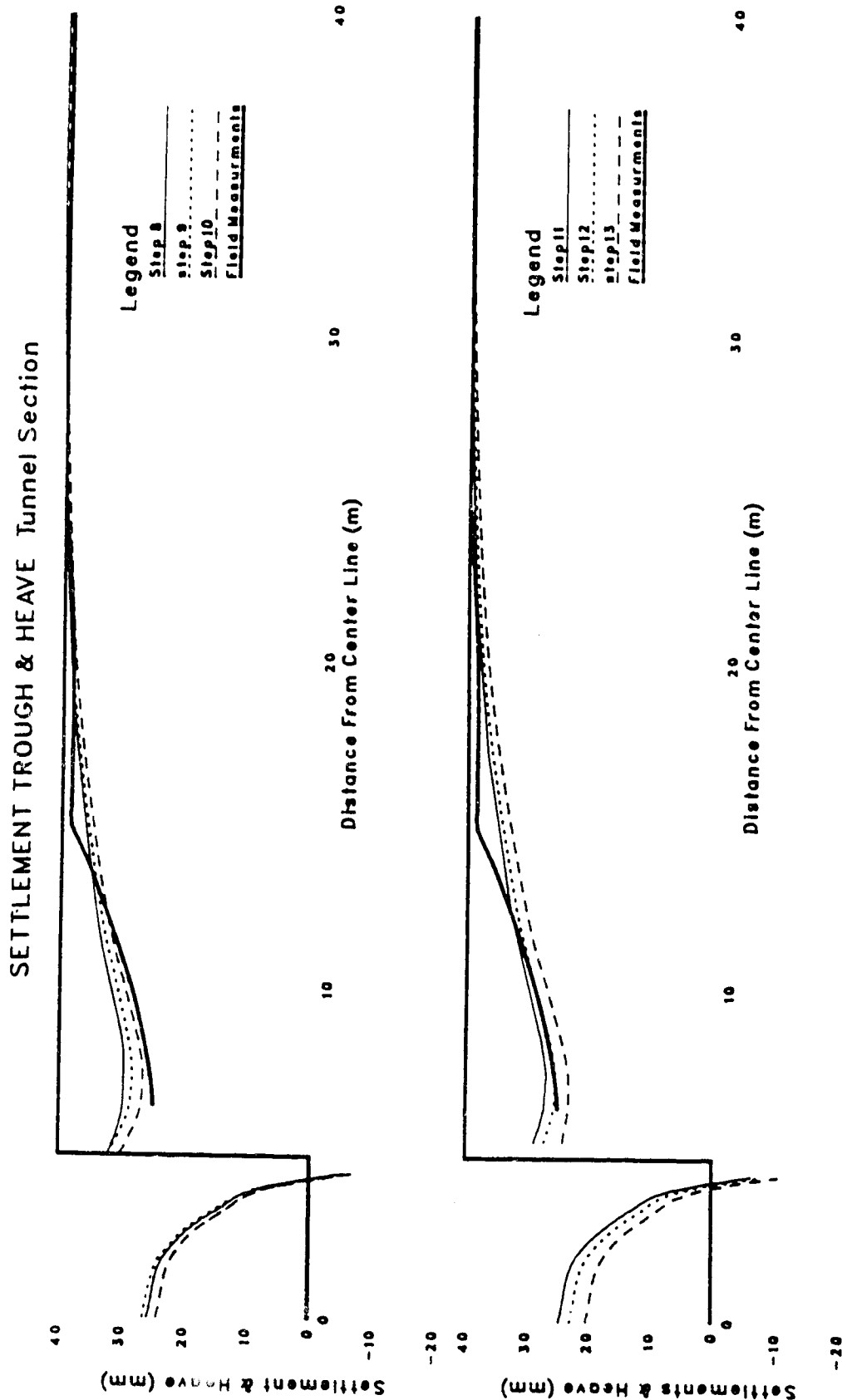


Figure 6.7 Settlement Trough and Heave for the Tunnel Section

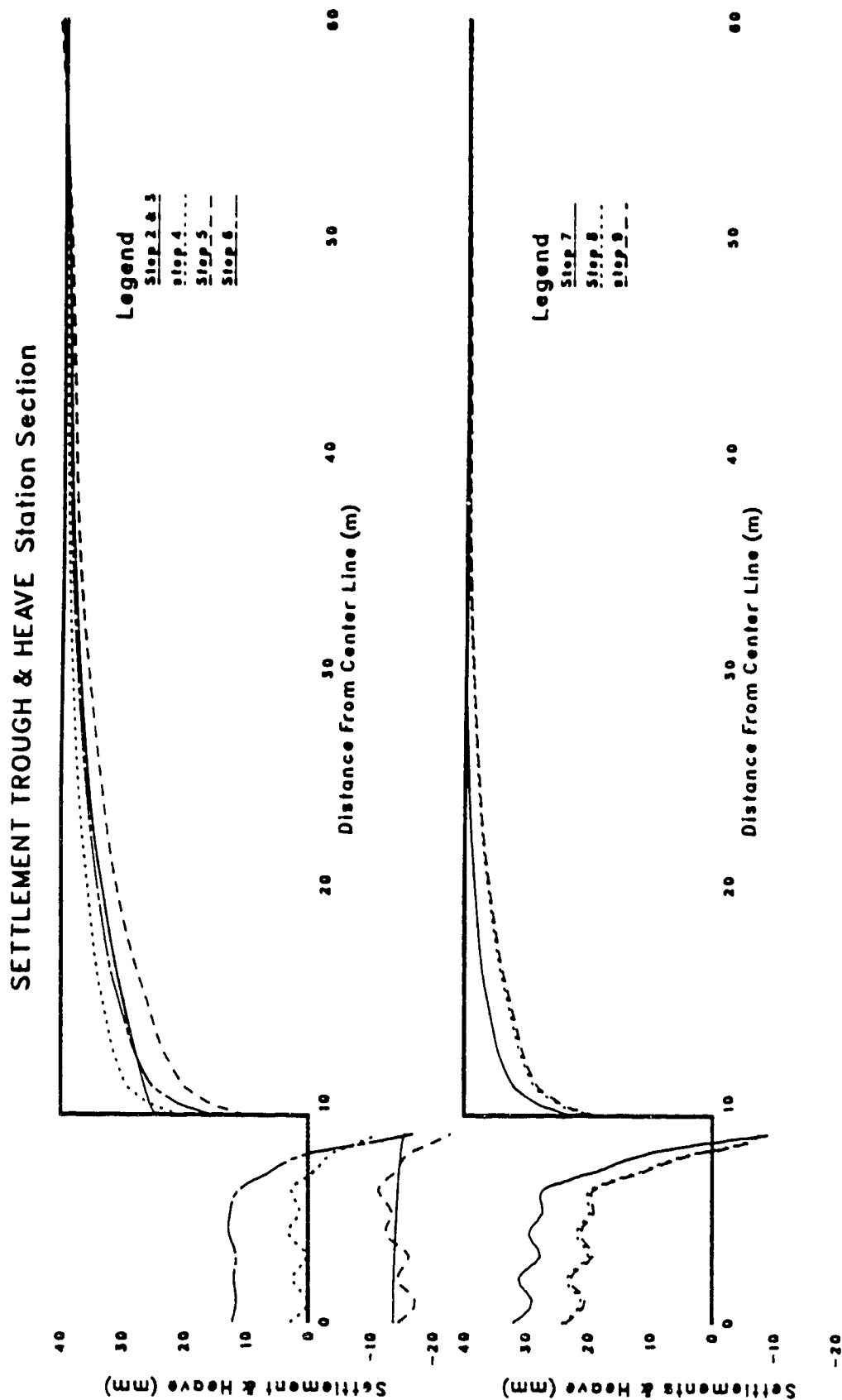


Figure 6.8 Settlement Trough and Heave for the Station Section

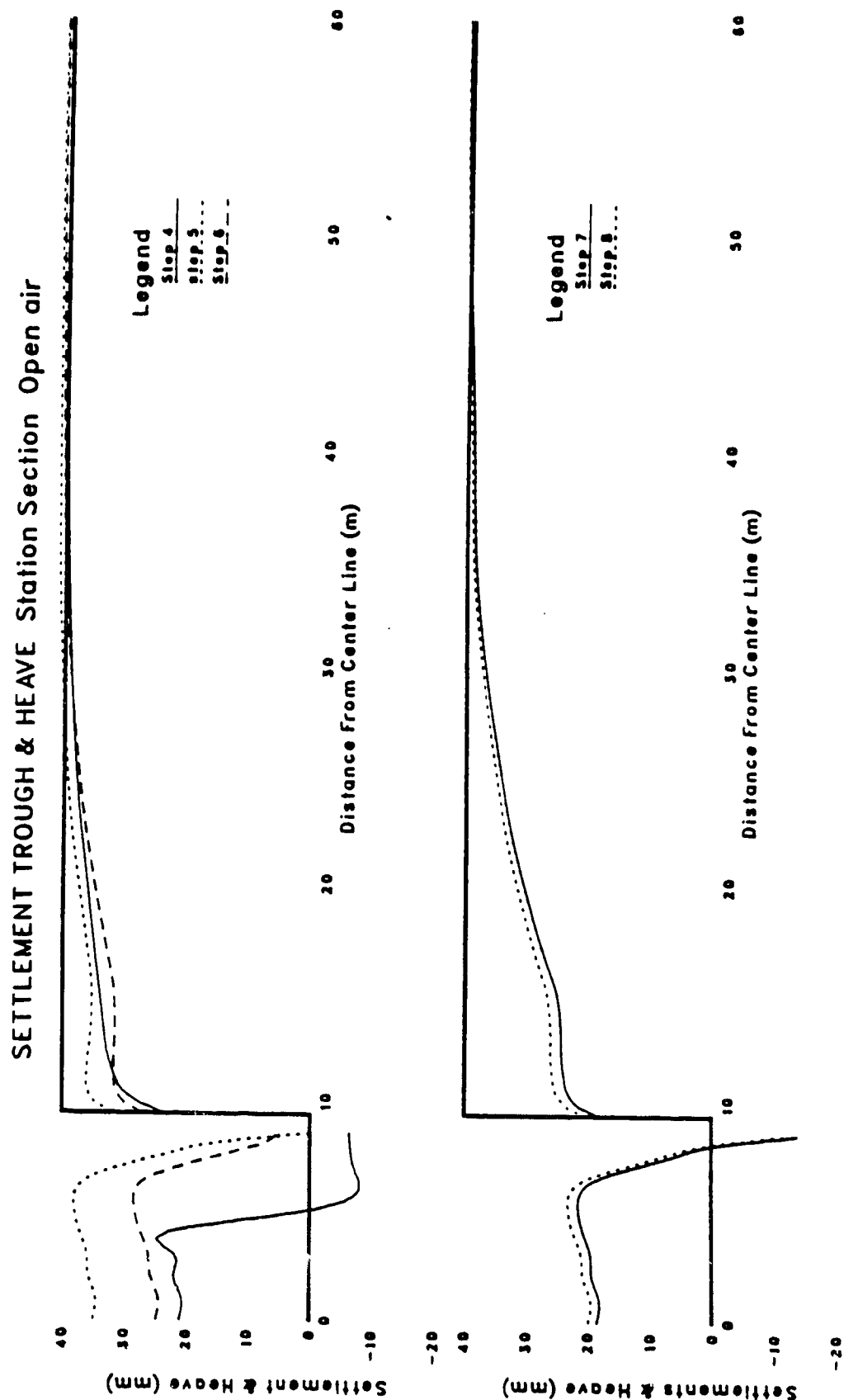


Figure 6.9 Settlement trough and Heave for Station Section as Open Air Excavation

The settlement troughs for the station section analysed as an undercover excavation are plotted in Figure 6.8. Higher values were calculated very close to the wall for a short distance and at a distance of 1.5 m from the wall they were 11.5 mm. A maximum of 20 mm was reached in Step 5, but reduced to 11.5 mm in the final case due to heave. The open air excavation analysis is shown in Figure 6.9. A gradual increase in settlement due to progress of the excavation was recorded with a maximum value of 16.77 mm at 1.5 m from the wall. Comparing the final settlement for both excavation procedures, it is concluded that the undercover procedure reduces surface settlement by approximately 30%.

Figure 6.10 compares the field measurements using multipoint extensometer (ME1) for the tunnel section and the predicted values using the F.E.M. (the final case). Field data showed an increase in vertical movement with depth while the predicted values showed a reduction with increasing depth. This discrepancy may be attributed to the idealized and simplified soil profile used in the F.E.M. analysis and the repair work conducted to salvage the line as the replacement of the instruments was not viable.

6.5.1 Vertical Displacement of the Excavation Base

An attempt was made to observe the base heave but it was not possible to obtain any reliable data. The development of predicted base heave of the tunnel section as a result of the progress of excavation is shown in Figure

6.7. The heave reached a maximum of 26 mm in Step 9 and reduced to 20 mm in the final step. It occurred at the centre line of the excavation rapidly decreasing as the wall was approached. Adjacent to the wall, 10 mm settlement was calculated in the final stage. The analysis of the station section as an undercover excavation is shown in Figure 6.8. The maximum value of 32 mm was reached in Step 7. A final value of 23.5 mm was recorded. Close to the wall, the behaviour was similar to that of the tunnel section. Figure 6.9 indicated that the maximum heave predicted in the open air excavation analysis was approximately 38 mm in Step 5 at a distance of 5 m from the centre line. It reduced to 23 mm in the final case at the same location. Comparing the results for the tunnel and station sections, taking into account the difference in base width, it is concluded that the behaviour in the undercover analysis is in agreement with that in the tunnel section. The comparison with the open air analysis, shows that the increase in width resulted in a 30% increase in the maximum value.

Abdel Salam (1984) explained the design criteria submitted by the contractor for the excavation base stability and for the determination of the bottom level of the grouting plug as follows:

$$(h + f) F.S > 2.1 f$$

where

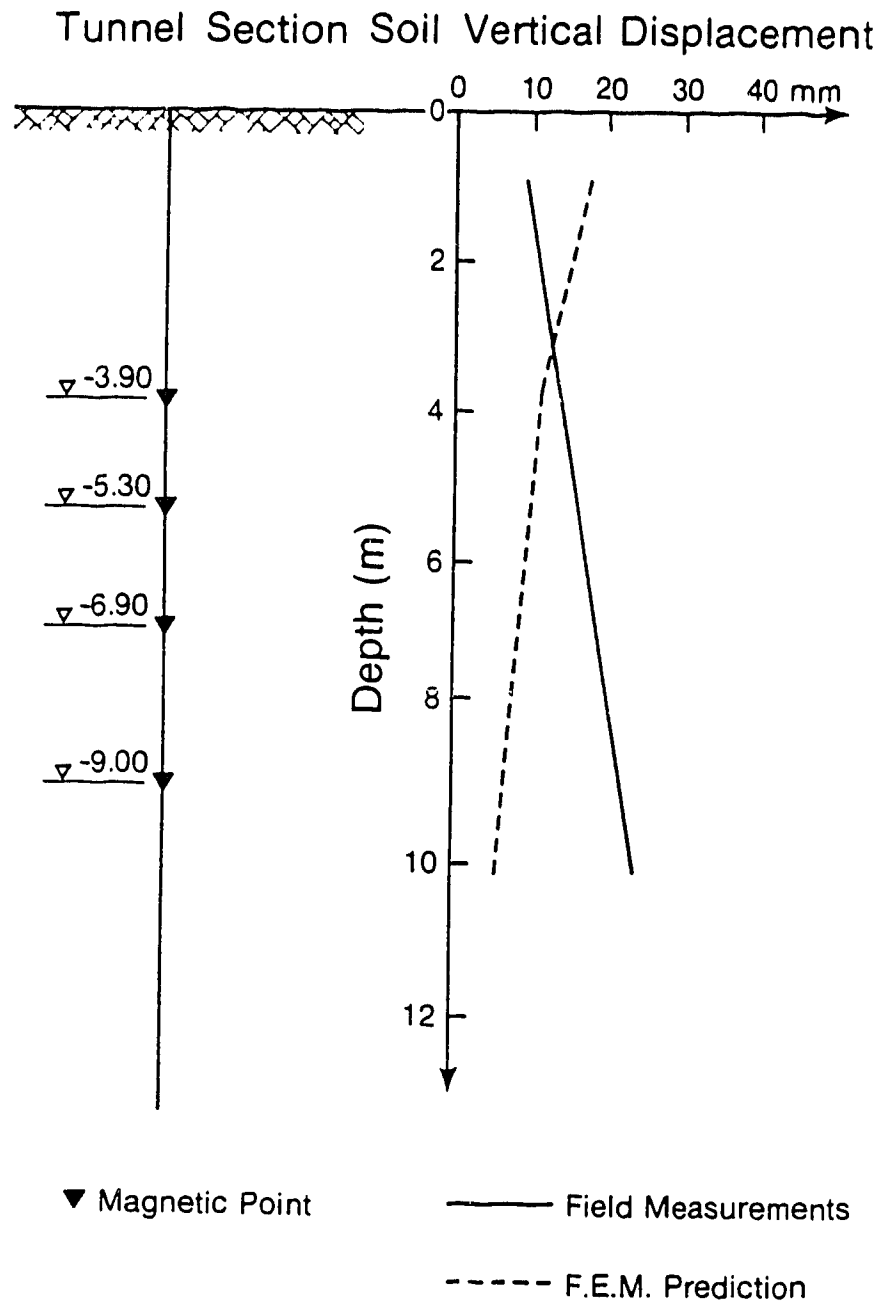


Figure 6.10 Vertical Displacement of the Soil for the Tunnel Section (ME1)

h = distance from the ground water level to the excavation bottom

f = distance from the excavation bottom to the bottom of the grouted plug

F.S. = factor of safety, taken as 1.1

Applying this to each section, the calculated factor of safety for the tunnel section is 1.13 and for the station section is 1.15, which is more than the F.S. of 1.1 suggested and used for the design. Using the actual dimensions and calculating the uplift pressure and resisting forces, the factor of safety for the tunnel section at the critical step of the analysis was 1.26 times higher than the one used by the contractor, reducing the risk of base failure. The factor of safety for the station section was 1.22. This difference in the factor of safety was attributed to the fact that the design criteria did not account for ground water fluctuations. Also the grouted plug, as a thick stiff layer, improved the ability of the soil to resist deformation. The grouting pipes acted as micro-piles also improving the soil stability. These factors increased the factor of safety of the excavated zone.

6.6 Strut and Normal Loads

The strut loads were measured by weldable vibrating wire strain gauges mounted on each side of the strut at approximately the zero bending moment point. The use of strain gauges has been documented by Rott and Veder (1980),

Baggett and Buttling (1981), Wood and Perrin (1984), Yih and Khara (1988) and Riker and Dailer (1988). A series of embedded strain gauges were installed in each section to observe the normal loads acting on the floor and roof slabs adjacent to the wall.

In Tables 5.2 and 5.3, the results of the finite element predictions are tabulated. The field measurements yielded values of 15 kN/m' for both rows of struts in the tunnel section and 60 kN/m' in the station section. The normal forces measured in the tunnel for the raft and roof were 70 kN/m' compressions and 80 kN/m' in tension, respectively. For the station, these values were 40 kN/m' compression in floor and tension in the roof. The field data was in reasonable agreement with the predictions for the first strut installed (lower strut) while much lower values were predicted for the upper struts. The low values could be attributed to the fact that the upper strut worked only to prevent further lateral movement. The majority of the lateral movement occurred before their introduction. The field conditions may differ from the ideal case used in the F.E.M. analysis as a result of the unexpected live loads (i.e. driving forces for sheet pile walls).

The struts in the station section were in the undercover excavation area. The results of the finite element analysis underestimated the measured values by about 40%. It is concluded that the temporary support system for

struts for the tunnel do not work up to reasonable capacity as a result of their later activation. The forces in the roof and raft slabs as measured using the embedded strain gauges were overestimated by the finite element predictions.

From the results of the tunnel and the station (undercover) test sections, it may be concluded that the early introduction of a temporary support system at the top of the open air excavation, will result in reduced lateral movement close to the undercover excavation. This will reduce the risk to adjacent buildings. The size of the struts could be less than the size used if they were especially manufactured for this project. Also the use of a single row of temporary support for the station section during the F.E.M. analysis allowed for more deformation, while it was expected to produce lower deformation values using two rows as for the tunnel section, the difference in stiffness of each section substitute for the use of a single row of temporary support, producing almost the same profile for both sections.

Medeiros and Eisenstein (1983) presented a diagram to explain the influence of the wall thickness on the strut and lateral loads acting on a tangent pile wall, which is considered similar to a diaphragm wall. The diagram was divided into zones, which showed the loads that will be carried by the struts and the soil. The results of this study showed that the load of the tunnel section will be primarily carried by the struts, and for the station section

higher values were shown for the lateral earth pressure. These were still in the same zone as the tunnel section. It must be noted that the lateral earth pressure predicted by the finite element for the station section as undercover and open air excavation showed slight differences, due to the the different values of deformation, but accounting for the second row of struts in the open air excavation will reduce this difference.

6.7 Shear Stresses at the Soil-Structure Interaction Zone

The problems concerning the soil-structure interaction during the F.E.M. analysis were dealt with based on the experience reported by Chan et al. (1986) and McRoberts et al. (1988). It was assumed that a no slip condition existed at the soil-structure element interface and that the soil can withstand the shear stresses which occur as a result of soil deformation. The initial results from the linear elastic analysis supported this assumption for the active zone which is the major concern in this study.

The angle of wall friction, δ , depends on the roughness of the contact face and can not exceed the angle of shear resistance, ϕ . Common practice for precast diaphragm walls yields a value between one and two-thirds the angle of shearing resistance. For the cast-in-situ panels at the station section, the interaction surface is considered rough and the value of δ could reach the ϕ value. The ϕ values are listed in Table 4.1

SHEAR STRESSES Tunnel Section

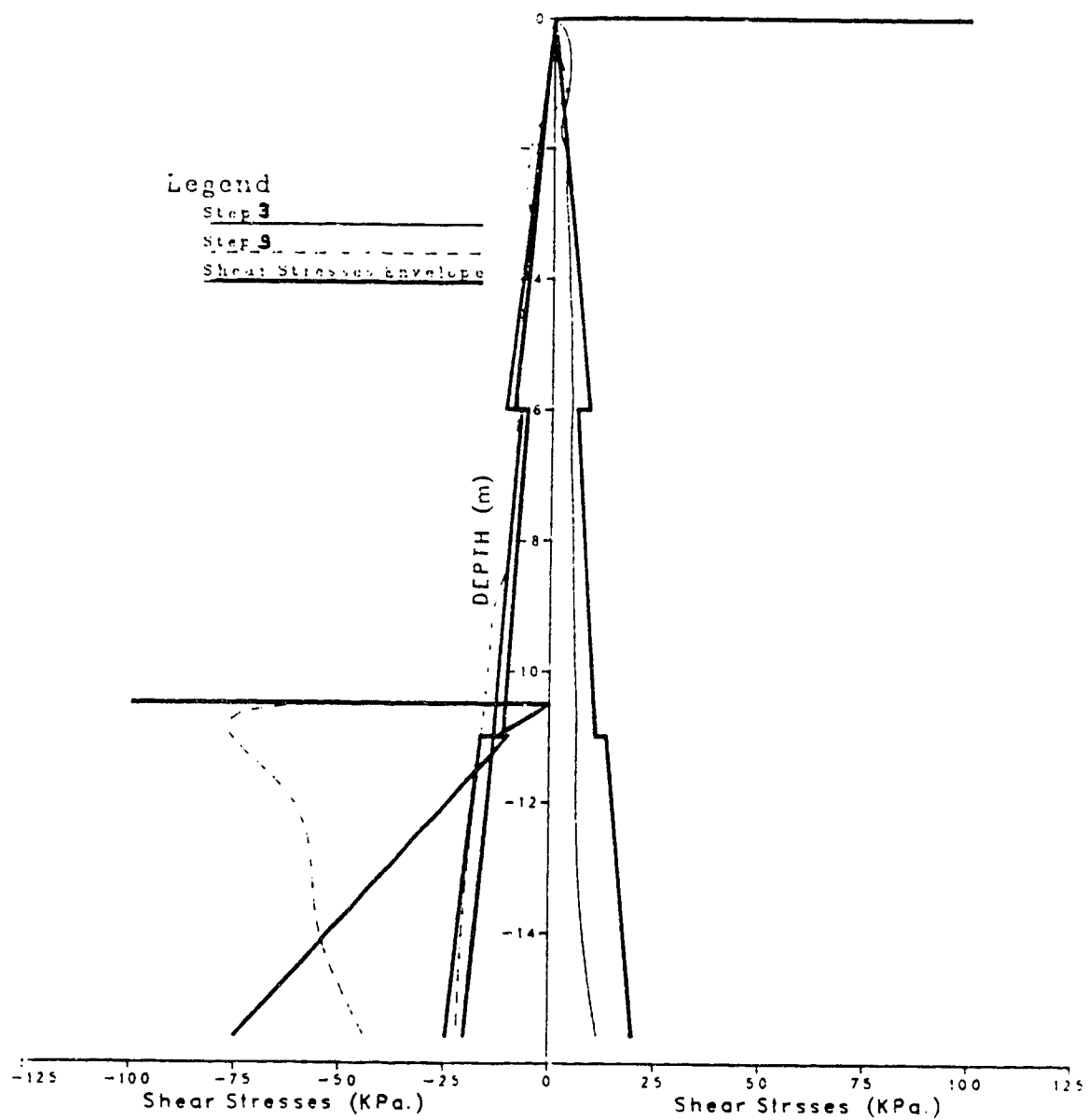


Figure 6.11 The Predicted Shear Stresses and the Allowable Shear Stress Envelope for the Tunnel Section

SHEAR STRESSES Station Section

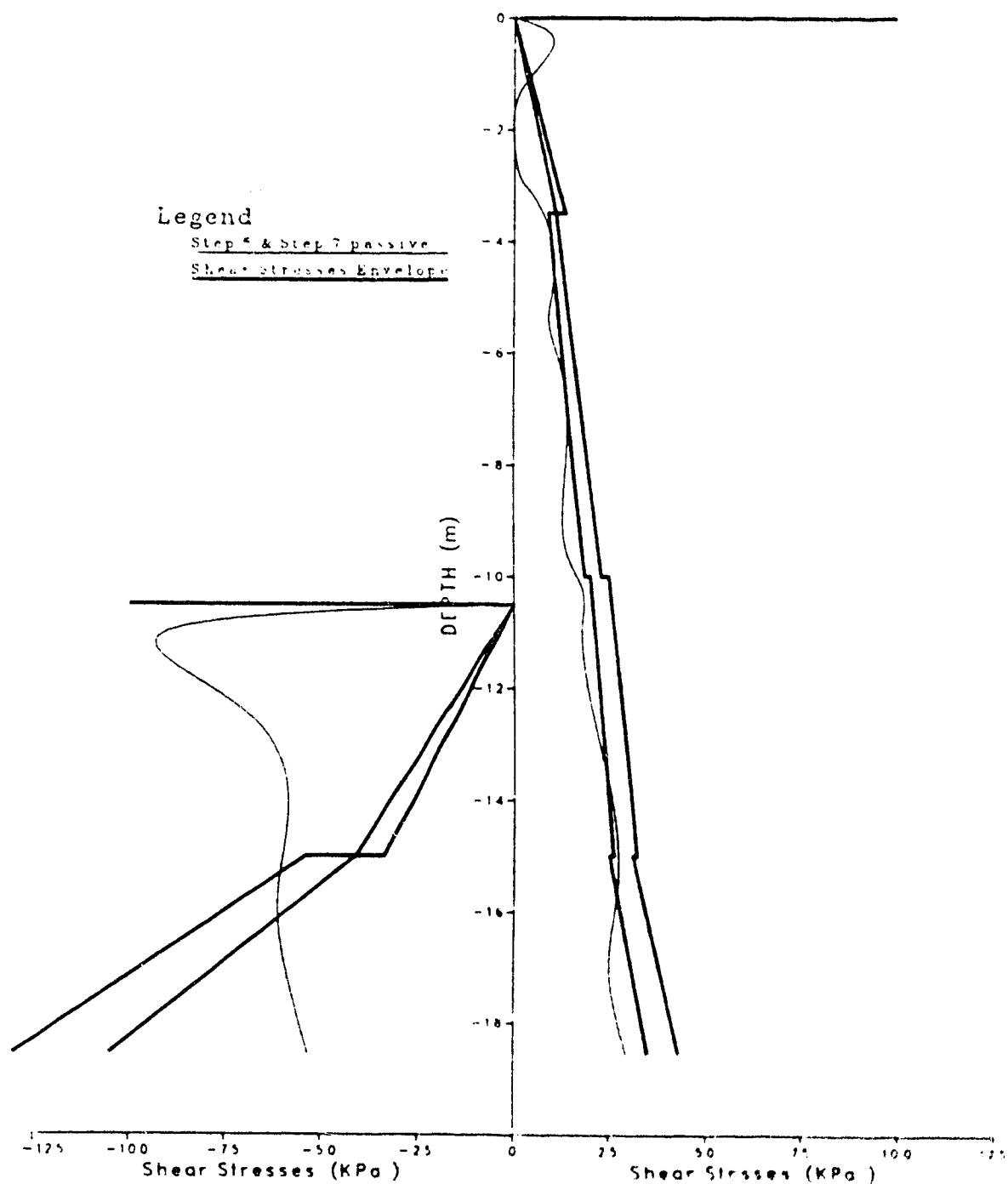


Figure 6.12 The Predicted Shear Stresses and the Allowable Shear Stress Envelope for the Station (Undercover) Section

SHEAR STRESSES Station Section Open Air

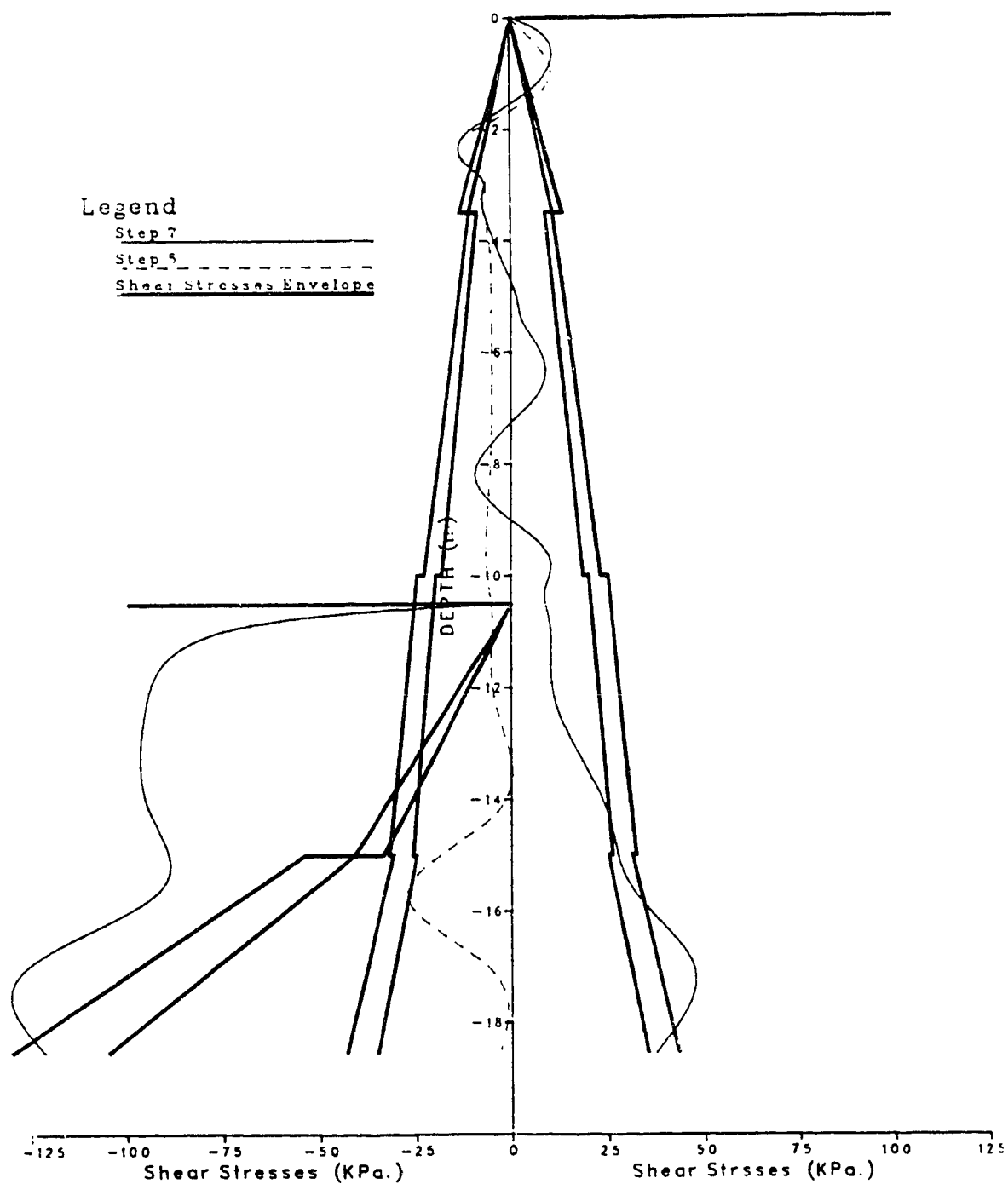


Figure 6.13 The Predicted Shear Stresses and the Allowable Shear Stress Envelope for the Station (Open Air) Section

Figure 6.11 presents the results of the analysis which form an envelope for the maximum values and the solid thick line represents the allowable shear stress envelope. Due to the upward and downward movement of the soil around the wall, the envelope has been drawn for both sides of the wall. The active side showed that the predicted shear stresses are within the allowable range. The upward movements lie between the two envelopes for δ values of $2/3$ and $1 \times \phi$. A slight increase near the elevation corresponding to the excavation base is noted. This is considered negligible as the predicted values are covered by the allowable shear stress envelop. The undercover analysis of the station section is presented in Figure 6.12. The predicted shear stresses are within the allowable range and are enclosed by the envelop defined by $\delta = 2/3 \phi$. Following in Figure 6.13, the open air analysis is shown. The behaviour is similar to that of the tunnel section. It may be concluded that the assumption of no slip was justified and there was no need to introduce an interface element or slip element for the active zone.

Comparing the results for the passive side shown in the previous three figures, it is clear that the predicted values exceeded the allowable shear stresses indicating the need for a slip element in this zone, as reported by Chan et al. (1986) and McRoberts et al. (1988). The use of a slip element reduced the shear stresses dramatically, especially close to the excavation base. This study is primarily

concerned with the stresses in the active zone, and therefore the time and cost to use a slip element was not justified. Also the analysis did not account for the soil stabilization inside the excavated zone due to the grouting procedure. The influence of micro-piles (or soil nailing) and soil grouted on the performance of the excavation base and factor of safety has been reported by Broms (1988). The factor of safety against base failure was discussed in the previous section. There it was shown that the actual factor of safety is higher than the one used in design.

6.8 Lateral Earth Pressures Acting on the Wall

The lateral earth pressure diagram suggested by Terzaghi and Peck (1967) for calculating strut loads of strutted excavations are the most commonly used in practice. Broms (1988) reports that most research work uses the strut load measured in the field. This method is completely dependent on the strut spacing, method of measurement, the sequence of installation, and method of activating the struts. The second most common way of predicting the lateral earth pressure is by calculating the bending moments in the structural element and back calculating the load causing the bending moments. Some researchers used slope indicator results to calculate the bending moments, but it has been proven that this may be applicable only to sheet pile walls with flexible stiffness. All these methods are academic since there is no direct way of measuring the lateral

pressures acting on the wall due to unloading during excavation.

In this study, a new concept for predicting the lateral earth pressure is attempted. Using soil parameters depends on the actual behaviour of the soil and feeding it to the finite element analysis. The finite element analysis is sensitive to computing the soil displacements, especially near failure. Therefore, by using the appropriate constitutive model and ensuring a close match of the field displacement measurements, the computed horizontal stresses will represent the actual lateral earth pressure distribution. As stated previously, a reasonable and close agreement was obtained, therefore, the finite element results from different analyses will be used as the field measured lateral pressures. The results have been confirmed with the use of the simple PFT program.

A complete set of results is provided in Appendix D. Figures 6.14 to 6.16 show the predicted lateral pressures for the last steps of the analysis for both test sections in comparison with Rankine's earth pressure diagrams which were used in the design. Figure 6.14 shows the predicted pressures to be less than the Rankine's earth pressure (P_A). It must be noted that in Step 11 of the analysis, the closest elements to the wall for a depth of about 3 m were deleted for simulation of the excavation. When an element has been deleted the program does not account for its previous stress history and when it is reintroduced to the

system, it is considered a newly birthed element. The results are presented as total stress including the hydrostatic pressures. Hansoen and Clough (1981) reported similar lateral earth pressure distributions for soft to medium clay in their investigation on the influence of clay anisotropy in the finite element analysis of a supported excavation. They stated that it is possible for a stiff clay to exhibit lower earth pressures than those calculated using Rankine's earth pressure theory. The predicted passive earth pressure was shown to be higher than Rankine's passive earth pressure. The results of the undercover analysis of the station section are graphed in Figure 6.15. The predicted values up to the excavation level are higher than Rankine's pressure and are in close agreement below the excavation depth. This may be attributed to the reduction in the lateral movement of the wall due to the early support by the roof slab. The deviation of the passive earth pressure from the predicted is reduced with depth, and below 15 m is in close agreement with Rankine's passive earth pressure. The open air excavation analysis is graphed in Figure 6.16. In the upper 2.5 m, a tension zone is evident, indicating separation between the wall and soil. In general, the results were in good agreement. The passive earth pressure showed similar behaviour as observed for the undercover excavation analysis. The predicted lateral earth pressure is close to the active earth pressure (K_a conditions) as calculated using Rankine's earth pressure theory in terms of

LATERAL EARTH PRESSURE Tunnel Section

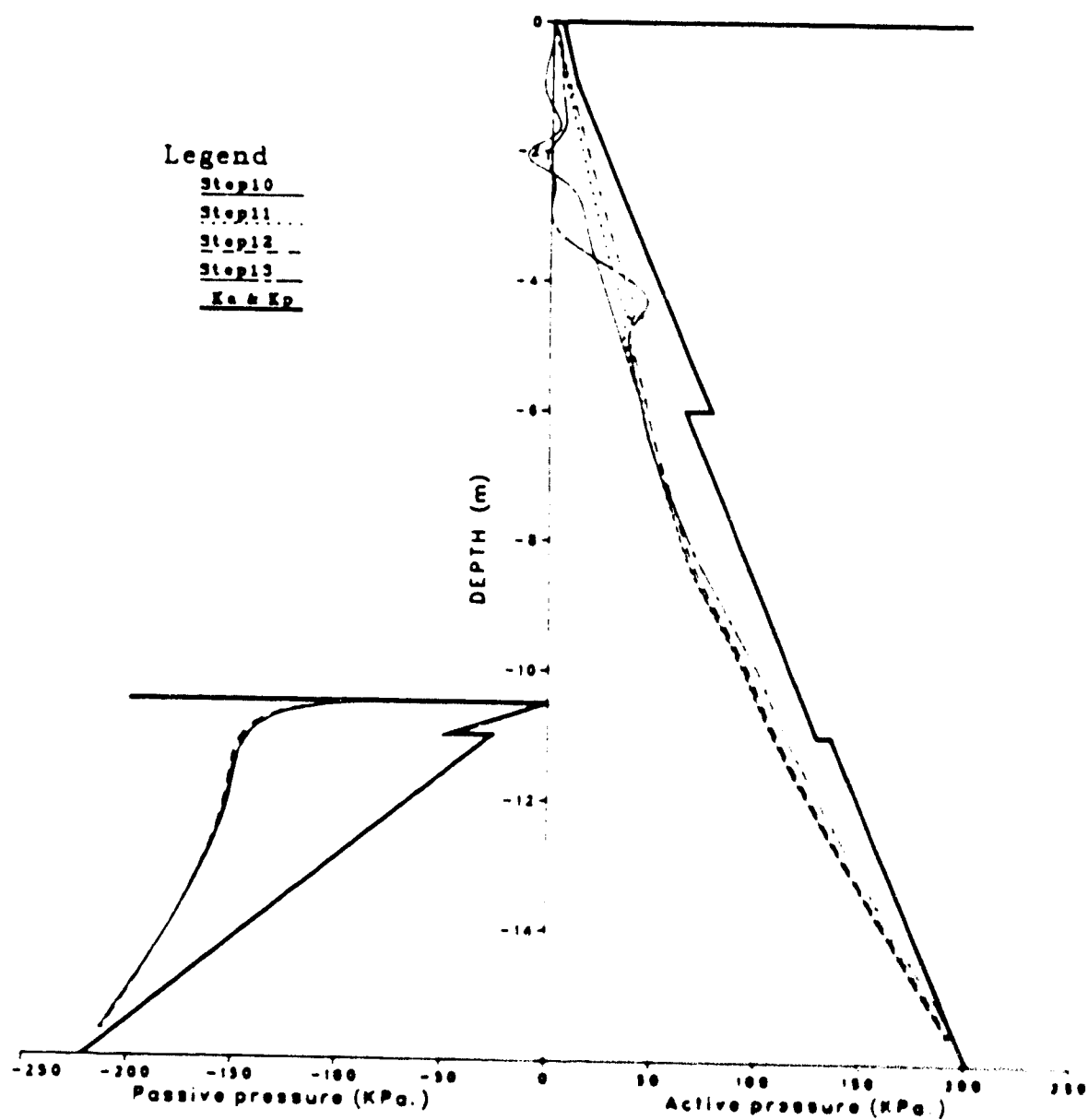


Figure 6.14 Final Predicted Lateral Total Earth Pressure for

LATERAL EARTH PRESSURE Station Section

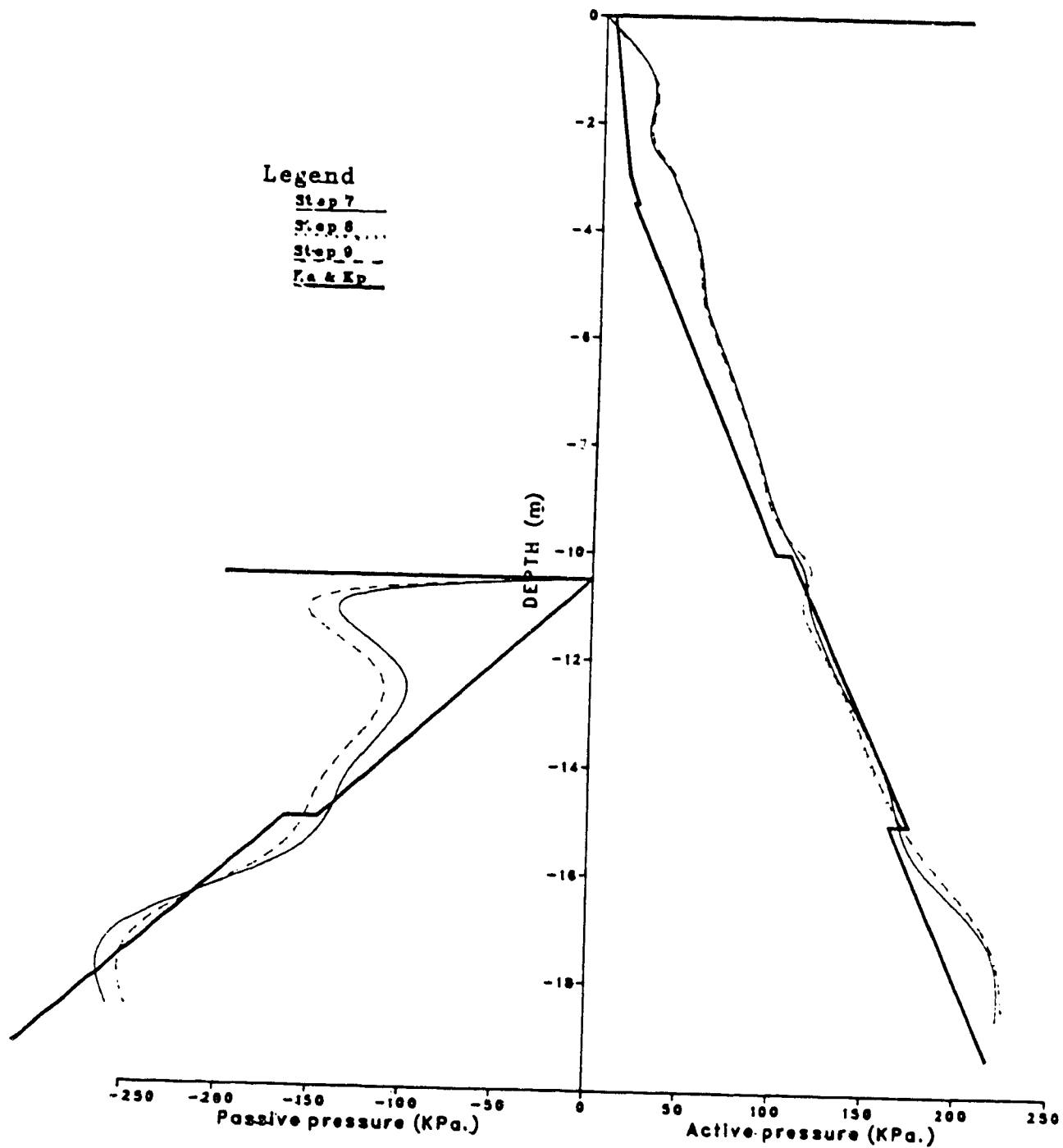


Figure 6.15 Final Predicted Lateral Total Earth Pressure for the Station Section Excavated Under Cover

LATERAL EARTH PRESSURE Station Section Open Air

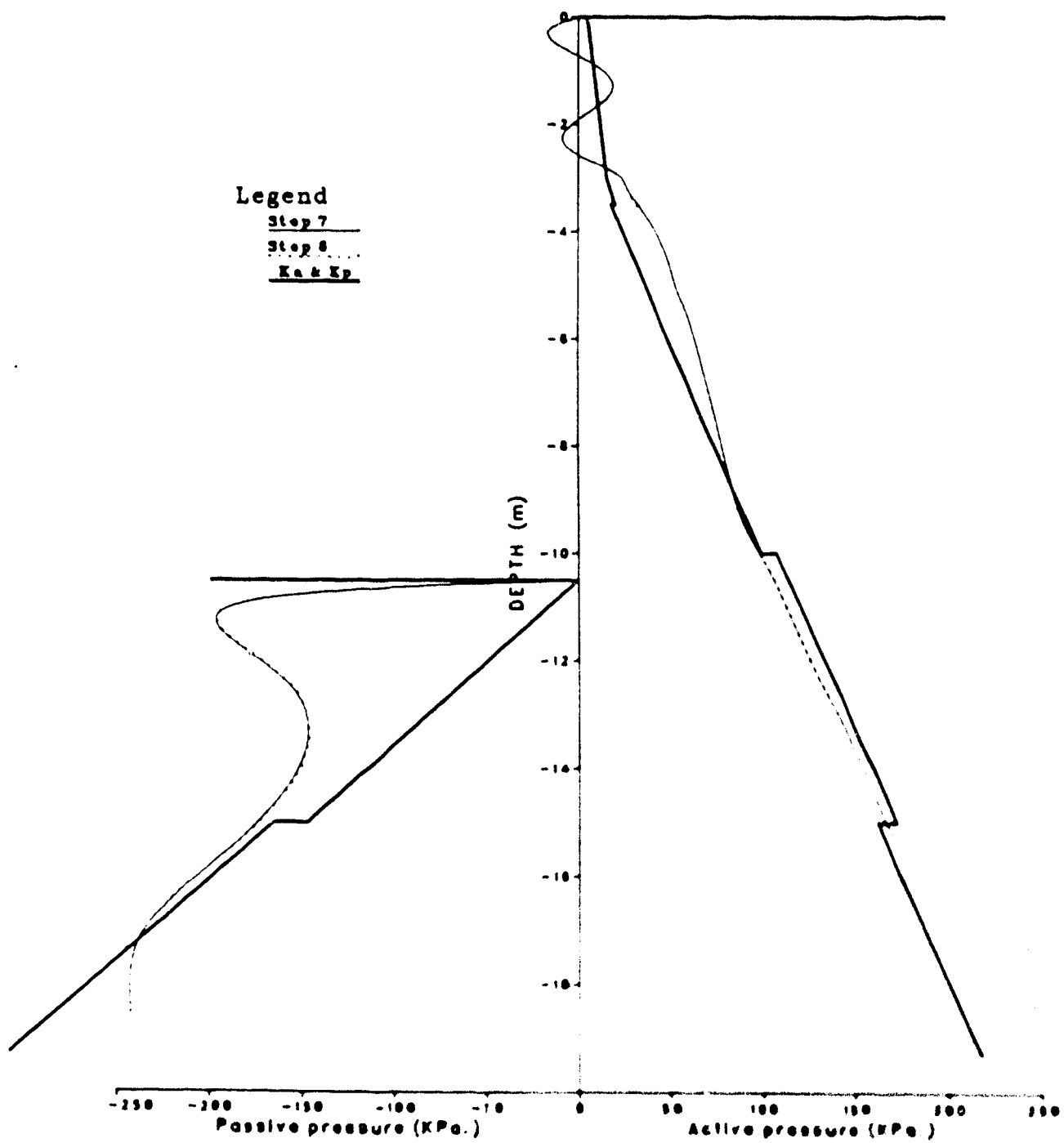


Figure 6.16 Final Predicted Lateral Total Earth Pressure for

the Station Section Open Air

total stresses. The effective stress results are shown in Figure 6.17 for the tunnel section. The field measurements of the pore water pressure proved that the pressures remained hydrostatic throughout the construction period. It is clear from the figure that the major source of lateral earth pressure is the hydrostatic pressure. Comparing the apparent earth pressure diagrams suggested by Terzaghi and Peck (1967), one can conclude that it is safe to use reduced allowable pressures in the design. Terzaghi and Peck's diagrams for a stiff clay are described as trapezoidal with height ratios of 0.25, 0.5 and 0.25 and the pressure is varied between 0.2 to $0.4\gamma'h$ where h is the excavation height and γ is the total unit weight of the soil. In Figures 6.17 and 6.18, Terzaghi and Peck's (1967) diagrams are produced for the effective and total unit weight, respectively. It is apparent that the use of the total unit weight overestimates the lateral earth pressure for such host materials and construction conditions. This is supported by the results of the station section analysis. Enlarged plots illustrating the difference in using effective and total unit weights are found in Figures 6.19 and 6.20. The calculations yielded 21 kN/m^2 and 42 kN/m^2 for 0.2 and $0.4\gamma'h$ using the effective unit weight (i.e. γ submerged) and 36.4 kN/m^2 and 72.8 kN/m^2 using the total unit weight (i.e. γ saturated). The calculated values for Terzaghi and Peck's diagrams as illustrated in the figures showed evidence to support the conclusion of using 0.2 to $0.4\gamma'h$ for similar problems in

LATERAL EARTH PRESSURE Tunnel Section

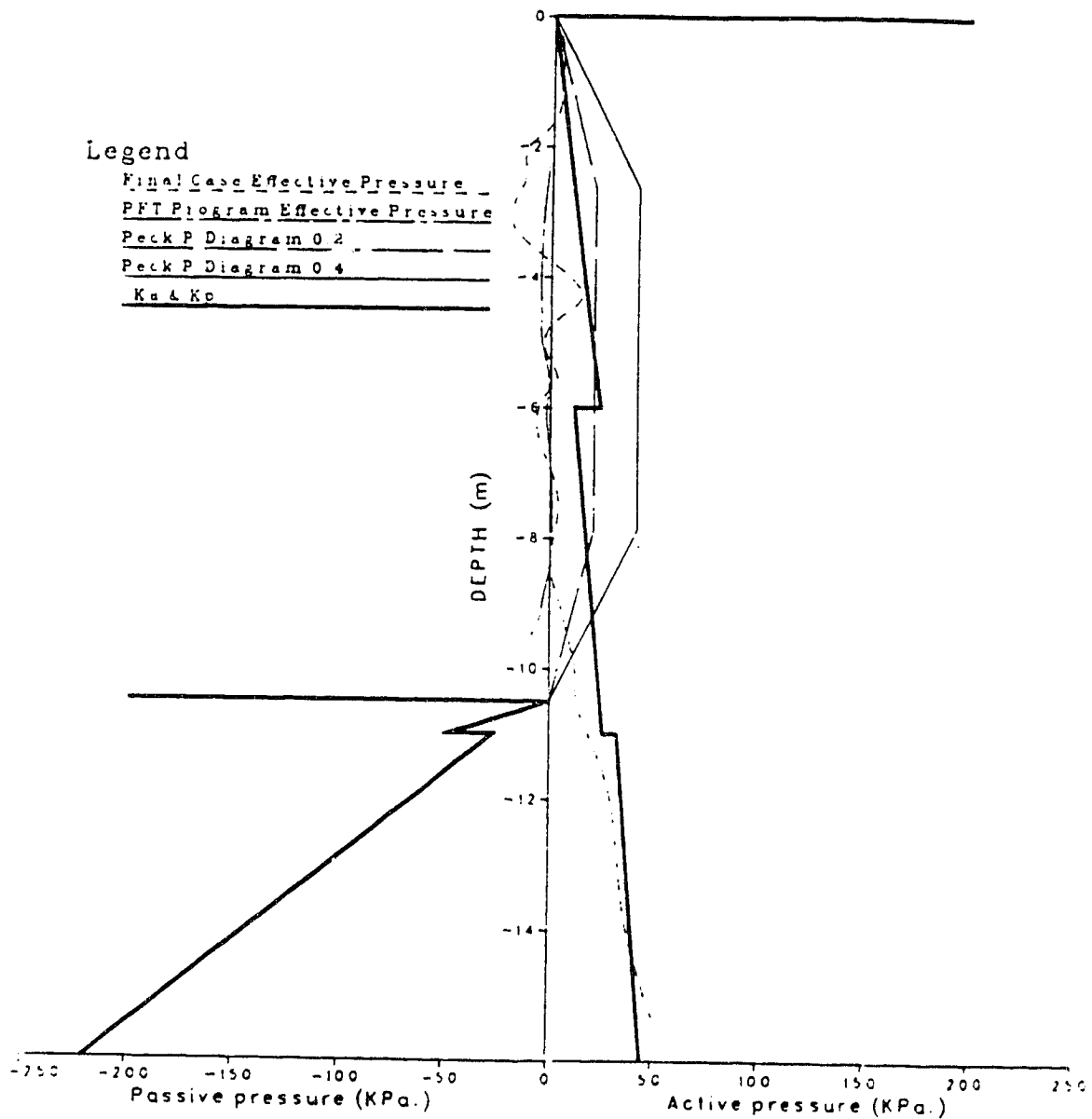


Figure 6.17 Final Effective Lateral Earth Pressure for the Tunnel Section with Effective Unit Weight for Terzaghi and Peck's Diagrams

LATERAL EARTH PRESSURE Tunnel Section

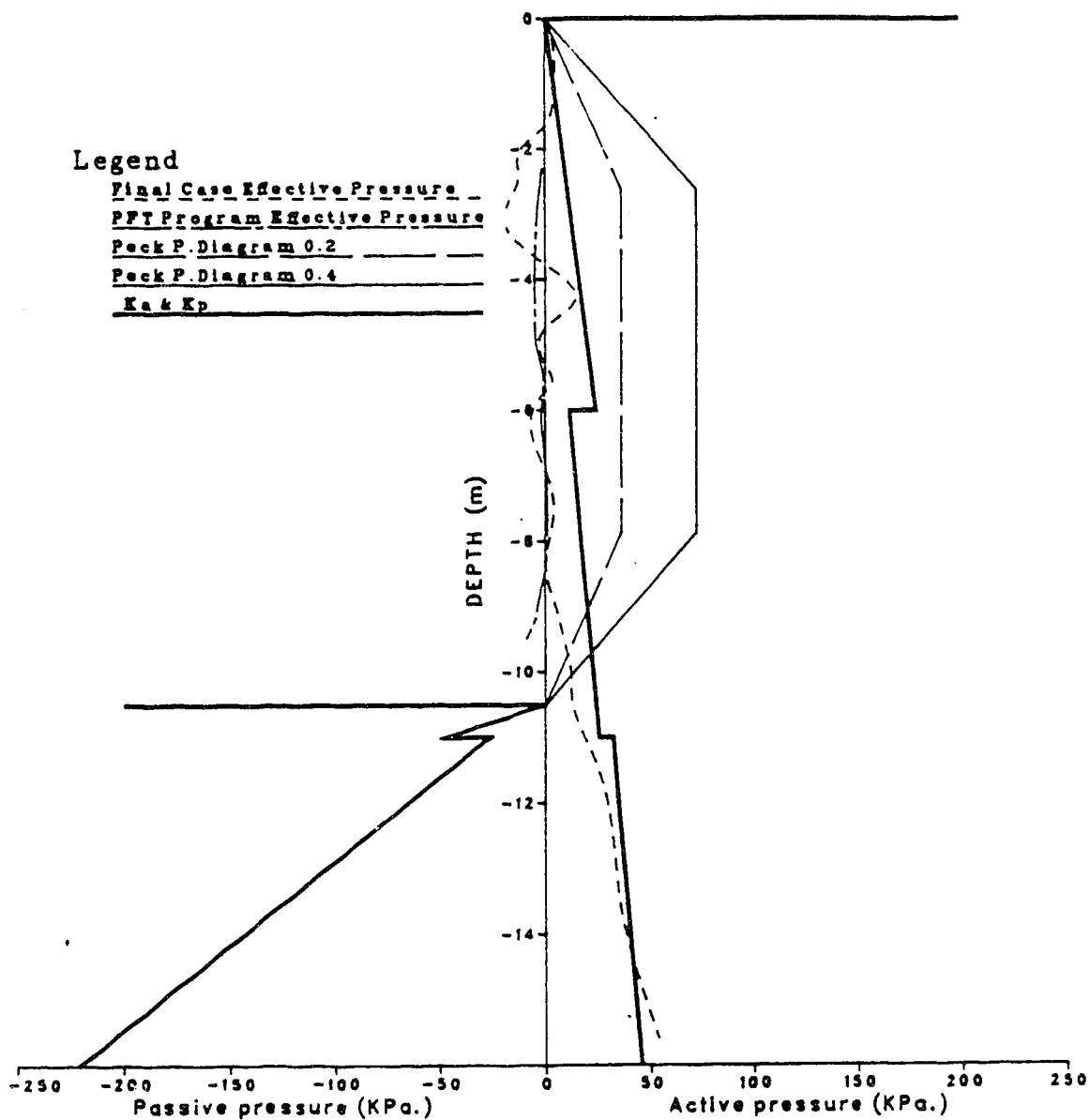


Figure 6.18 Final Effective Lateral Earth Pressure for the Tunnel Section with Total Unit Weight for Terzaghi and Peck's Diagrams

the future.

Figures 6.21 and 6.22 illustrate the differences between the predicted lateral earth pressures, the pressures calculated using Rankine's earth pressure theories and the recommended Terzaghi and Peck pressure diagrams. Figure 6.21 shows Terzaghi and Peck's diagram calculated using the total unit weight and Figure 6.22 presents the data based on the effective unit weight. The analysis is repeated in Figures 6.23 and 6.24 using the open air excavation method. The results are in agreement with the analysis of the tunnel section.

In Figures 6.25 and 6.26, a comparison of the lateral earth pressure diagrams for both the undercover and open air excavation methods are presented using the total and submerged unit weight in Terzaghi and Peck's diagrams, respectively. It is apparent that the use of the effective unit weight for Terzaghi and Peck's diagrams is the most appropriate. Figures 6.27 and 6.28 illustrate this by expanding the view of the area of intersection in the figures. Using the total unit weight, a good agreement results for the undercover excavation using $0.2\gamma_h$. The use of the effective unit weight produced a reasonable and conservative agreement with $0.4\gamma_h$. The use of the effective unit weight yields values of 20.2 and 40.4 kN/m² for 0.2 to $0.4\gamma_h$ respectively and the total unit weight yields 36.7 and 73.3 kN/m². The results of both the undercover and open air excavation analyses lie between 0.2 and $0.4\gamma_h$. This

LATERAL EARTH PRESSURE Tunnel Section

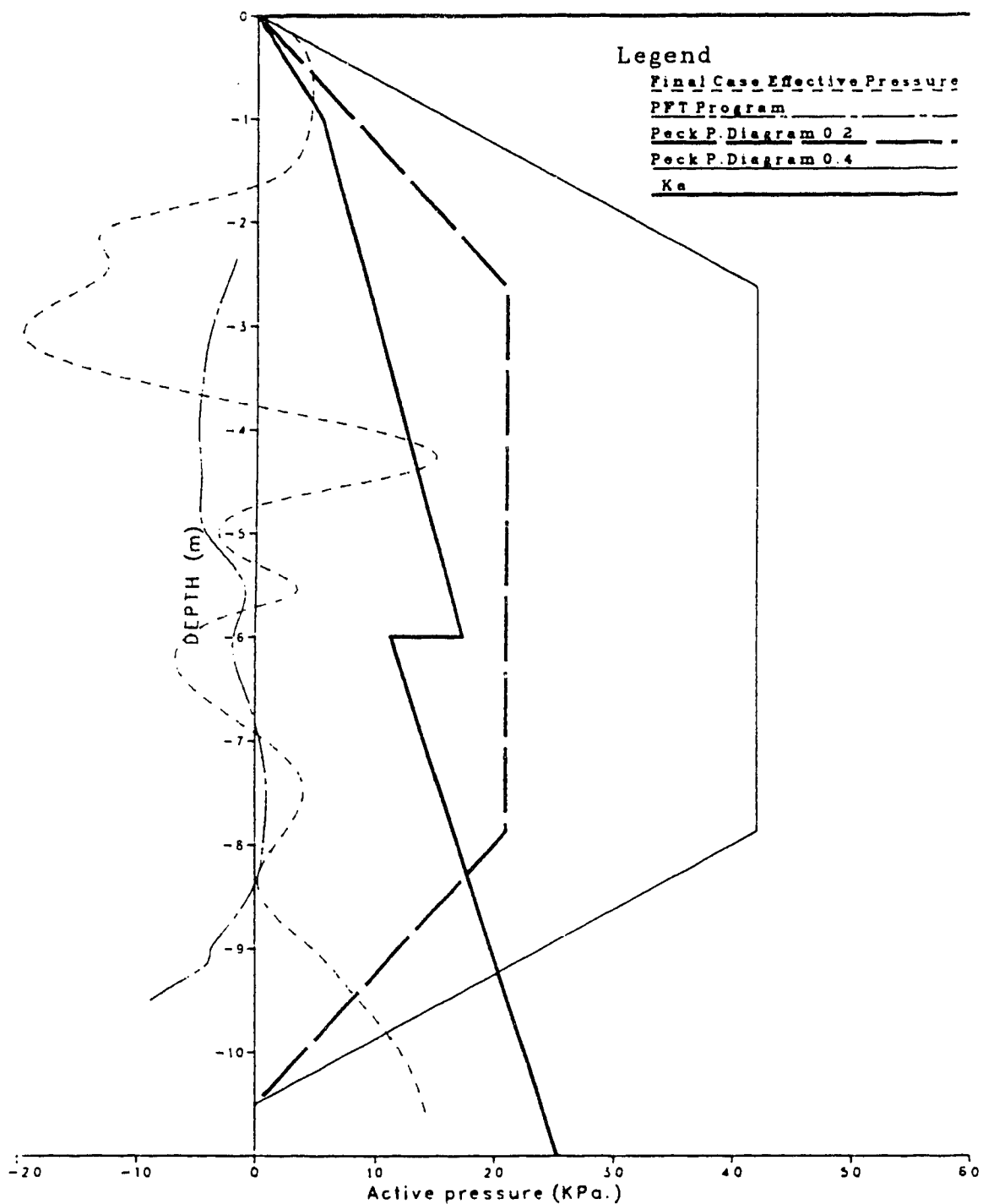


Figure 6.19 Final Lateral Earth Pressure Diagrams for the Tunnel Section using Effective Unit Weight for Terzaghi and Peck Diagrams

LATERAL EARTH PRESSURE Tunnel Section

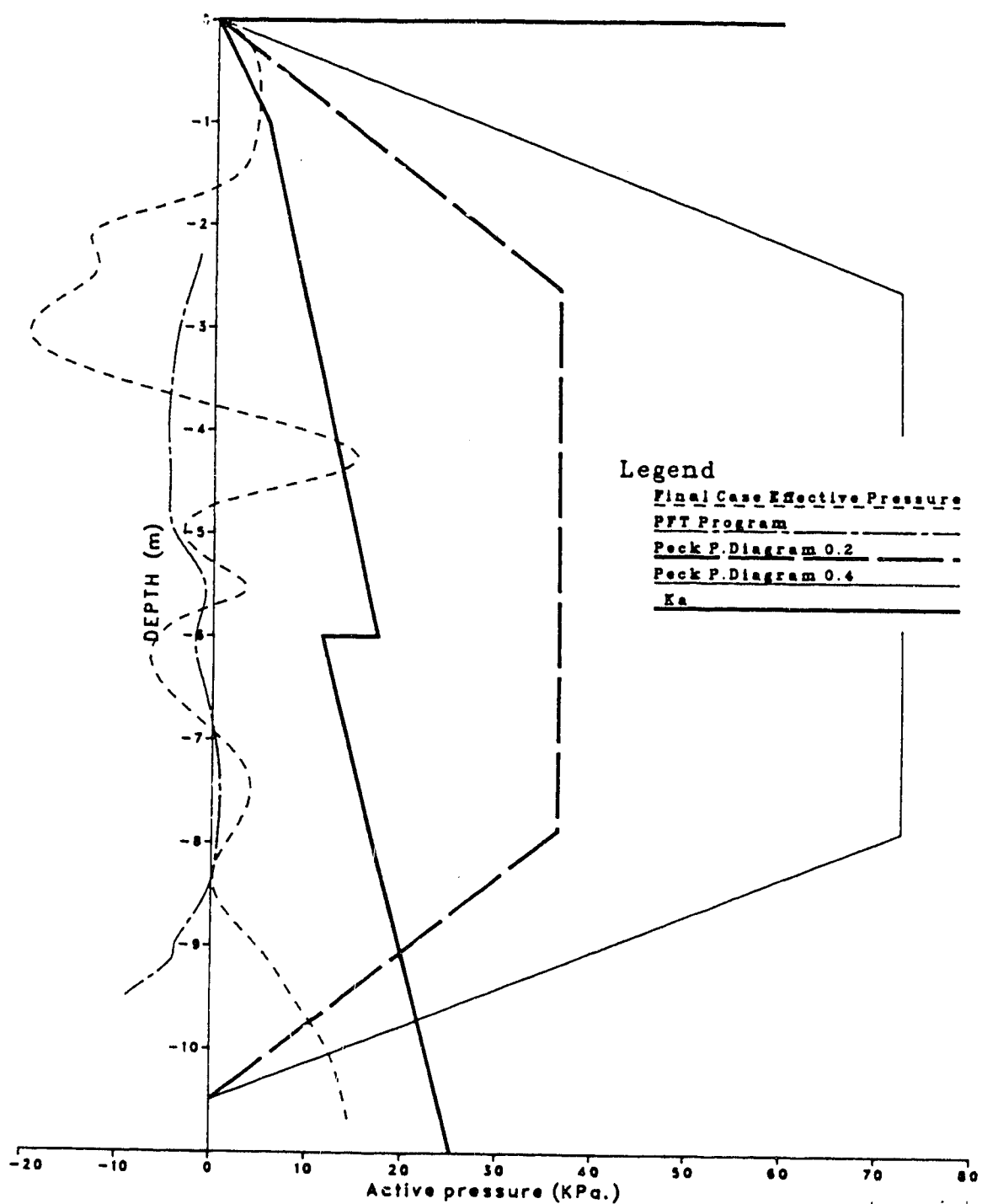


Figure 6.20 Final Lateral Earth Pressure Diagrams for the Tunnel Section using Total Unit Weight for Terzaghi and Peck Diagrams

LATERAL EARTH PRESSURE Station Section

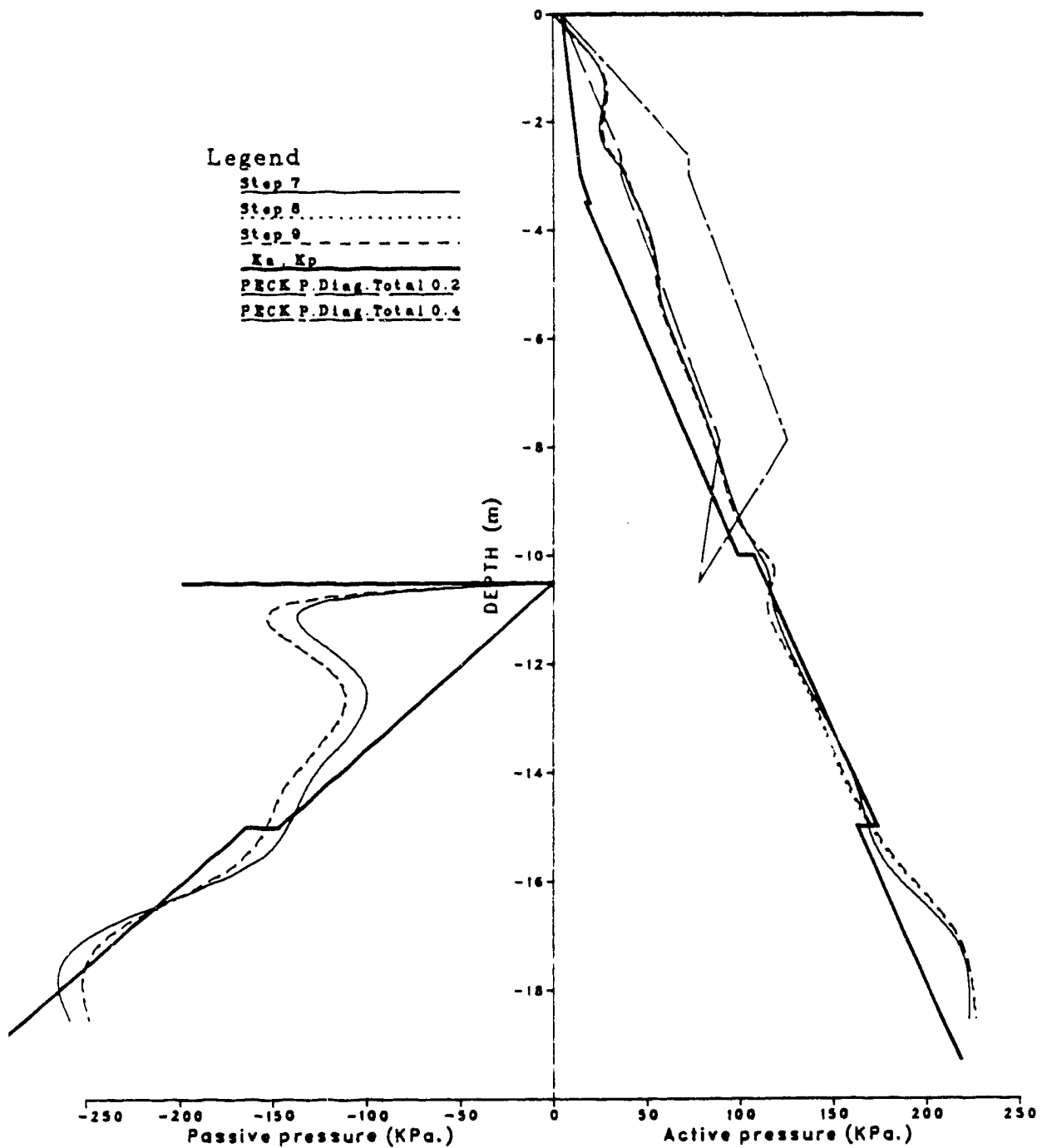


Figure 6.21 Final Lateral Earth Pressure Diagrams for the Station (Undercover) Section using Total Unit Weight for Terzaghi and Peck Diagrams

LATERAL EARTH PRESSURE Station Section

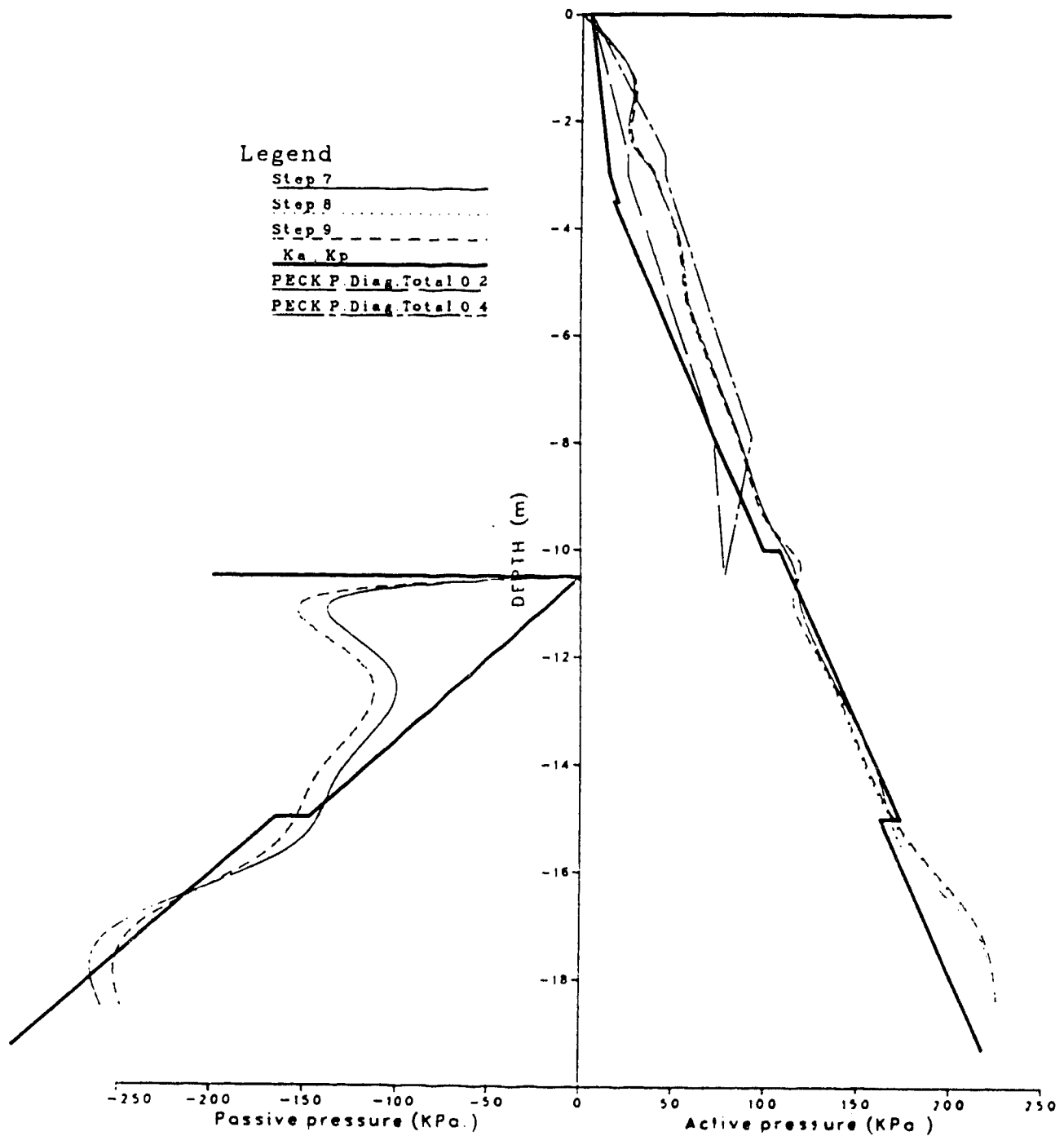


Figure 6.22 Final Lateral Earth Pressure Diagrams for the Station (Undercover) Section using Effective Unit Weight for Terzaghi and Peck Diagrams

LATERAL EARTH PRESSURE Station Section Open Air

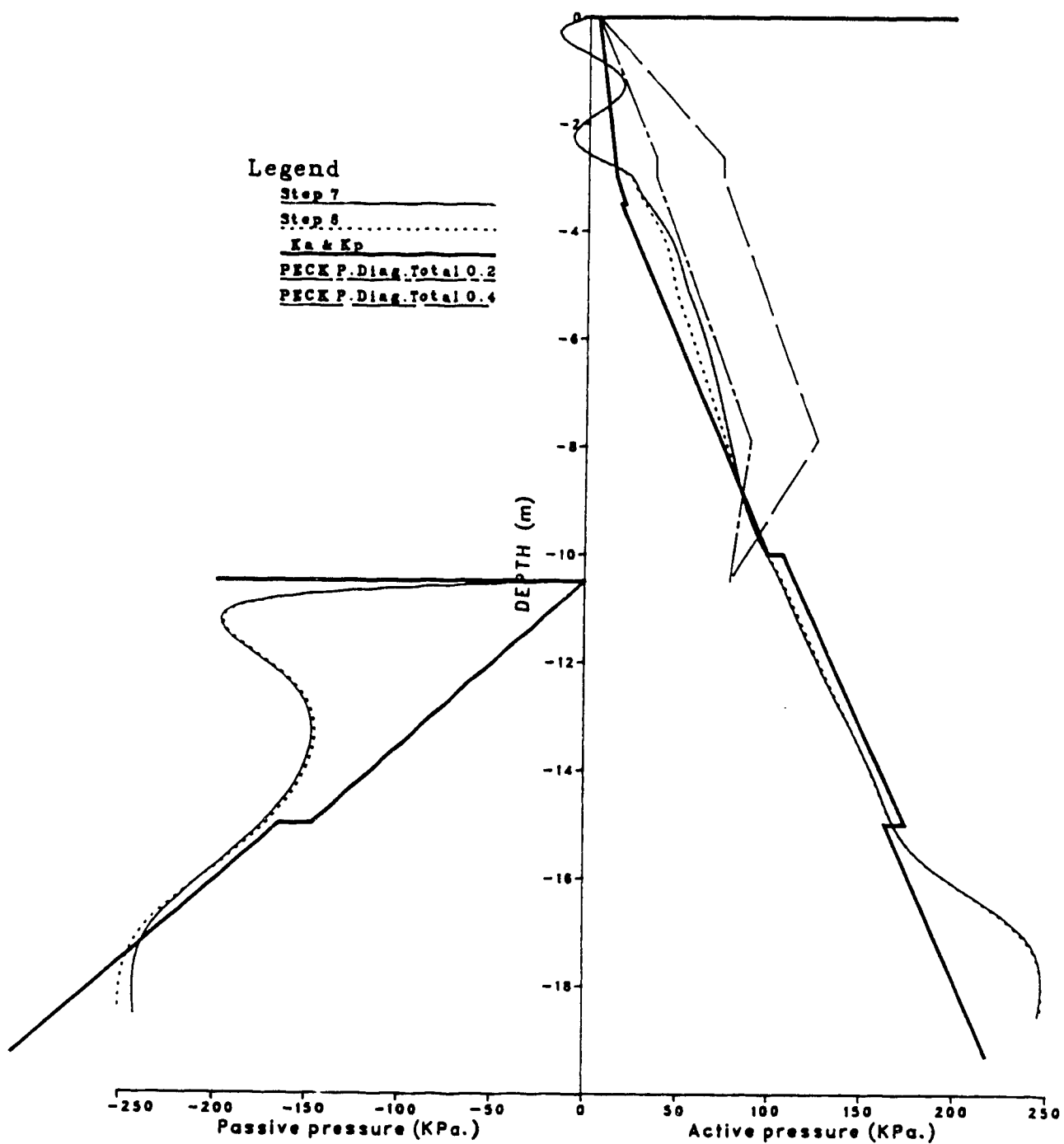


Figure 6.23 Final Lateral Earth Pressure Diagrams for the Station (Open Air) Section using Total Unit Weight for Terzaghi and Peck Diagrams

LATERAL EARTH PRESSURE Station Section Open Air

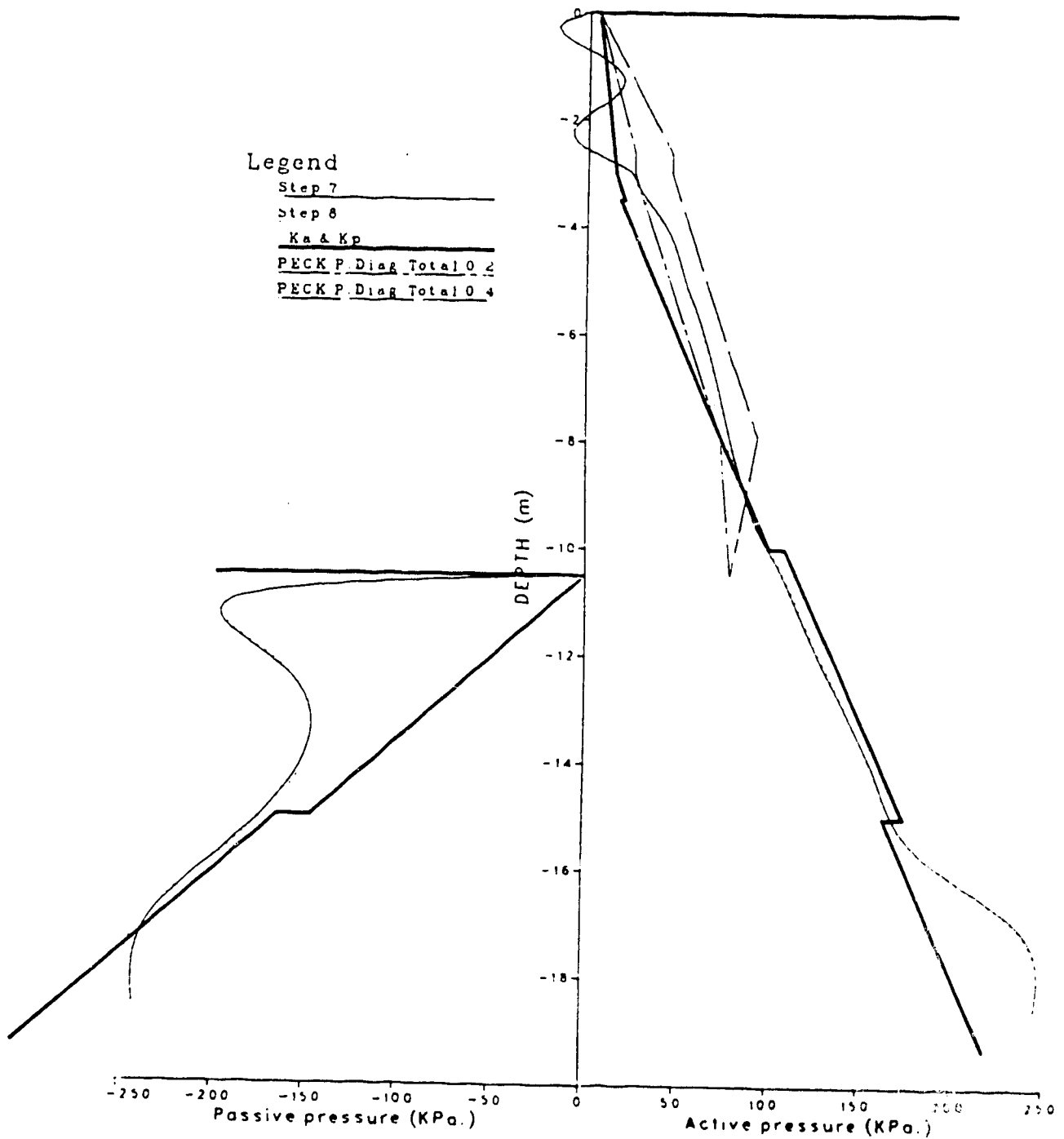


Figure 6.24 Final Lateral Earth Pressure Diagrams for the Station (Open Air) Section using Effective Unit Weight for Terzaghi and Peck Diagrams

EFFECTIVE LATERAL EARTH PRESSURE Station Section

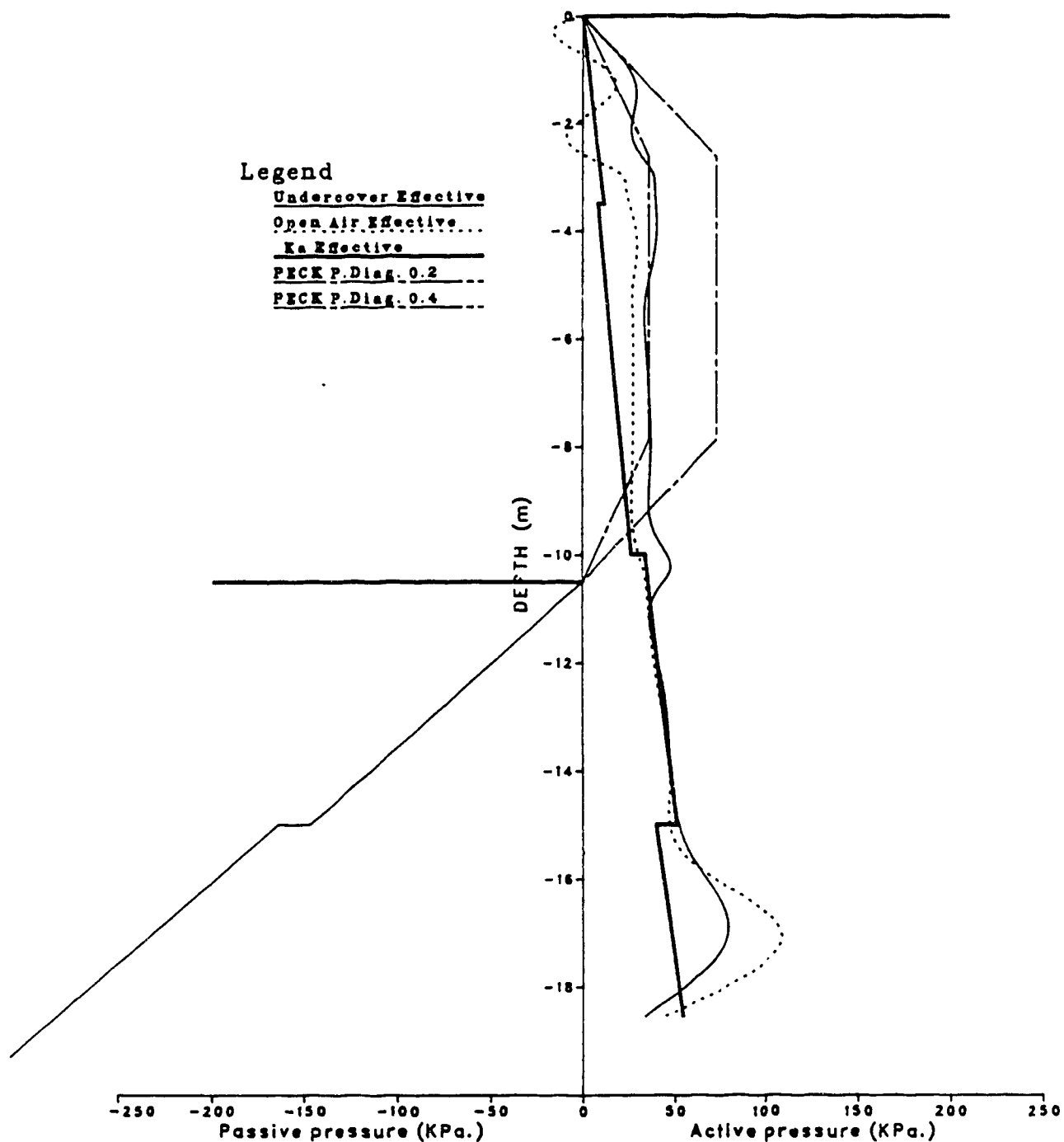


Figure 6.25 Final Effective Lateral Earth Pressure Diagrams
for the Station (Undercover) Section using Total Unit Weight
for Terzaghi and Peck Diagrams

EFFECTIVE LATERAL EARTH PRESSURE Station Section

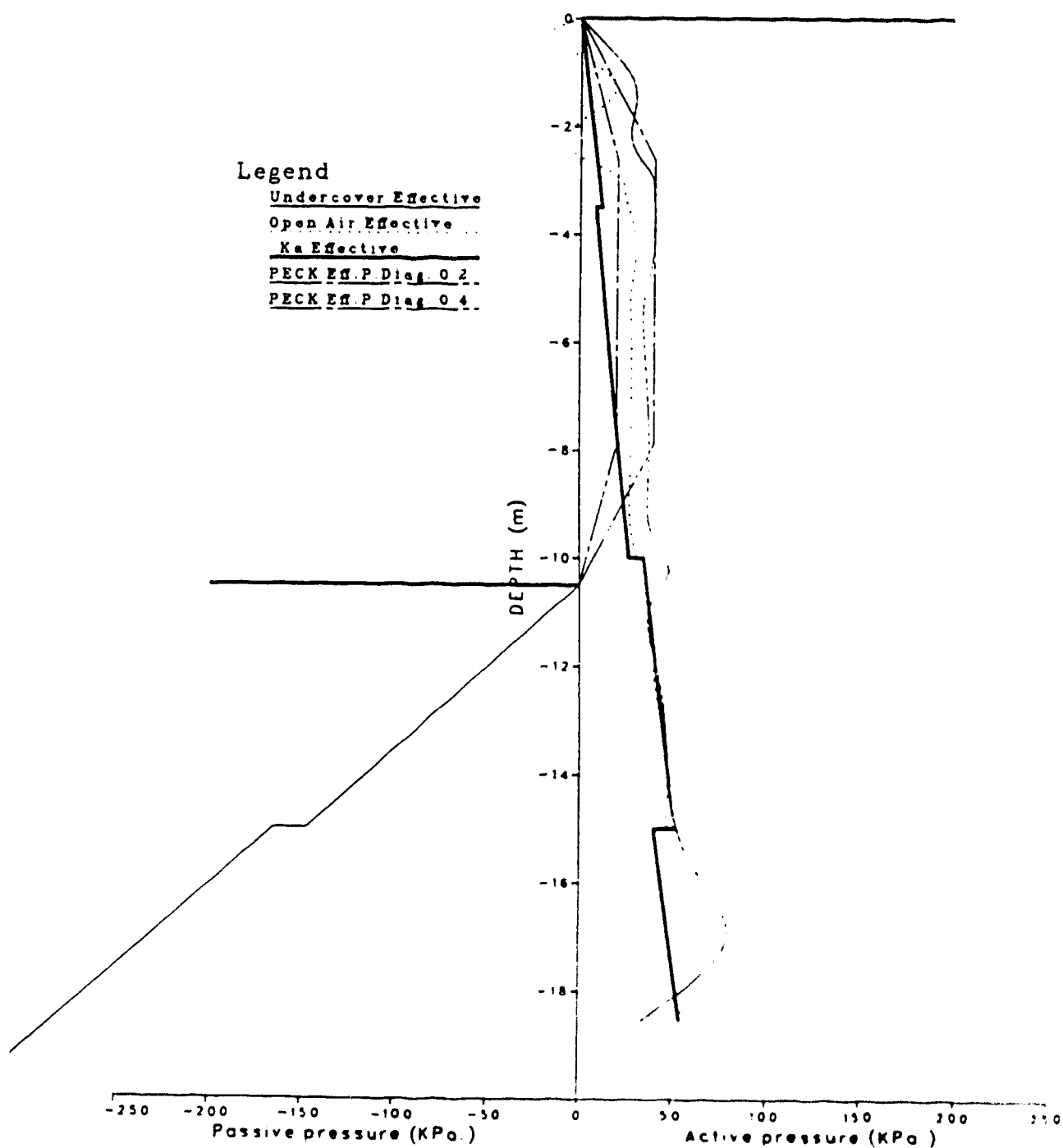


Figure 6.26 Final Effective Lateral Earth Pressure Diagrams
for the Station (Undercover) Section using Effective Unit
Weight for Terzaghi and Peck Diagrams

supported the use of the effective unit weight for Terzaghi and Peck's diagrams as most appropriate. It may be recommended that the pressure distribution for such host materials is better illustrated in Figure 6.29 where the height distribution will be divided into two parts only $0.25 H$ at the top and $0.75 H$ at the bottom rather than the trapezoidal distribution. Where H is the depth from the ground surface to the base of the excavation, as defined by Terzaghi and Peck (1967). The proposed diagram, a modification of the Terzaghi and Peck diagram, has been obtained from an envelope of the lateral earth pressures computed by F.E.M..

Mederios (1979) studied the influence of wall stiffness on the lateral earth pressure diagrams. He concluded that lower stiffness produces lower pressure and the increasing stiffness (i.e. increase in thickness of the concrete wall), the lateral earth pressure increases up to a limit. At this point any further increase in the wall stiffness (or thickness) has no significant effect on the lateral earth pressure diagrams. This conclusion was supported by Hubbard et al. (1984). Broms (1988) reported results on the effect of jet grouting and the use of micro-piles of 100 mm diameter on the predicted earth pressure for a soft clay in Singapore. The main aim of the use of jet grouting and the micro piles was to improve the stability of the excavation by improving the material properties of the base of the excavation. The results showed a reduction in the lateral

LATERAL EARTH PRESSURE Station Section

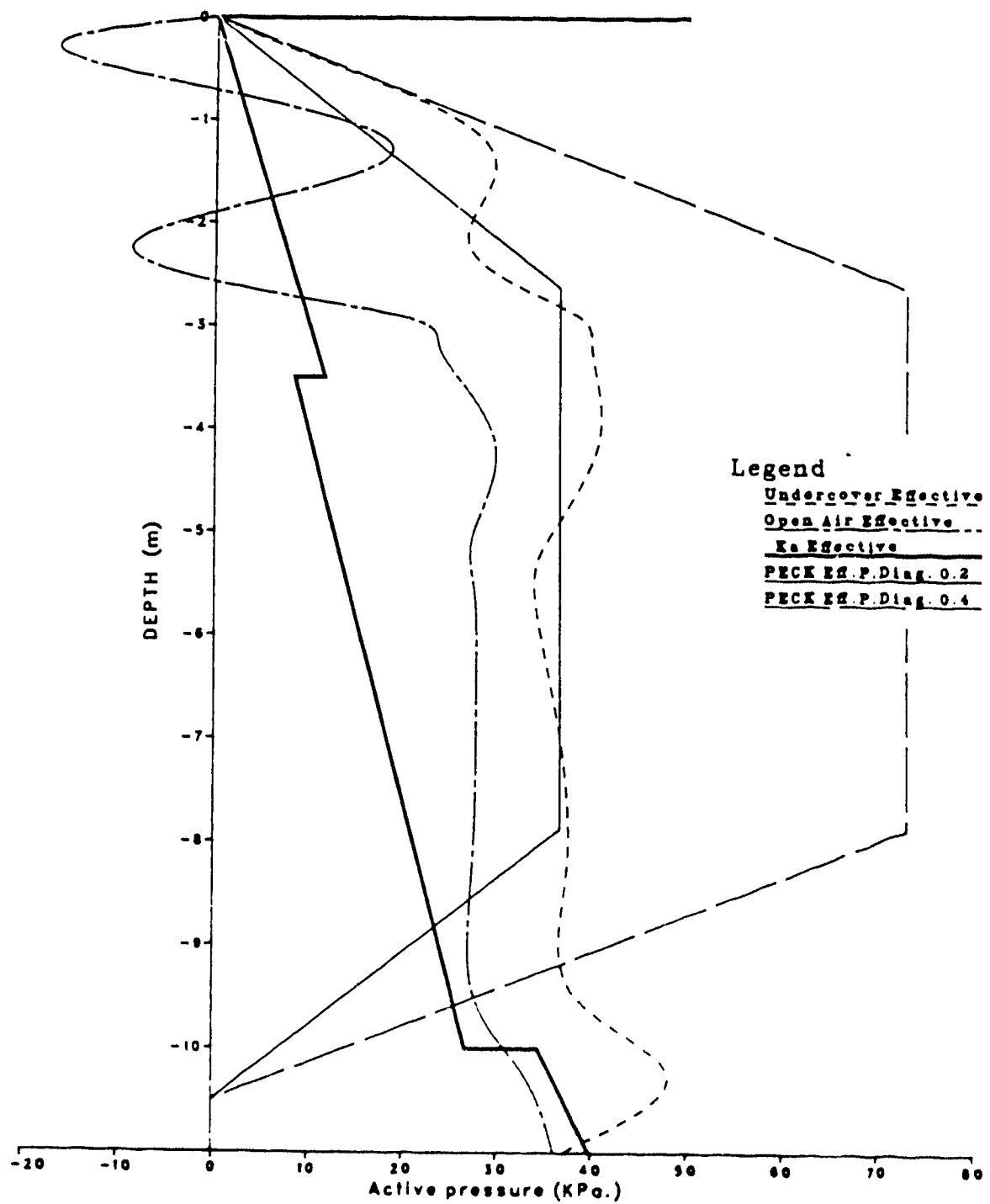


Figure 6.27 Final Effective Lateral Earth Pressure Diagrams for the Station (Undercover) Section using Total Unit Weight for Terzaghi and Peck Diagrams - Expanded View

Metro research project - final report. Submitted to the IDRC and NAT.

EL-Nahhas, F., 1980. The behaviour of tunnels in stiff soils. Ph.D. Thesis, Department of Civil Engineering, University of Alberta, Canada.

EL-Nahhas, F., 1987. Prediction of ground movement adjacent to a supported deep excavation. Proceedings Ninth African Regional Conference, Lagos, Nigeria, September.

EL-Nahhas, F., Eisenstein, Z., Shalaby, A., Abdel Salam, M., and EL-bedaiwy, S., 1988. Geotechnical performance of diaphragm walls during construction of Cairo Metro tunnel. Proceedings of the International Congress on Tunnels and Water, ITA, Madrid, Vol. 1, pp. 259-266.

EL-Nahhas, F., Eisenstein, Z., Shalaby, A., Abdel Salam, M., and EL-bedaiwy, S., 1989. Behaviour of diaphragm walls during construction of Cairo Metro, Submitted for publication in the XII International Conference of Soil Mechanics and Foundation Engineering, Rio de Janeiro, Brazil.

EL-Nahhas, F., Eisenstein, Z., Shalaby, A., Abdel Salam, M., and EL-bedaiwy, S., 1989. In situ behaviour of Orabi subway station during construction. Submitted for publication in the International Congress on Progress and Innovations in Tunnelling, Sept., 1989, Toronto, Ontario.

EL-Ramli, A.H., 1985. A geotechnical study of the greater Cairo zone as related to the behaviour of a Mighty River. Proceedings of Seminar on Some Foundation Problems in Egypt and Northern Germany, pp. 106-123.

EL-Sohby, M.A., and Mazen, O., 1985. Geological aspects in Cairo subsoil development. Proceedings 11th ICSMFE, San Francisco, Vol. 3, pp. 2401-2405.

Evison, S.E., 1988. A ring and spring model for tunnel liner design. M.Sc. Thesis, Department of Civil Engineering, University of Alberta, Canada.

Fang, M.L., 1987. A deep excavation Taipei Basin.

- Proceedings 9th Southeast Asian Geotechnical Conference, Bangkok, Thailand, pp. 2.35-2.41.
- Finno, R.J., Nerby, S.M., Atmatzidis, D.K., 1988. Ground response to sheet pile installation in clay. Proceedings Second International Conference on Case Histories in Geotechnical Engineering. June, St. Louis, Mo., Paper No. 6.43, pp. 1297-1301.
- Fourtean, R., 1897. Note sur la stratigraphie du NukaHam, Bulletin Societe Geologie France, (25), pp. 208-211.
- Green, G.R., 1973. Principles and performance of two inclinometers for measuring horizontal ground movements. Proceedings of Symposium on Field Instrumentation in Geotechnical Engineering, Butterworth and Co., London.
- Hanna, T.H., 1973. Foundation instrumentation. Trans-Tech Publications, Cleveland.
- Hansmire, W., 1975. Field measurements of ground displacements about a tunnel in soil. Ph.D. Thesis, University of Illinois at Urbana-Champaign.
- Hanson, L.A., Clough, G.W., 1981. The significance of clay anisotropy in finite element analysis of supported excavations. Proceedings of the Symposium held at Chicago, Illinois, August, pp. 73-92.
- Hubbard, H.W., Potts, D.M., Miller, D., and Burland, J.B., 1984. Design of the retaining walls for the M25 cut and cover tunnel at Bell Common. Geotechnique, Vol. 34, No. 4, pp. 495-521.
- Hurst, H.E., 1944. A short account of the Nile basin. Allen and Unwin, London.
- Hurst, H.E., 1966. The Nile Basin. Allen and Unwin, London.
- Janbu, N., 1963. Soil compressibility as determined by oedometer and triaxial tests. European Conference on Soil Mechanics and Foundation Engineering, Weissbaden, Germany, Vol. 1, pp. 19-25.

- Kaiser, P., Chan, D.H., Tannant, D., Pelli, F., and Neville, 1987. Numerical simulation of room 209 instrument rig. A report submitted to Atomic Energy of Canada Ltd., Whiteshell Nuclear Research Establishment, Pinawa, Manitoba, Canada.
- Konokike, K., and Ono, K., 1987. Prediction of the behaviour of earth retaining walls. Proceedings 9th Southeast Asian Geotechnical Conference. pp. 2.13-2.22.
- Lee, F.H., Yong, K.Y., Lee, S.L., and Toh, C.T., 1989. Finite element modelling of a strutted excavation. Proceedings of the Third International Symposium on Numerical Models of Geomechanics (NUM OGIII), May, Niagra Falls, Canada, pp. 577-584.
- Ludwig, E., 1936. The Nile. Third Edition of the English Translation, Allen and Unwin, London.
- Mana, A.I., and Clough, G.W., 1981. Prediction of movements for braced cut in clay. Journal of soil mechanics and foundation devision. ASCE. volume 107, GT6, pp 759-777
- Marsland, A., 1973. Instrumentation of flood defence banks along the River Thames. Field Instrumentation in Geotechnical Engineering. Butterworth and Co., London, pp. 287-303.
- Marsland, A., and Quarterman, R., 1974. Further development of multipoint extensometer for use in highly compressible ground. Geotechnique, Vol. 24, pp. 429-433.
- Medeiros, L.V., 1979. Deep excavation in stiff soils. Ph.D. Thesis, Department of Civil Engineering, University of Alberta, Canada.
- Medeiros, L., and Eisenstein, Z., 1983. A deep retaining structure in till and sand. Part I, Canadian Geotechnical Journal, Vol. 20, No. 1, pp. 120-130.
- Medeiros, L., and Eisenstein, Z., 1983. A deep retaining structure in till and sand. and II, Canadian Geotechnical Journal, Vol. 20, No. 1, pp. 131-140.

- Morgenstern, N.R., and Eisenstein, Z., 1970. Methods of estimating lateral loads and deformations. Proceedings ASCE Specialty Conference on Lateral Stresses and Earth Retaining Structures. Cornell University, State-of-the-Art Volume, pp. 51-102.
- Morton, D.J., 1982. Cut and cover excavation. Chapter 14, Tunnel Engineering Handbook, Ed. by Bickel, J.O. and Kuesel, T.R., Van Nostrand, ISBN:0.442.28127-7, pp. 395-416.
- McCarthy, D.F., 1982. Essentials of soil mechanics and foundations - basic geotechnics. Reston Publishing Company Inc. Reston, Virginia, 516 p.
- McRoberts, E.C., Barlow, J.P., and Plewes, H.D., 1988. Geotechnical design considerations for SLRT Grandin station - Edmonton. Proceedings of the 7th Annual Canadian Tunnelling Conference, May, Edmonton, Alberta, pp. 73-84.
- Norwegian Geotechnical Institute, 1962. Vibrating wire measuring devices used at strutted excavations. Technical Report No. 9, 151 p.
- Peck, R.B., 1969. Deep excavation and tunnelling in soft ground. Proceedings Seventh International Conference on Soil Mechanics and Foundation Engineering. Mexico, State-of-the-Art Volume. pp. 225-290.
- Peck, R.B., 1985. The last sixty years. Proceedings of the 11th International Conference on Soil Mechanics and Foundation Engineering, San Francisco, U.S.A., Golden Jubilee Volume, pp. 123-133.
- Pit Slope Manual, Chapter 4, 1977. Cement Report 77-13 prepared for Canada Centre for Mineral and Energy Technology, Energy, Mines and Resources Canada.
- Potts, D.M., and Fourie, A.B., 1984. The behaviour of a propped retaining wall, results of a numerical experiment. Geotechnique 34, No. 3, pp. 383-404.
- Project documents and reports. A series of documents and reports for Greater Cairo regional metro line - provided

by the National Authority for Tunnels (NAT), Egypt, Cairo.

- Riker, R., and Dailer, D., 1988. Design, construction and performance of a deep excavation in soft clay. Proceedings Second International Conference on Case Histories in Geotechnical Engineering, June, St. Louis, Mo., Paper No. 6.32, pp. 1263-1269.
- Robertson, P.K., Campanella, R.G., and Wightman, A., 1983. A SPT-CPT correlation. Journal of Geotechnical Division of American Society of Civil Engineers, Vol. 29, pp. 1449-1459.
- Rott, W. and Veder, Ch., 1980. Earth pressure experiment on Diaphragm Walls. Ground Engineering, volume 13, no. 13, April, pp 35-36
- Said, R., 1962. Geology of Egypt. Elsevier, Amsterdam and New York, 377 p.
- Said, R., 1981. The geological evaluation of the river Nile. Springer Verlag, N.Y., 151 p.
- Savigny, K.w., 1980. In Situ analysis of naturally occurring creep in ice-rich permafrost soil. Ph.D thesis, Department of civil Engineering, University of Alberta.
- Schlosser, F., Magnan, J.P. and Holtz, R.D. 1985. Geotechnical engineering construction (in french), proceeding Eleventh ICSMFE, San Francisco, volume 1, pp 211-254
- Schmidt, B., and Dunnicliff, C.J., 1974. Construction monitoring of soft ground rapid transit tunnels. Volume I: A definition of needs and potential developments. Report prepared for Transportation System Center, NTIS NO. PB241536.
- Schweiger, H.F., and Hass, W., 1988. Application of a thin layer interface element to the geotechnical problems. Proceedings Numerical Methods in Geomechanics, Balkema, Rotterdam, pp. 907-912.
- Shenouda, N., 1973. A comparative study of soil formation in

Cairo. M.Sc. Thesis, The University of Cairo.

Shi, L.P., Chang, K.T., and Yeh, H.Y., 1987. Performance evaluation of foundation excavation in Rong Cuang Building. Proceedings 9th Southeast Asian Geotechnical Conference, Bangkok, Thailand, pp. 2.43-2.52.

Simmonds, S.H., 1981. User manual for computer program (PFT). Internal Note, Department of Civil Engineering, Univerisity of Alberta, Canada.

Simmonds, S.H., 1988. Personal Communication.

Smith, P.D.K., and Burland, J.B., 1976. Performance of a high precision multipoint borehole extensometer in soft rock. Canadian Geotechnical Journal, Vol. 13, pp. 172-176.

Terzaghi, K., and Peck, R.B., 1967. Soil mechanics in engineering practice. Second Edition. John Wiley, New York, (Chapter 8).

Thomas, H.S.H., 1965. The measurement of strains in tunnel linings using the vibrating wire technique. Conference on Strain Measurement in Difficult Environments.

Timber Design Manual, 1980. (Metric Edition). Laminated Timber Institute of Canada, p. 404, Table 9a.

Tominaga, M., Vchiyama, H., Koseki, T., and Fukuwaka, M., 1985. A computerized construction control system and its application to an excavation. Proceedings of the Fifth International Conference on Numerical Methods in Geomechanics, Nagoya, Japan, April, pp. 927-934.

Tschebotarioff, G., 1949. Large scale earth pressure test with model flexible bulckheads. Princeton university, final report, Bur.Yards Docks ,U.S. Navey, January ,272pp

Tschebotarioff, G., 1973. Foundation, retaining and earth structures. Second Edition, McGraw Hill Book Company, New York, 427 p.

- Wolosick, J.R., Feldman, A.I., 1987. Reliability of bending moments backcalculated from inclinometer measurements. Geotechnical News, September, pp. 26-27.
- Wood, L.A., and Perrin, A.J., 1984. Observations of a strutted diaphragm wall in London clay. A preliminary assessment. Geotechnique 24, No. 4, pp. 563-579.
- Yih, C., and Khera, R.P., 1988. Slurry wall instrumentation and monitoring in Taipei. Proceedings Second International Conference on Case Histories in Geotechnical Engineering, June, St. Louis, Mo., Paper No. 5.18, pp. 985-988.

For the Steel Struts

Diameter for tunnel test section - 400 mm

Diameter for station tests section - 600 mm

The following relationship was used to calculate the force from the strains measured in the field.

$$P = \epsilon E_s A \quad [A.1]$$

where

P = force

ϵ = Axial strain (microns, μ)

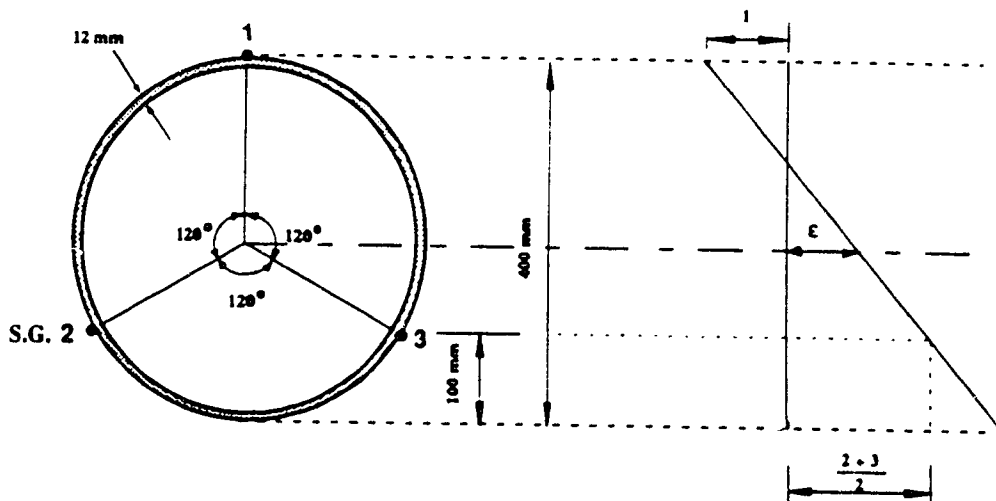
E = Young's modulus for steel = 206.85×10^6 kPa

A = cross-sectional area

for example

A = cross-sectional area for tunnel section = 0.0146 m²

P = 0.308 e tons



For the Embedded Strain Gauges

using a transformed section

$$N = \frac{P}{A} I y \frac{M}{I} \quad [A.2]$$

where

N = normal stress at the top and bottom of the section

P = normal force

A = area of concrete and transformed steel

M = moment of inertia of the section

I = distance from centre line to top or bottom

Modulus of elasticity for concrete has been determined to be:

$$E_c = 31\,250 \text{ MPa}$$

As a result of low range of the measured strains in concrete, it is assumed that the concrete stress-strain curve is linear for these calculations (i.e. the working range is in the straight line portion of the stress-strain curve).

N will be calculated from the measured strains

A is 0.9 m² for tunnel roof for station 1 m²

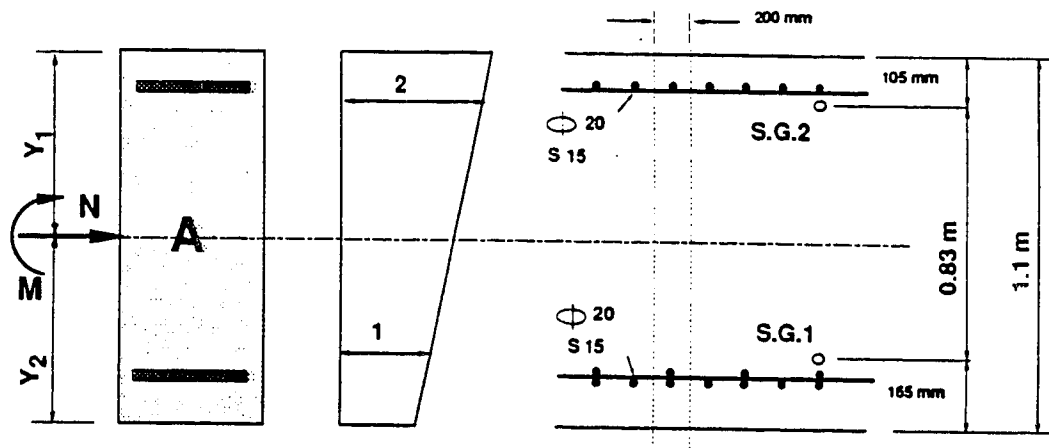
A is 1.1 m² for tunnel raft for station 1 m²

Using the correct dimension for each section according to the exact location of the embedded strain gauges,

equation A.2 can be solved for P, the normal force. Solving A.2 for P can be expressed in this case as

$$P = \frac{N_1 + N_2}{2} A$$

where $A = 6\,597.0 \text{ mm}^2$ for tension using steel area only
therefore $P = 3\,288.5 (N_1 + N_2) \text{ tons}$.



Example of Geometry at Tunnel Test Section Raft

B. Field and Laboratory Tests

This appendix contains samples of the field and laboratory tests conducted and used in this study.

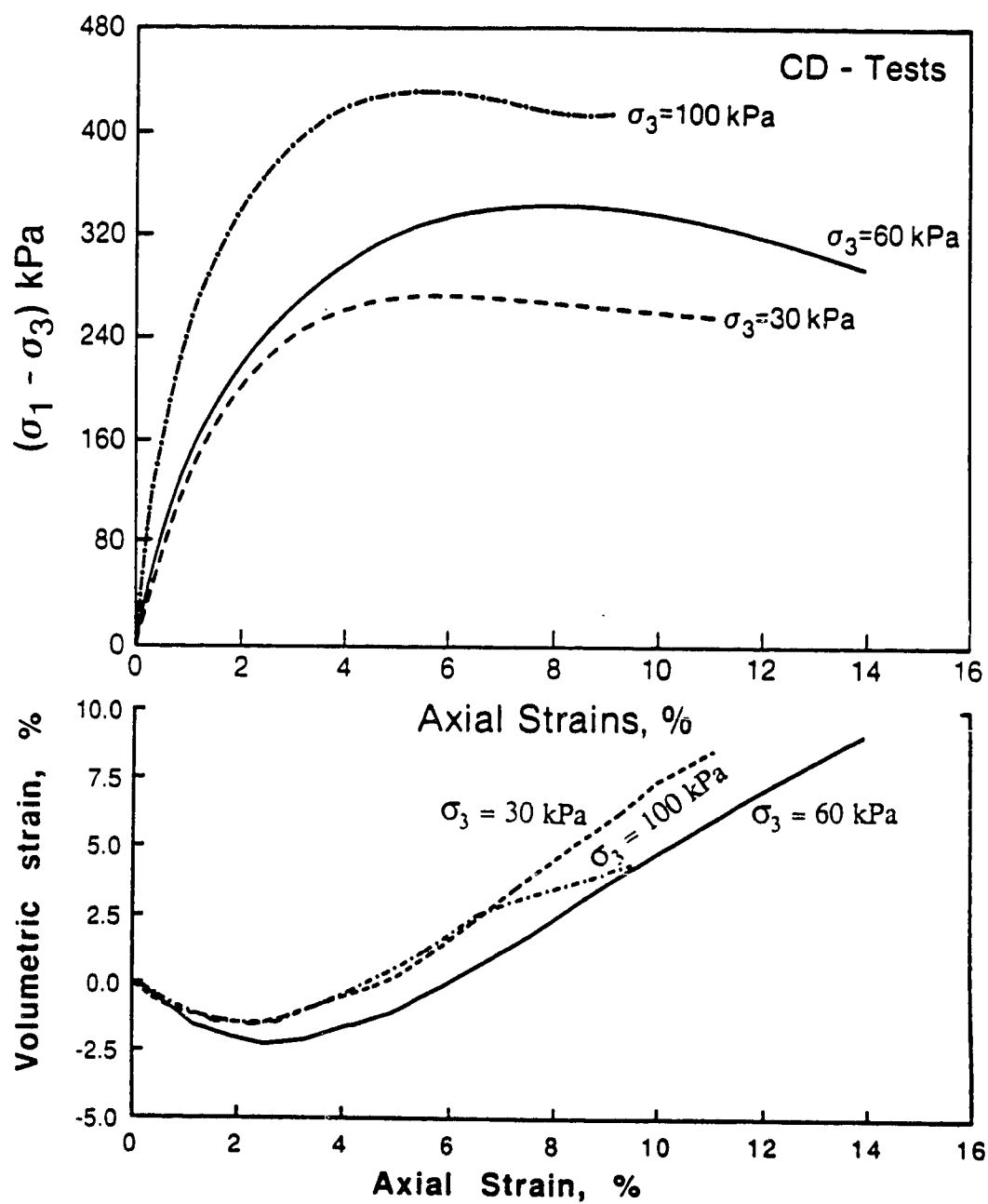


Figure B.1 Consolidated Drained Triaxial Test Results for
Silty Clay

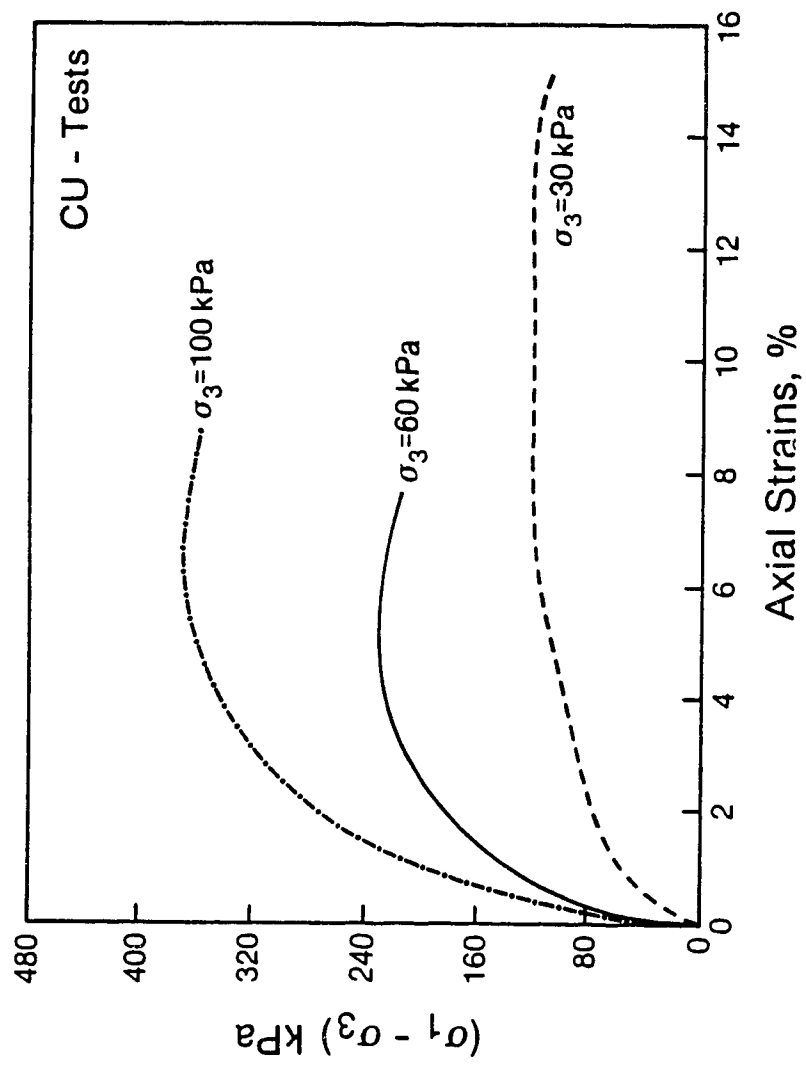
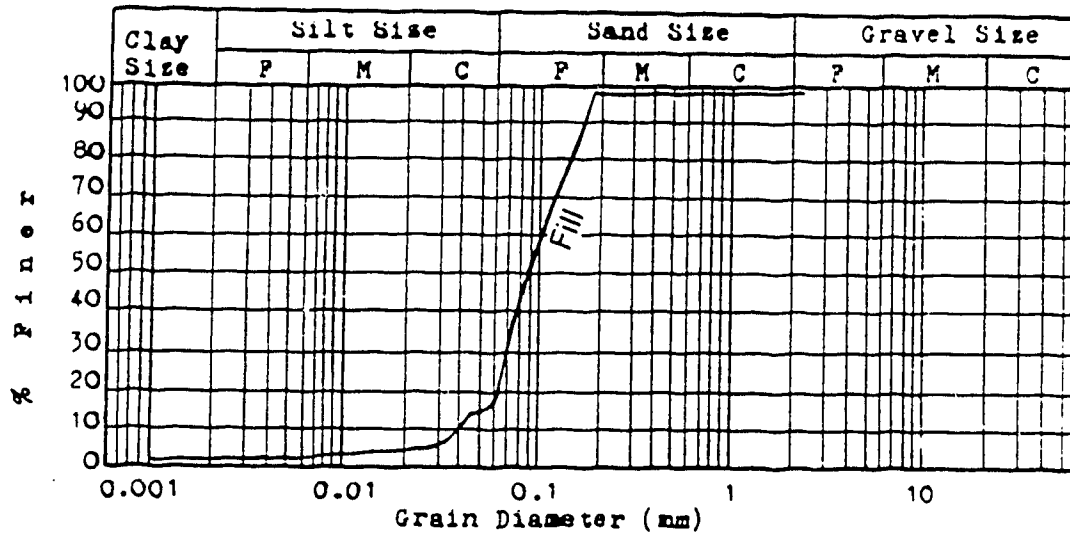


Figure B.2 Consolidated Undrained Triaxial Test Results for Silty clay

A - Station Test Section



B - Tunnel Test Section

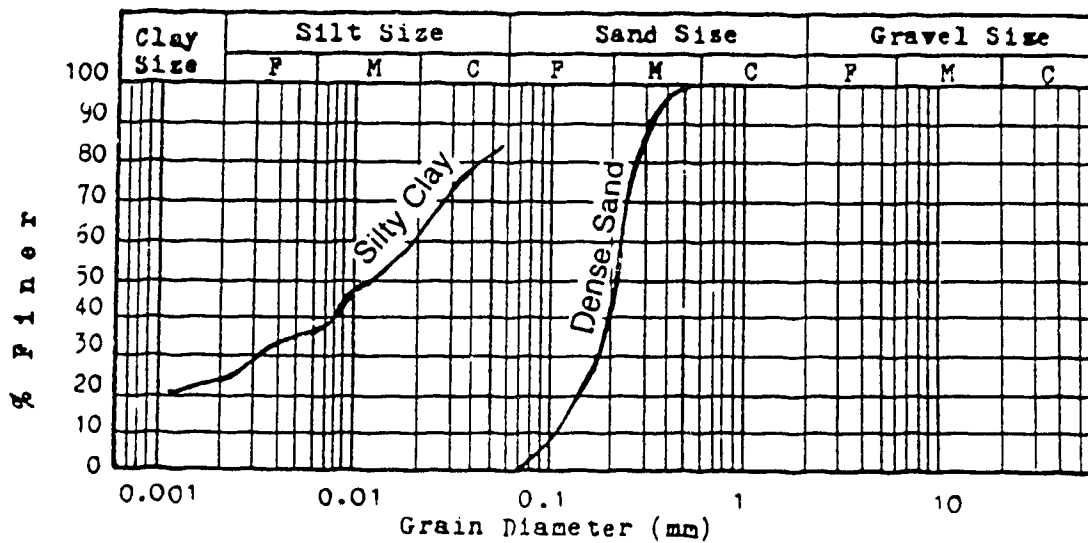
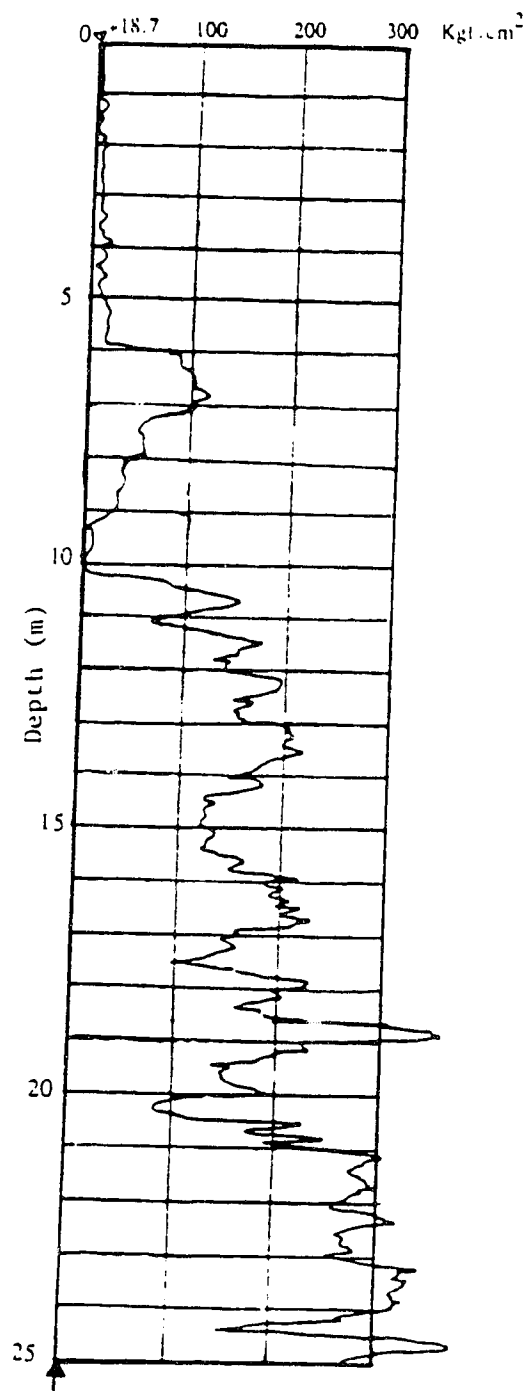
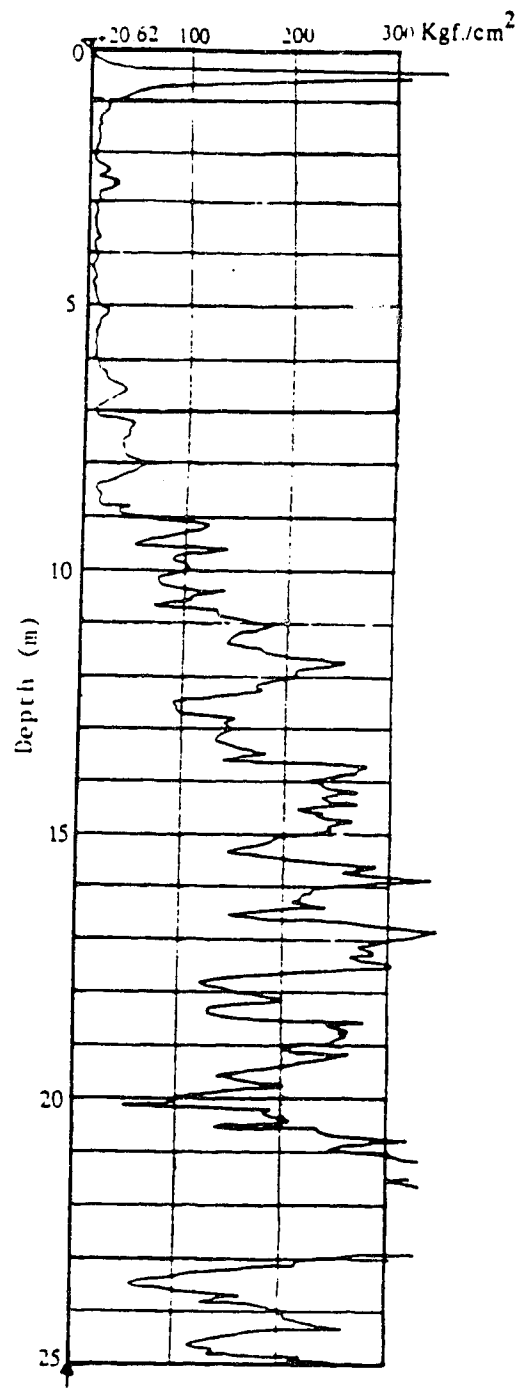


Figure B.3 Grain Size Distribution of Soils



CPT 2003
(18/2/1984)

Tunnel Section



CPT 9000
(14/2/1984)

Station Section

Figure B.4 CPT Results at the Test Sections

C. Determination of Concrete Properties

In order to determine the concrete properties used for each test section, specimens were collected during the pouring of concrete at each step of construction for both sections. Some of the specimens were instrumented with embedded strain gauges as shown in Plate 4.1. This was to assist in estimating the axial strain during testing. A standard test procedure explained by ASTM C469-83 (1983) was followed to determine the properties. The results were compared with the available results of the tests conducted by the National Authorities for Tunnels. Table C.1 summarizes the results to determine the compressive strength and the unit weight with an average value for the results.

To determine the elasticity modulus of the concrete used, nine specimens were tested and the results are shown in Table C.2. Figure C.1 shows a sample of the stress-strain relationship obtained for the tunnel test section.

The Canadian Concrete Manual provides an empirical equation to determine the modulus of elasticity as follows:

$$E_c = \gamma_c^{1.5} 0.043 \sqrt{f_c}$$

where

γ_c kg/m³ (range 2000-2500 kg/m³)

f_c MPa (range 20 - 40 MPa)

using the average values obtained from the tests

$f_c = 40.02 \text{ MPa}$ and $\gamma_c = 2375 \text{ kg/m}^3$

will yield $E_c = 31\,477 \text{ MPa}$

The average value for the modulus of elasticity as determined from our tests is $E_c = 31\,134 \text{ MPa}$. So, the modulus of elasticity for the concrete used in the analyses is

$E = 31\,250 \text{ MPa}$

The results provided by the contractor are as follows:
average unit weight = 23.9 kN/m^3 and the average for the compressive strength of 41.11 MPa , while the previously mentioned results yielded an average of 23.7 kN/m^3 - unit weight and 39.54 for the compressive strength. The average value was for all tests regardless of the test section. The average values used in the analysis were
unit weight = 2.5 t/m^3
compressive strength = 40 MPa

Table C.1 The Results of the Concrete Tests

No. & location of Specimen	Weight kg	Cross-section Area cm ²	Failure Load t	Unit f_c kN/m ³	Compressive strength f_c MPa
TUNNEL SECTION					
Raft *1	12.82	182.65	75.0	23.05	42.42
2	13.16	177.42	80.75	24.36	44.60
*3	13.68	181.54	77.50	24.15	41.84
4	12.72	172.50	61.20	24.22	34.77
5	12.67	179.08	60.50	23.48	33.11
Roof 6	13.00	180.98	72.25	23.59	39.12
7	12.82	181.53	76.00	23.19	41.03
8	12.94	179.08	69.25	23.73	37.90
*9	12.94	180.98	66.75	23.48	36.14
*10	13.00	180.27	81.75	23.68	44.44
STATION SECTION					
Roof 11	13.12	179.79	81.25	23.97	44.29
12	12.84	180.27	57.75	23.39	31.39
13	12.98	179.32	76.00	23.77	41.53
*14	13.10	179.08	74.25	24.02	40.63
*15	12.86	177.65	68.75	23.77	37.92
Raft 16	12.80	181.46	77.00	23.17	41.58
17	12.94	172.03	73.00	24.70	41.58
18	12.84	177.89	77.50	23.66	42.69
*19	13.24	181.46	80.25	23.96	43.34
Average	12.97	179.21	72.98	23.75	40.02

* Tests with embedded strain gauges

Table C.2 Moduli of Elasticity for Concrete based on
Laboratory Test Results

Test No.	Unit Weight γ_c kN/m ³	Compressive Strength f_c MPa	Elasticity Modules E_c MPa
*1	23.05	42.42	24,189.0
*3	24.15	41.84	31,848.0
*9	23.48	36.14	26,214.0
*10	23.68	44.44	26,132.0
12	23.39	31.39	34,788.0
*14	24.02	40.63	35,367.0
*15	23.77	37.92	35,278.0
16	23.17	41.58	34,788.0
*19	23.96	43.34	31,603.0
Average	23.63	39.97	31,134.0

* Tests with embedded strain gauges

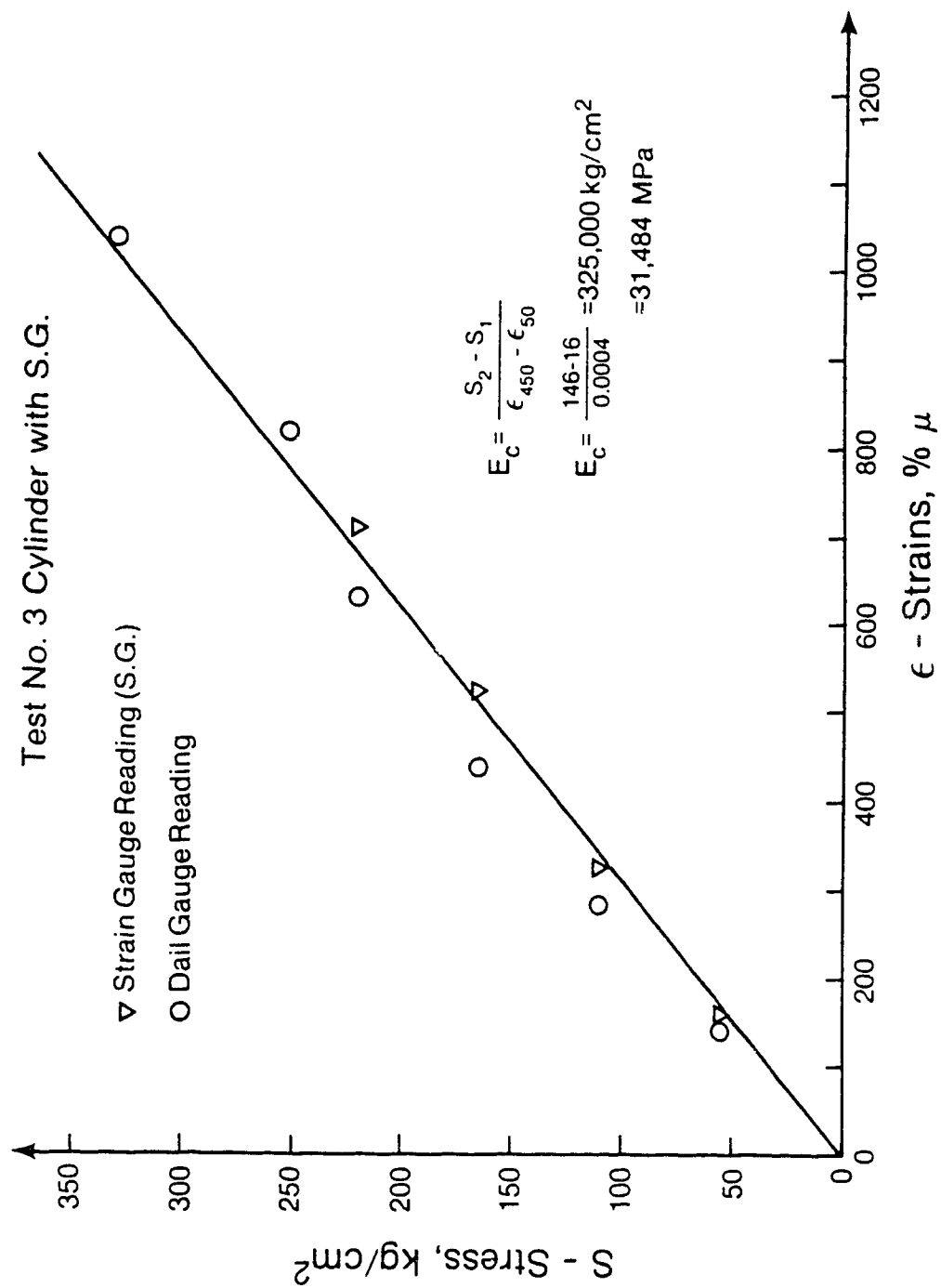
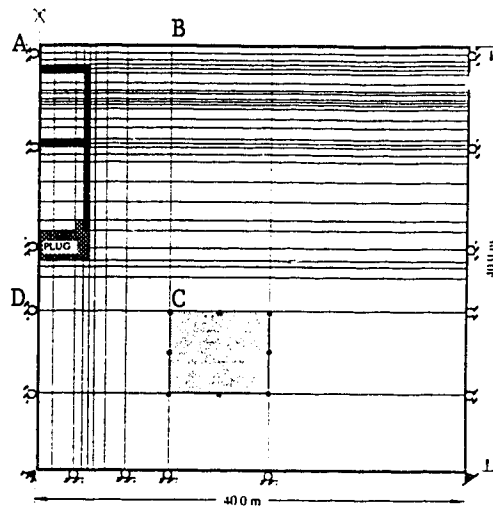


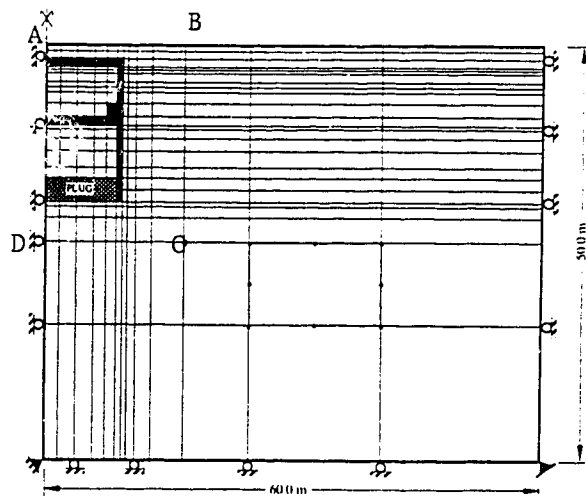
Figure C.1 Stress-Strain Relationship for Concrete

D. Finite Element Results

This appendix contains the results of the finite element analyses of this study for the running tunnel and station test sections. The analyses for the station were conducted for two different construction methods. Displacement arrows shown in the figures refer to the portion ABCD of the F.E.M. meshes shown below. The scale for the arrows is 1:5 mm .



Running Tunnel Test Section Finite Element Mesh



Station Test Section Finite Element Mesh

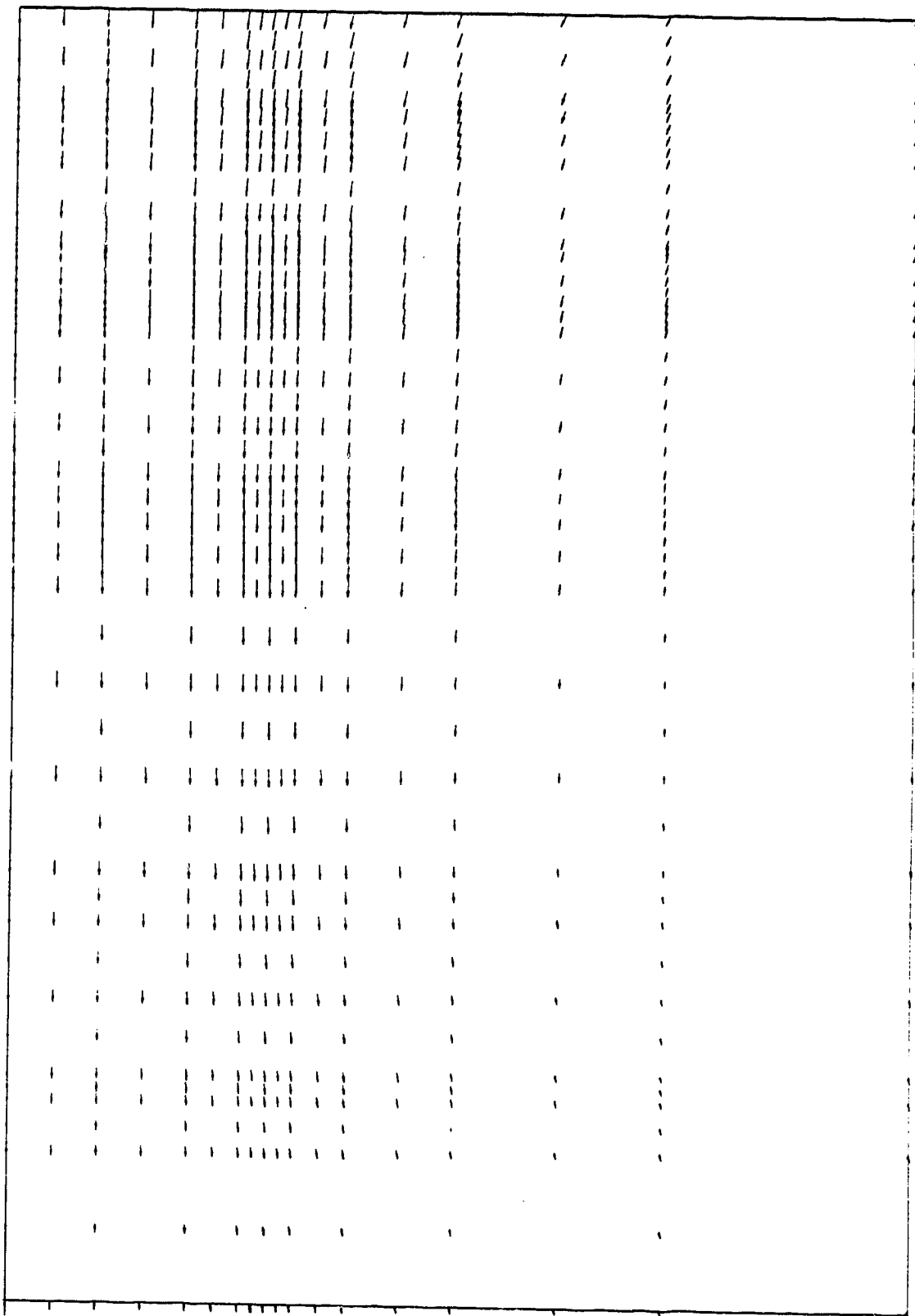


Figure D.1 Displacement Arrows - Tunnel Section - Step (2)

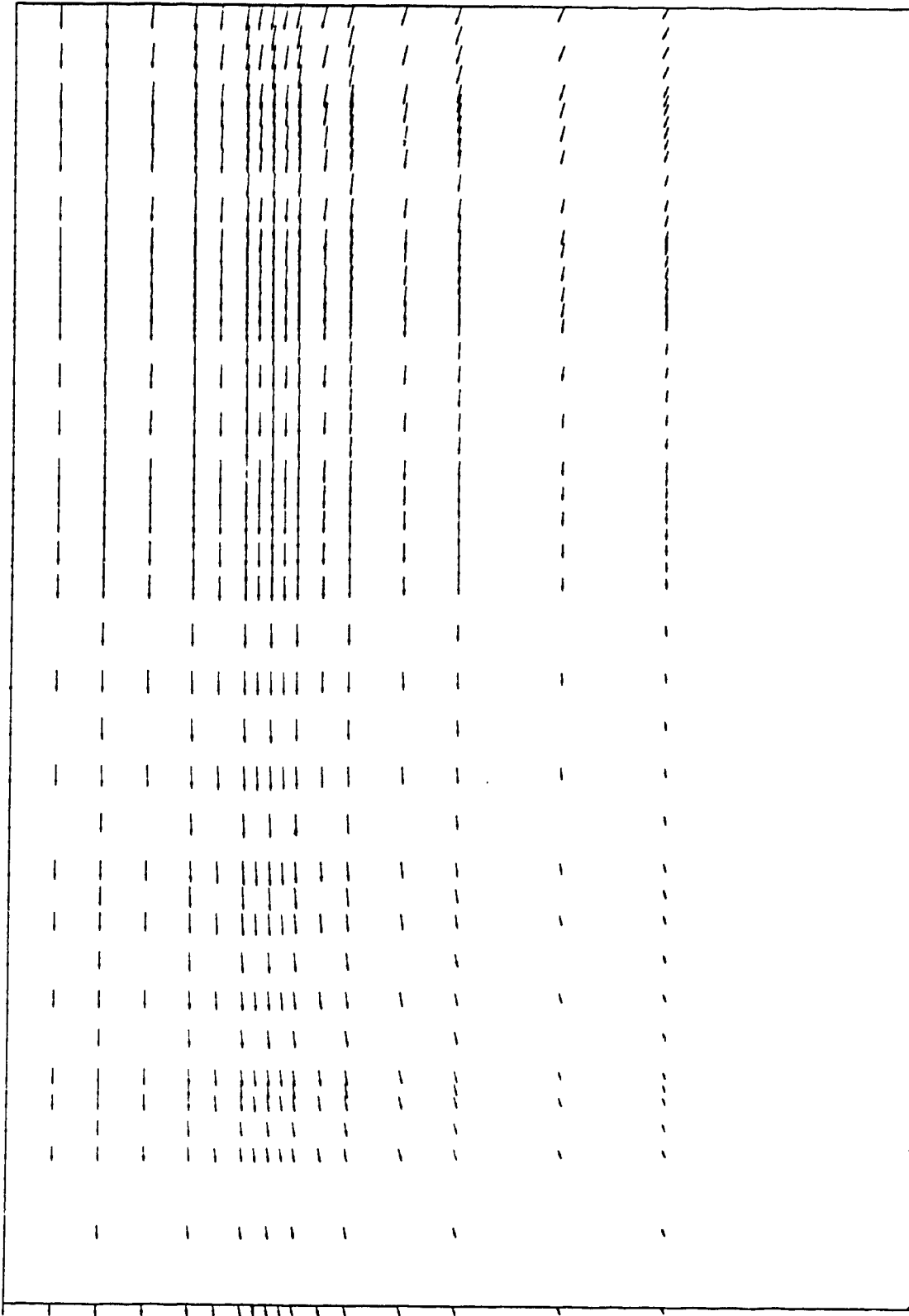


Figure D.2 Displacement Arrows - Tunnel Section - Step (3)

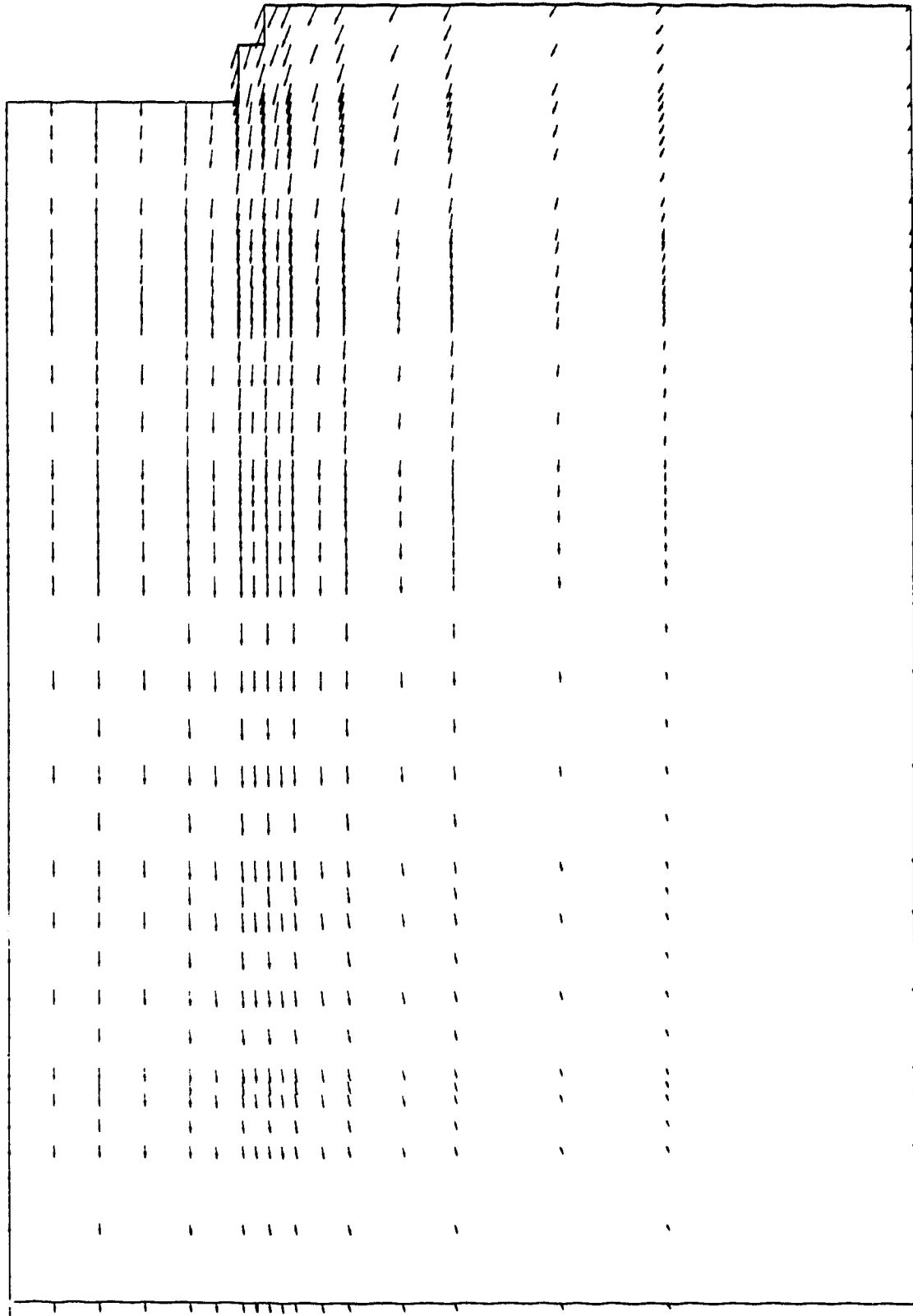


Figure D.3 Displacement Arrows - Tunnel Section - Step (4)

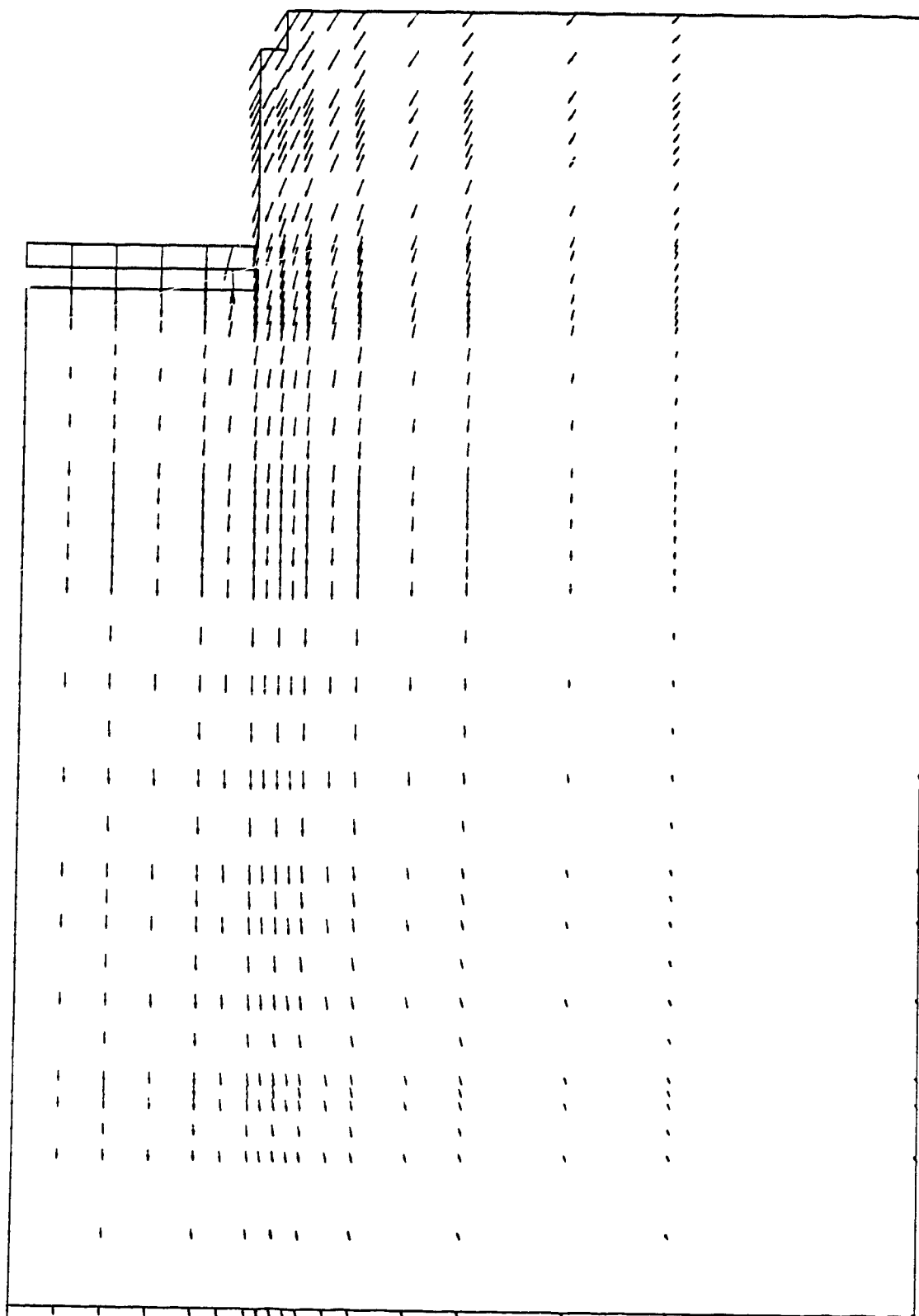


Figure D.4 Displacement Arrows - Tunnel Section - Step (5)

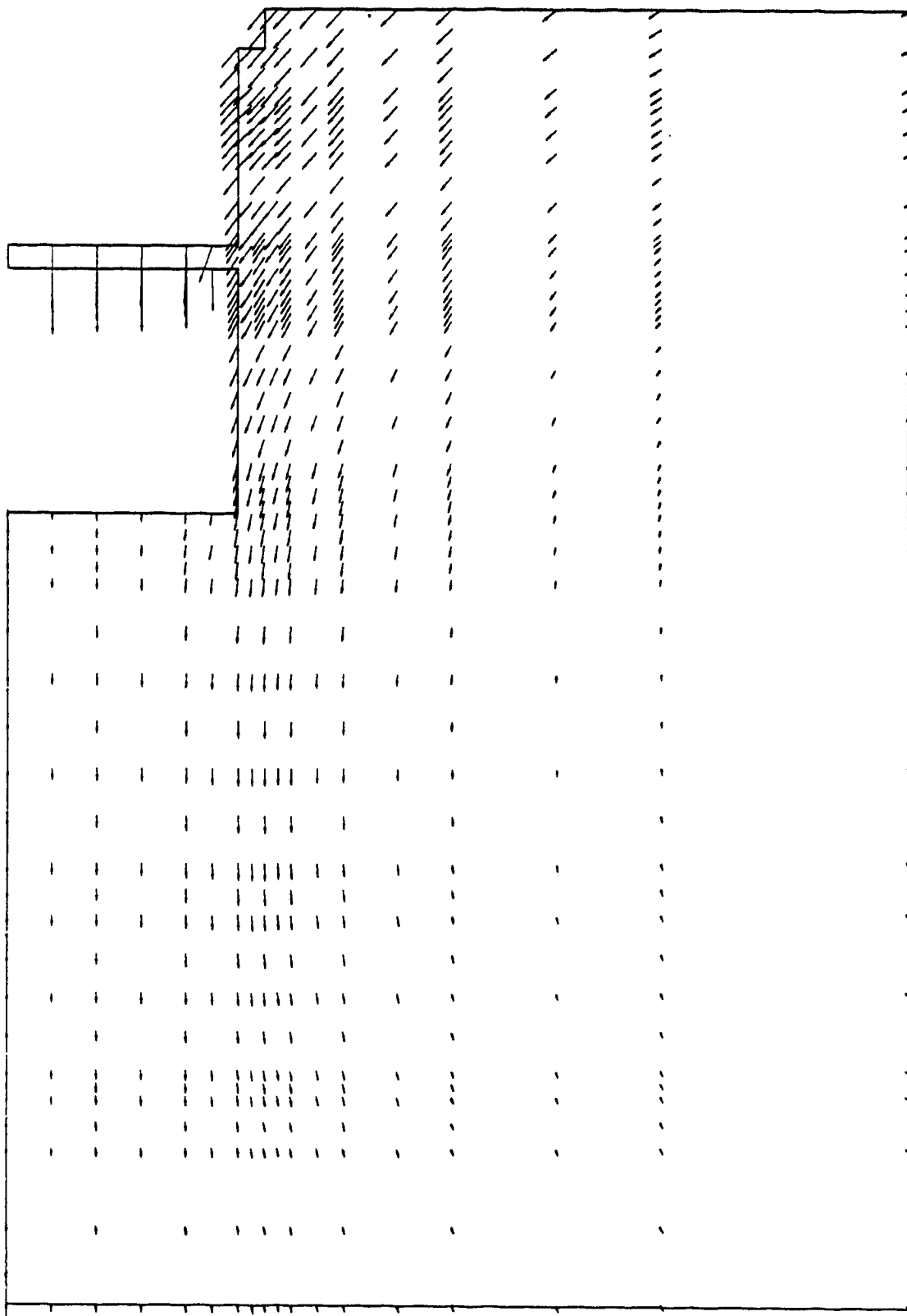


Figure D.5 Displacement Arrows - Tunnel Section - Step (6)

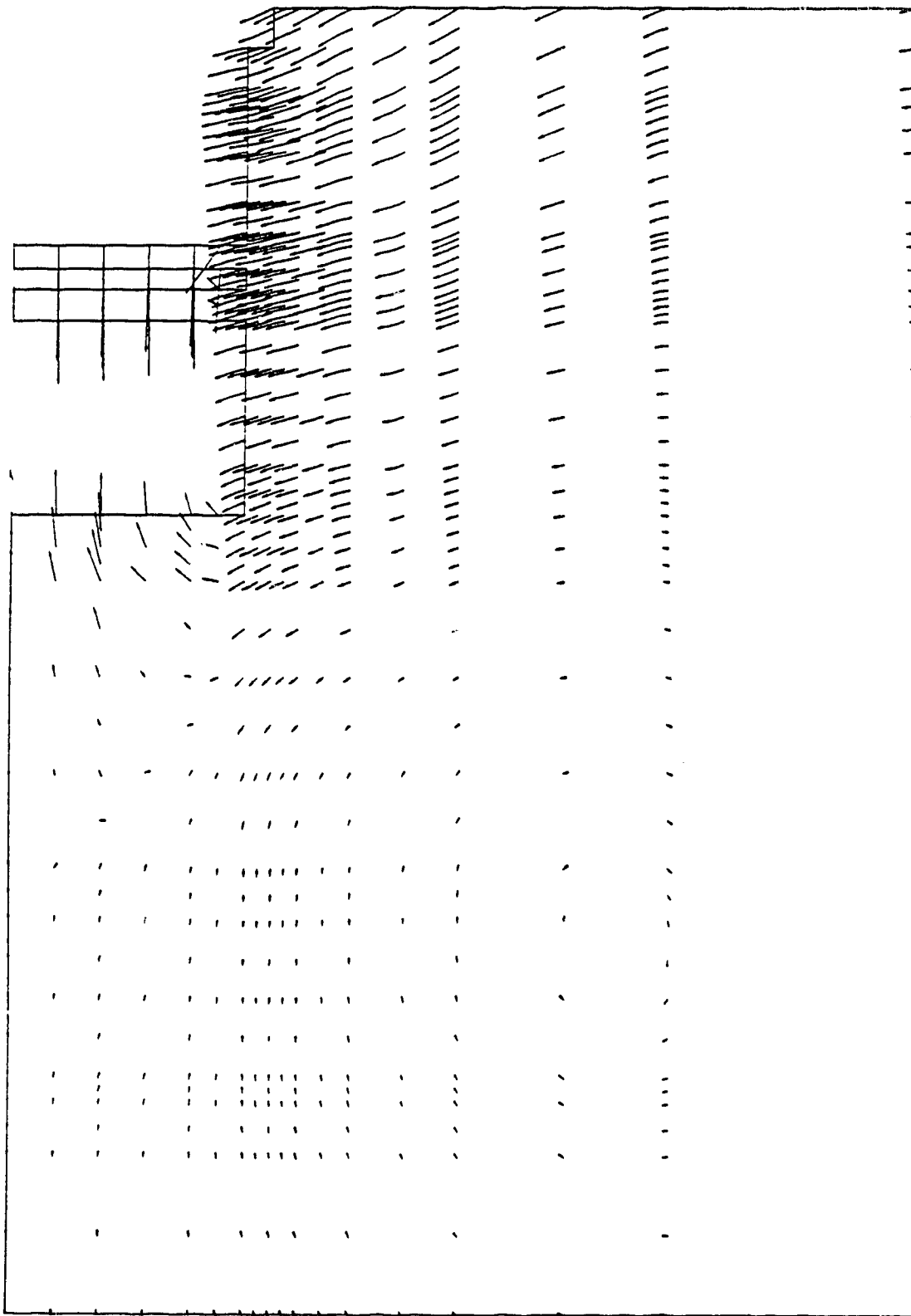


Figure D.6 Displacement Arrows - Tunnel Section - Step (7)

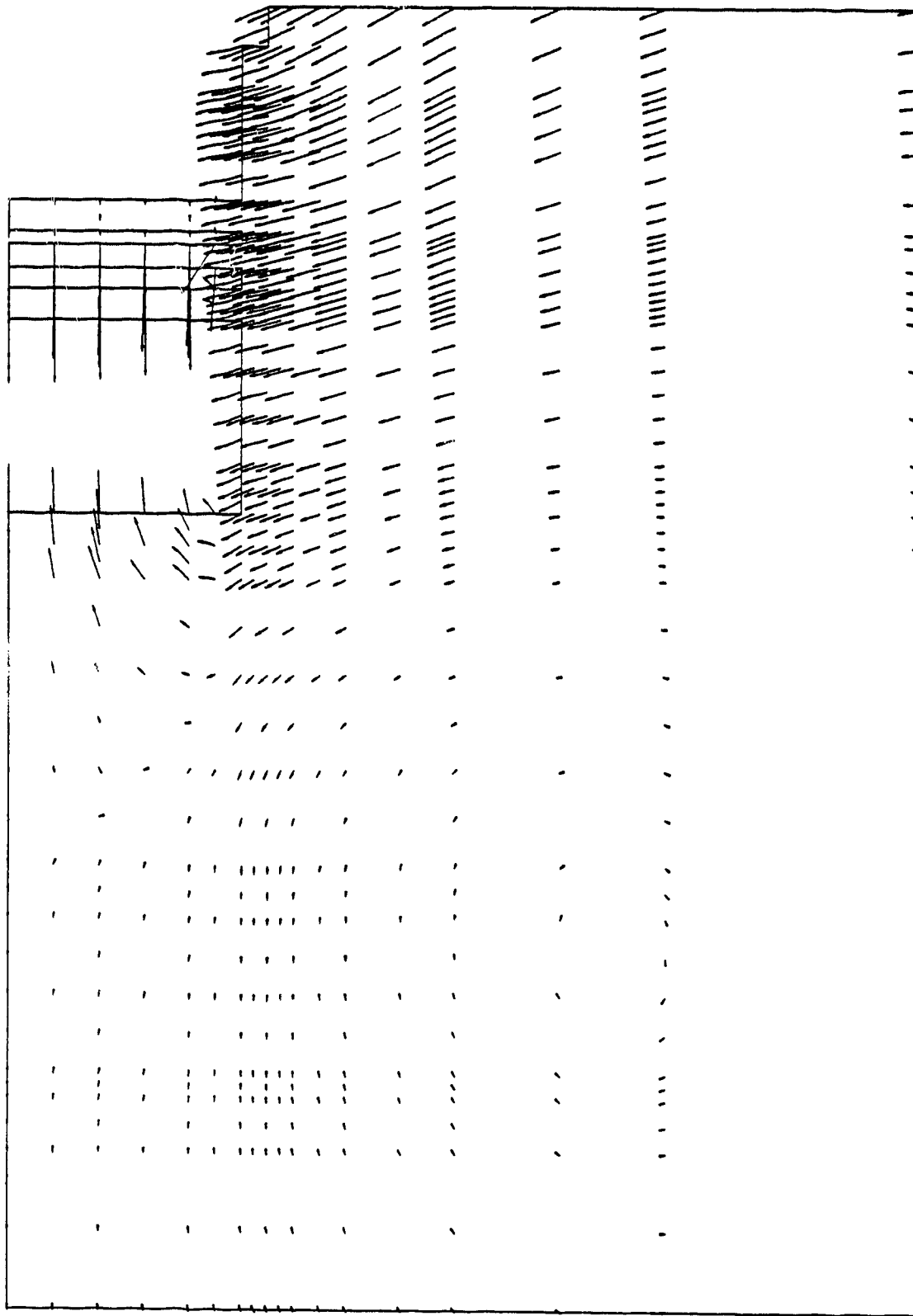


Figure D.7 Displacement Arrows - Tunnel Section - Step (8)

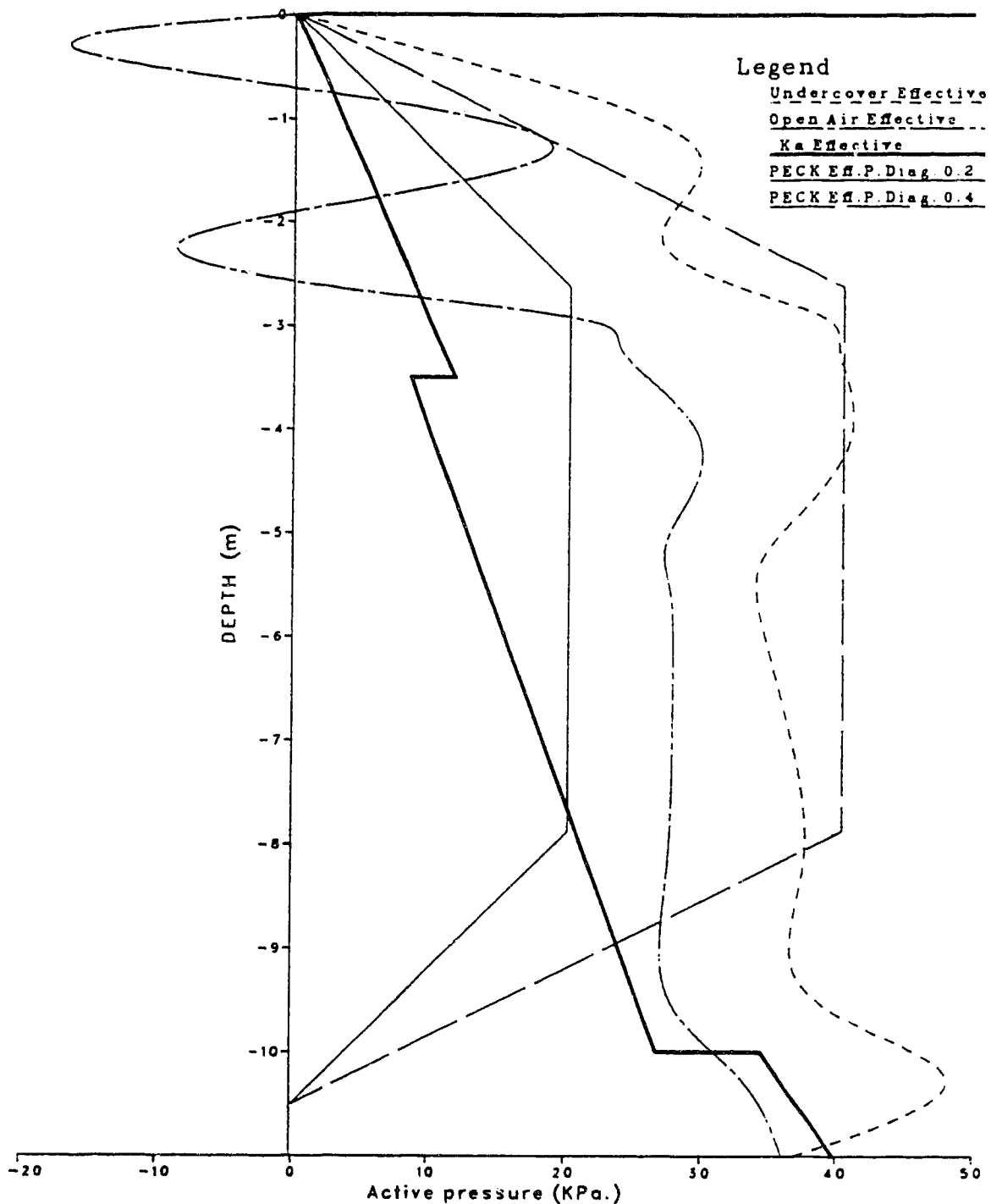


Figure 6.28 Final Effective Lateral Earth Pressure Diagrams for the Station (Undercover) Section using Effective Unit Weight for Terzaghi and Peck Diagrams - Expanded View

The material contained in this page has been removed because of the unavailability of copy right permission for part of this material.

Figure 6.29 presents the proposed recommendation for the lateral earth pressure diagrams for diaphragm walls compared with the proposed diagrams by Tschebotarioff(1949) and Terzaghi and Peck (1969).

earth pressure as a result of the use of each of these methods. This was supported by the present study on stiff clays. It may be concluded that the construction procedure employed minimized the soil deformation around the tunnel.

The pressure diagrams suggested by Tschebotarioff (1949), (1973) for stiff clay using temporary and permanent support are presented in Figure 6.29. The study showed that such distributions are economical for lower stiffness walls such as the tunnel wall but underestimate when used for higher stiffness walls. It is deemed not conservative to apply the proposed diagrams for the diaphragm walls. McCarthy (1982) studied the type and magnitude of lateral movements required to reach the active lateral earth pressure. He recommended a value of $0.01 H$ to $0.02 H$ at the top of the cantilever. Movements in this study would be 105 to 210 mm. This can be widely applied, but would be appropriate for the backfill of the retaining wall. The highest predicted and measured value for the wall and soil at the top did not exceed 40 mm. For the stiffer wall (the open air excavation), a tension zone of approximately 2.5 m depth existed. This indicated that the soil can stand free without any support to this depth. The lateral movement predicted suggests that the ratio will be about $0.004 H$ or less, where H is the excavation depth. The excavation is primarily through fill and clays underlain by sands. The fill properties are very similar to those of the clay. If one material is assumed, the theoretical calculation for the

depth at which the clay can maintain vertical banks without providing any lateral support yields a value of $2c/\sigma_v K_A$ (see Crag, 1978) or 3.125 m. For the station section this is applicable, but in the tunnel section the hydrostatic pressure provided the major force causing the soil and wall deformations. This difference in behaviour is explained by the variations in wall thickness and stiffness. It is concluded that the deformation pattern will influence the lateral earth pressure distribution.

6.9 A Comparison Between SAFE and PFT

A comparison of the highly sophisticated finite element program, SAFE, and the PFT program will be performed with the tunnel section data. The same soil parameters were used in both programs.

In Figure 6.30, analyses for the final case are presented for both programs. A good agreement was found. Comparing the time and cost, the PFT program proved to be a good tool for estimating the lateral earth pressures based on given lateral displacements. The only limitation of the PFT program is that it only predicts the lateral earth pressure and not the movements around the tunnel, but the results are very encouraging. It may be used during on site evaluation of the lateral earth pressure with the available deformation profile. This saves valuable time, cost and effort as opposed to conducting a full scale finite element analysis. A pilot analysis to ensure proper simulation of

the on site conditions is suggested.

The deviation in the upper portion of the 2 curves is due to

1. deletion of elements in the SAFE program
2. PFT calculation begins at the centreline of the roof elevation.

In Figures 6.31 and 6.32, a comparison of the results with Terzaghi and Peck's pressure diagrams calculated with total and effective unit weights, respectively is shown. As before, the effective unit weight is the most appropriate with $0.2\gamma H$ for the lower stiffness walls.

The PFT program can be used for the prediction of the lateral movement of the wall based on the lateral earth pressure diagram. The PFT program has been used successfully as explained in Chapter 5 in handling geotechnical and structural problems in a comparative, simplified manner with reasonable accuracy.

6.10 The Ground Control Analysis

One of the most important goals of the excavation method employed in this project was to achieve optimum ground control by minimizing the soil deformation around the tunnel. Peck (1969) introduced a normalized settlement trough for evaluating the ground control based on the soil type. He divided it into three zones; Zone I for sand and soft to hard clay, average workmanship; Zone II for very soft to soft clay with some conditions, 1) limited depth of

LATERAL EARTH PRESSURE Tunnel Section

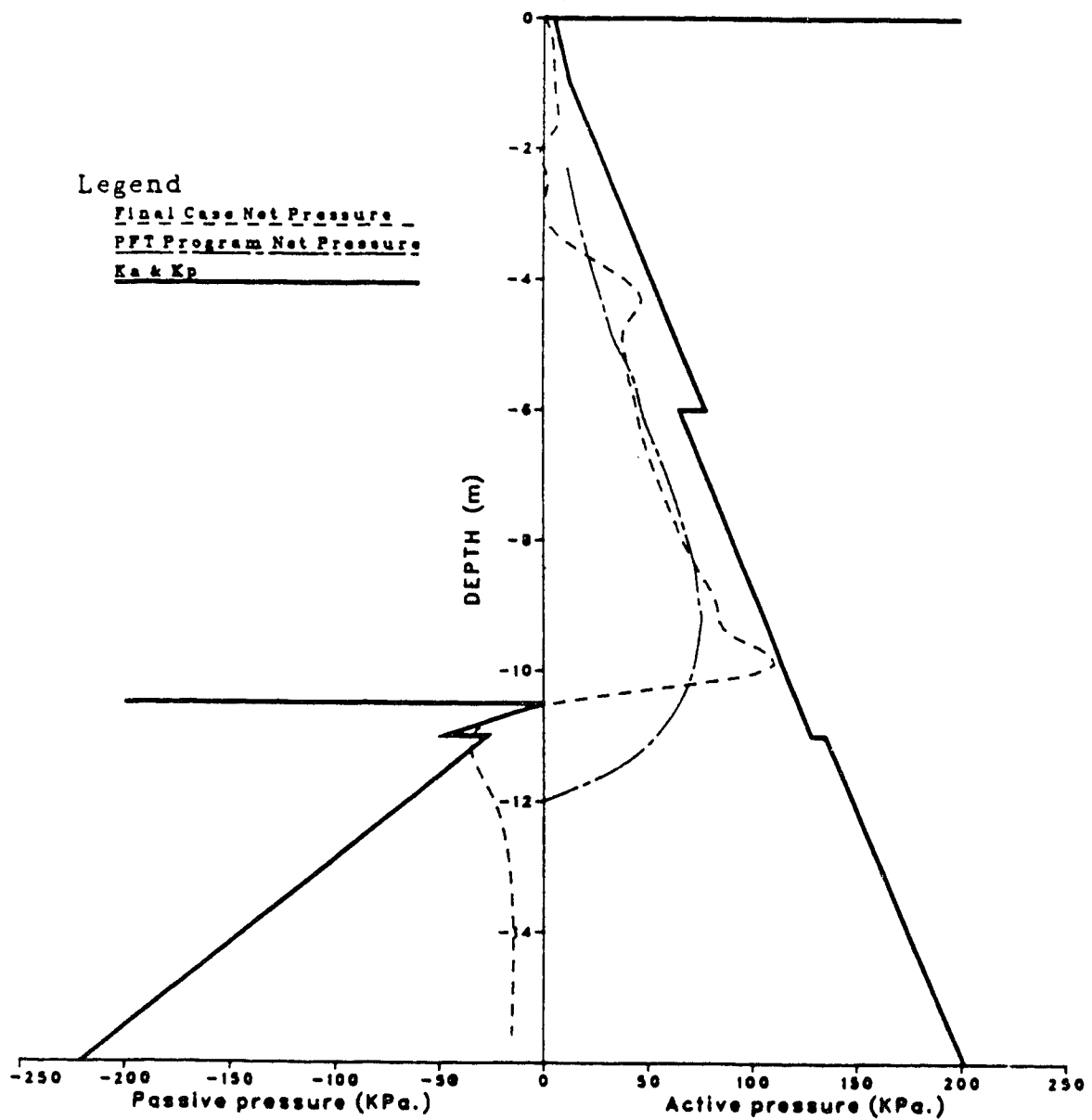


Figure 6.30 Results of SAFE and PFT programs for the Tunnel
Test Section in Terms of Net Pressures

LATERAL EARTH PRESSURE Tunnel Section

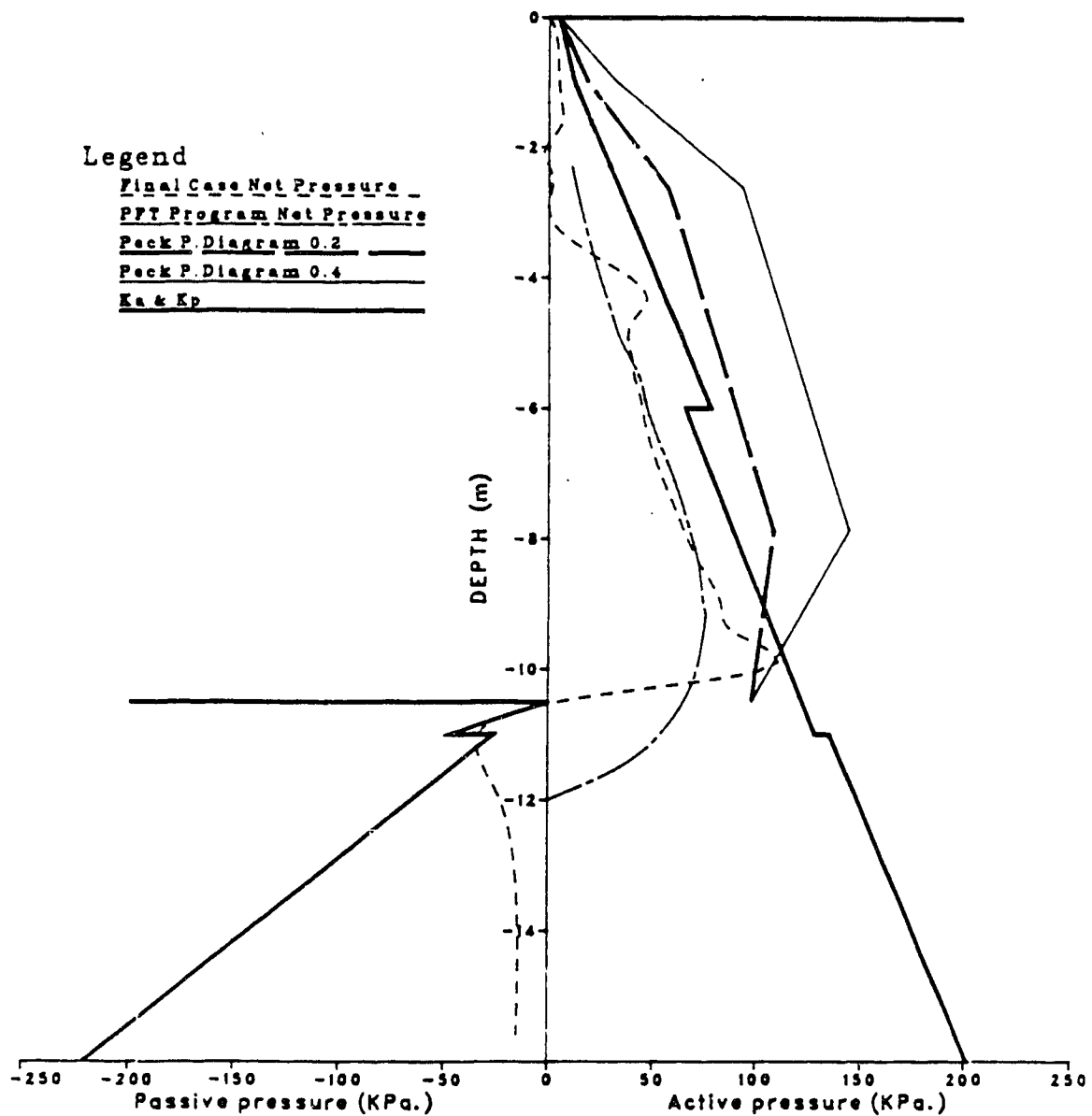


Figure 6.31 Net Lateral Earth Pressure Diagrams for the Tunnel Section Using the Total Unit Weight for Terzaghi and Peck Diagrams

LATERAL EARTH PRESSURE Tunnel Section

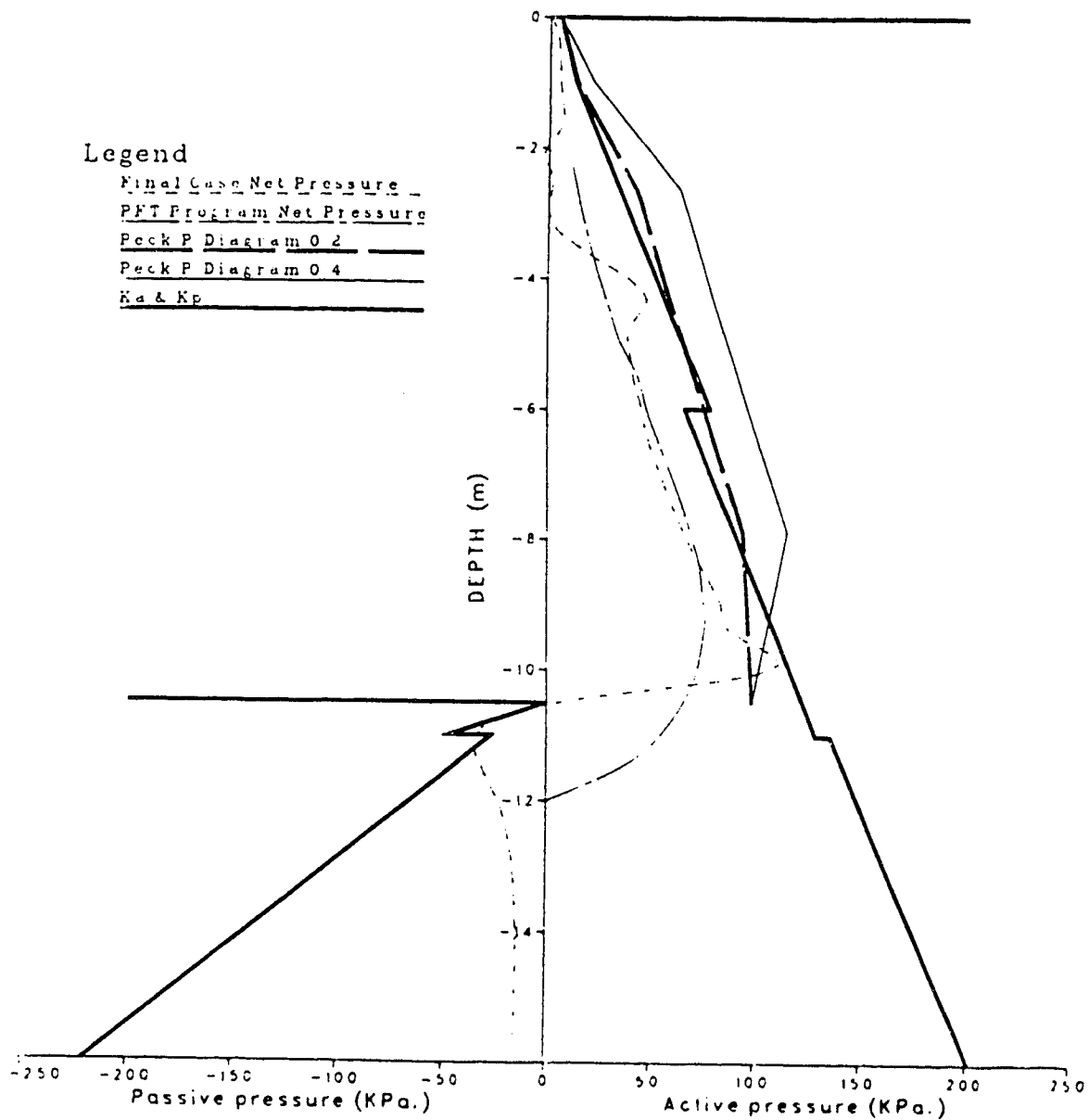


Figure 6.32 Net Lateral Earth Pressure Diagrams for the Tunnel Section Using the Effective Unit Weight for Terzaghi and Peck Diagrams

clay below bottom of excavation, 2) significant depth of clay below the bottom of excavation and 3) the settlement affected by construction difficulties; Zone III for very soft and soft clay in the excavation and at significant depth below the excavation. All the data are for Standard soldier piles or sheet piles braced with cross-bracing or tie backs. El-Nahhas (1987) used this figure for comparing the predicted and measured normalized settlement trough for Edmonton till (very stiff clay). Figure 6.33 shows the entire figure with the predicted and measured data with both results plotting in the upper portion of Zone I. Figure 6.34 presents an enlarged view of Zone I, showing all the data in the upper 15% of Zone I indicating the good ground control produced by the use of the diaphragm wall. The field data showed that the highest measure of ground control was for the tunnel section. In the station section, the excavation procedure has no significant influence. Close to the excavation, there is no significant difference between the settlement troughs for the station and tunnel sections. Peck's figure shows only the relationship between the settlement trough and ground control. Figure 6.35 presents the relationship between maximum settlement and maximum lateral wall movements. It should be noted that the first element of temporary support was erected at about half of the excavation depth (5 m) which represents about twice the undrained shear strength (S_u) divided by the total unit weight. Peck (1969) considered this depth as the maximum

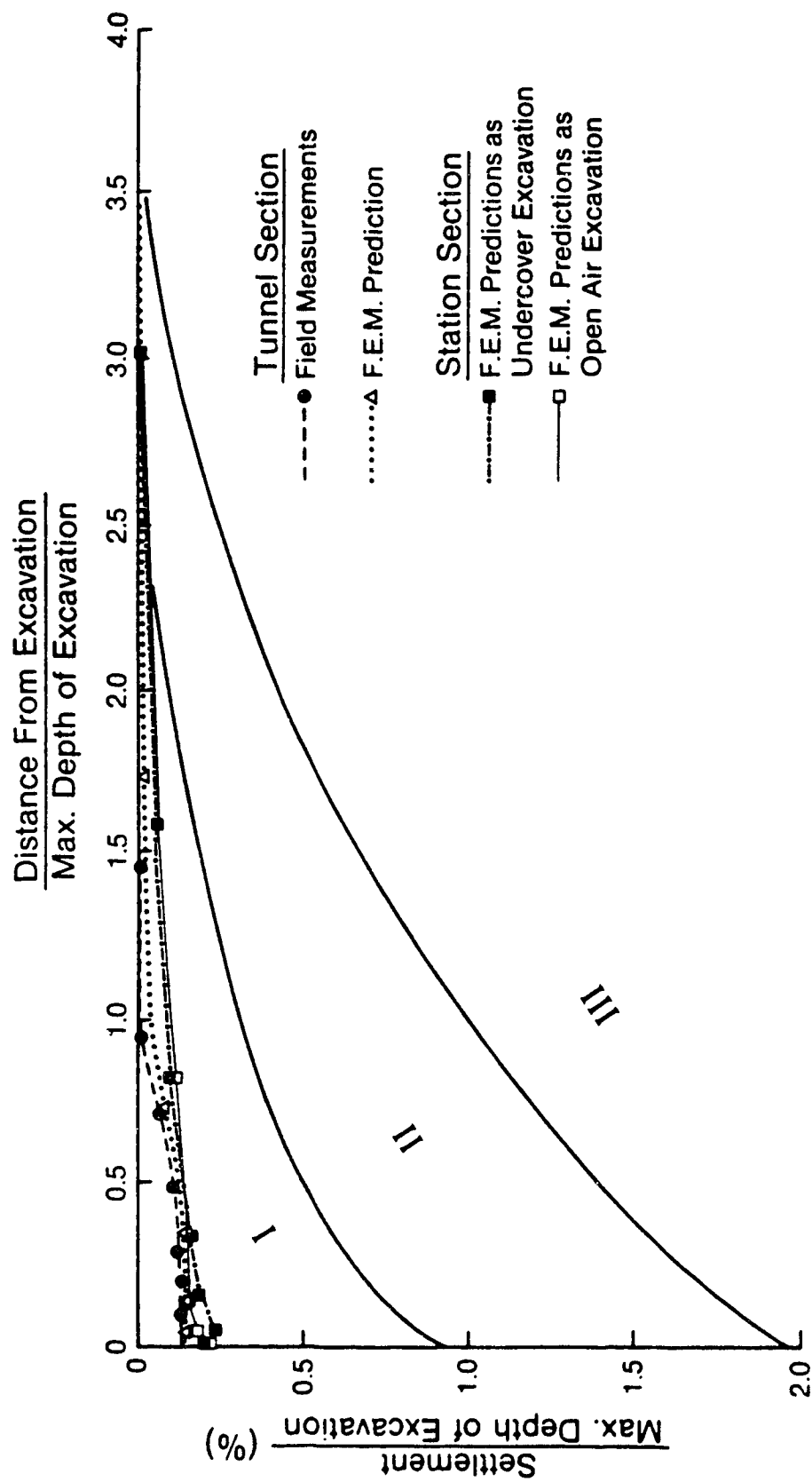


Figure 6.33 Normalized Settlement Troughs (Suggested by Peck (1969); modified)

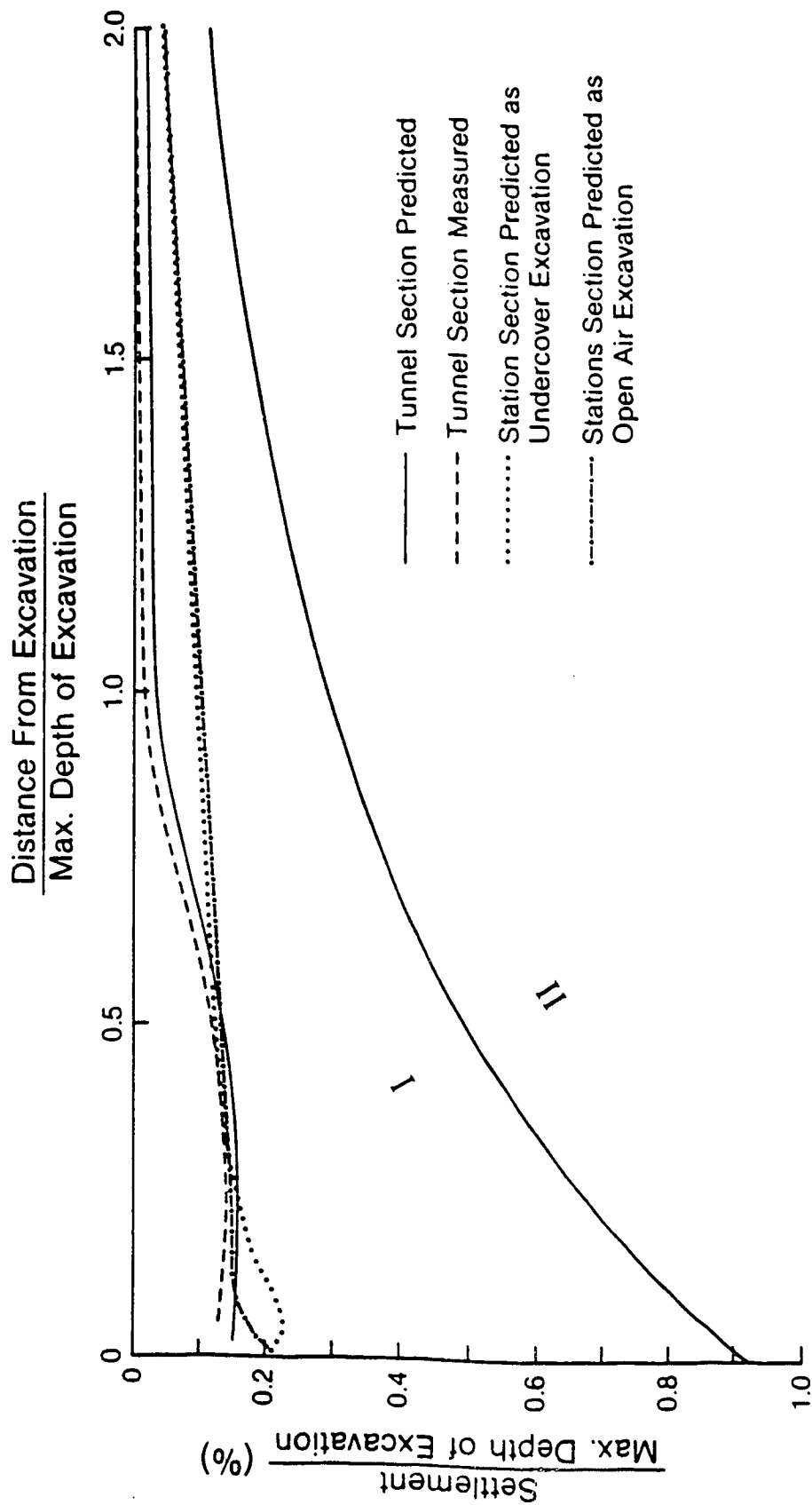


Figure 6.34 Zone I Normalized Settlement Troughs

height of a supported excavation which can be left unbraced in order to avoid excessive ground loss and settlement.

The guidelines given by Mana and Clough (1981) and Schlosser et al. (1985) considered a braced excavation to be adequately controlled if the ratio between maximum settlement of the ground surface and the maximum lateral movement was in the order of 0.5 to 1.0. As shown in Figure 6.35, the measured ratio for the test sections lies in this range with the exception of the undercover excavation analysis. This value was greater than unity, indicating greater ground control. This may be due to the early introduction of the first permanent support. The measured ratio for the tunnel section was 0.75 to 0.6 and the predicted value was 0.5. For the station section, the predicted values were 8 (undercover) and 0.71 (open air).

Figure 6.36 compares the volumes of ground surface settlement and lateral wall deflection at different stages of the analysis as well as the field measured values. For the tunnel section, the measured volume for the settlement trough was approximately 60% of the lateral deformation volume of the wall. The predicted values at the final stages of the analysis tended toward the $V_v = V_s$ line. The undercover analysis of the station section indicates that the lateral wall deflection was very small in comparison with the settlement trough volumes, similar to the tunnel section. The normalized maximum ground surface settlement relationship to the normalized volume of the lateral wall

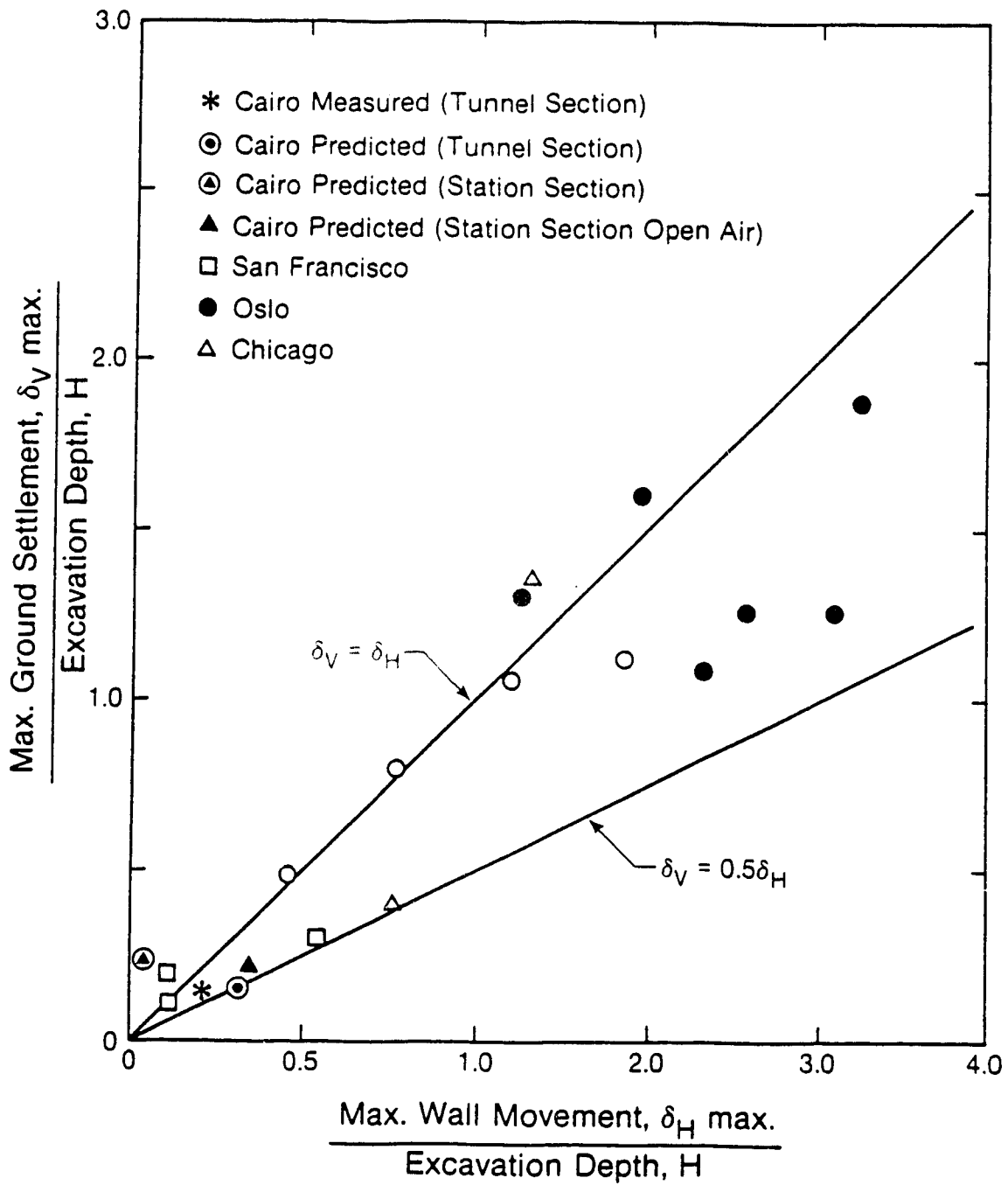


Figure 6.35 The Relationship Between Maximum Settlements and Maximum Lateral Wall Movements for Test Sections

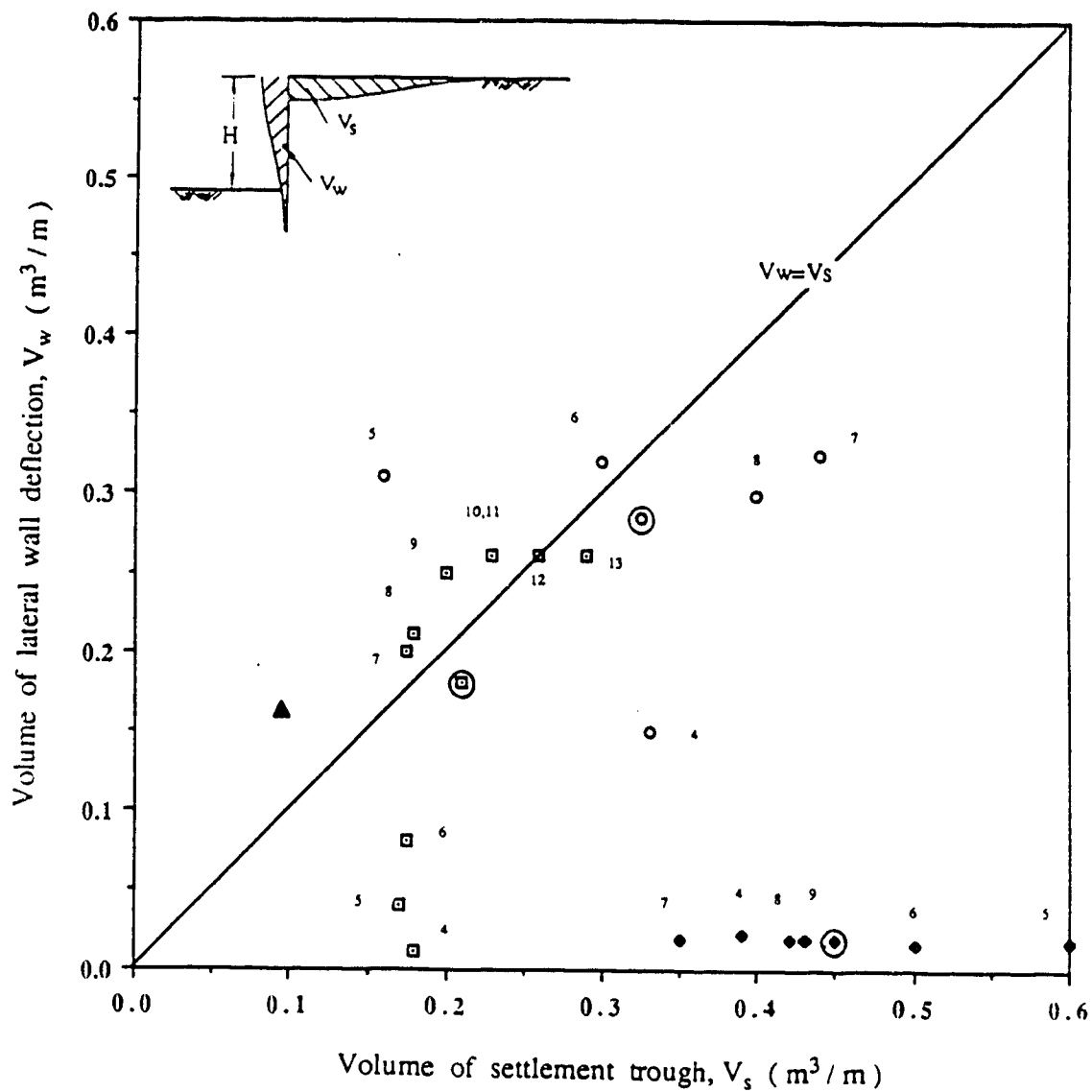


Figure 6.36 Comparison of volume of Ground Surface Settlement and Lateral Wall Deflection

deflection is presented in Figure 6.37. These results support the conclusions drawn from Figure 6.36.

In general, the construction method employed in this study resulted in good ground control. The best ground control could be achieved either by using the undercover excavation procedure or by the early introduction of the first temporary support element at its elevations. It must be noted that this high degree of ground control was achieved in conjunction with the grouted plug and good quality control of the ground water table outside the excavated area. The observed settlement trough with a slope of 1:740 (a very conservative value) indicates that there is no significant influence on adjacent buildings.

6.11 Summary

The field measurements and the F.E.M. analysis have been coupled to indirectly measure the lateral earth pressure acting on the diaphragm walls as it is not viable to obtain direct field pressure measurements. The use of the grouting procedure achieved good control of the groundwater table keeping the pore water pressure hydrostatic throughout the construction procedure. The sequence of temporary and permanent support installation influenced the lateral deformation of the walls which in turn affects the lateral earth pressure.

An on-line search was conducted at the University of Alberta library and revealed little published research on

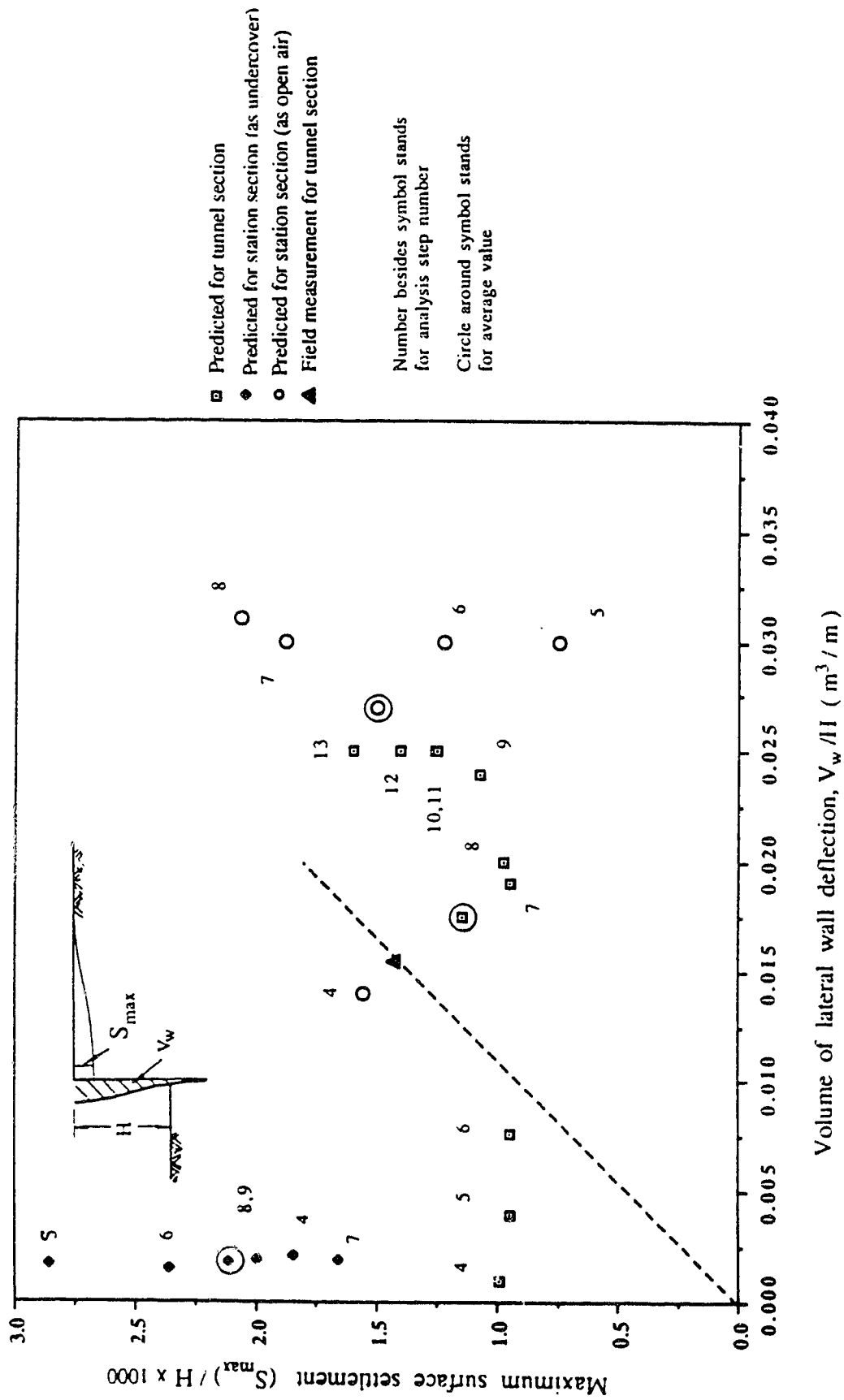


Figure 6.37 Maximum Ground Surface Settlement versus Volume of Lateral Wall Deflections

diaphragm walls. Most of the available work deals with construction aspects, case histories and field observation reporting. The literature on the design and performance of the retaining walls deals with sheetpile and tie back walls. This indicates the need for research on the behaviour and performance of the diaphragm walls. The influence of the soil profile and the determination of soil parameters are very important factors in prediction of the soil behaviour during the analysis. The use of some simple programs with simplified models to analyse and predict the field measurements as on site aids in decision making and can save time and money during construction. The need for high quality ground control justifies the high cost to achieve it, the use of the grouted plug not only prevented water from flowing into the excavation but improved the stability of the excavation base. The results indicate that the use of semi-empirical pressure diagrams presented by Terzaghi and Peck should be applied with the effective unit weight rather than the total unit weight for such host materials and construction procedures.

Peck (1969) suggested that for clays with stability number, N , less than 4 ($N = \gamma H / S_u$ where S_u is the undrained shear strength, the classical earth pressure theory suggests that the earth pressure acting on the bracing system should be zero. If the total unit weight is used, the stability number will be approximately 3.5 and will reduce to 2 if the effective unit weight is used. He suggested that the

discrepancy between the theory and reality may be due to an attempt to apply a theory of plastic equilibrium to a case not in a plastic state. He also reported that " for values of N less than 3 or 4, earth pressure theory should not be used, whether the cut is a shallow one in soft clay or deeper one in stiff clay".

Morgenstern and Eisenstein (1970) reviewed the method of estimating lateral loads and deformations associated with earth retaining structures, stating the limitation of the available analytical tools. They classified the methods into three groups depending on the deformation; small, moderate or large, and pointed out the importance of the determination of the soil properties and the pore pressures. They stated that the change in pore pressure and subsequent consolidation may control the deformation behaviour of an excavation, and the most recent reported failures have seldom been the result of inadequacies in modern earth pressure theories. They stated that if the aim of the design is to prevent failure in the most economical way, the conventional methods of design are clearly not satisfactory and the requirements in accuracy of theoretical deformation prediction have not been established. Morton (1982) reported that Peck recommended that for clays the highest values of Terzaghi and Peck's diagrams, but sheeting for braced subway cuts in stiff to hard clays is reported to be satisfactory if lower values of pressure were used. This has been confirmed by instrumentation programs. The high cost of

construction imposes the minimization of the design loads while maintaining the safety standard. The results of this study indicate that with the introduction of the correct soil properties, parameters and pore pressures, the lateral earth pressure diagrams and the deformation around the excavation may be minimized reducing the cost of construction. The finite element analysis does not imply any earth pressure theory. It calculates the stress in the element as a result of the stress level corresponding to the laboratory stress-strain relationships. The results of the F.E.M. indicated that the total lateral earth pressure produced by the earth pressure theory is in reasonable agreement with the predicted total lateral earth pressures, suggesting the use of the classical earth pressure theory for such host materials. It seems logical that with the minimum deformation and the high quality ground control, the lateral earth pressure will be close to the in situ condition (K_0 conditions), but the soil improvement due to grouting reduces the lateral earth pressures as indicated by Broms (1988). A new apparent pressure diagram has been presented adapting the diagrams suggested by Terzaghi and Peck (1967) to be suitable for use with diaphragm walls. The influence of the wall thickness and stiffness can be introduced to the diagram by the use of the lower value of 0.2 for the small thickness and 0.4 for the higher thickness.

It can be concluded from this study that the construction procedure achieved its goals justifying the high cost of such a procedure when it is needed.

7. CONCLUSIONS AND RECOMMENDATIONS

Geotechnical design problems are encountered when the designer is uncertain of the properties of the materials. This type of problem is particularly evident in Egypt where no database exists on soil behaviour, not only with respect to tunnelling but also in foundation design. There is then a tendency to employ costly construction methods to overcome this deficiency.

In this project, the Cairo Metro, the observational method was employed. In this manner, data was collected for use in this particular design, as well as establishing a general corpus of knowledge as reference for other studies.

The main objective of this construction method was to minimize ground deformation due to excavation. Consideration of the ground water level and diversion of the present surface traffic flow influenced both the design and construction method.

To fulfill the requirements, two test sections were instrumented in the Regional line of the Cairo Metro. These provided measurements of the movement of the soil and diaphragm wall, loads in the struts and structural elements, and the pore water pressures. The data was used to determine the deformation pattern and lateral earth pressures as a function of material type and construction procedure. These results were compared with finite element analyses.

A summary of the project is presented below.

1. A new concept to predict lateral earth pressures from

field measurements has been introduced (i.e. γ_{sub} instead of γ_{sat}), and the hydrostatic pressure effect is considered a separate component of the loads acting on the wall. It uses the soil parameters obtained from laboratory tests. Then by matching the field deformation with predicted values, the lateral earth pressure is evaluated as the forces causing these movements.

2. The most commonly used earth pressure diagram for this type of material is that by Terzaghi and Peck for stiff clays. Analyses showed that it was more appropriate to use the effective unit weight of the soil rather than the total unit weight and hydrostatic pressure as recommended.
3. The influence of wall stiffness on the lateral earth pressure was evaluated. For diaphragm walls of lower stiffness, $0.2\gamma'H$ should be used in the calculations, and for walls of higher stiffness, $0.4\gamma'H$.
4. For clays underlain by sand, a modified pressure diagram is proposed, with height ratios of 0.25 and 0.75 H from the top, respectively keeping the pressure constant at the bottom with no reduction.
5. To calculate the permanent (i.e. long term) earth pressure acting on the walls, the use of the Rankin earth pressure theory is suggested. For the case of wall with lower stiffness, reduced pressures may be used.
6. The construction of the grouted plug and the improvement of the excavation base as a result of the grouting

procedure (i.e. micro piles or soil nailing) contributed to the reduction of the active earth pressure and therefore minimized soil deformations.

7. The construction method succeeded in sealing the excavation zone during construction, keeping pore pressures hydrostatic. This reduced the risk of damage to adjacent buildings.
8. The undercover excavation procedure significantly reduced deformation around the tunnel. Using an extruded liner in the tunnel construction method is the only other procedure which may lay claim to such a high degree of ground control.
9. The construction method employed in this project achieved its goals of minimizing deformation, thereby justifying its high cost.
10. The installation sequence of the temporary support influenced the deformation pattern. Early activation of the struts will minimize the deformation.
11. A set of numerical analyses were verified in this study and the behaviour of such host material was investigated.
12. The use of the PFT program to predict lateral earth pressures based on the measured deformation, proved to be an important tool in preliminary studies and on site evaluation.
13. The ground control analyses showed that the construction method produced high quality ground control. This

encourages the use of diaphragm walls under these conditions.

14. The use of the SAFE program produced satisfactory results with the use of the appropriate parameters. It is independent of any earth pressure theory.
15. The use of multipoint extensometers to measure the base heave of an excavation is not recommended due to the difficulties encountered.
16. In general, the width of the excavation base with the presence of the plug and soil nailing has no significant effect on the earth pressures or soil deformation.

It is suggested that further studies be conducted in the following areas.

1. More data is required to confirm the recommendations.
2. Three dimensional numerical analyses would be more appropriate to simulate the third dimension effect due to excavation of material adjacent to the analysed section.
3. A direct method or instrument to measurement the lateral earth pressure in the field would be greatly appreciated accounting for the advancements in technical and theoretical aspects.
4. The parameters used in this study can be used in the design of the new Cairo Metro lines and thier reliability may be checked through a field instrumentation program.
5. This study was primarily concerned with stiff clays

underlain by sands. Studies on the behaviour of different materials would be valuable.

6. Long term observation is needed to evaluate the influence of the actual loading conditions during operation.

REFERENCES

- Abdel Salam, M.E., 1984. Grouting of alluvial soil in Cairo underground method. Proceedings of the Tunnelling in Soft and Water-Bearing Grounds, Lyon, France, pp. 135-142.
- Abu AL-Izz, M.S., 1971. Land forms of Egypt. The American Univeristy in Cairo, Cairo, 281 p.
- American Standard Test Method, 1983. Static modulus of elasticity and Poisson's ratio of concrete in compression. ASTM Designation C469-83, pp. 303-307.
- Attia, M., 1954. Deposits in the Nile valley and the delta. Government Press-Cairo.
- Baggett, J.K., and Buttling, S., 1981. Design and in situ performance of a sheet pile wall. Proceedings of the 10th International Conference on Soil Mechanics and Foundation Engineering, Stockholm, Vol. 3, pp. 3-7.
- Barratt, D.A., and Tyler, R.G., 1976. Measurements of ground movement and lining behaviour on the London underground at Regents Park. TRRL Laboratory, Report 584, Crowthorne, Berkshire, U.K.
- Bozozuk, M., 1968. The spiral-foot settlement gauge. Canadian Geotechnical Journal. Vol. 5, No. 2, pp. 123-125.
- Broms, B.B., Wong, I.H., and Wong, K.S., 1986. Experience with finite element analysis of braced excavation in Singapore. Proceedings 2nd International Symposium on Numerical Models in Geomechanics, Ghent, pp. 309-324.
- Broms, B.B., 1988. Design and construction of anchored and strutted sheet pile walls in soft clay. Proceedings Second International Conference on Case Histories in Geotechnical Engineering, June, St. Louis, Mo., Invited Paper, pp. 1515-1559.
- Burland, J.B., Moore, J.F.A., and Smith, P.D.K., 1972. A simple and precise borehole extensometer. Geotechnique, Vol. 22, pp. 174-177.

- Burland, J.B., and Moore, J.F.A., 1973. The measurement of ground displacement around deep excavations. Field Instrumentation in Geotechnical Engineering, Butterworth and Co., London, pp. 7084.
- Canadian Standards Association [CSA], 1984. Design of concrete structures for buildings. CAN3-A23.3-M84, Canadian Standards Association, Rexdale, Ontario, Canada.
- Cappelari, G., and Ottaviani, M., 1981. Finite element analysis of horizontal loading test on a precast concrete diaphragm wall. Proceedings of the Symposium held at Chicago, Illinois, August. Implementation of Computer Procedures and Stress-Strain Laws in Geotechnical Engineering, Vol. 1, pp. 185-196.
- Chalaturnyk, R., Chan, D., and Scott, J.D., 1987. Finite element analysis of reinforced soil. Presented at the NATO Advanced Research Workshop - Application of Polymeric Reinforcement in Soil Retaining Structures. Royal Military College of Canada, June, Kingston, Ontario, Sponsored by the NATO Scientific Affairs Division.
- Chan, D.H., 1986. Analysis of strain softening material. Ph.D. Thesis, Department of Civil Engineering, Univeristy of Alberta, Canada.
- Chan, D., and McRobert, E.C., 1986. Government Centre station, summary report on finite element analysis, light rail transit system in Edmonton, Alberta. Special Report by Hardy Associates, Edmonton, Alberta.
- Chan, D.H., Morgenstern, N., 1987. Analysis of progressive deformation of the Edmonton Convention Centre. Canadian Geotechnical Journal, Vol. 24, No. 3, pp. 430-440.
- Chan, D.H., Barlow, J.P., and Plewes, H.D., 1987. Government centre station. Results of finite element analysis. Report submitted to the City of Edmonton Transportation. Transportation and Stanley Associated Engineering Ltd. r
- Chan, D.H., and Chan, Z.H., 1988. SAFE - A computer program for soil analysis by finite element method. User Manual, Department of Civil Engineering, Univerisity of Alberta,

Canada.

- Cording, E.J., Hendron, A.J., MacPherson, H.H., Hansmire, W.H., Jones, R.A., Mahar, J.W., and O'Rourke, T.D., 1975. Methods for geotechnical observations and instrumentation in tunnelling. Report prepared for U.S. National Science Foundation, Washington, D.C., NTIS No. PB25258-PB252286.
- Crag, R.F., 1978. Soil Mechanics. Second Edition, Van Nostrand Reinhold Company, London, 122 p.
- Cuvilier, J., 1924. Contribution a l'etude geologique du. Bulletin Inst. Egypt, (16), pp. 95-102.
- Deardorff, G.B., Lumsten, A.M., and Ittefferson, W.M., 1980. Pneumatic piezometers: multiple and single installations in vertical and inclines boreholes. Canadian Geotechnical Journal, Vol. 17, pp. 313-320.
- Desai, C., and Christian, J., 1977. Numerical methods in geotechnical engineering. McGraw Hill, New York.
- Duncan, J.M., and Chang, C.Y., 1970. Non linear analysis of stress and strain in soils. Journal of Soil Mechanics and Foundation Division, ASCE, Vol. 96, No. SM5, Sept.
- Duncan, J.M., Byrne, P., Wong, K.S., and Mabry, P., 1980. Strength, stress-strain and bulk modulus parameters for finite element analysis of stresses and movements in soil masses. Report No. UCB/GT/80-01, College of Engineering, University of California, Berkeley, California, U.S.A.
- Dunnicliff, C.J., 1971. Equipment for field deformation measurements. Proceedings Fourth Panamerican Conference on Soil Mechanics and Foundation Engineering, San Juan, Vol. 2, pp. 319-332.
- Dunnicliff, C.J., 1988. Geotechnical instrumentation for monitoring field performance. A Wiley-Interscience Publication. ISBN 0.471.09614-8.
- Eisenstein, Z., EL-Nahhas, F., Thalaby, A., 1987. Cairo

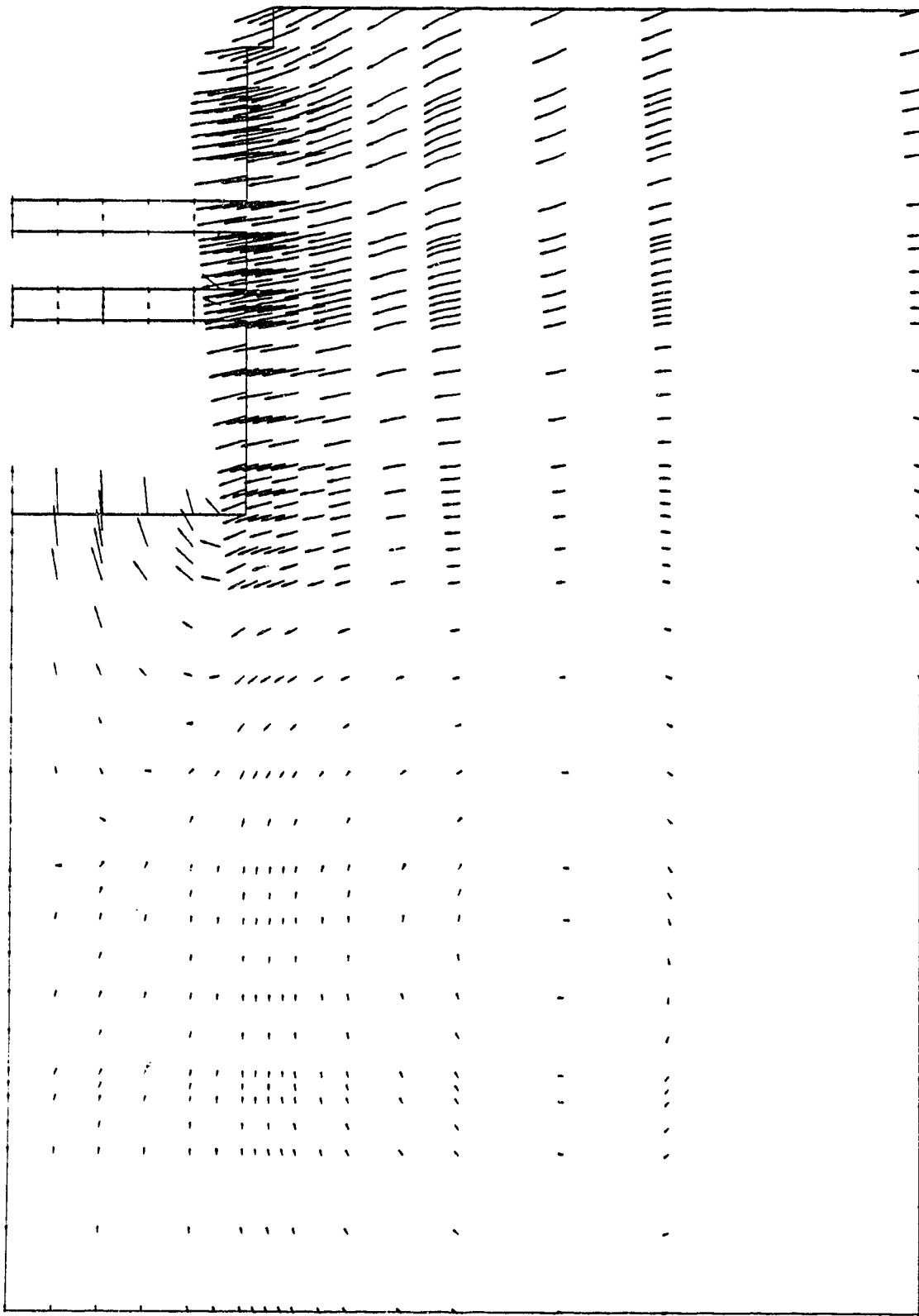


Figure D.8 Displacement Arrows - Tunnel Section - Step (9)

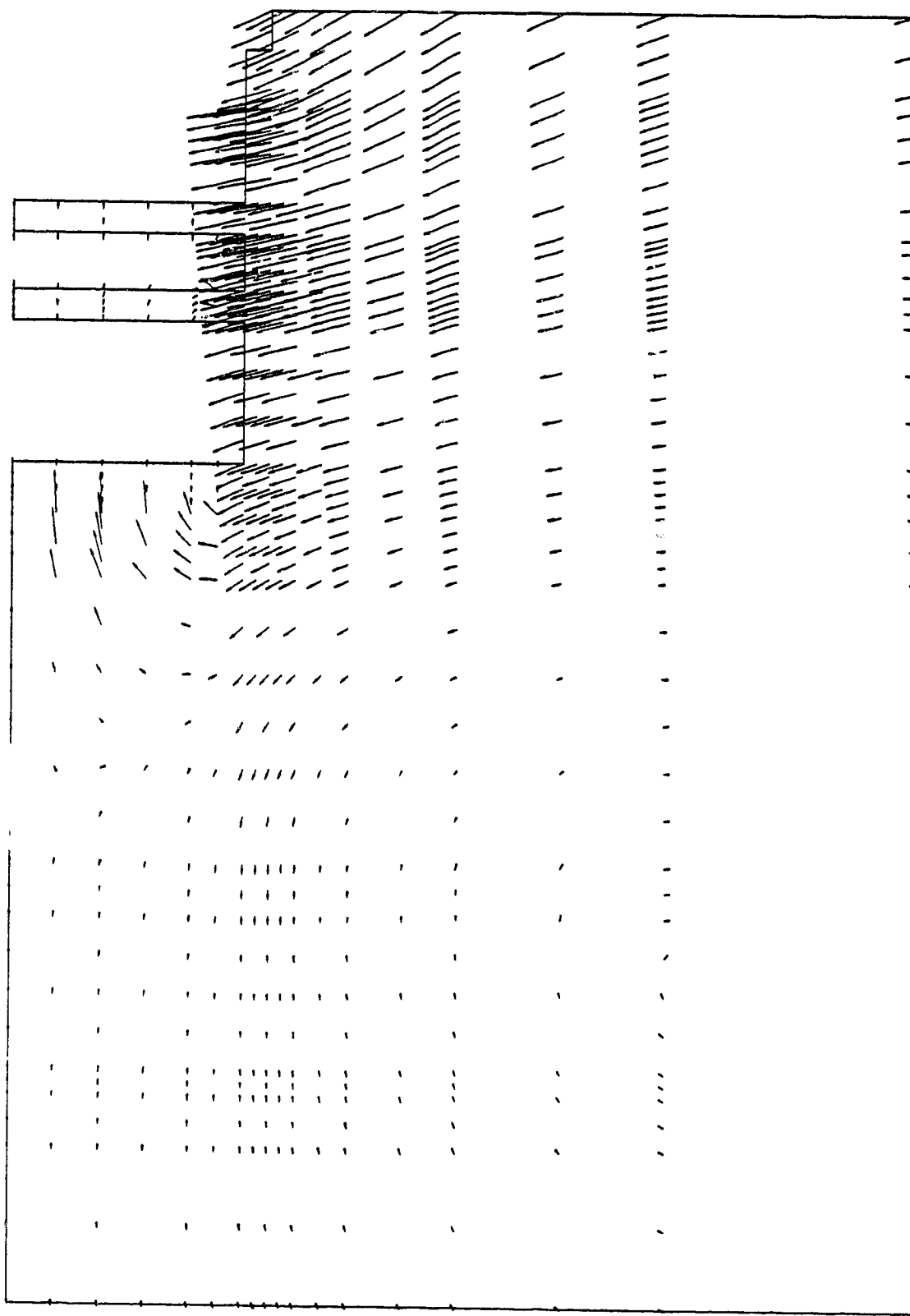


Figure D.9 Displacement Arrows - Tunnel Section - Step (10)

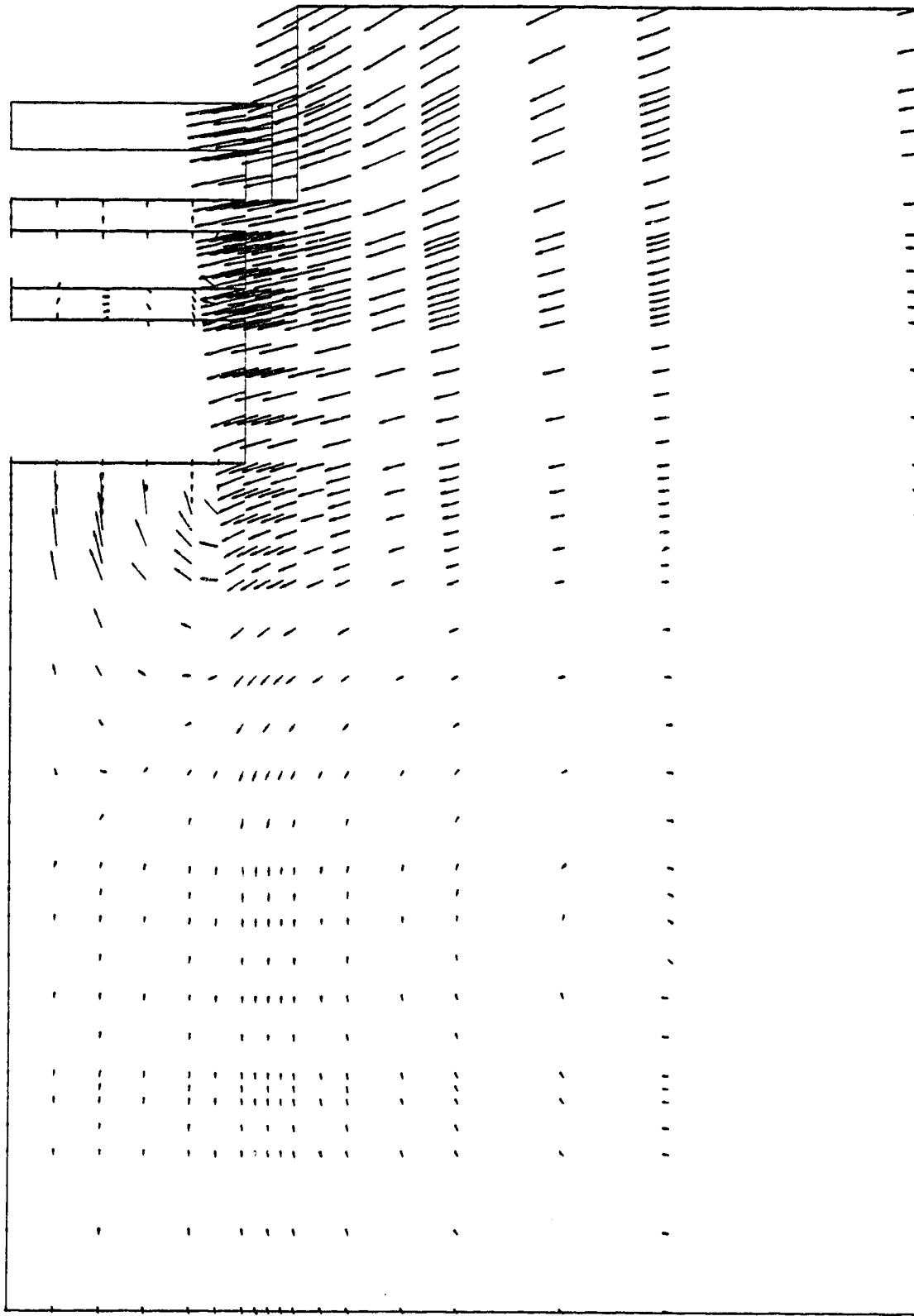


Figure D.10 Displacement Arrows - Tunnel Section - Step (11)

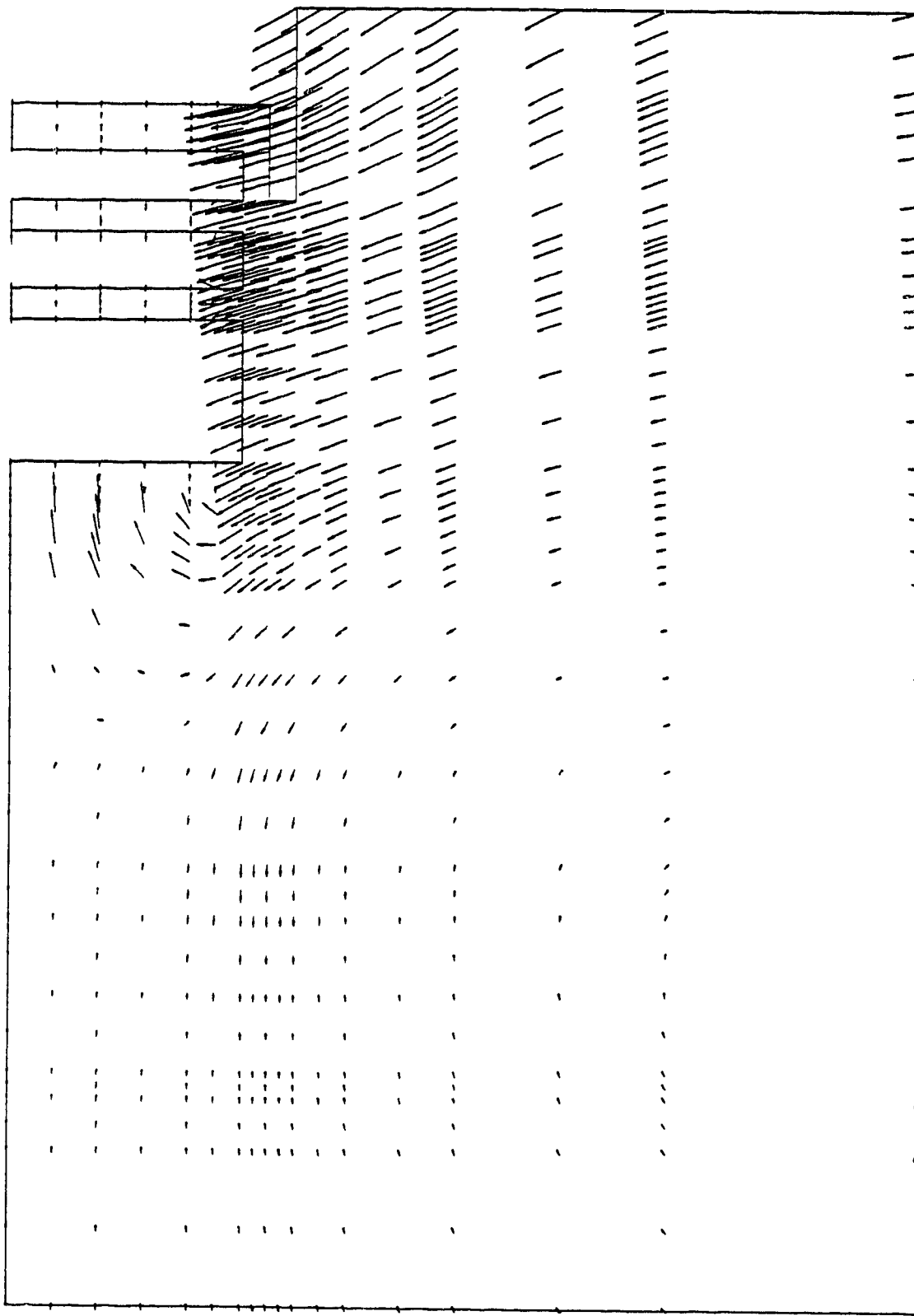


Figure D.11 Displacement Arrows - Tunnel Section - Step (12)

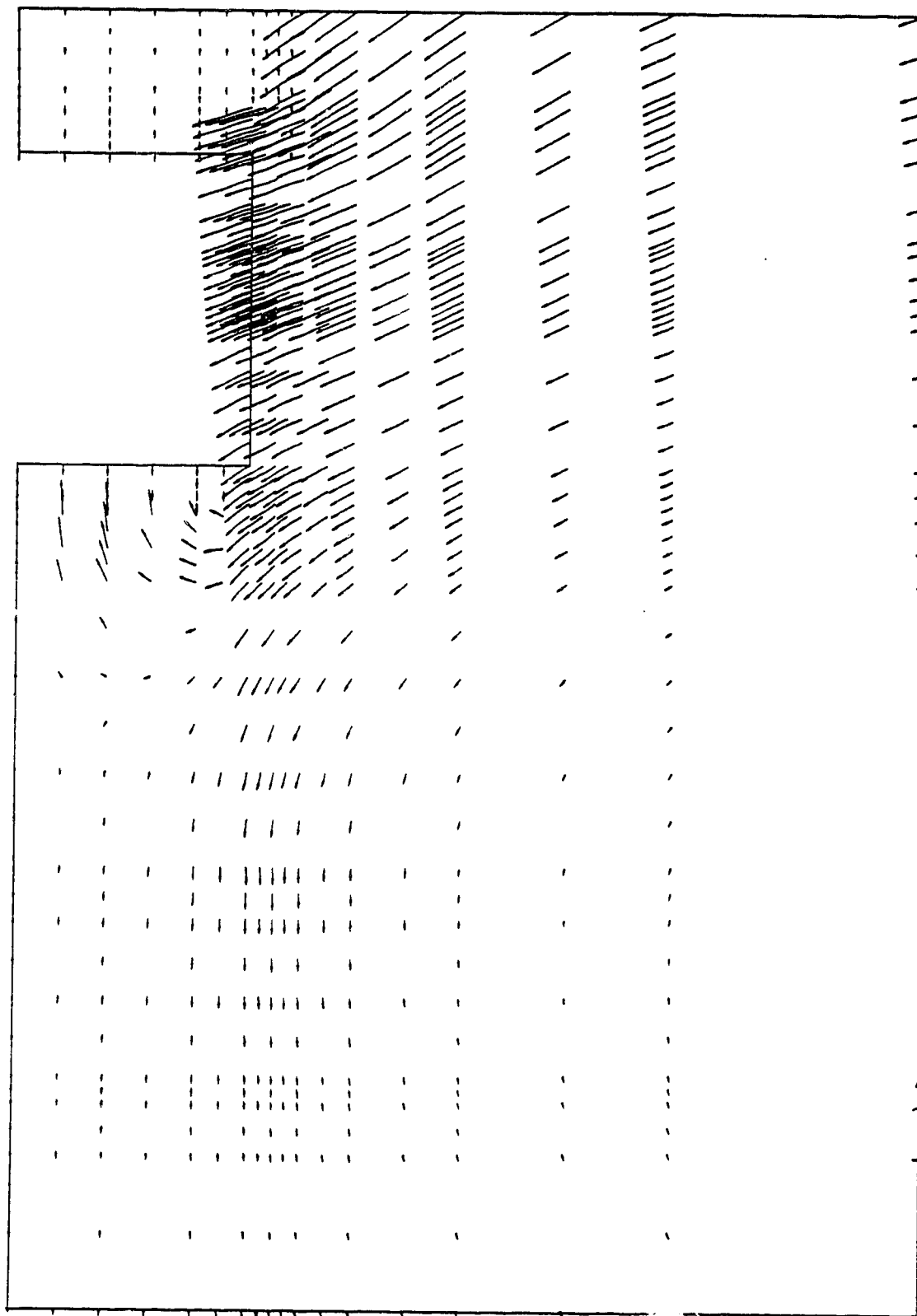
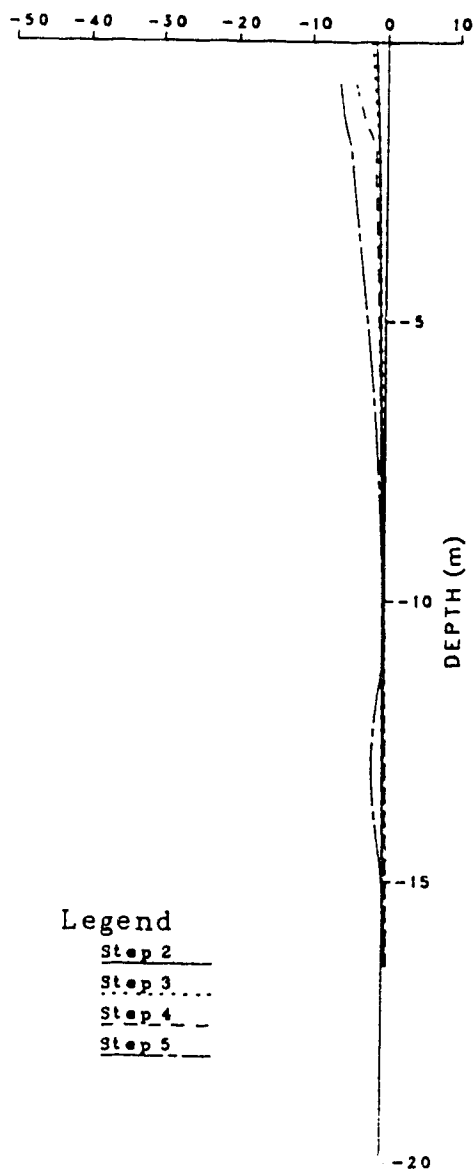


Figure 12 Displacement Arrows - Tunnel Section - Step (13)

HORIZONTAL DISPLACEMENT (mm)
Tunnel Section

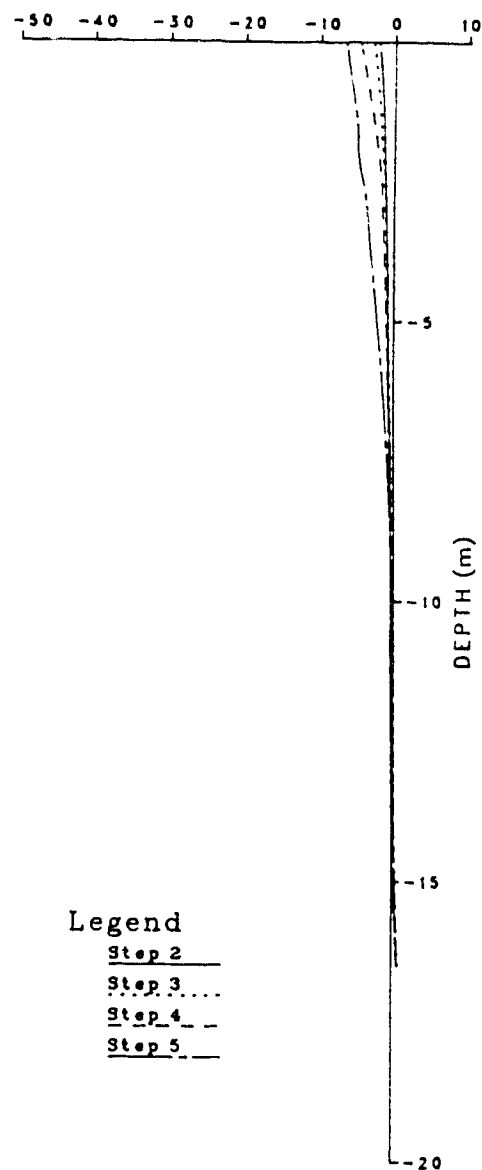


Legend

Step 2
Step 3....
Step 4 - -
Step 5 - - -

WALL DISPLACEMENT

HORIZONTAL DISPLACEMENT (mm)
Tunnel Section



Legend

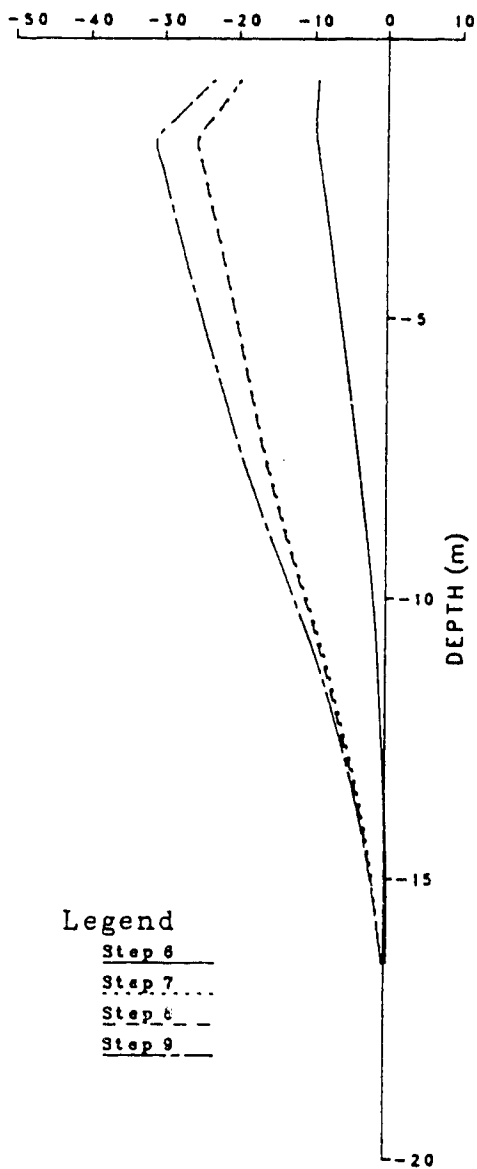
Step 2
Step 3....
Step 4 - -
Step 5 - - -

SOIL DISPLACEMENT

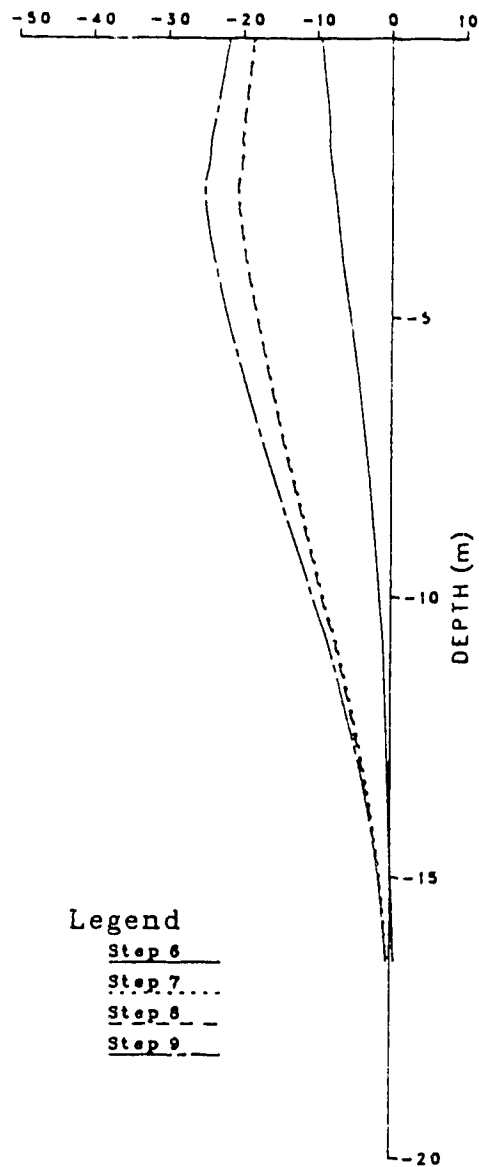
Figure D.13 Horizontal Displacement - Tunnel Section - Set

HORIZONTAL DISPLACEMENT (mm)
Tunnel Section

HORIZONTAL DISPLACEMENT (mm)
Tunnel Section



WALL DISPLACEMENT



SOIL DISPLACEMENT

Figure D.14 Horizontal Displacement - Tunnel Section - Set

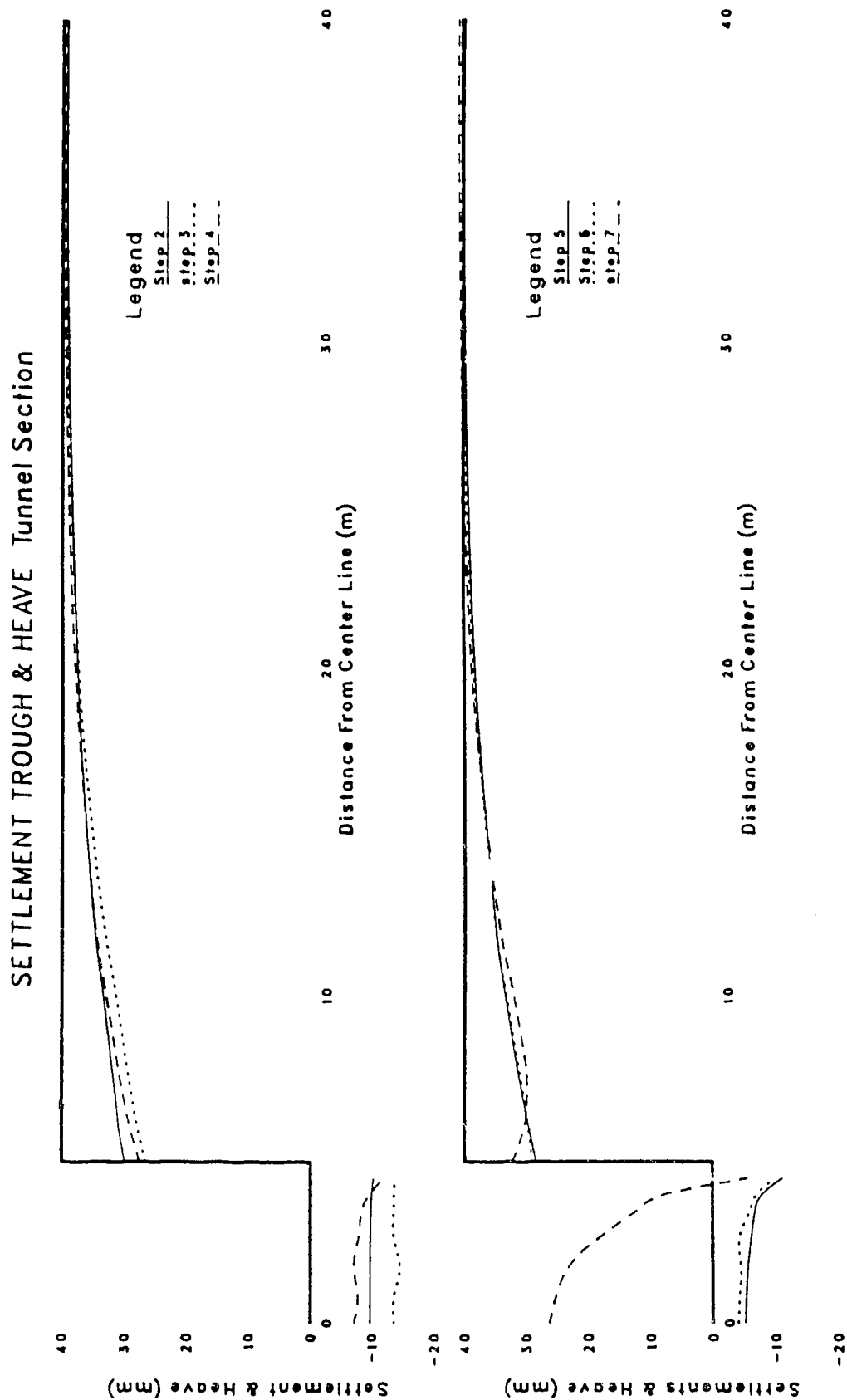


Figure D.15 Settlement Trough and Excavation Base Heave - Tunnel Section Set (1)

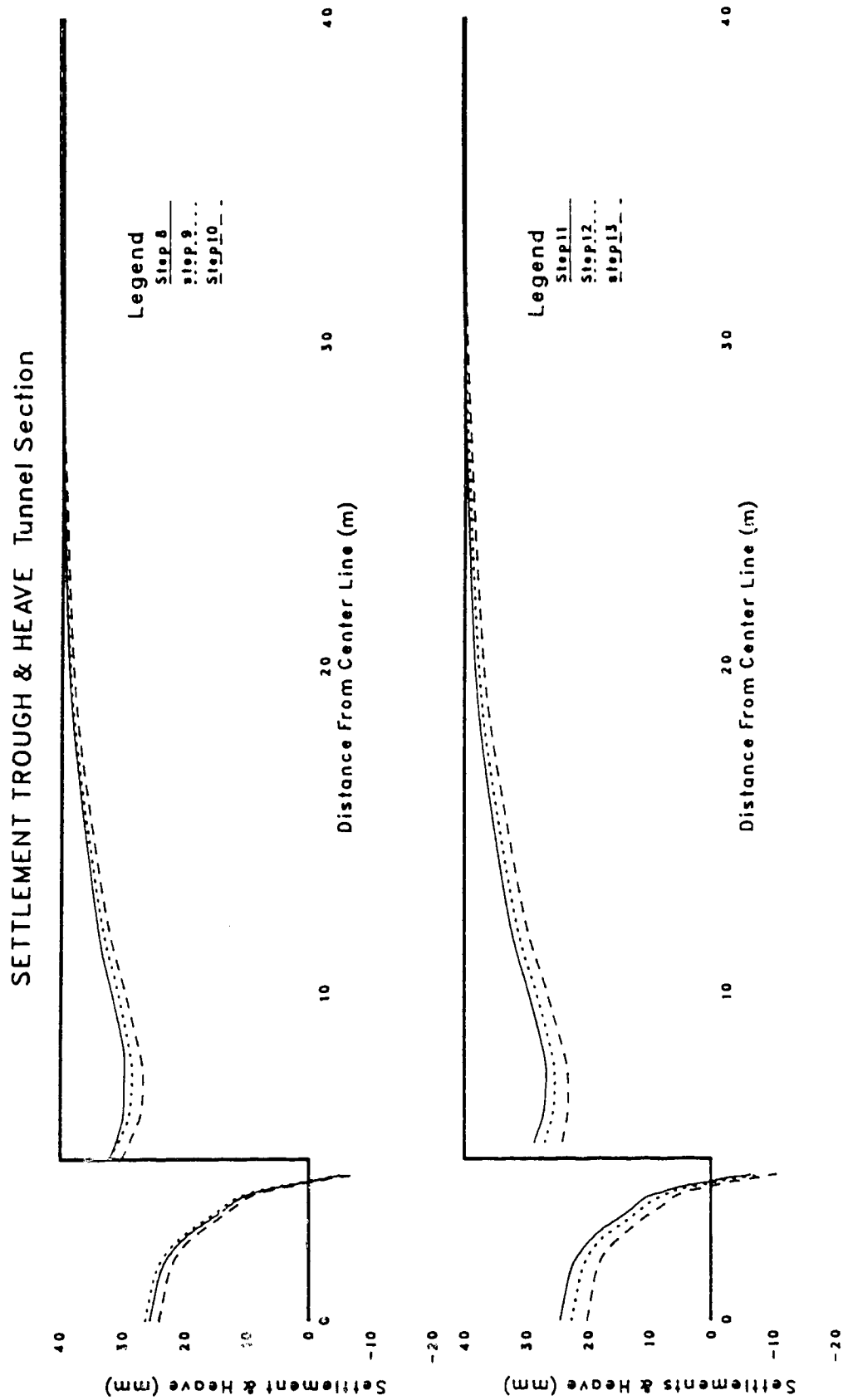


Figure D.16 Settlement Trough and Excavation Base Heave - Tunnel Section Set (2)

LATERAL EARTH PRESSURE Tunnel Section

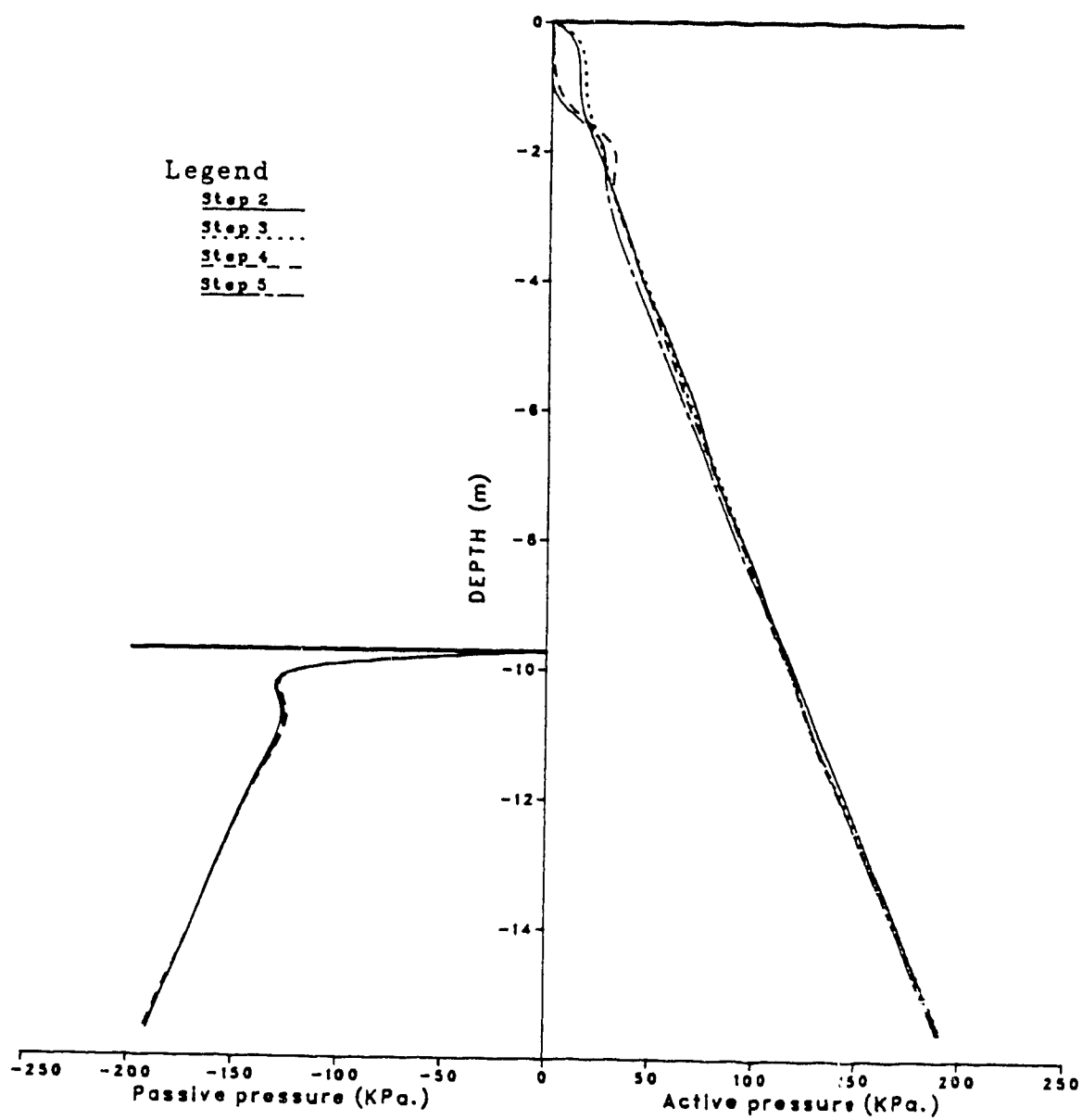


Figure D.17 Lateral Earth Pressure - Tunnel Section Set (1)

LATERAL EARTH PRESSURE Tunnel Section

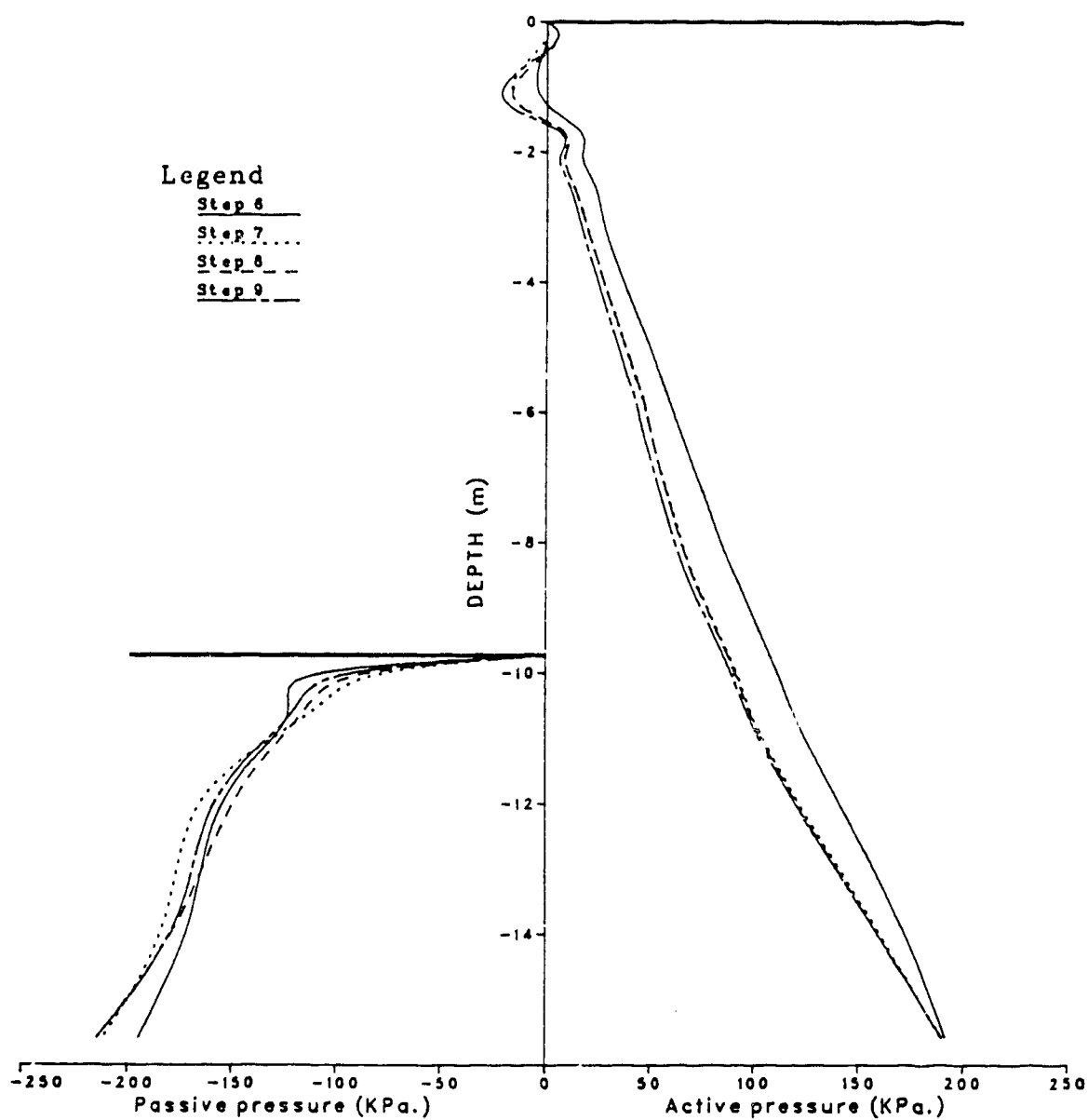


Figure D.18 Lateral Earth Pressure - Tunnel Section Set (2)

LATERAL EARTH PRESSURE Tunnel Section

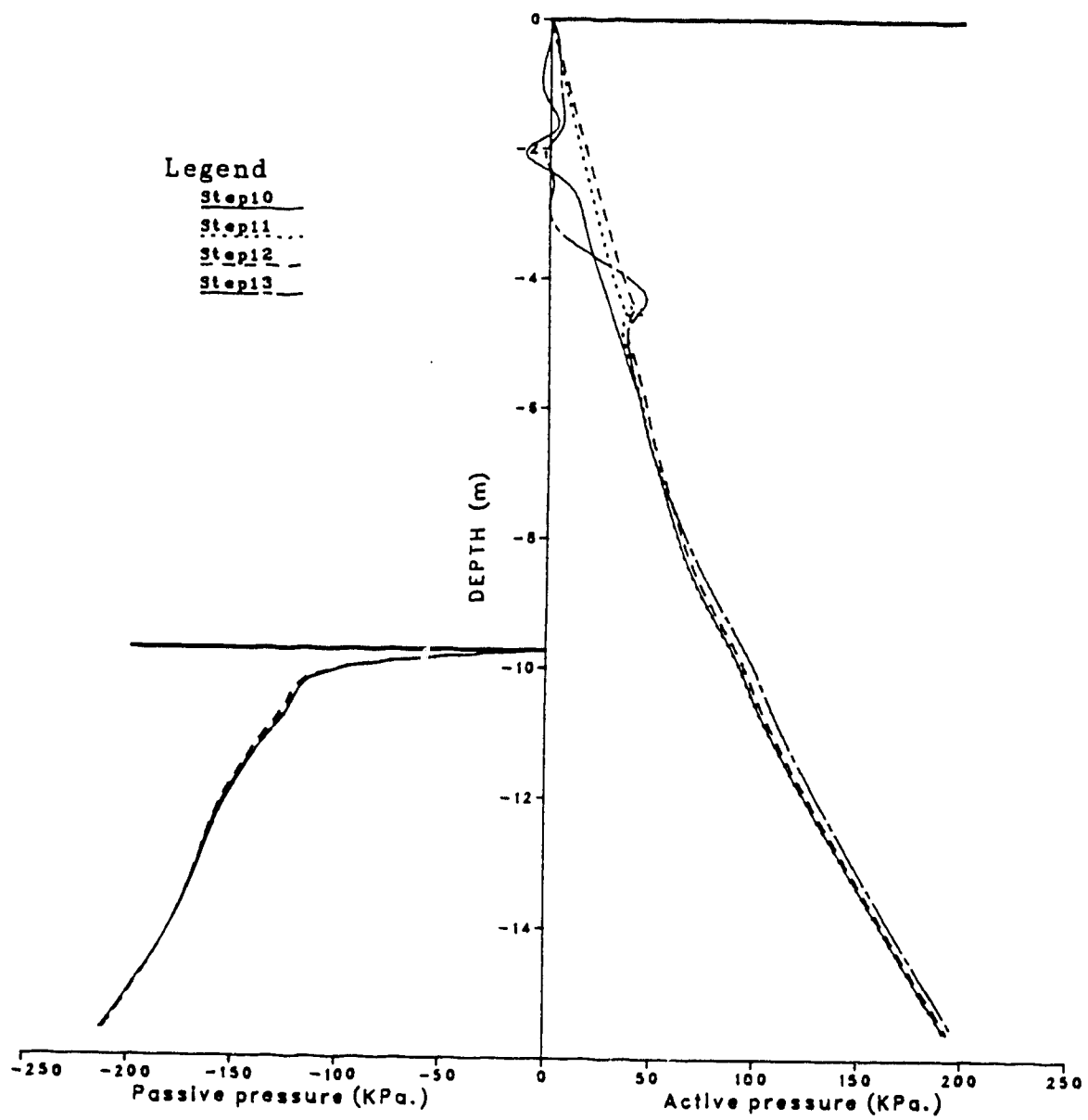


Figure D.19 Lateral Earth Pressure - Tunnel Section Set (3)

SHEAR STRESSES Tunnel Section

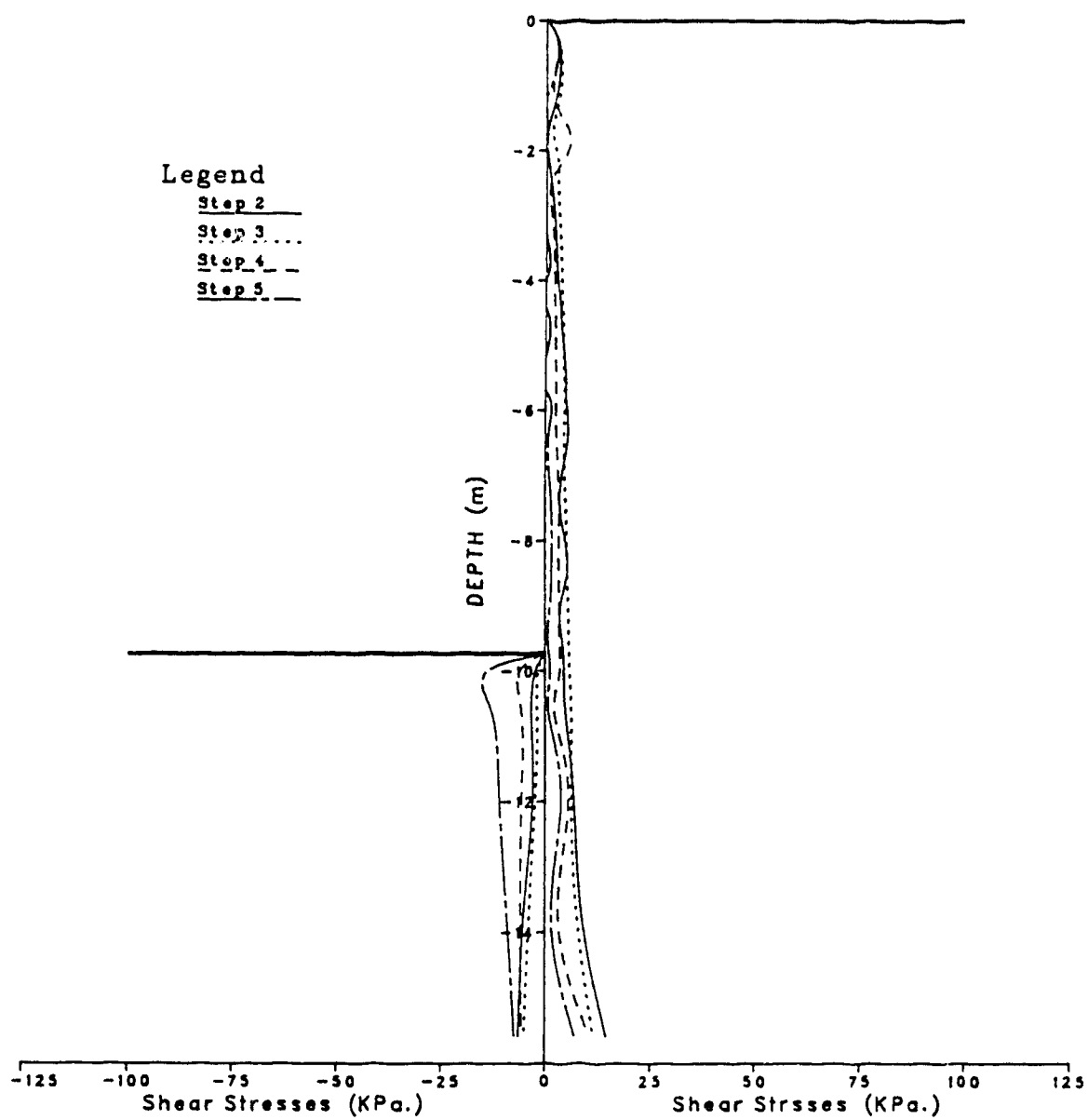


Figure D.20 Shear Stresses - Tunnel Section Set (1)

SHEAR STRESSES Tunnel Section

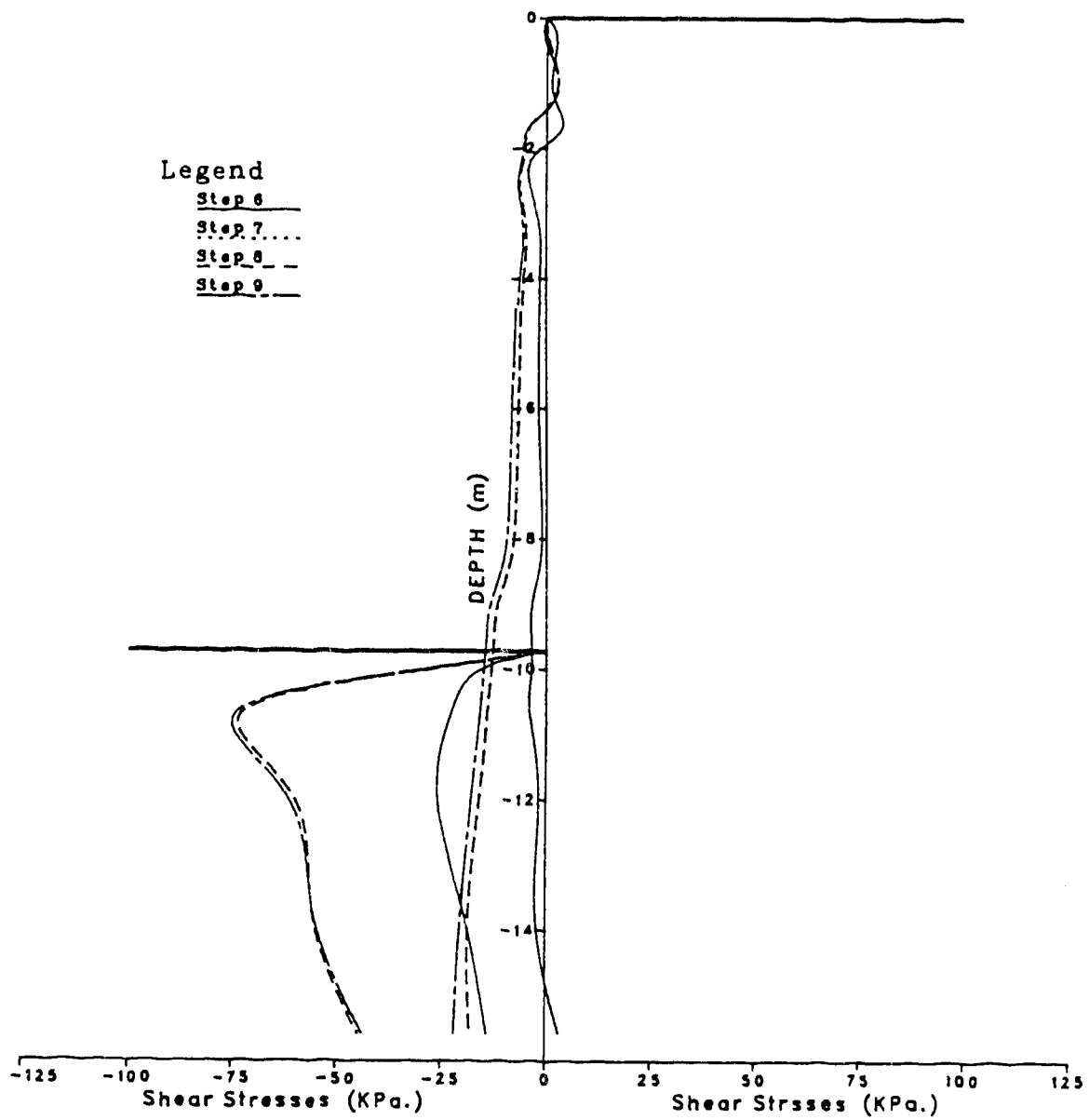


Figure D.21 Shear Stresses - Tunnel Section Set (2)

SHEAR STRESSES Tunnel Section

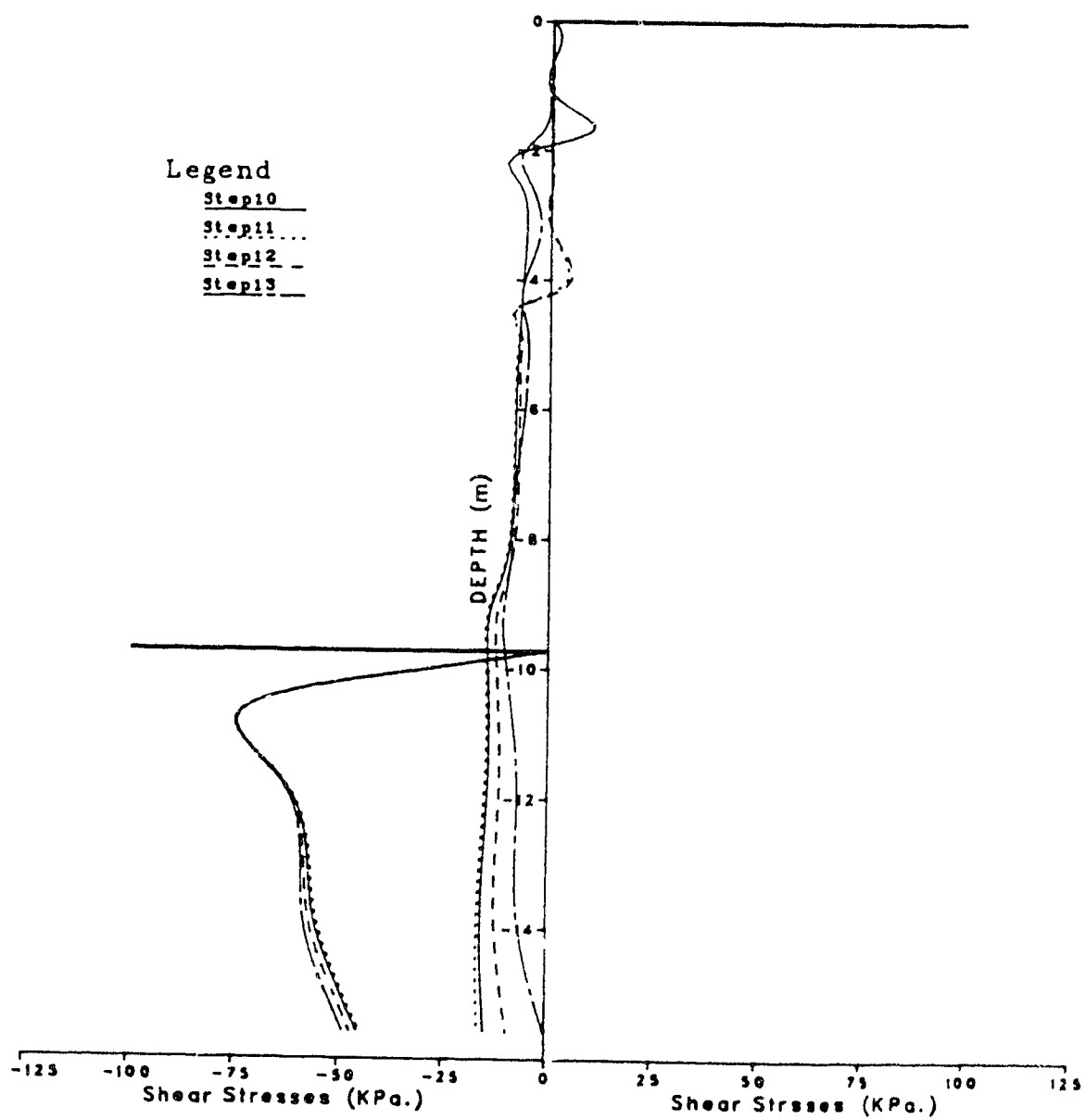


Figure D.22 Shear Stresses - Tunnel Section Set (3)

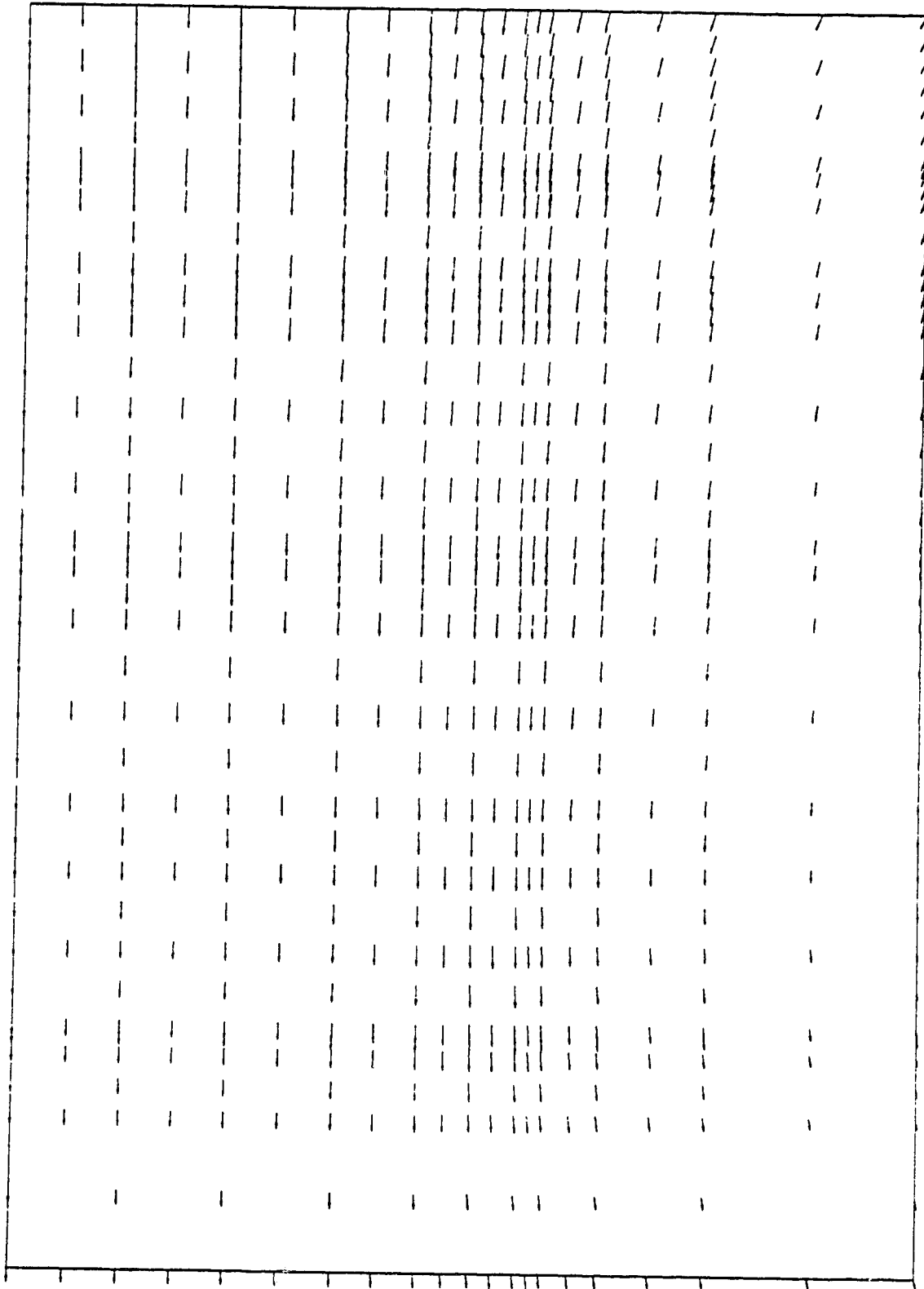


Figure D.23 Displacement Arrows - Station Section Steps (2)
and (3)

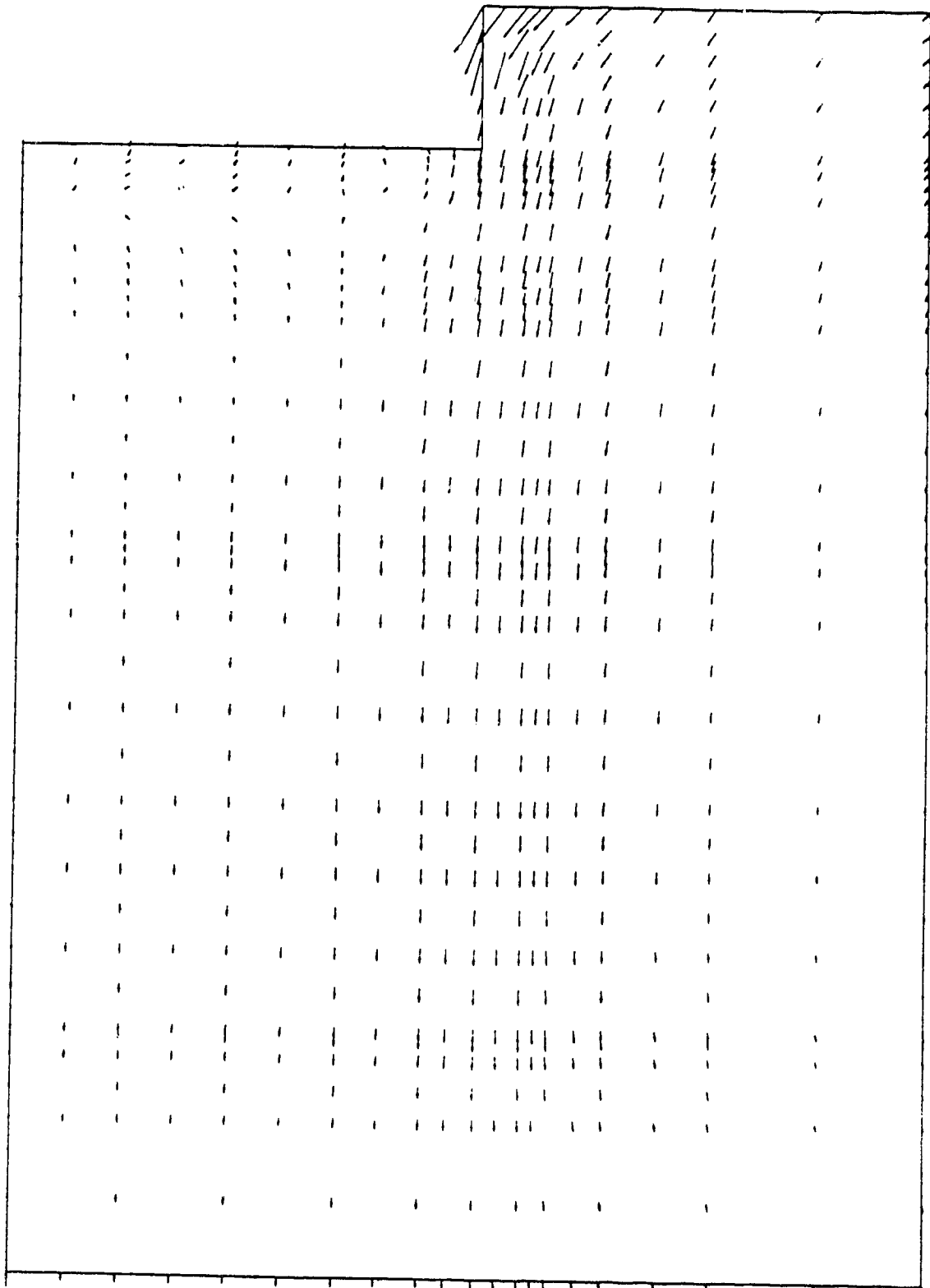


Figure D.24 Displacement Arrows - Station Section -
Undercover Step (4)

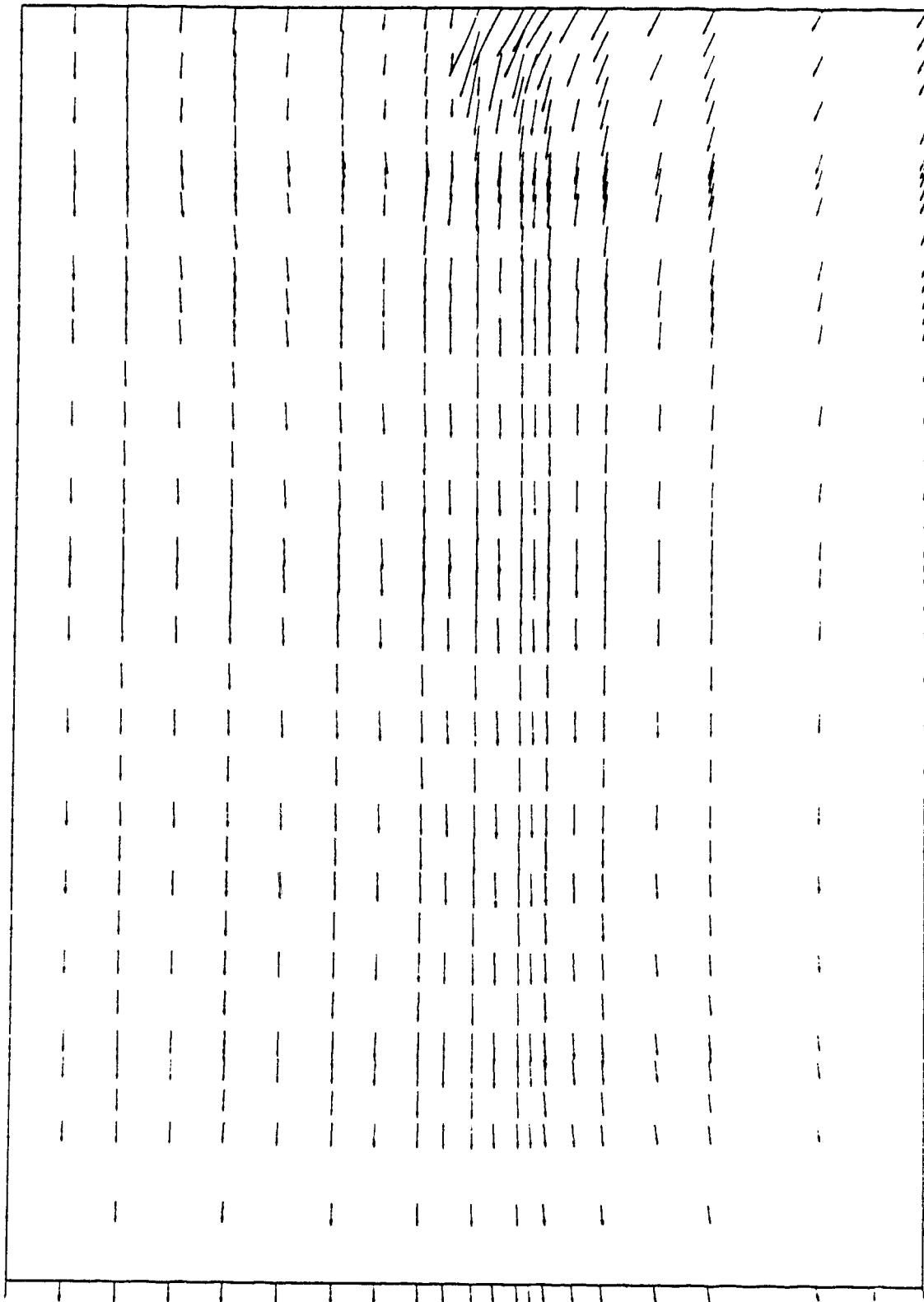


Figure D.25 Displacement Arrows - Station Section -
Undercover Step (5)

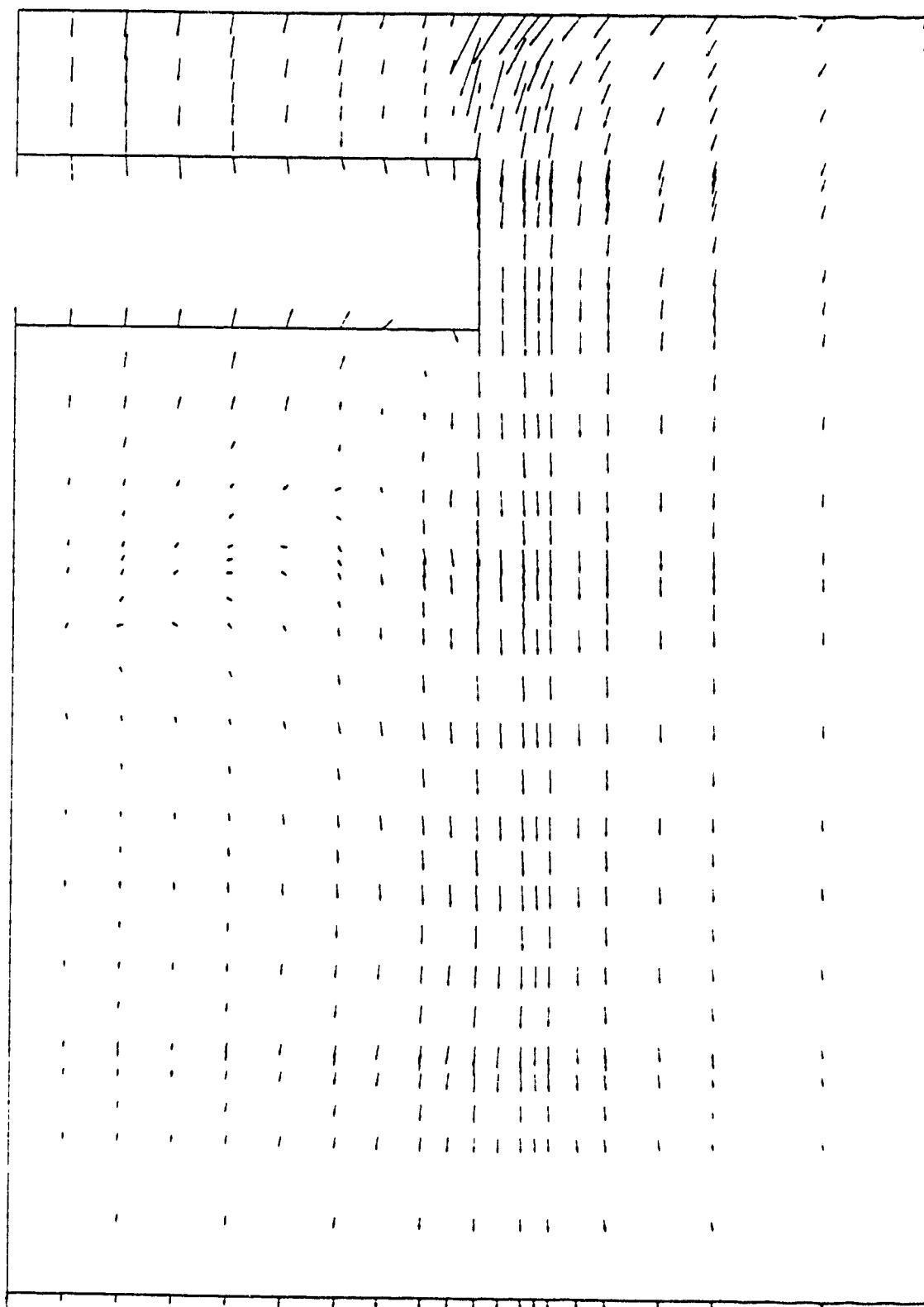


Figure D.26 Displacement Arrows - Station Section -
Undercover Step (6)

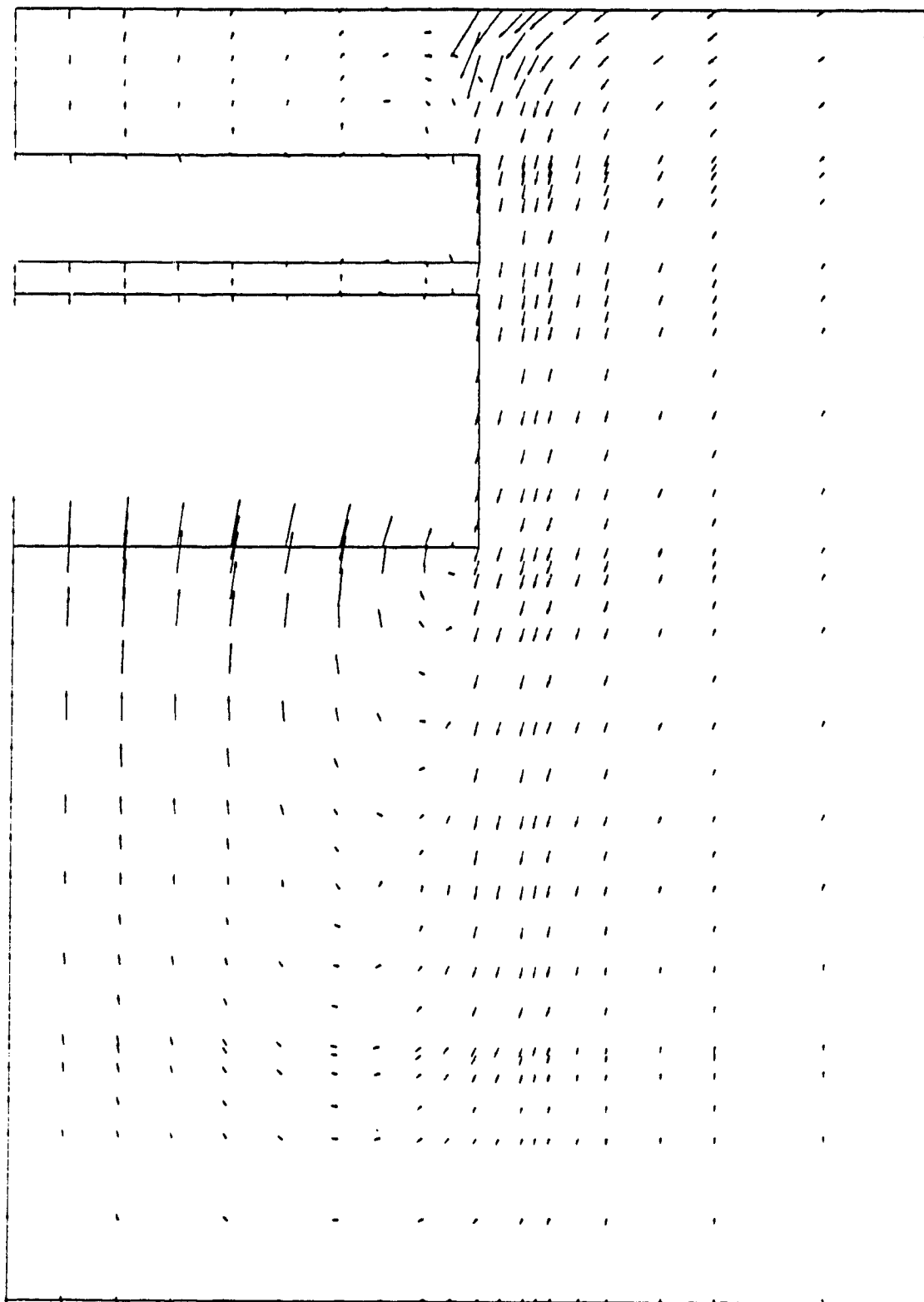


Figure D.27 Displacement Arrows - Station Section -
Undercover Step (7)

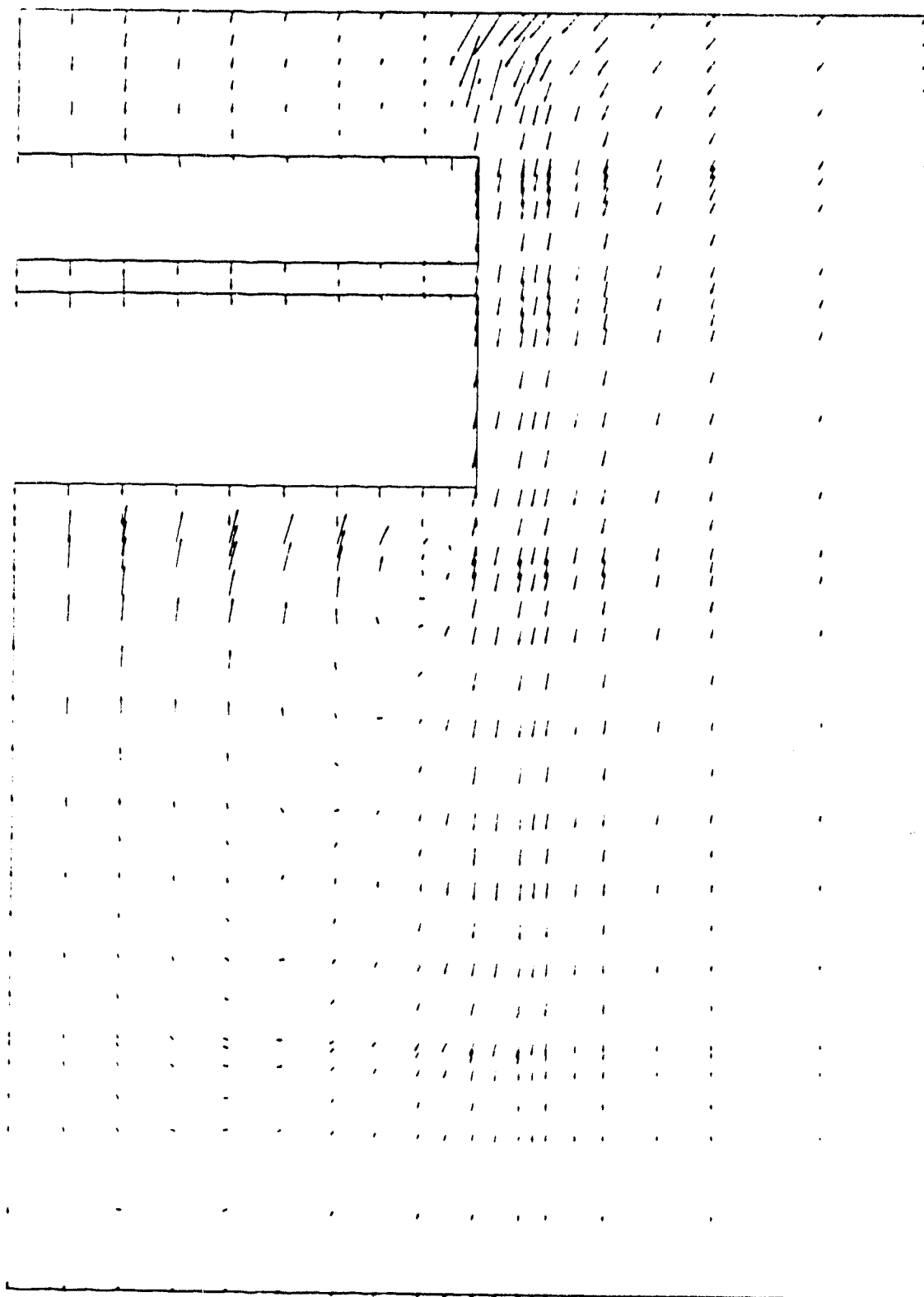


Figure D.28 Displacement Arrows - Station Section -
Undercover Step (8)

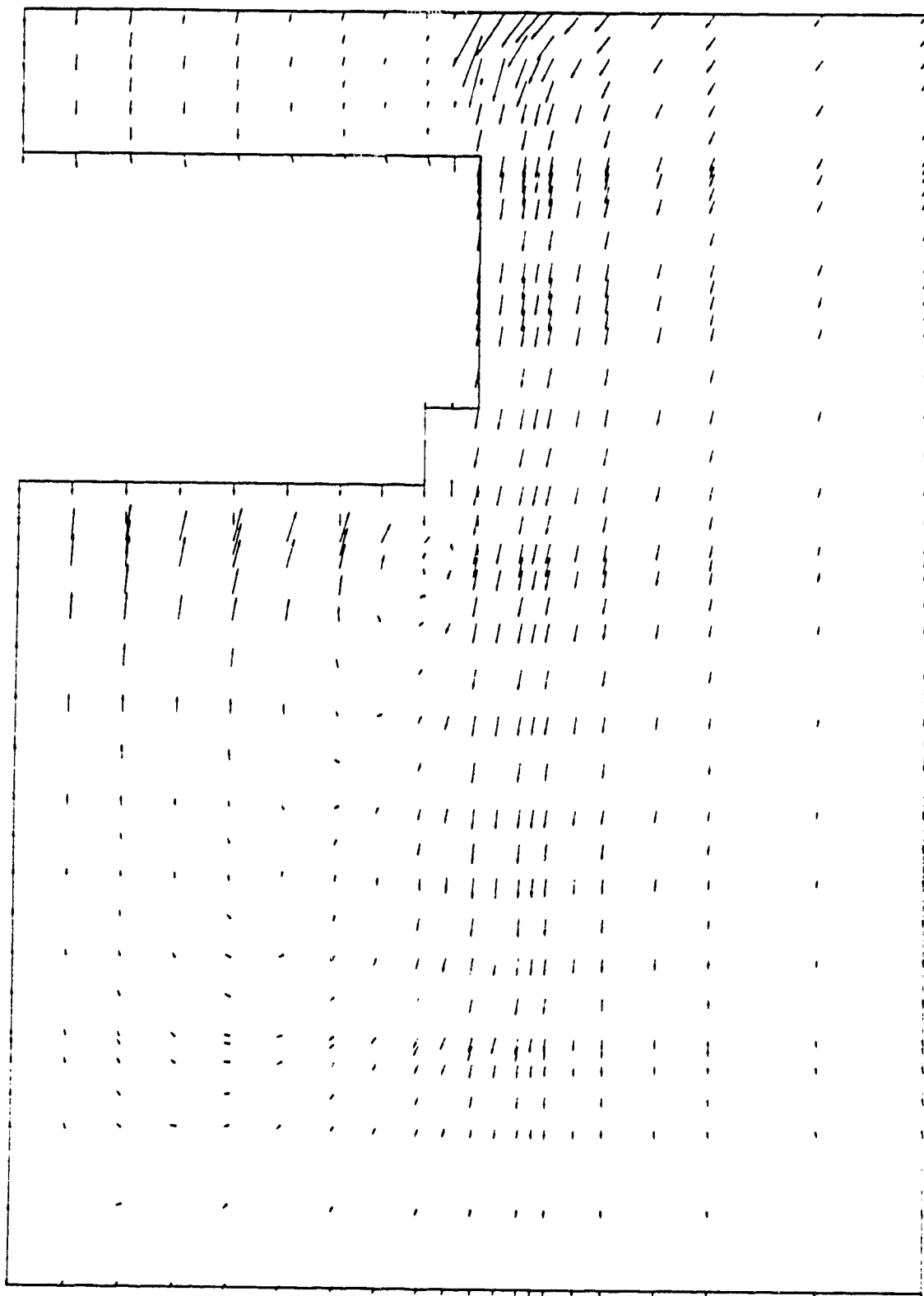


Figure D.29 Displacement Arrows - Station Section -
Undercover Step (9)

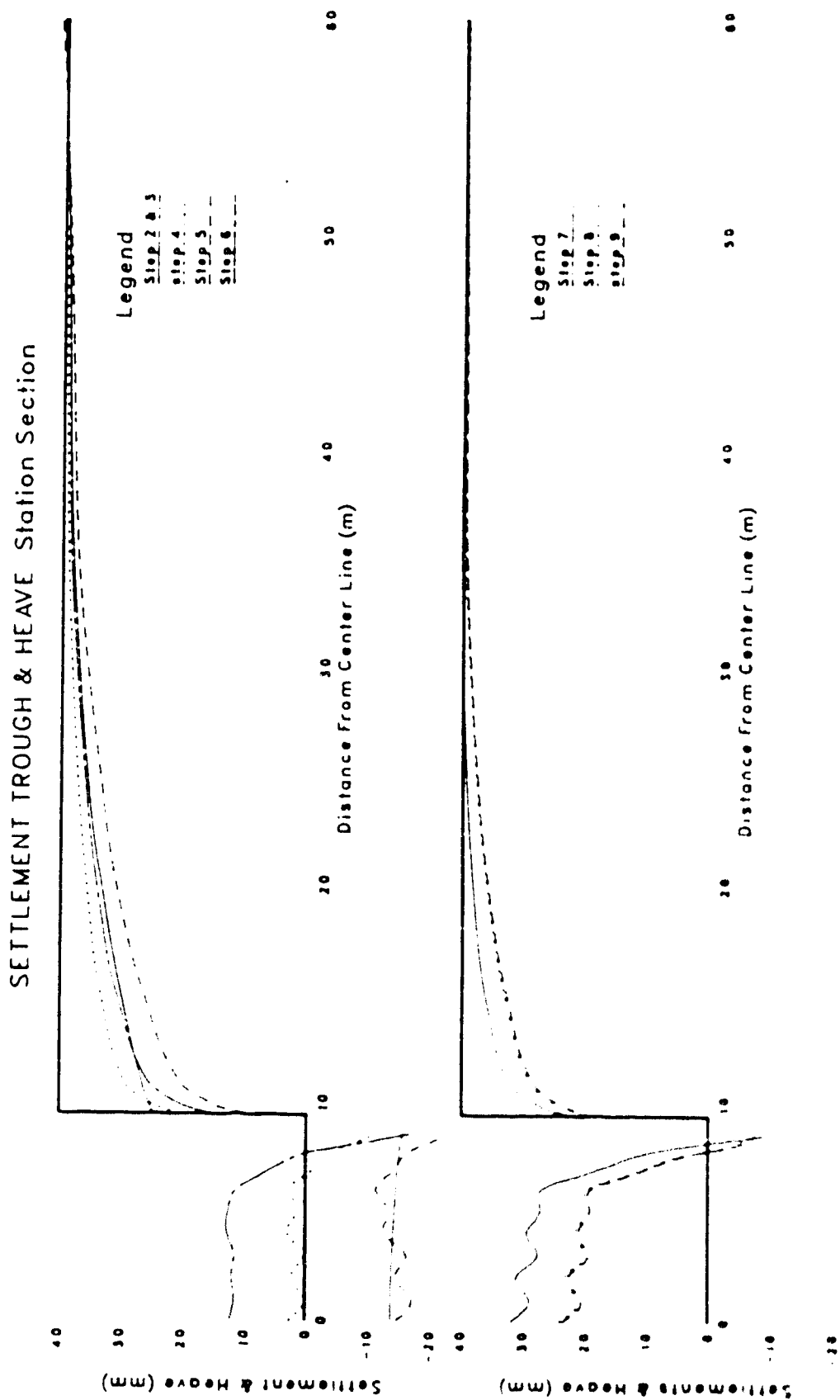
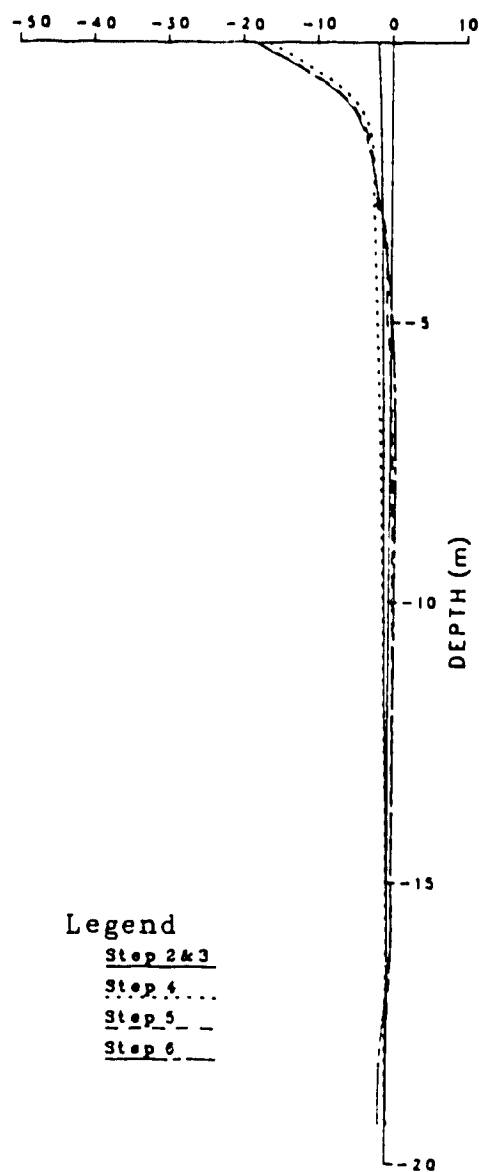


Figure D.30 Settlement Troughs and Excavation Base Heave - Station Section - Undercover

HORIZONTAL DISPLACEMENT (mm)
Station Section

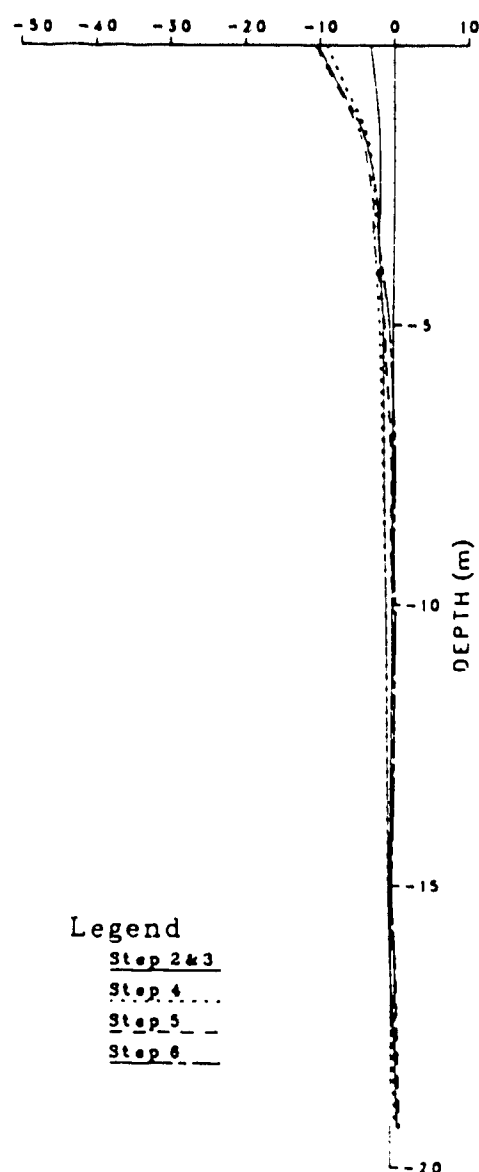
HORIZONTAL DISPLACEMENT (mm)
Station Section



Legend

Step 2 & 3
Step 4 ...
Step 5 - -
Step 6 - . -

WALL DISPLACEMENT



Legend

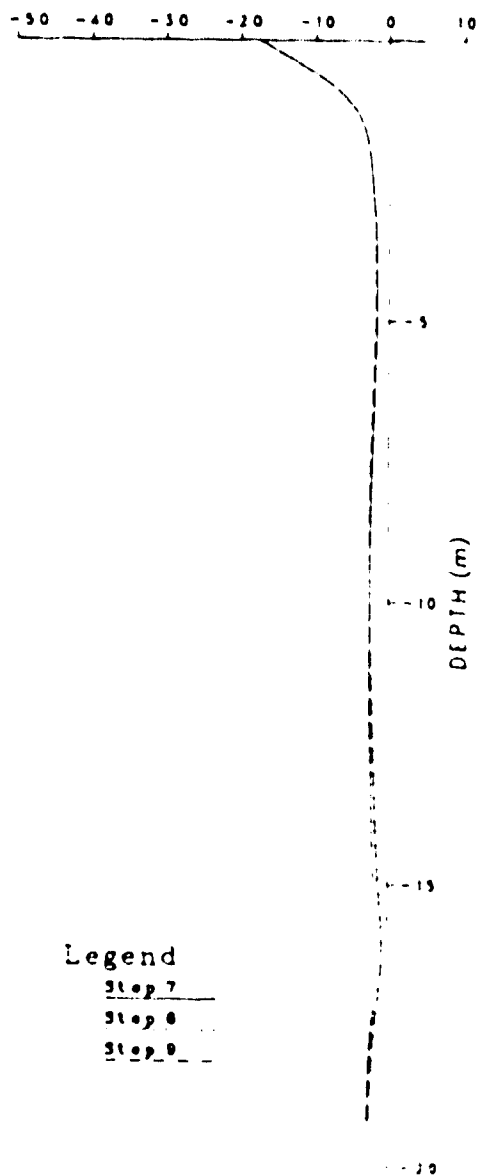
Step 2 & 3
Step 4 ...
Step 5 - -
Step 6 - . -

SOIL DISPLACEMENT

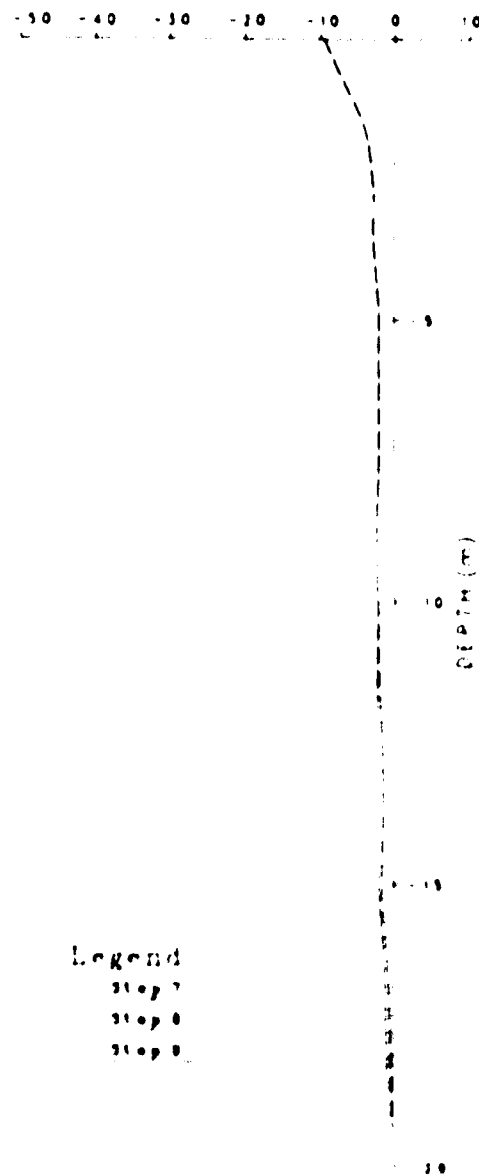
Figure D.31 Horizontal Displacement - Station Section -
Undercover - Set (1)

HORIZONTAL DISPLACEMENT (mm)
Station Section

HORIZONTAL DISPLACEMENT (mm)
Station Section



WALL DISPLACEMENT



SOIL DISPLACEMENT

Figure D.32 Horizontal Displacement - Station Section -

Undercover - Set (2)

LATERAL EARTH PRESSURE Station Section

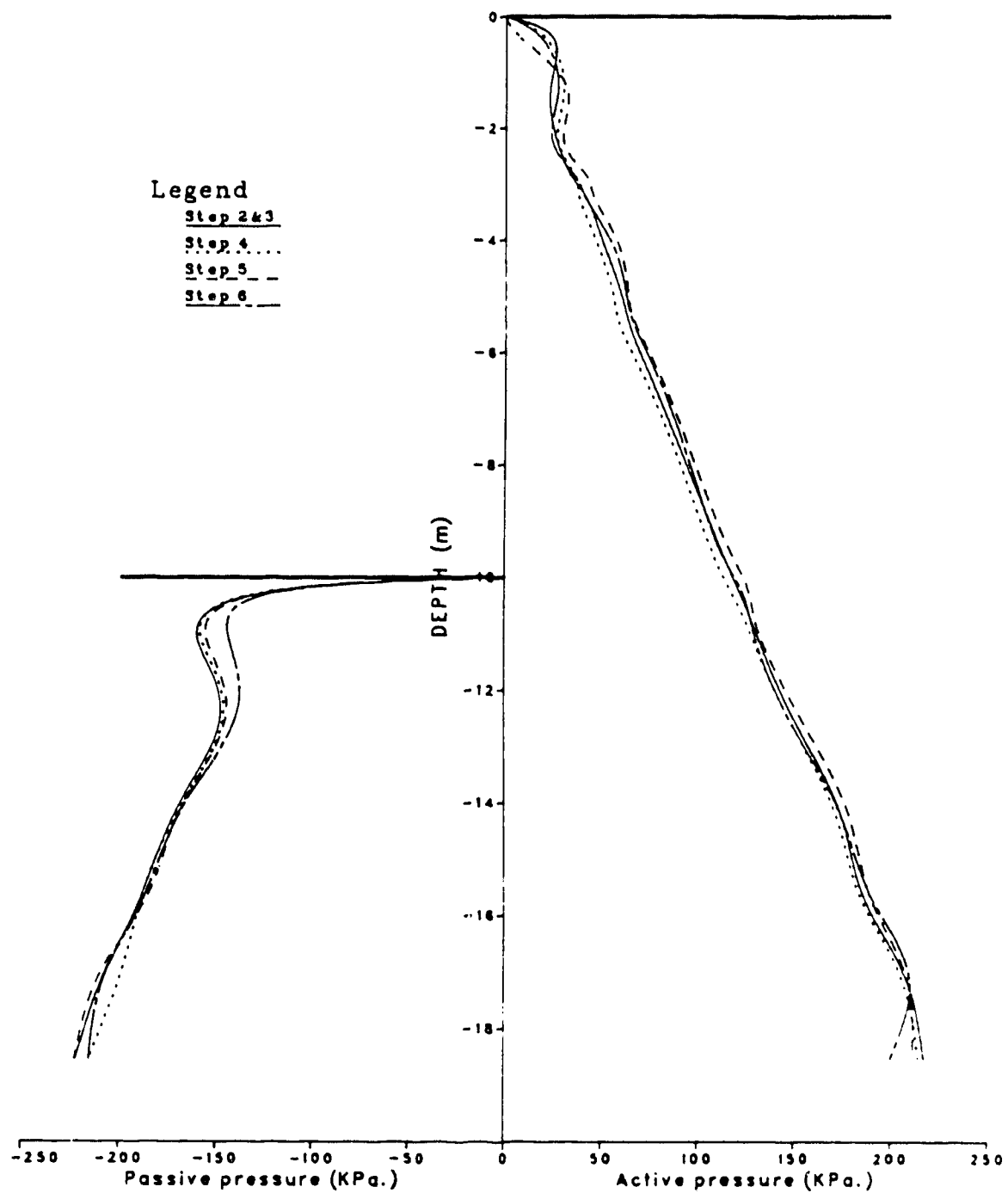


Figure D.33 Lateral Earth Pressure Station Section -
Undercover - Set (1)

LATERAL EARTH PRESSURE Station Section

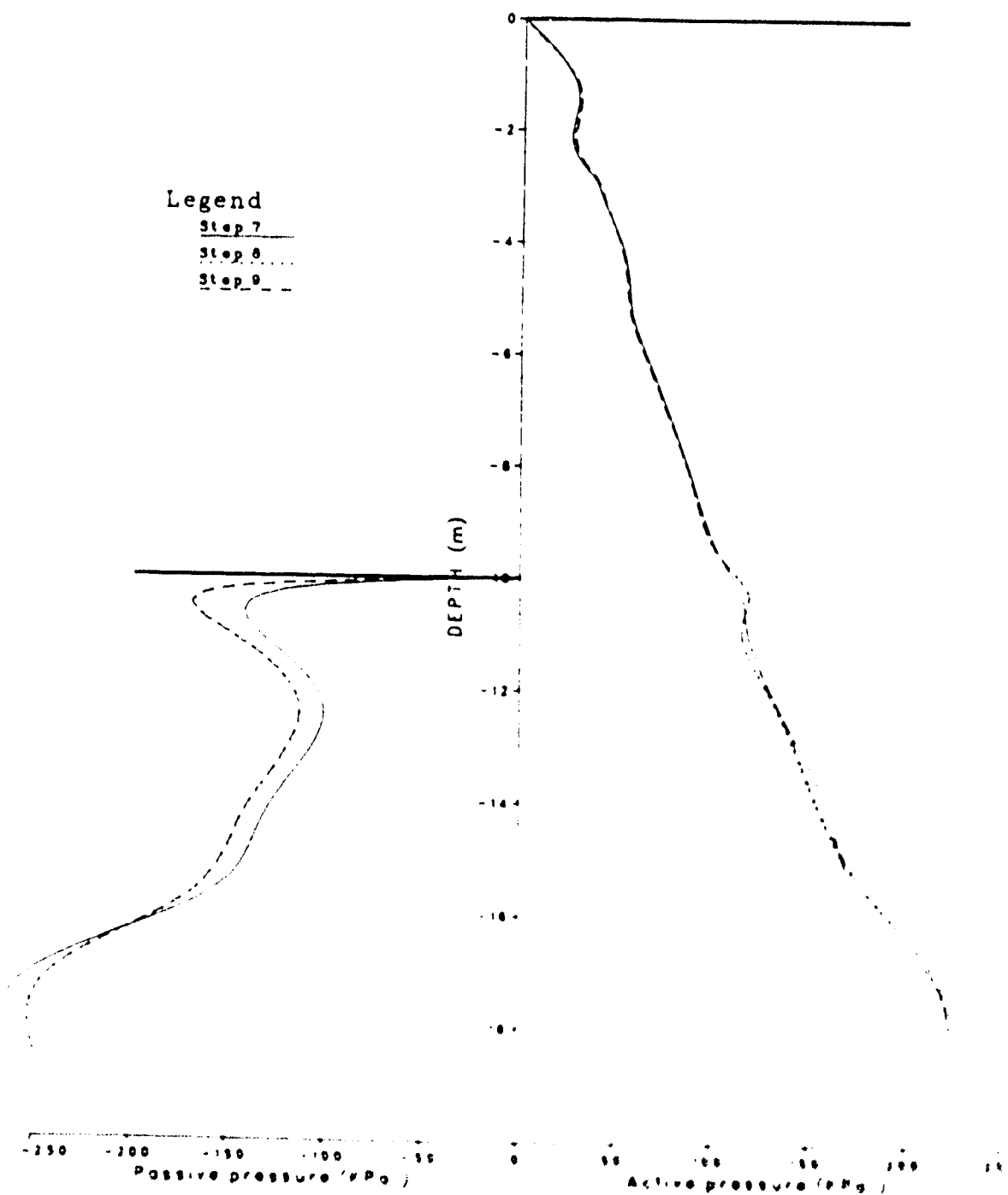


Figure D.34 Lateral Earth Pressure Station Section -
Undercoffer - Set (2)

SHEAR STRESSES Station Section

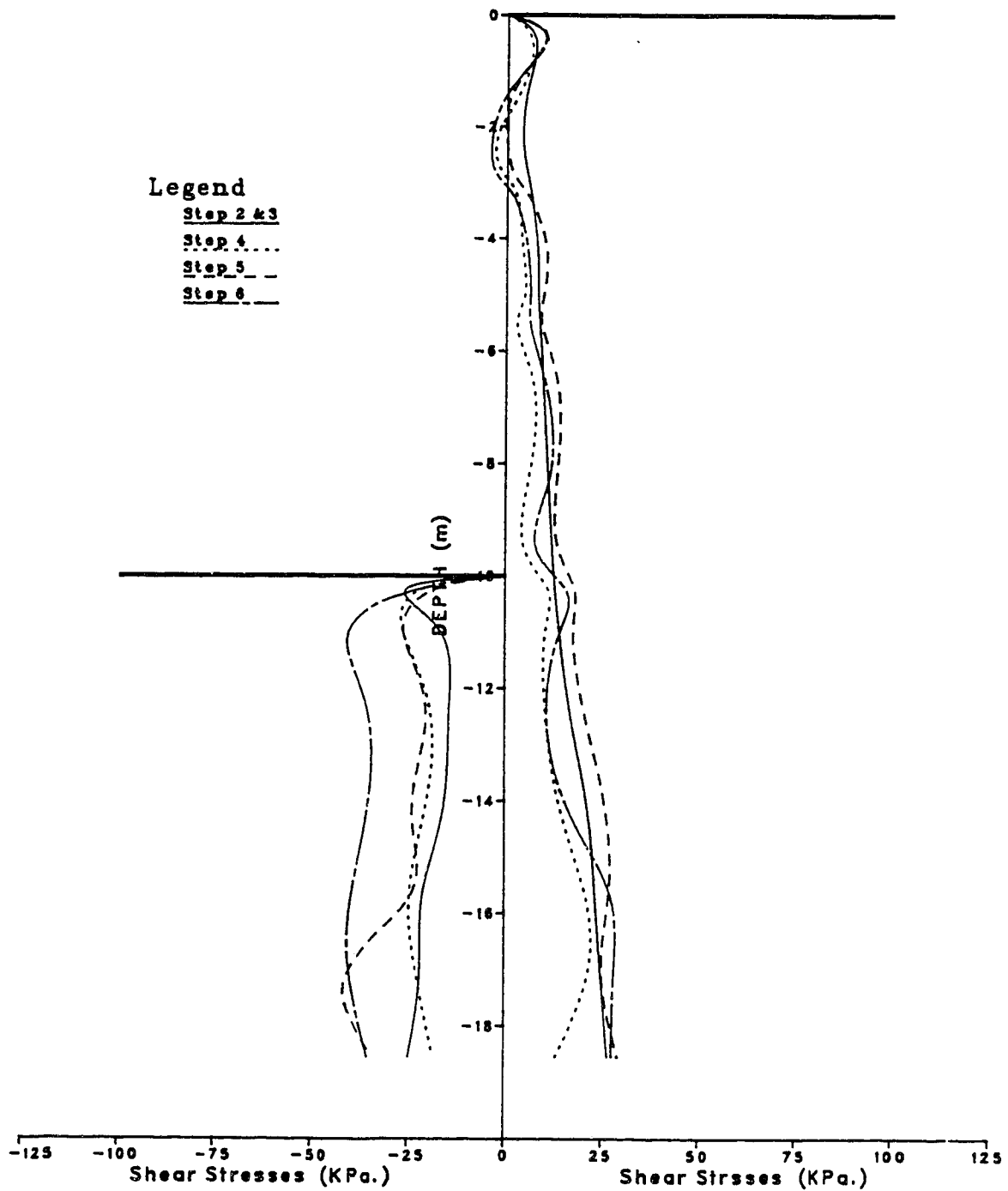


Figure D.35 Shear Stress - Station Section - Undercover -
Set (1)

SHEAR STRESSES Station Section

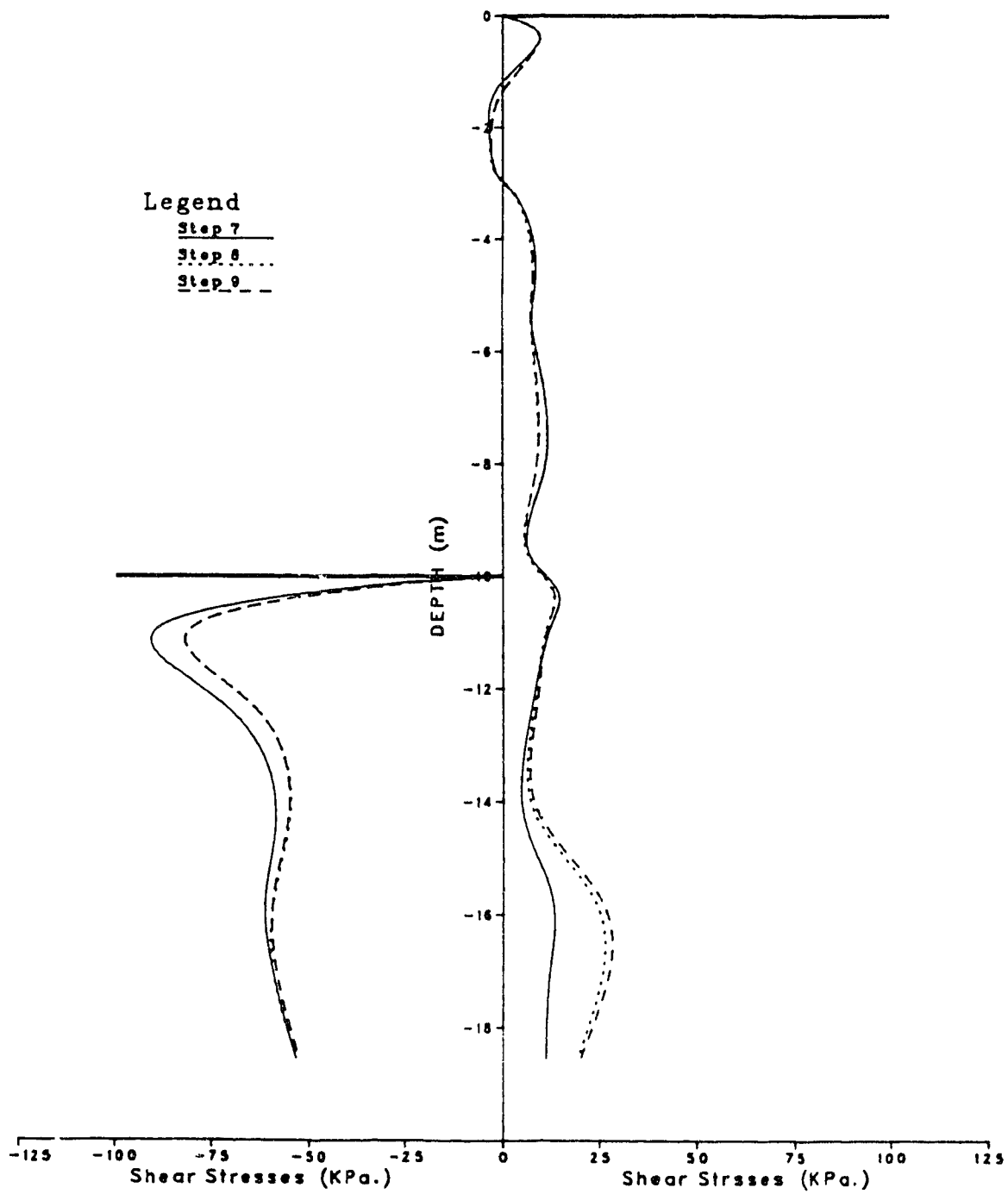


Figure D.36 Shear Stress - Station Section - Undercover -
Set (2)

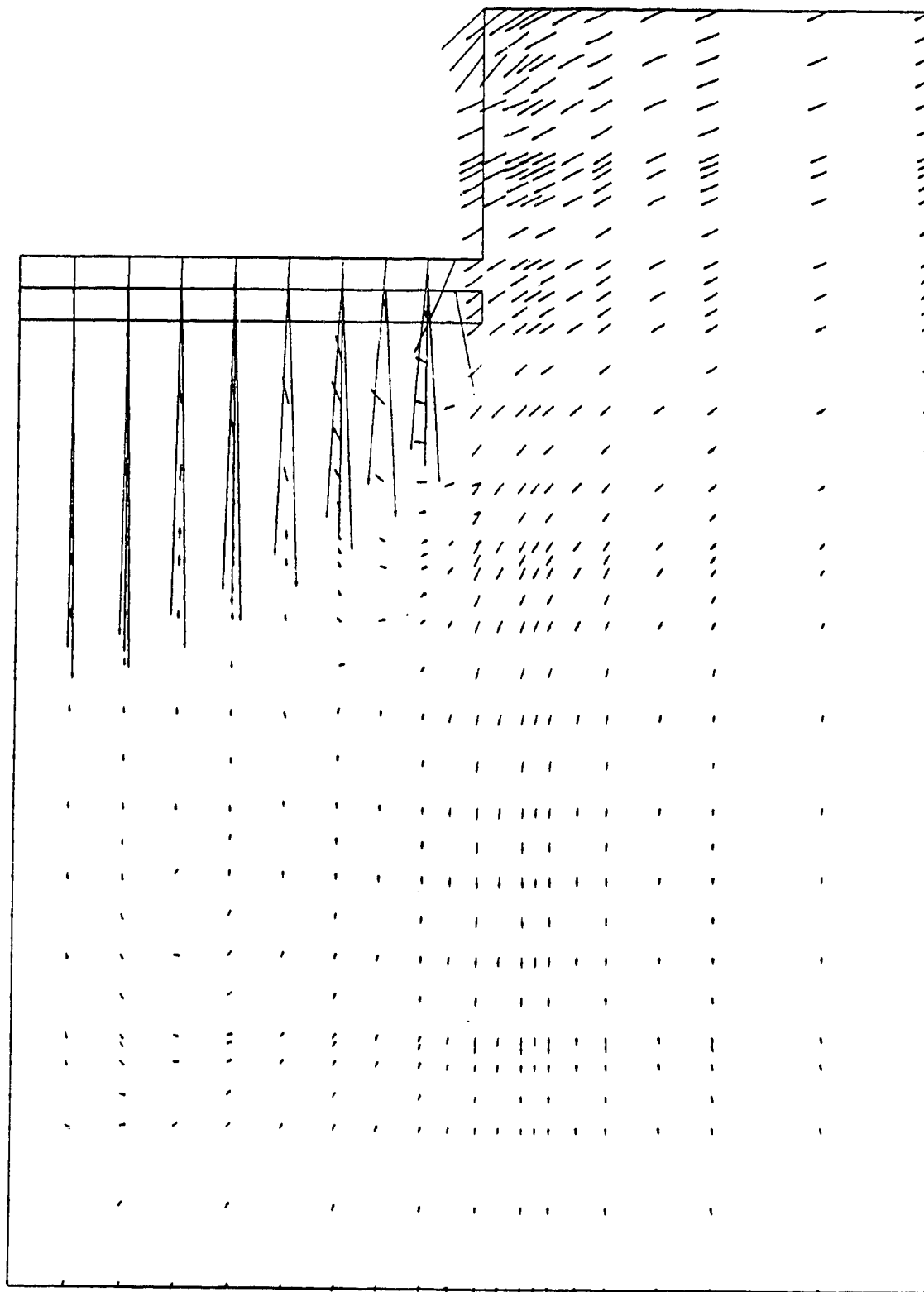


Figure D.37 Displacement Arrows - Station Section - Open Air
Excavation Step (4)

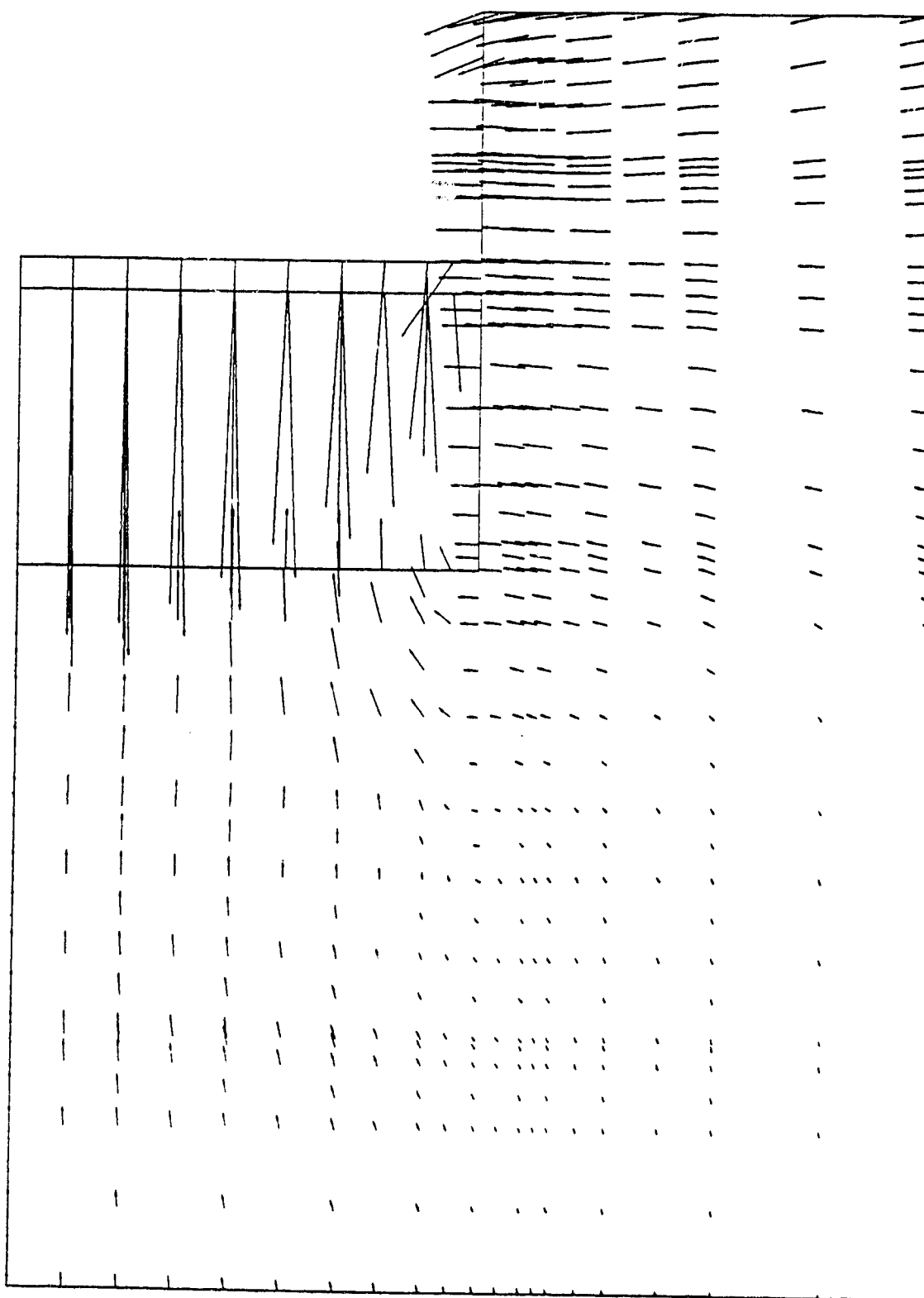


Figure D.38 Displacement Arrows - Station Section - Open Air
Excavation Step (5)

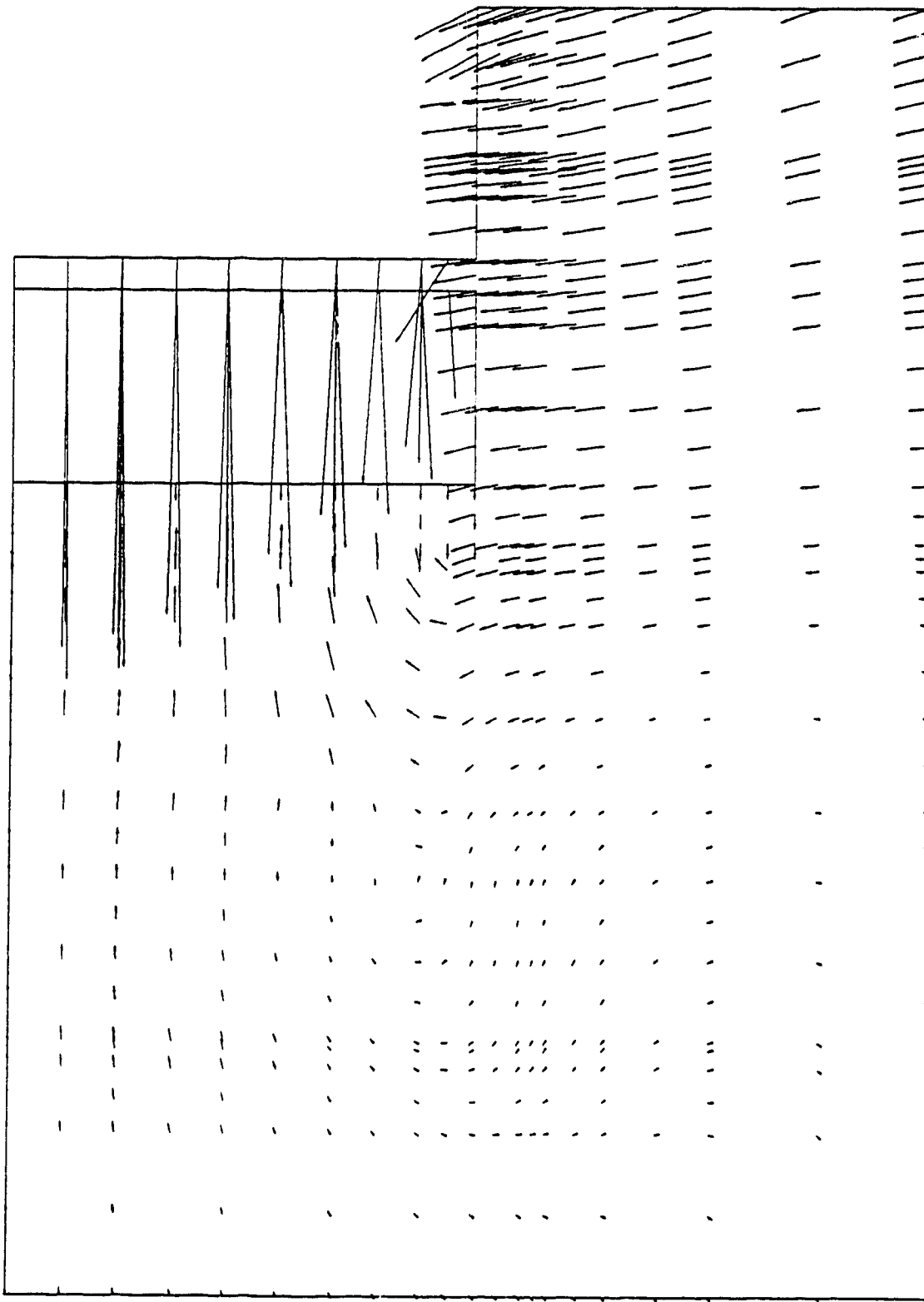


Figure D.39 Displacement Arrows - Station Section - Open Air
Excavation Step (6)

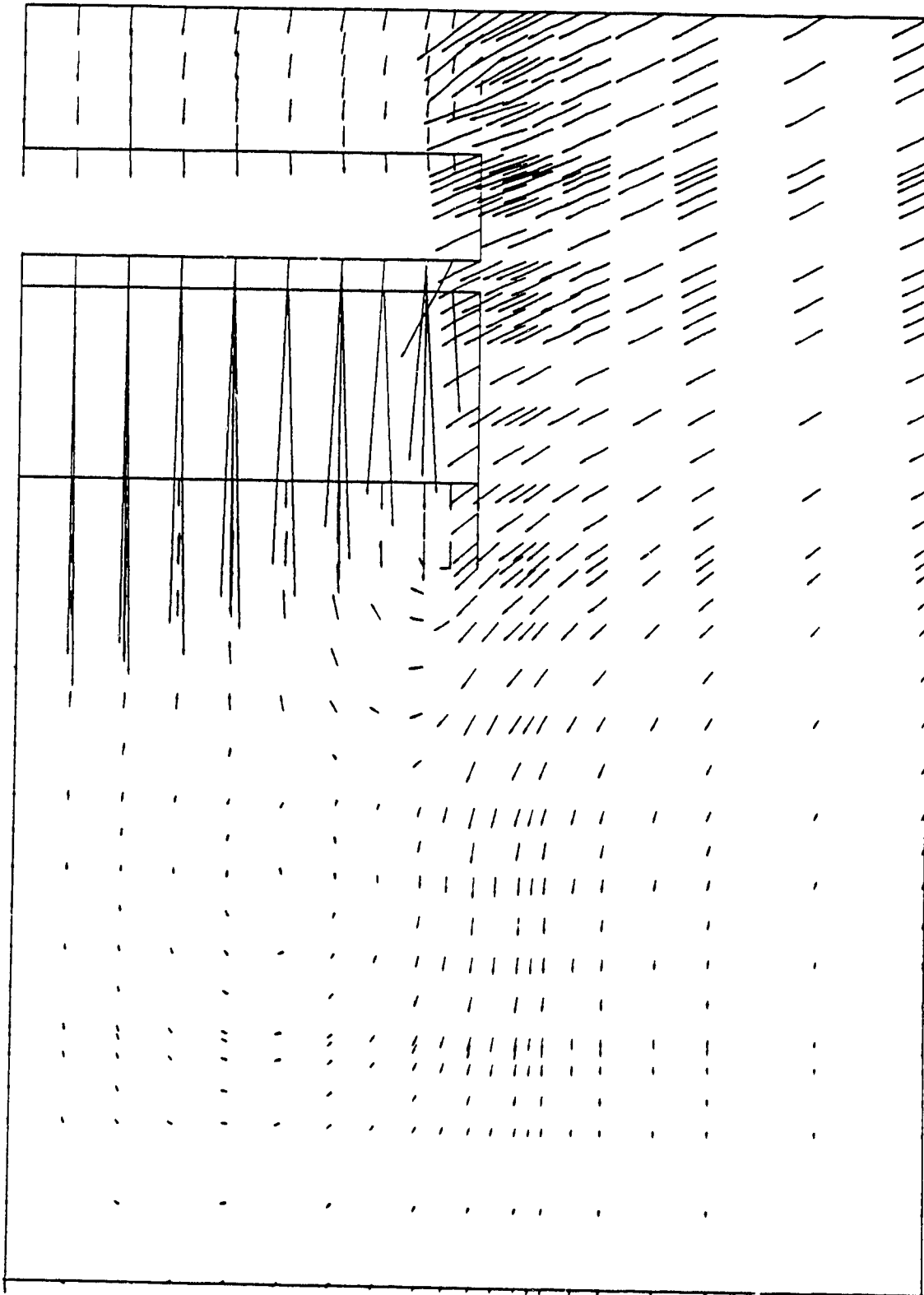


Figure D.40 Displacement Arrows - Station Section - Open Air
Excavation Step (7)

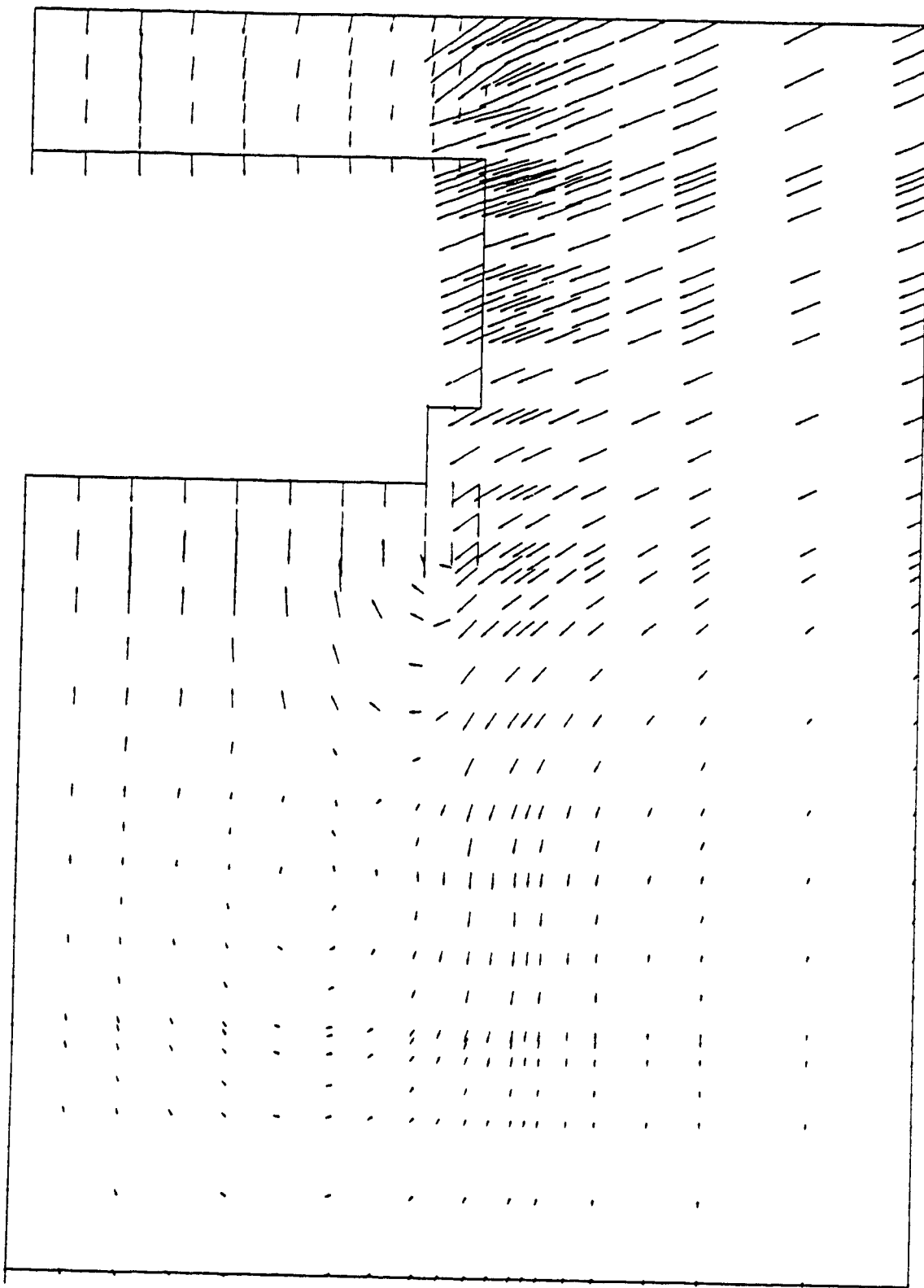


Figure D.41 Displacement Arrows - Station Section - Open Air
Excavation Step (8)

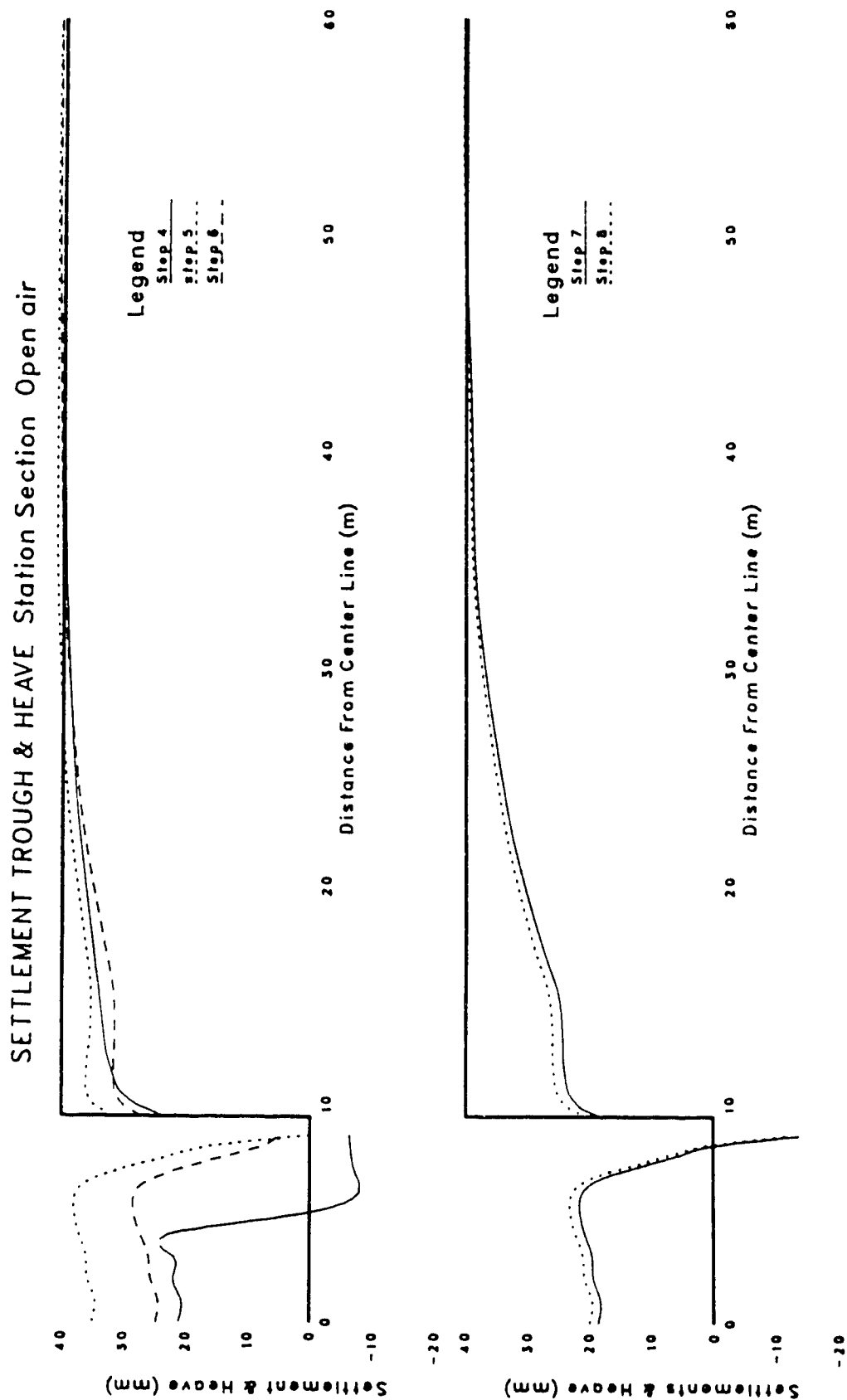
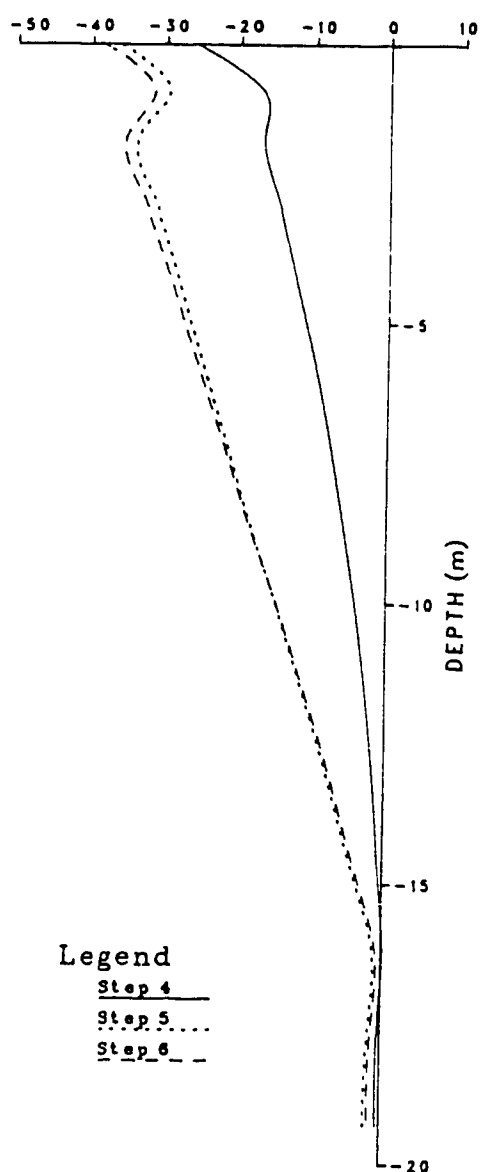


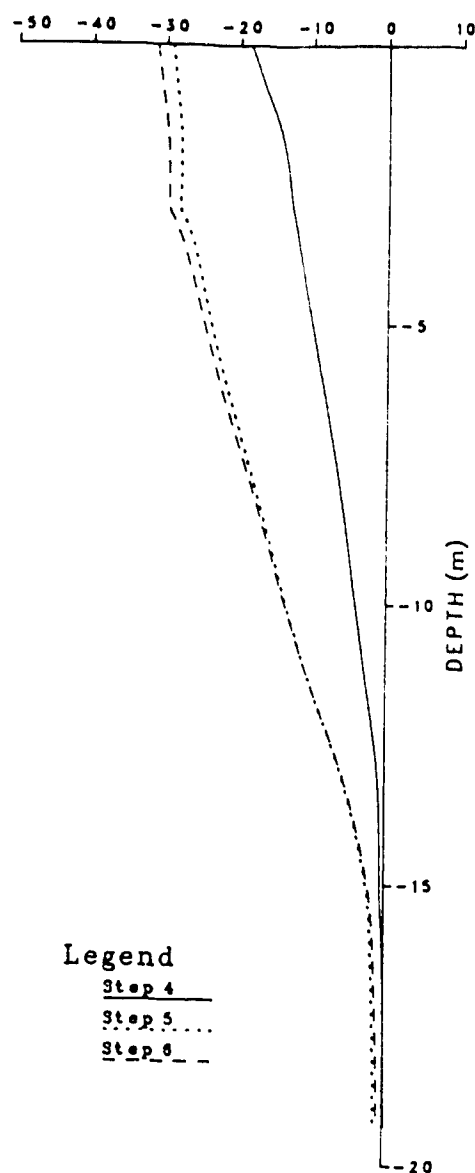
Figure D.42 Settlement Trough and Excavation Base Heave - Station Section - Open Air
Excavation

HORIZONTAL DISPLACEMENT (mm)
Station Section Open Air

HORIZONTAL DISPLACEMENT (mm)
Station Section Open Air



WALL DISPLACEMENT

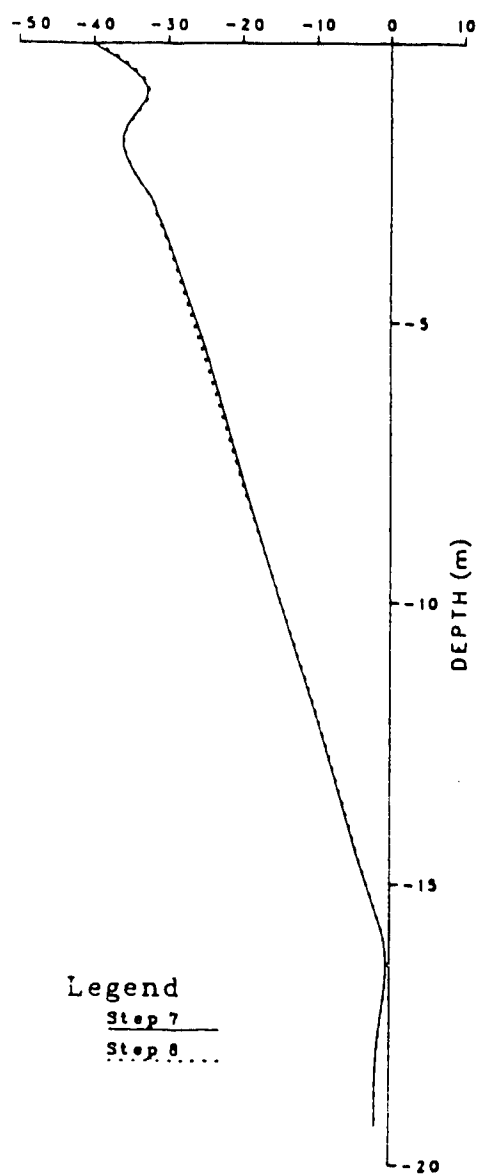


SOIL DISPLACEMENT

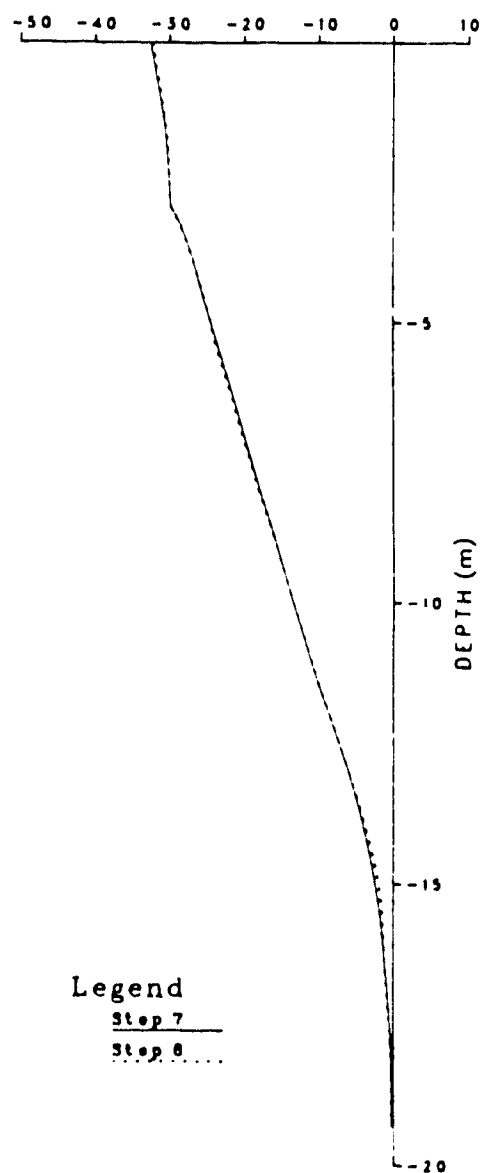
Figure D.43 Horizontal Displacement - Station Section - Open
Air - Set (1)

HORIZONTAL DISPLACEMENT (mm)
Station Section Open Air

HORIZONTAL DISPLACEMENT (mm)
Station Section Open Air



WALL DISPLACEMENT



SOIL DISPLACEMENT

Figure D.44 Horizontal Displacement - Station Section - Open
Air - Set (2)

LATERAL EARTH PRESSURE Station Section Open Air

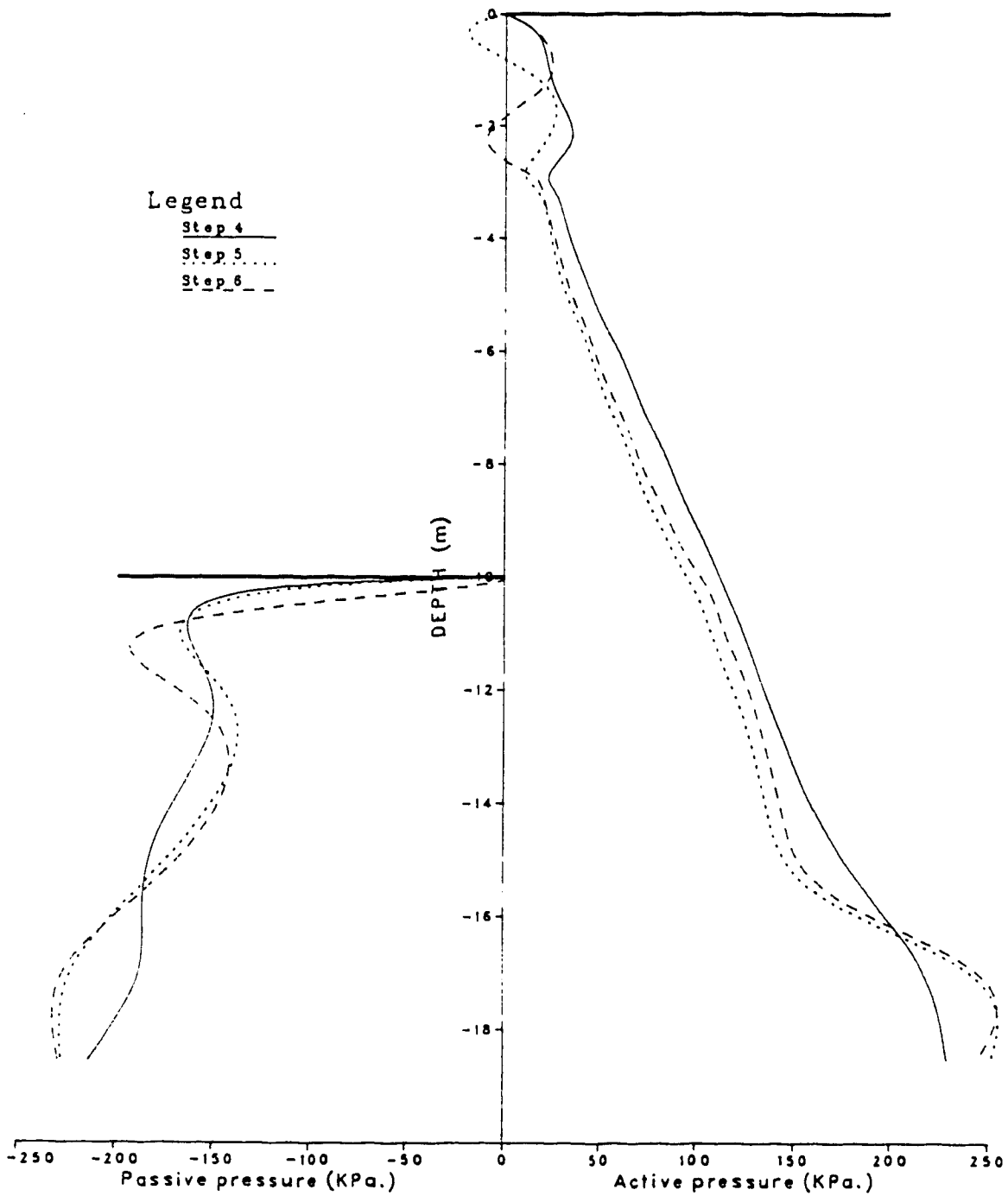


Figure D.45 Lateral Earth Pressure Station Section - Open
Air - Set (1)

LATERAL EARTH PRESSURE Station Section Open Air

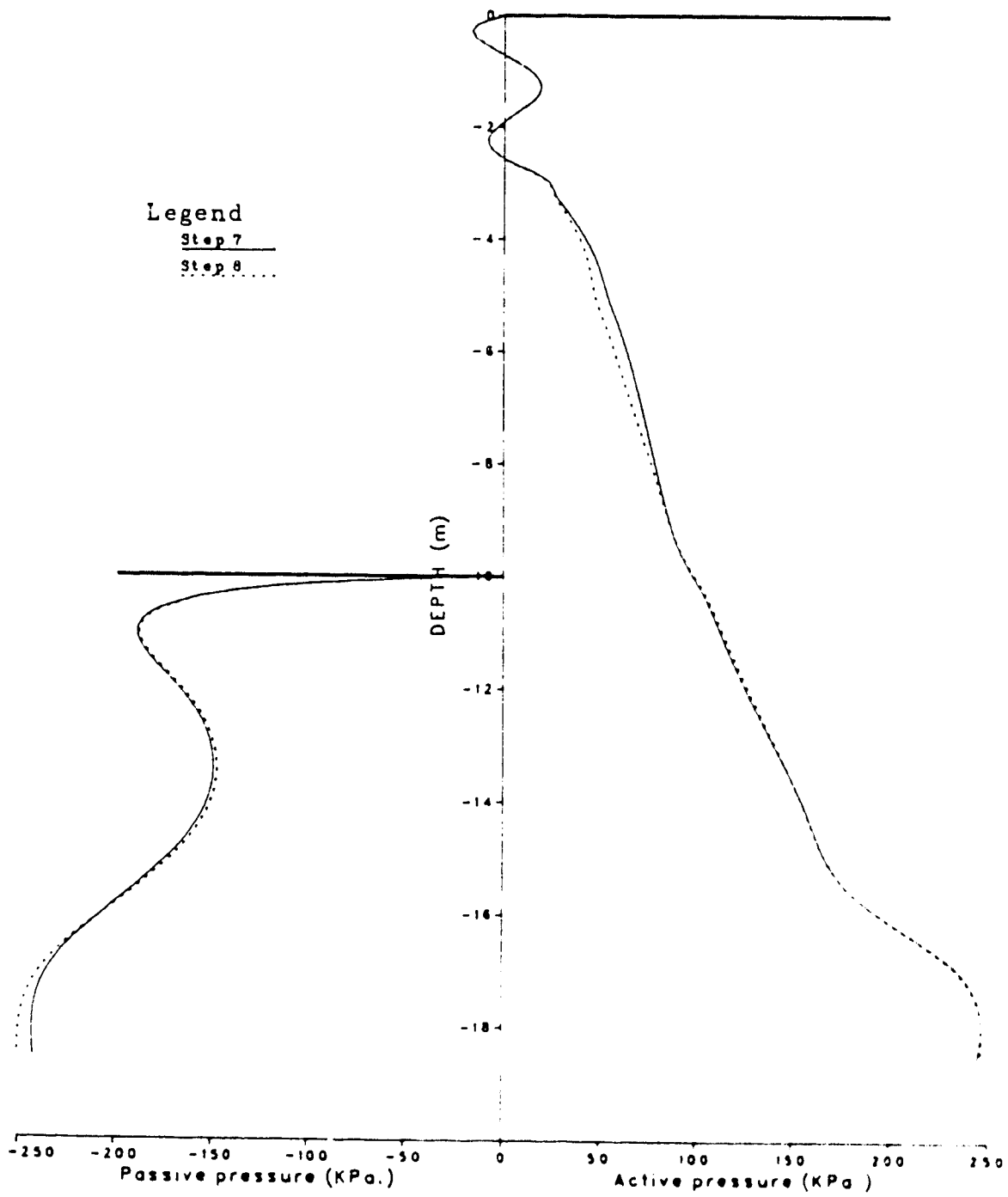


Figure D.46 Lateral Earth Pressure Station Section - Open
Air - Set (2)

SHEAR STRESSES Station Section Open Air

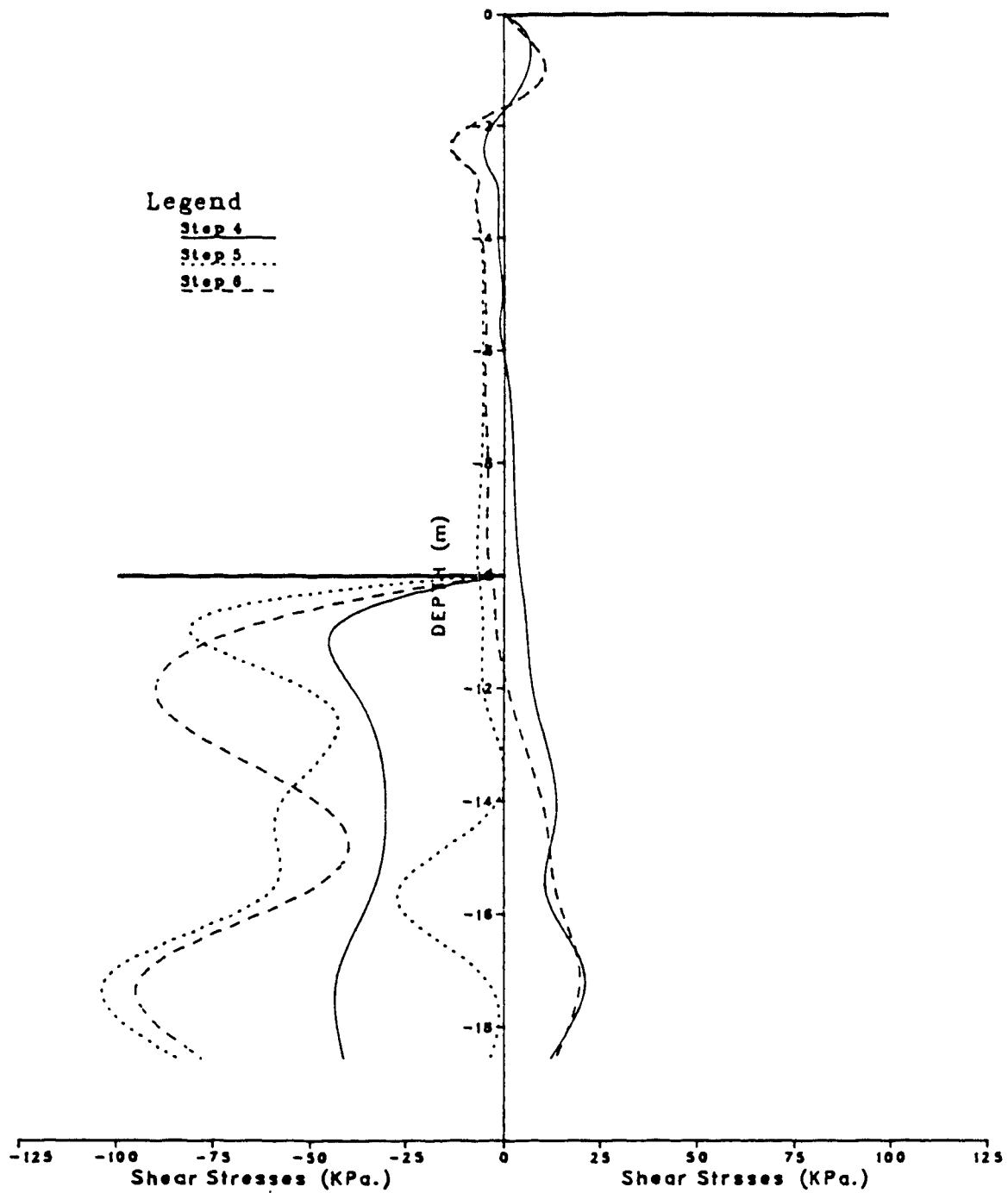


Figure D.47 Shear Stress - Station Section - Open Air - Set

SHEAR STRESSES Station Section Open Air

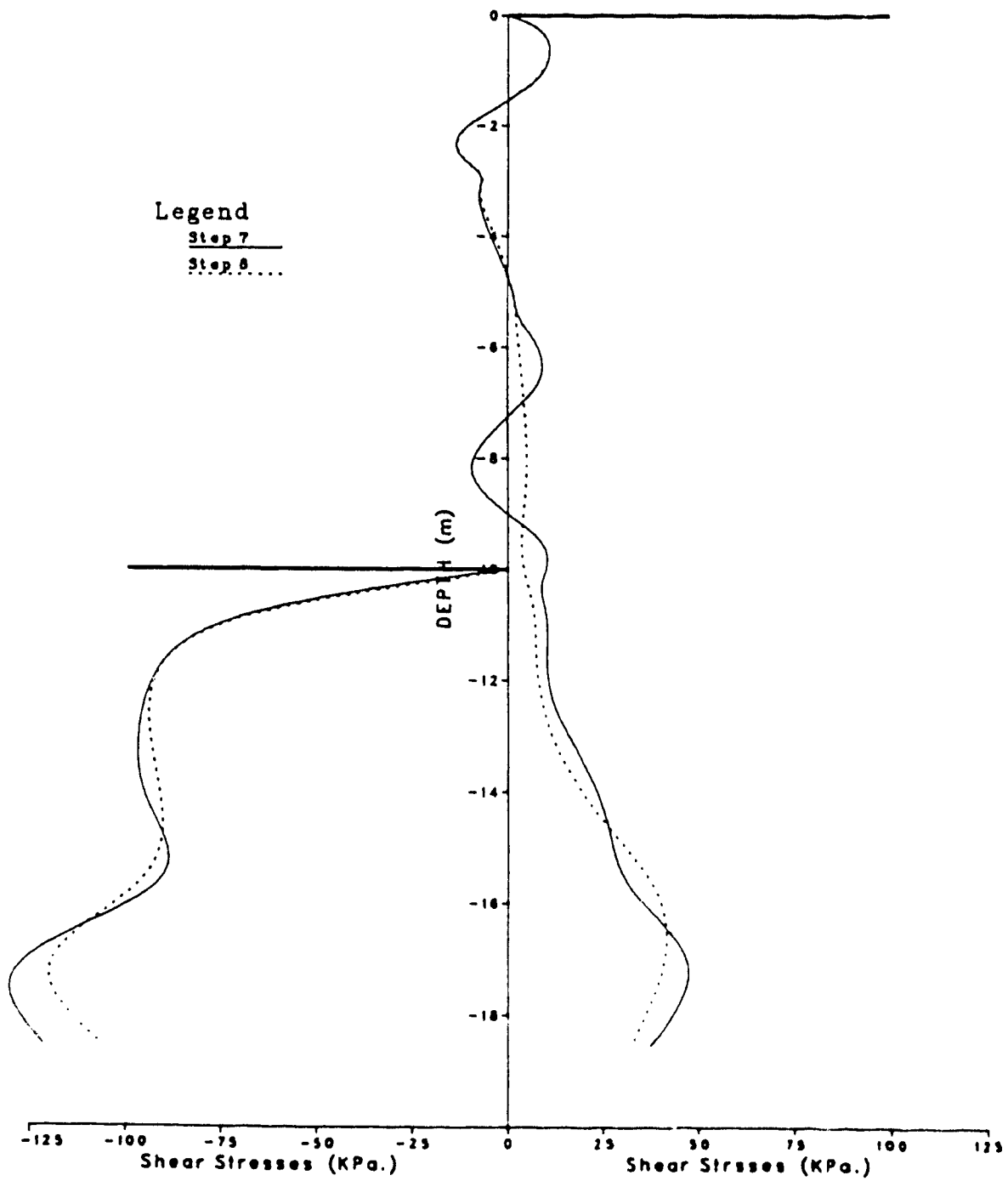


Figure D.48 Shear Stress - Station Section - Open Air - Set

E. Input/Output Files for SAFE

This appendix contains the Input and Output files for SAFE , each contains a sample of control cards and output components (i.e.these are not the complete files).

CAIRO	METRO	PROJECT	TUNNEL	SECTION
3	2	0	0.0	15 15 1 1 1 8 0
13	13	300 981	2	13 -1 0 0 1
1	15	0.000500		
2	10	0.001000		
0	0	0.0010 0		
0.0		0.0	0 0	
0.85800		0.0	0 0	
1.71500		0.0	0 0	
2.57300		0.0	0 0	
22.00000	40.00000	1 1		
31.00000	40.00000	1 1		
40.00000	40.00000	0 1		
1	3	35 33	2 23 34 22	2 1 1 0
4				
3	5	37 35	4 24 36 23	2 1 1 0
4				
5	7	39 37	6 25 38 24	2 1 1 0
4				
7	9	41 39	8 26 40 25	2 1 1 0
4				
9	11	43 41	10 27 42 26	2 1 1 0
4				
11	13	45 43	12 28 44 27	2 1 1 0
4				
13	15	47 45	14 29 46 28	2 1 1 0
	1.0	750.0	0.0	-13.04 0.0 15.E3
	0.4	0.0	0.0	0.0 0.0 0.0
	0.0	0.0	0.0	0.0 0.0 0.0
	11.	0.0	0.0	-18.0 0.0 200.
	450.0	0.79	0.69	0.60 33.0 101.33
	120.	0.37	0.0	0.1 0.99
	0.0	0.0	0.0	0.0 0.0
Step: (1)	for Intial	Stress Calculation		
1	0	0 0	0 0 0	
1	1	1 0	0 300	
Step: (2)	Slurry Trench + Pannel			
53	0	0 0	0 0	
1	1	0 0	10 110	
111	1	0 0	9 180	
181	1	0 0	8 280	
54	0	0 0	0 0	
64	0	0 0	0 0	
Step : (13)	Final Case			
9	6	0 0	0 0 0	
245	1	1 0	1 0	
255	1	1 0	1 0	
265	1	1 0	1 0	
271	1	1 0	1 275	
281	1	1 0	1 285	
291	1	1 0	1 295	
181	0	0 0	0 183	
191	0	0 0	0 193	
231	0	0 0	0 233	
886	0	1 0		
897	0	1 0		
918	0	1 0		
929	0	1 0		
950	0	1 0		
961	0	1 0		

DATE : DEC 20, 1988 TIME (HRS:MIN:SEC) : 00:27:41

**THIS IS A SMALL DEFORMATION NON-LINEAR ELASTIC-PLASTIC
TWO DIMENSIONAL PLANE STRAIN ANALYSIS**

TOTAL STRESS ANALYSIS DIFF. 0

TOTAL NUMBER OF STEPS IN THE ANALYSIS =	13	ANALYSIS STARTS AT STEP NUMBER =	13
---	----	----------------------------------	----

TOTAL NUMBER OF ELEMENTS (NEL) = 300 TOTAL NUMBER OF NODES (NNOD) = 981

NUMBER OF INTEGRATION POINTS (NIP) = 2

NO. OF MATERIAL TYPE = 13 THICKNESS = 1.00000

IN-SITE DISPLACEMENT CODE: (IDGR) = -1

IDGR = 0. DISPLACEMENTS WILL BE SET TO ZERO AFTER THE FIRST ANALYSIS

IDGR < 0. DISPLACEMENTS AND STRAINS WILL BE SET ZERO AFTER THE FIRST ANALYSIS

IN-SITE STRESS AND STRAIN CODE: (ISITE) = 0

ISITE = 0. NO INITIAL STRESS IS GIVEN

ISITE = 1, ONLY SIGMA-XX WILL BE GIVEN

ISITE - 2. SIGMA-XX AND SIGMA-VY WILL BE GIVEN

ISITE = 3, SIGMA-XX, SIGMA-YY AND SIGMA-XY WILL BE GIVEN

INFORMATION CODE (INFORM) - 0

INFORM = 1. EXECUTION WILL STOP AFTER DETERMINING THE SIZE OF THE GLOBAL MATRIX

INFORM = 0, PROGRAM PROCEED WITHOUT INTERRUPTION

PRINT-OUT CONTROL (IPRINT)

```

PRINT-OUT CONTROL (IPRINT)
IPRINT(1) = 15  DISPLACEMENTS ,STRESSES AND STRAINS PRINT-OUT

```

IF IPRINT(1) = 0, NO PRINT-OUT IS REQUIRED DURING EQUILB. ITERATION. ONLY FINAL VALUES ARE PRINTED
IF IPRINT(1) = 15, DISPLACEMENTS, STRESSES AND STRAINS PRINT-OUT

```

IF IPRINT(1) = 0, NO PRINT-OUT IS REQUIRED DURING EQUILB. ITERATION. ONLY FINAL VAL
IF IPRINT(1) > 0, INTERMEDIATE RESULTS WILL BE GIVEN FOR EVERY IPRINT(1) ITERATION

```

```

17. PRINT(7) = 0, INTERMEDIATE RESULTS WILL BE GIVEN FOR EVERY
IPRINT(2) = 15 UNBALANCED LOAD VECTOR DURING EQUILB. ITERATION

```

IF IPRINT(2) = 0, NO PRINT-OUT IS REQUIRED

IF IPRINT(2) > 0, UNBALANCED LOAD VECTOR WILL BE GIVEN FOR EVERY IPRINT(1) ITERATION ABOVE

```

IPRINT(3) = 1      FINAL UNBALANCED LOAD VECTOR

```

IF IPRINT(3) = 0, NO FINAL UNBALANCED LOAD VECTOR WILL BE PRINTED

IF IPRINT(3) > 0, FINAL UNBALANCED VECTOR WILL BE GIVEN

IPRINT(4) = 1 ELEMENT LOAD VECTOR

IF IPRINT(4) = 0, NO ELEMENT LOAD VECTOR WILL BE PRINTED

IF IPRINT > 0, ELEMENT LOAD VECTOR FOR SURFACE TRACTION WILL BE PRINTED

IPRINT(5) = 1 LISTING OF DEGREES OF FREEDOM

A COMPLETE PROGRAM FOR
ON ANALYSIS OF FINITE ELEMENT

1	2	3	4	5	6	7	8	9	10	11	12	13	14	15	16	17	18	19	20	21	22	23	24	25	26	27	28	29	30	31	32	33	34	35	36	37	38	39	40	41	42	43	44	45	46	47	48	49	50	51	52	53	54	55	56	57	58	59	60	61	62	63	64	65	66	67	68	69	70	71	72	73	74	75	76	77	78	79	80	81	82	83	84	85	86	87	88	89	90	91	92	93	94	95	96	97	98	99	100	101	102	103	104	105	106	107	108	109	110	111	112	113	114	115	116	117	118	119	120	121	122	123	124	125	126	127	128	129	130	131	132	133	134	135	136	137	138	139	140	141	142	143	144	145	146	147	148	149	150	151	152	153	154	155	156	157	158	159	160	161	162	163	164	165	166	167	168	169	170	171	172	173	174	175	176	177	178	179	180	181	182	183	184	185	186	187	188	189	190	191	192	193	194	195	196	197	198	199	200	201	202	203	204	205	206	207	208	209	210	211	212	213	214	215	216	217	218	219	220	221	222	223	224	225	226	227	228	229	230	231	232	233	234	235	236	237	238	239	240	241	242	243	244	245	246	247	248	249	250	251	252	253	254	255	256	257	258	259	260	261	262	263	264	265	266	267	268	269	270	271	272	273	274	275	276	277	278	279	280	281	282	283	284	285	286	287	288	289	290	291	292	293	294	295	296	297	298	299	300	301	302	303	304	305	306	307	308	309	310	311	312	313	314	315	316	317	318	319	320	321	322	323	324	325	326	327	328	329	330	331	332	333	334	335	336	337	338	339	340	341	342	343	344	345	346	347	348	349	350	351	352	353	354	355	356	357	358	359	360	361	362	363	364	365	366	367	368	369	370	371	372	373	374	375	376	377	378	379	380	381	382	383	384	385	386	387	388	389	390	391	392	393	394	395	396	397	398	399	400	401	402	403	404	405	406	407	408	409	410	411	412	413	414	415	416	417	418	419	420	421	422	423	424	425	426	427	428	429	430	431	432	433	434	435	436	437	438	439	440	441	442	443	444	445	446	447	448	449	450	451	452	453	454	455	456	457	458	459	460	461	462	463	464	465	466	467	468	469	470	471	472	473	474	475	476	477	478	479	480	481	482	483	484	485	486	487	488	489	490	491	492	493	494	495	496	497	498	499	500	501	502	503	504	505	506	507	508	509	510	511	512	513	514	515	516	517	518	519	520	521	522	523	524
---	---	---	---	---	---	---	---	---	----	----	----	----	----	----	----	----	----	----	----	----	----	----	----	----	----	----	----	----	----	----	----	----	----	----	----	----	----	----	----	----	----	----	----	----	----	----	----	----	----	----	----	----	----	----	----	----	----	----	----	----	----	----	----	----	----	----	----	----	----	----	----	----	----	----	----	----	----	----	----	----	----	----	----	----	----	----	----	----	----	----	----	----	----	----	----	----	----	----	-----	-----	-----	-----	-----	-----	-----	-----	-----	-----	-----	-----	-----	-----	-----	-----	-----	-----	-----	-----	-----	-----	-----	-----	-----	-----	-----	-----	-----	-----	-----	-----	-----	-----	-----	-----	-----	-----	-----	-----	-----	-----	-----	-----	-----	-----	-----	-----	-----	-----	-----	-----	-----	-----	-----	-----	-----	-----	-----	-----	-----	-----	-----	-----	-----	-----	-----	-----	-----	-----	-----	-----	-----	-----	-----	-----	-----	-----	-----	-----	-----	-----	-----	-----	-----	-----	-----	-----	-----	-----	-----	-----	-----	-----	-----	-----	-----	-----	-----	-----	-----	-----	-----	-----	-----	-----	-----	-----	-----	-----	-----	-----	-----	-----	-----	-----	-----	-----	-----	-----	-----	-----	-----	-----	-----	-----	-----	-----	-----	-----	-----	-----	-----	-----	-----	-----	-----	-----	-----	-----	-----	-----	-----	-----	-----	-----	-----	-----	-----	-----	-----	-----	-----	-----	-----	-----	-----	-----	-----	-----	-----	-----	-----	-----	-----	-----	-----	-----	-----	-----	-----	-----	-----	-----	-----	-----	-----	-----	-----	-----	-----	-----	-----	-----	-----	-----	-----	-----	-----	-----	-----	-----	-----	-----	-----	-----	-----	-----	-----	-----	-----	-----	-----	-----	-----	-----	-----	-----	-----	-----	-----	-----	-----	-----	-----	-----	-----	-----	-----	-----	-----	-----	-----	-----	-----	-----	-----	-----	-----	-----	-----	-----	-----	-----	-----	-----	-----	-----	-----	-----	-----	-----	-----	-----	-----	-----	-----	-----	-----	-----	-----	-----	-----	-----	-----	-----	-----	-----	-----	-----	-----	-----	-----	-----	-----	-----	-----	-----	-----	-----	-----	-----	-----	-----	-----	-----	-----	-----	-----	-----	-----	-----	-----	-----	-----	-----	-----	-----	-----	-----	-----	-----	-----	-----	-----	-----	-----	-----	-----	-----	-----	-----	-----	-----	-----	-----	-----	-----	-----	-----	-----	-----	-----	-----	-----	-----	-----	-----	-----	-----	-----	-----	-----	-----	-----	-----	-----	-----	-----	-----	-----	-----	-----	-----	-----	-----	-----	-----	-----	-----	-----	-----	-----	-----	-----	-----	-----	-----	-----	-----	-----	-----	-----	-----	-----	-----	-----	-----	-----	-----	-----	-----	-----	-----	-----	-----	-----	-----	-----	-----	-----	-----	-----	-----	-----	-----	-----	-----	-----	-----	-----	-----	-----	-----	-----	-----	-----	-----	-----	-----	-----	-----	-----	-----	-----	-----	-----	-----	-----	-----	-----	-----	-----	-----	-----	-----	-----	-----	-----	-----	-----	-----	-----	-----	-----	-----	-----	-----	-----	-----	-----	-----	-----	-----	-----

THIS PROGRAM IS DEVELOPED BY THE GEOTECHNICAL GROUP OF
THE DEPARTMENT OF CIVIL ENGINEERING
UNIVERSITY OF ALBERTA, EDMONTON ALBERTA

ALL RIGHTS RESERVED
© 1991

THE DEVELOPER OF THIS PROGRAM AND/OR THE UNIVERSITY OF ALABAMA MAKES NO WARRANTY WHATSOEVER, EXPRESSED OR IMPLIED, THAT THE PROGRAM AND ANY MODIFICATIONS, INCLUDING UPDATES, AND THE DOCUMENTATION ARE FREE FROM ERROR AND/OR DEFECTS.

```

IF IPRINT(5) = 0, NO LISTING OF DEGREES OF FREEDOM WILL BE PRINTED
IF IPRINT(5) > 0, LISTING OF DEGREES OF FREEDOM WILL BE PRINTED

BINARY OUTPUT CODE (ITAP8) = 8
IF ITAP8 < 0 OR = 0, ONLY CONVERGED RESULTS WILL BE STORED IN TAPE # 7
IF ITAP8 > 0, RESULTS OF THE LATEST EQUILIBRIUM ITERATION, OR FINAL RESULTS OF THE LAST STEP,
WILL BE STORED IN ITAP8

PROGRAM RESTARTING CODE (IRES) = 0
IF IRES < 0 OR = 0, PROGRAM RESTART AT THE BEGINNING OF THE LOADING STEP
IF IRES = 1, PROGRAM RESTART IN BETWEEN LOADING STEPS

ADDITIONAL OUTPUT CODE (ITAP9) = 0
IF ITAP9 < 0, NO ADDITIONAL OUTPUT IS REQUIRED
IF ITAP9 > 0, ADDITIONAL OUTPUT INDICATING THE CONVERGING CHARACTERISTIC OF THE PROBLEM IS PROVIDED IN FILE ITAP9

NUMBER OF FILE PROVIDE IN RESTARTING FILE = 1

EQUILIBRIUM ITERATION
METHOD OF EQUILIBRIUM ITERATION (IEQM) = 1
IEQM = 1: FULL NEWTON-RAPHSON ITERATION
IEQM = 2: FULL NEWTON EVERY OTHER ITERATION
IEQM = 3: FULL NEWTON EVERY SECOND ITERATION ETC.
MAXIMUM NUMBER FOR EVERY LOAD INCREMENT (MITEQ) = 15
CONVERGENCE TOLERANCE (EQTOL) = 0.5000E-03
IF EQTOL IS LESS THAN OR EQUAL TO ZERO, DEFAULT IS 0.001
AITKEN ACCELERATOR DURING MODIFY NEWTON-RAPHSON ITERATION (IEQIT) = 0

STRESS CALCULATION ITERATION
METHOD OF STRESS CALCULATION ITERATION (ISM) = 2
ISM = 1: EULER FORWARD SCHEME
ISM = 2: IMPROVED EULER SCHEME
ISM = 3: RUNGE-KUTTER METHOD
NUMBER OF SUBINTERVALS DURING STRESS CALCULATION (MITS) = 10
CONVERGENCE TOLERANCE (STOL) = 0.1000E-02
IF STOL IS LESS THAN OR EQUAL TO ZERO, DEFAULT IS 0.001

NO-TENSION ANALYSIS
CODE OF NO TENSION ANALYSIS (INTM) = 0
IF INTM=0 ALL MATERIALS ARE CAPABLE TO SUSTAIN TENSION
INTM > 0 SOME MATERIALS CANNOT SUSTAIN TENSION
MAXIMUM NUMBER OF ITERATION ALLOWED TO DETERMINE PRINCIPAL STRESSES IN 3- DIMENSIONAL ANALYSIS (MITNT) = 0
CONVERGENCE TOLERANCE IN 3-DIMENSIONAL ANALYSIS (TNTOL) = 0.1000E-02
IF TNTOL IS LESS THAN OR EQUAL TO ZERO, DEFAULT IS E-15

```

MODAL COORDINATES

MODE	X-COORD.	Y-COORD.	U	V	NODE	X-COORD.	Y-COORD.	U	V
1	0.0	0.0	0	0	2	0.858000E+00	0.0	0	0
4	0.257300E+01	0.0	0	0	5	0.343000E+01	0.0	0	0
7	0.443000E+01	0.0	0	0	8	0.493000E+01	0.0	0	0
10	0.518000E+01	0.0	0	0	11	0.543000E+01	0.0	0	0
13	0.643000E+01	0.0	0	0	14	0.746500E+01	0.0	0	0
16	0.105000E+02	0.0	0	0	17	0.125000E+02	0.0	0	0
19	0.220000E+02	0.0	0	0	20	0.310000E+02	0.0	0	0
22	0.0	0.375000E+01	0	1	23	0.171500E+01	0.375000E+01	1	1
25	0.443000E+01	0.375000E+01	1	1	26	0.493000E+01	0.375000E+01	1	1
					27	0.543000E+01	0.375000E+01	1	1

MATERIAL PROPERTIES FOR MODEL NUMBER 1

MAT. TYPE	MODEL	LINEAR ELASTIC ISOTROPIC MODEL									
		TEN.	SIGTH X	BODY FORCE	Y	BODY FORCE	Z	BODY FORCE	E-MODULUS	POI. RATIO	EMPTY
1	1.	750.00	0.0	0.0	-13.040	0.0	0.0	0.0	15000.	0.40000	0.0
		0.0	0.0	0.0	0.0	0.0	0.0	0.0	0.0	0.0	0.0
2	1.	0.0	0.0	0.0	-18.000	0.0	0.0	0.0	15000.	0.40000	0.0
		0.0	0.0	0.0	0.0	0.0	0.0	0.0	0.0	0.10000	0.99000
3	1.	0.0	0.0	0.0	-18.300	0.0	0.0	0.0	20000.	0.40000	0.0
		0.0	0.0	0.0	0.0	0.0	0.0	0.0	0.0	0.10000	0.99000
4	1.	0.0	0.0	0.0	-20.000	0.0	0.0	0.0	22000.	0.40000	0.0
		0.0	0.0	0.0	0.0	0.0	0.0	0.0	0.0	0.10000	0.99000
5	1.	1200.0	0.0	0.0	-5.0000	0.0	0.0	0.0	0.20000E+06	0.40000	0.0
		0.0	0.0	0.0	0.0	0.0	0.0	0.0	0.0	0.0	0.0
6	1.	3350.0	0.0	0.0	-25.000	0.0	0.0	0.0	0.31250E+08	0.20000	0.0
		0.0	0.0	0.0	0.0	0.0	0.0	0.0	0.0	0.0	0.0
7	1.	36000.	0.0	0.0	-1.9100	0.0	0.0	0.0	0.50340E+07	0.40000	0.0
		0.0	0.0	0.0	0.0	0.0	0.0	0.0	0.0	0.0	0.0
13	1.	0.0	0.0	0.0	-0.60000	0.0	0.0	0.0	10000.	0.40000	0.0
		0.0	0.0	0.0	0.0	0.0	0.0	0.0	0.0	0.0	0.0

MATERIAL PROPERTIES FOR MODEL NUMBER 11

MAT. TYPE	MODEL	HYPERBOLIC NON-LINEAR ELASTIC MODEL									
		TEN.	SIGTH X	BODY FORCE	Y	BODY FORCE	Z	BODY FORCE	K-MODULUS	N-EXPONENT	RF-FACTOR
8	11.	0.0	0.0	0.0	-18.000	0.0	0.0	0.0	200.00	0.79000	0.69000
		0.60000	33.000	101.33	101.33	120.00	120.00	0.0	0.37000	0.10000	0.99000
9	11.	0.0	0.0	0.0	-18.300	0.0	0.0	0.0	225.00	0.79000	0.70000
		0.60000	32.000	101.33	101.33	140.00	140.00	0.0	0.37000	0.10000	0.99000
10	11.	0.0	0.0	0.0	-20.000	0.0	0.0	0.0	300.00	0.45000	0.70000
		0.0	30.000	101.33	101.33	150.00	150.00	0.0	0.20000	0.10000	0.99000
11	11.	0.0	0.0	0.0	4.4400	0.0	0.0	0.0	225.00	0.79000	0.69000
		0.60000	32.000	101.33	101.33	140.00	140.00	0.0	0.37000	0.0	0.0
12	11.	0.0	0.0	0.0	4.9600	0.0	0.0	0.0	200.00	0.79000	0.69000
		0.60000	33.000	101.33	101.33	120.00	120.00	0.0	0.37000	0.0	0.0

ANALYSIS STEP NUMBER 13

TITLE FOR THIS STEP: **Step : (13) Final Case**

NUMBER OF LINE	INPUT FOR NEW ELEMENT	9
NUMBER OF LINE	INPUT FOR NEW MODES	6
NUMBER OF LINE	INPUT FOR SLOPE BOUNDARY	0
NUMBER OF LINE	INPUT FOR NEW POINT LOAD	0
NUMBER OF LINE	INPUT FOR NEW DISPLACEMENT	0
NUMBER OF LOAD INCREMENTS		1
LOAD INCREMENT BEGIN AT INCREMENT NUMBER		1

♦♦NEW ELEMENT ADDED OR DELETED♦♦

FROM EL.	TO EL.	15	16	17	18	19
245	245	1	1	0	1	0
252	255	1	1	0	1	1
265	265	1	1	0	1	0
271	275	1	1	0	1	0
281	285	1	1	0	1	1
291	295	1	1	0	1	0
181	183	0	0	0	0	0
191	193	0	0	0	0	0
231	233	0	0	0	0	0

♦♦NEW NODES ADDED OR DELETED♦♦

FROM NODE TO NODE D.O.F. CODE

886	886	0	1
887	887	0	1
918	918	0	1
929	929	0	1
950	950	0	1
961	961	0	1

LISTING OF DEGREES OF FREEDOM

[illegible]

TOTAL DEGREE OF FREEDOM = 1652													MAX. HALF BANDWIDTH NO DIA. EL. = 66													STIFFNESS MATRIX SIZE = 82364																																																																																																																																																																																																																																																																																																																																																																																																																																																																																																																																																																																																																																																																																																																																																																																																																																																																																																																																																																																																																																																																																																																																																																																																																																																																																																																																																																																																											
561	980	981	562	982	983	563	984	985	564	986	987	565	0	988	566	0	989	1000	567	0	990	1001	1002	568	0	991	0	992	569	0	993	1003	994	0	995	1004	1005	570	0	996	1006	1007	571	0	997	1008	1009	572	0	998	1010	1011	573	0	999	1012	1013	574	0	1000	1014	1015	575	0	1001	1016	1017	576	0	1002	1018	1019	577	0	1003	1020	1021	578	0	1004	1022	1023	579	0	1005	1024	1025	580	0	1006	1026	1027	581	0	1007	1028	1029	582	0	1008	1030	1031	583	0	1009	1032	1033	584	0	1010	1034	1035	585	0	1011	1036	1037	586	0	1012	1038	1039	587	0	1013	1040	1041	588	0	1014	1042	1043	589	0	1015	1044	1045	590	0	1016	1046	1047	591	0	1017	1048	1049	592	0	1018	1050	1051	593	0	1019	1052	1053	594	0	1020	1054	1055	595	0	1021	1056	1057	596	0	1022	1058	1059	597	0	1023	1060	1061	598	0	1024	1062	1063	599	0	1025	1064	1065	600	0	1026	1066	1067	601	0	1027	1068	1069	602	0	1028	1070	1071	603	0	1029	1072	1073	604	0	1030	1074	1075	605	0	1031	1076	1077	606	0	1032	1078	1079	607	0	1033	1080	1081	608	0	1034	1082	1083	609	0	1035	1084	1085	610	0	1036	1086	1087	611	0	1037	1088	1089	612	0	1038	1090	1091	613	0	1039	1092	1093	614	0	1040	1094	1095	615	0	1041	1096	1097	616	0	1042	1098	1099	617	0	1043	1100	1101	618	0	1044	1102	1103	619	0	1045	1104	1105	620	0	1046	1106	1107	621	0	1047	1108	1109	622	0	1048	1110	1111	623	0	1049	1112	1113	624	0	1050	1114	1115	625	0	1051	1116	1117	626	0	1052	1118	1119	627	0	1053	1120	1121	628	0	1054	1122	1123	629	0	1055	1124	1125	630	0	1056	1126	1127	631	0	1057	1128	1129	632	0	1058	1130	1131	633	0	1059	1132	1133	634	0	1060	1134	1135	635	0	1061	1136	1137	636	0	1062	1138	1139	637	0	1063	1140	1141	638	0	1064	1142	1143	639	0	1065	1144	1145	640	0	1066	1146	1147	641	0	1067	1148	1149	642	0	1068	1150	1151	643	0	1069	1152	1153	644	0	1070	1154	1155	645	0	1071	1156	1157	646	0	1072	1158	1159	647	0	1073	1160	1161	648	0	1074	1162	1163	649	0	1075	1164	1165	650	0	1076	1166	1167	651	0	1077	1168	1169	652	0	1078	1170	1171	653	0	1079	1172	1173	654	0	1080	1174	1175	655	0	1081	1176	1177	656	0	1082	1178	1179	657	0	1083	1180	1181	658	0	1084	1182	1183	659	0	1085	1184	1185	660	0	1086	1186	1187	661	0	1087	1188	1189	662	0	1088	1190	1191	663	0	1089	1192	1193	664	0	1090	1194	1195	665	0	1091	1196	1197	666	0	1092	1198	1199	667	0	1093	1200	1201	668	0	1094	1202	1203	669	0	1095	1204	1205	670	0	1096	1206	1207	671	0	1097	1208	1209	672	0	1098	1210	1211	673	0	1099	1212	1213	674	0	1100	1214	1215	675	0	1101	1216	1217	676	0	1102	1218	1219	677	0	1103	1220	1221	678	0	1104	1222	1223	679	0	1105	1224	1225	680	0	1106	1226	1227	681	0	1107	1228	1229	682	0	1108	1230	1231	683	0	1109	1232	1233	684	0	1110	1234	1235	685	0	1111	1236	1237	686	0	1112	1238	1239	687	0	1113	1240	1241	688	0	1114	1242	1243	689	0	1115	1244	1245	690	0	1116	1246	1247	691	0	1117	1248	1249	692	0	1118	1250	1251	693	0	1119	1252	1253	694	0	1120	1254	1255	695	0	1121	1256	1257	696	0	1122	1258	1259	697	0	1123	1260	1261	698	0	1124	1262	1263	699	0	1125	1264	1265	700	0	1126	1266	1267	701	0	1127	1268	1269	702	0	1128	1270	1271	703	0	1129	1272	1273	704	0	1130	1274	1275	705	0	1131	1276	1277	706	0	1132	1278	1279	707	0	1133	1280	1281	708	0	1134	1282	1283	709	0	1135	1284	1285	710	0	1136	1286	1287	711	0	1137	1288	1289	712	0	1138	1290	1291	713	0	1139	1292	1293	714	0	1140	1294	1295	715	0	1141	1296	1297	716	0	1142	1298	1299	717	0	1143	1300	1301	718	0	1144	1302	1303	719	0	1145	1304	1305	720	0	1146	1306	1307	721	0	1147	1308	1309	722	0	1148	1310	1311	723	0	1149	1312	1313	724	0	1150	1314	1315	725	0	1151	1316	1317	726	0	1152	1318	1319	727	0	1153	1320	1321	728	0	1154	1322	1323	729	0	1155	1324	1325	730	0	1156	1326	1327	731	0	1157	1328	1329	732	0	1158	1330	1331	733	0	1159	1332	1333	734	0	1160	1334	1335	735	0	1161	1336	1337	736	0	1162	1338	1339	737	0	1163	1340	1341	738	0	1164	1342	1343	739	0	1165	1344	1345	740	0	1166	1346	1347	741	0	1167	1348	1349	742	0	1168	1350	1351	743	0	1169	1352	1353	744	0	1170	1354	1355	745	0	1171	1356	1357	746	0	1172	1358	1359	747	0	1173	1360	1361	748	0	1174	1362	1363	749	0	1175	1364	1365	750	0	1176	1366	1367	751	0	1177	1368	1369	752	0	1178	1370	1371	753	0	1179	1372	1373	754	0	1180	1374	1375	755	0	1181	1376	1377	756	0	1182	1378	1379	757	0	1183	1380	1381	758	0	1184	1382	1383	759	0	1185	1384	1385	760	0	1186	1386	1387	761	0	1187	1388	1389	762	0	1188	1390	1391	763	0	1189	1392	1393	764	0	1190	1394	1395	765	0	1191	1396	1397	766	0	1192	1398	1399	767	0	1193	1400	1401	768	0	1194	1402	1403	769	0	1195	1404	1405	770	0	1196	1406	1407	771	0	1197	1408	1409	772	0	1198	1410	1411	773	0	1199	1412	1413	774	0	1200	1414	1415	775	0	1201	1416	1417	776	0	1202	1418	1419	777	0	1203	1420	1421	778	0	1204	1422	1423	779	0	1205	1424	1425	780	0	1206	1426	1427	781	0	1207	1428	1429	782	0	1208	1430	1431	783	0	1209	1432	1433	784	0	1210	1434	1435	785	0	1211	1436	1437	786	0	1212	1438	1439	787	0	1213	1440	1441	788	0	1214	1442	1443	789	0	1215	1444	1445	790	0	1216	1446	1447	791	0	1217	1448	1449	792	0	1218	1450	1451	793	0	1219	1452	1453	794	0	1220	1454	1455	795	0	1221	1456	1457	796	0	1222	1458	1459	797	0	1223	1460	1461	798	0	1224	1462	1463	799	0	1225	1464	1465	800	0	1226	1466	1467	801	0	1227	1468	1469	802	0	1228	1470	1471	803	0	1229	1472	1473	804	0	1230	1474	1475	805	0	1231	1476	1477	806	0	1232	1478	1479	807	0	1233	1480	1481	808	0	1234	1482	1483	809	0	1235	1484	1485	810	0	1236	1486	1487	811	0	1237	1488	1489	812	0	1238	1490	1491	813	0	1239	1492	1493	814	0	1240	1494	1495	815	0	1241	1496	1497	816	0	1242	1498	1499	817	0	1243	1500	1501	818	0	1244	1502	1503	819	0	1245	1504	1505	820	0	1246	1506	1507	821	0	1247	1508	1509	822	0	1248	1510	1511	823	0	1249	1512	1513	824	0	1250	1514	1515	825	0	1251	1516	1517	826	0	1252	1518	1519	827	0	1253	1520	1521	828	0	1254	1522	1523	829	0	1255	1524	1525	830	0	1256	1526	1527	831	0	1257	1528	1529	832	0	1258	1530	1531	833	0	1259	1532	1533	834	0	1260	1534	1535	835	0	1261	1536	1537	836	0	1262	1538	1539	837	0	1263	1540	1541	838	0	1264	154

UNBALANCED NODAL FORCES									
NODE	X-FORCE	Y-FORCE	NODE	X-FORCE	Y-FORCE	NODE	X-FORCE	Y-FORCE	Y-FORCE
1	0.0	0.0	2	0.0	0.0	3	0.0	0.0	0.0
5	0.0	0.0	6	0.0	0.0	7	0.0	0.0	0.0
9	0.0	0.0	10	0.0	0.0	11	0.0	0.0	0.0
13	0.0	0.0	14	0.0	0.0	15	0.0	0.0	0.0
17	0.0	0.0	18	0.0	0.0	19	0.0	0.0	0.0
21	0.0	0.0	22	0.0	-0.857833E+02	23	-0.52946E-06	-0.171500E+03	-0.135717E+03
25	-0.485759E-06	-0.750000E+02	26	-0.328938E-06	-0.500000E+02	27	-0.557898E-06	-0.750000E+02	-0.153500E+03
29	-0.204483E-05	-0.303500E+03	30	-0.169214E-05	-0.675000E+03	31	-0.238211E-05	-0.137500E+04	-0.900000E+03
33	0.0	0.428583E+02	34	-0.125205E-06	-0.171500E+03	35	0.254389E-06	0.857500E+02	-0.171500E+03
37	0.521585E-06	0.678917E+02	38	-0.503010E-06	-0.100000E+03	39	0.447795E-06	0.375000E+02	-0.500000E+02
41	0.313681E-06	0.250000E+02	42	-0.285785E-06	-0.500000E+02	43	0.451645E-06	0.375000E+02	-0.100000E+03
45	0.523980E-06	0.767500E+02	46	-0.653542E-06	-0.207000E+02	47	-0.776486E-06	0.151750E+03	-0.400000E+03
49	-0.698637E-06	0.337500E+03	50	-0.130554E-05	-0.950000E+03	51	0.409780E-06	0.687500E+03	-0.180000E+04
53	0.0	0.450000E+03	54	0.0	-0.857833E+02	55	-0.329126E-06	-0.171500E+03	-0.135717E+03
57	-0.824028E-06	-0.750000E+02	58	-0.617060E-06	-0.137500E+03	59	-0.800813E-06	-0.750000E+02	-0.153500E+03
61	0.296765E-05	0.303500E+03	62	0.867267E-05	-0.120050E+03	63	-0.236433E-05	0.137500E+04	-0.900000E+03
65	0.0	0.300008E+02	66	0.109930E-05	-0.120050E+03	67	-0.155658E-05	0.600350E+02	-0.120050E+03
69	-0.823007E-06	0.475242E+02	70	-0.107433E-05	-0.700000E+02	71	0.720420E-06	0.262500E+02	-0.350000E+02
73	0.17268E-05	0.175000E+02	74	-0.133906E-05	-0.350000E+02	75	0.171715E-05	0.262500E+02	-0.700000E+02
77	0.155377E-05	0.537250E+02	78	-0.120183E-05	-0.144900E+02	79	-0.210115E-05	0.106225E+03	-0.280000E+03
81	-0.108336E-05	0.236250E+03	82	0.925469E-05	-0.665000E+03	83	-0.318955E-05	0.481250E+03	-0.126000E+04
85	0.0	0.315000E+03	86	0.0	-0.343133E+02	87	0.555476E-05	-0.686000E+02	-0.542867E+02
89	-0.209949E-05	-0.300000E+02	90	-0.310719E-05	-0.200000E+02	91	-0.482451E-05	-0.300000E+02	-0.614000E+02
93	0.228439E-05	-0.121400E+03	94	0.212927E-04	-0.270000E+03	95	0.635175E-05	-0.550000E+03	-0.360000E+03
97	0.0	0.114289E+02	98	0.451721E-05	-0.457333E+02	99	-0.198628E-05	0.228667E+02	-0.457333E+02
101	-0.134994E-05	0.181044E+02	102	-0.565096E-06	-0.266667E+02	103	0.894354E-06	0.100000E+02	-0.133333E+02
105	0.257745E-05	0.666667E+01	106	-0.553108E-05	-0.133333E+02	107	0.222743E-05	0.100000E+02	-0.266667E+02
109	0.188556E-05	0.204667E+02	110	-0.656324E-05	-0.552000E+02	111	-0.245061E-05	0.404667E+02	-0.106667E+03
113	-0.249890E-05	0.900000E+02	114	0.142131E-04	-0.253333E+03	115	-0.494121E-05	0.183333E+03	-0.480000E+03
117	0.0	0.120000E+03	118	0.0	-0.114378E+02	119	-0.753554E-05	-0.228667E+02	-0.180955E+02
121	-0.334037E-05	-0.999999E+01	122	-0.694835E-05	-0.666667E+02	123	-0.622457E-05	-0.100000E+02	-0.204667E+02
125	-0.205555E-05	-0.404667E+02	126	0.105034E-04	-0.900000E+02	127	0.398183E-05	0.183333E+03	-0.171500E+02
129	0.0	0.428583E+01	130	0.440040E-05	-0.171500E+02	131	-0.260414E-05	0.857500E+01	-0.500000E+01
133	0.152696E-05	0.678917E+01	134	0.702987E-05	-0.999998E+01	135	0.101917E-05	0.375000E+01	-0.100000E+02
137	0.123955E-05	0.250000E+01	138	-0.397456E-05	-0.500001E+01	139	0.156106E-06	0.375000E+01	-0.400000E+02
141	0.204080E-05	0.767500E+01	142	-0.569420E-05	-0.207000E+02	143	-0.398207E-06	0.151750E+02	-0.180000E+03
145	-0.154934E-05	0.337500E+02	146	0.816908E-05	-0.950000E+02	147	-0.265789E-05	0.687500E+02	-0.180000E+03
149	0.0	0.450000E+02	150	0.0	-0.571889E+01	151	0.590483E-05	-0.114333E+02	-0.904777E+01
153	-0.291500E-05	-0.499999E+01	154	-0.999350E-05	-0.333334E+01	155	0.355981E-05	-0.500001E+01	-0.102333E+02
157	-0.275658E-05	-0.202333E+02	158	0.560549E-05	-0.450000E+02	159	0.233248E-05	-0.916667E+01	-0.600000E+02
161	0.0	0.571445E+01	162	0.137038E-05	-0.228667E+02	163	-0.318592E-05	0.114333E+02	-0.403966E-05
165	-0.565717E-05	0.905219E+01	166	-0.256086E-05	-0.133334E+02	167	0.198391E-05	0.531247E+01	-0.791669E+01
169	-0.328009E-04	0.364584E+01	170	0.324752E-04	0.666667E+01	171	-0.379083E-06	0.500000E+01	-0.133333E+02
173	0.632924E-05	0.102333E+02	174	-0.175421E-04	-0.276000E+02	175	-0.440520E-05	0.203333E+02	-0.533334E+02
177	-0.996628E-06	0.450000E+02	178	0.131884E-04	-0.126667E+03	179	-0.332844E-05	0.916667E+02	-0.240000E+03

EQUILIBRIUM ITERATION 1 UNBALANCED LOAD = 0.25774E-01 DISPLACEMENT ERROR = 0.13154E+00

EQUILIBRIUM ITERATION 2 UNBALANCED LOAD = 0.38335E-02 DISPLACEMENT ERROR = 0.54853E-02

EQUILIBRIUM ITERATION 3 UNBALANCED LOAD = 0.81376E-03 DISPLACEMENT ERROR = 0.12811E-02

EQUILIBRIUM ITERATION 4 UNBALANCED LOAD = 0.71700E-03 DISPLACEMENT ERROR = 0.67744E-03

EQUILIBRIUM ITERATION 5 UNBALANCED LOAD = 0.79058E-03 DISPLACEMENT ERROR = 0.37106E-03

[illegible]

ELEMENT STRESSES AND STRAINS												
II	X-COORD	Y-COORD	SIGMA-XX	SIGMA-YY	SIGMA-XY	SIGMA-ZZ	SIGMA-1	SIGMA-3	ANGLE	YIELD	STGTH-5	STGTH-2
STGTH-3		STGTH-4	STRAIN-XX	STRAIN-YY	GAMMA-XY	STRAIN-XX	STRAIN-1	STRAIN-3	ANGLE			STGTH-6
***** STRESSES AND STRAINS IN ELEMENT NUMBER *****												
11	0.3628E+00	0.1585E+01	-0.4982E+03	0.7350E+03	0.3479E-01	-0.4980E+03	-0.4982E+03	-0.7350E+03	0.8417E-02	-0.1000E+01	0.2532E+03	0.0
12	0.2368E+03	0.0	0.3173E-04	0.1787E-03	0.6889E-05	0.0	0.3178E-04	0.1787E-03	0.9376E+00	0.0	0.0	0.0
21	0.2632E+03	0.0	0.4113E+03	-0.6476E+03	0.1324E+03	-0.4402E+03	-0.4413E+03	-0.6476E+03	0.3677E-01	-0.1000E+01	0.2367E+03	0.0
22	0.1353E+01	0.1585E+01	-0.4982E+03	0.7350E+03	0.4966E-05	0.0	0.9121E-04	0.2341E-03	0.3960E+00	0.0	0.0	0.0
23	0.2369E+03	0.0	0.3132E-04	0.1777E-03	0.1234E+03	-0.4980E+03	-0.4982E+03	-0.7350E+03	0.3130E-01	-0.1000E+01	0.2532E+03	0.0
24	0.1353E+01	0.1585E+01	-0.4982E+03	0.7350E+03	0.4966E-05	0.0	0.9121E-04	0.2341E-03	0.3960E+00	0.0	0.0	0.0
25	0.2369E+03	0.0	0.3132E-04	0.1777E-03	0.1234E+03	-0.4980E+03	-0.4982E+03	-0.7350E+03	0.3130E-01	-0.1000E+01	0.2532E+03	0.0
26	0.1353E+01	0.1585E+01	-0.4982E+03	0.7350E+03	0.4966E-05	0.0	0.9121E-04	0.2341E-03	0.3960E+00	0.0	0.0	0.0
27	0.2369E+03	0.0	0.3132E-04	0.1777E-03	0.1234E+03	-0.4980E+03	-0.4982E+03	-0.7350E+03	0.3130E-01	-0.1000E+01	0.2532E+03	0.0
28	0.1353E+01	0.1585E+01	-0.4982E+03	0.7350E+03	0.4966E-05	0.0	0.9121E-04	0.2341E-03	0.3960E+00	0.0	0.0	0.0
29	0.2369E+03	0.0	0.3132E-04	0.1777E-03	0.1234E+03	-0.4980E+03	-0.4982E+03	-0.7350E+03	0.3130E-01	-0.1000E+01	0.2532E+03	0.0
30	0.1353E+01	0.1585E+01	-0.4982E+03	0.7350E+03	0.4966E-05	0.0	0.9121E-04	0.2341E-03	0.3960E+00	0.0	0.0	0.0
31	0.2369E+03	0.0	0.3132E-04	0.1777E-03	0.1234E+03	-0.4980E+03	-0.4982E+03	-0.7350E+03	0.3130E-01	-0.1000E+01	0.2532E+03	0.0
32	0.1353E+01	0.1585E+01	-0.4982E+03	0.7350E+03	0.4966E-05	0.0	0.9121E-04	0.2341E-03	0.3960E+00	0.0	0.0	0.0
33	0.2369E+03	0.0	0.3132E-04	0.1777E-03	0.1234E+03	-0.4980E+03	-0.4982E+03	-0.7350E+03	0.3130E-01	-0.1000E+01	0.2532E+03	0.0
34	0.1353E+01	0.1585E+01	-0.4982E+03	0.7350E+03	0.4966E-05	0.0	0.9121E-04	0.2341E-03	0.3960E+00	0.0	0.0	0.0
35	0.2369E+03	0.0	0.3132E-04	0.1777E-03	0.1234E+03	-0.4980E+03	-0.4982E+03	-0.7350E+03	0.3130E-01	-0.1000E+01	0.2532E+03	0.0
36	0.1353E+01	0.1585E+01	-0.4982E+03	0.7350E+03	0.4966E-05	0.0	0.9121E-04	0.2341E-03	0.3960E+00	0.0	0.0	0.0
37	0.2369E+03	0.0	0.3132E-04	0.1777E-03	0.1234E+03	-0.4980E+03	-0.4982E+03	-0.7350E+03	0.3130E-01	-0.1000E+01	0.2532E+03	0.0
38	0.1353E+01	0.1585E+01	-0.4982E+03	0.7350E+03	0.4966E-05	0.0	0.9121E-04	0.2341E-03	0.3960E+00	0.0	0.0	0.0
39	0.2369E+03	0.0	0.3132E-04	0.1777E-03	0.1234E+03	-0.4980E+03	-0.4982E+03	-0.7350E+03	0.3130E-01	-0.1000E+01	0.2532E+03	0.0
40	0.1353E+01	0.1585E+01	-0.4982E+03	0.7350E+03	0.4966E-05	0.0	0.9121E-04	0.2341E-03	0.3960E+00	0.0	0.0	0.0
41	0.2369E+03	0.0	0.3132E-04	0.1777E-03	0.1234E+03	-0.4980E+03	-0.4982E+03	-0.7350E+03	0.3130E-01	-0.1000E+01	0.2532E+03	0.0
42	0.1353E+01	0.1585E+01	-0.4982E+03	0.7350E+03	0.4966E-05	0.0	0.9121E-04	0.2341E-03	0.3960E+00	0.0	0.0	0.0
43	0.2369E+03	0.0	0.3132E-04	0.1777E-03	0.1234E+03	-0.4980E+03	-0.4982E+03	-0.7350E+03	0.3130E-01	-0.1000E+01	0.2532E+03	0.0
44	0.1353E+01	0.1585E+01	-0.4982E+03	0.7350E+03	0.4966E-05	0.0	0.9121E-04	0.2341E-03	0.3960E+00	0.0	0.0	0.0
45	0.2369E+03	0.0	0.3132E-04	0.1777E-03	0.1234E+03	-0.4980E+03	-0.4982E+03	-0.7350E+03	0.3130E-01	-0.1000E+01	0.2532E+03	0.0
46	0.1353E+01	0.1585E+01	-0.4982E+03	0.7350E+03	0.4966E-05	0.0	0.9121E-04	0.2341E-03	0.3960E+00	0.0	0.0	0.0
47	0.2369E+03	0.0	0.3132E-04	0.1777E-03	0.1234E+03	-0.4980E+03	-0.4982E+03	-0.7350E+03	0.3130E-01	-0.1000E+01	0.2532E+03	0.0
48	0.1353E+01	0.1585E+01	-0.4982E+03	0.7350E+03	0.4966E-05	0.0	0.9121E-04	0.2341E-03	0.3960E+00	0.0	0.0	0.0
49	0.2369E+03	0.0	0.3132E-04	0.1777E-03	0.1234E+03	-0.4980E+03	-0.4982E+03	-0.7350E+03	0.3130E-01	-0.1000E+01	0.2532E+03	0.0
50	0.1353E+01	0.1585E+01	-0.4982E+03	0.7350E+03	0.4966E-05	0.0	0.9121E-04	0.2341E-03	0.3960E+00	0.0	0.0	0.0
51	0.2369E+03	0.0	0.3132E-04	0.1777E-03	0.1234E+03	-0.4980E+03	-0.4982E+03	-0.7350E+03	0.3130E-01	-0.1000E+01	0.2532E+03	0.0
52	0.1353E+01	0.1585E+01	-0.4982E+03	0.7350E+03	0.4966E-05	0.0	0.9121E-04	0.2341E-03	0.3960E+00	0.0	0.0	0.0
53	0.2369E+03	0.0	0.3132E-04	0.1777E-03	0.1234E+03	-0.4980E+03	-0.4982E+03	-0.7350E+03	0.3130E-01	-0.1000E+01	0.2532E+03	0.0
54	0.1353E+01	0.1585E+01	-0.4982E+03	0.7350E+03	0.4966E-05	0.0	0.9121E-04	0.2341E-03	0.3960E+00	0.0	0.0	0.0
55	0.2369E+03	0.0	0.3132E-04	0.1777E-03	0.1234E+03	-0.4980E+03	-0.4982E+03	-0.7350E+03	0.3130E-01	-0.1000E+01	0.2532E+03	0.0
56	0.1353E+01	0.1585E+01	-0.4982E+03	0.7350E+03	0.4966E-05	0.0	0.9121E-04	0.2341E-03	0.3960E+00	0.0	0.0	0.0
57	0.2369E+03	0.0	0.3132E-04	0.1777E-03	0.1234E+03	-0.4980E+03	-0.4982E+03	-0.7350E+03	0.3130E-01	-0.1000E+01	0.2532E+03	0.0
58	0.1353E+01	0.1585E+01	-0.4982E+03	0.7350E+03	0.4966E-05	0.0	0.9121E-04	0.2341E-03	0.3960E+00	0.0	0.0	0.0
59	0.2369E+03	0.0	0.3132E-04	0.1777E-03	0.1234E+03	-0.4980E+03	-0.4982E+03	-0.7350E+03	0.3130E-01	-0.1000E+01	0.2532E+03	0.0
60	0.1353E+01	0.1585E+01	-0.4982E+03	0.7350E+03	0.4966E-05	0.0	0.9121E-04	0.2341E-03	0.3960E+00	0.0	0.0	0.0
61	0.2369E+03	0.0	0.3132E-04	0.1777E-03	0.1234E+03	-0.4980E+03	-0.4982E+03	-0.7350E+03	0.3130E-01	-0.1000E+01	0.2532E+03	0.0
62	0.1353E+01	0.1585E+01	-0.4982E+03	0.7350E+03	0.4966E-05	0.0	0.9121E-04	0.2341E-03	0.3960E+00	0.0	0.0	0.0
63	0.2369E+03	0.0	0.3132E-04	0.1777E-03	0.1234E+03	-0.4980E+03	-0.4982E+03	-0.7350E+03	0.3130E-01	-0.1000E+01	0.2532E+03	0.0
64	0.1353E+01	0.1585E+01	-0.4982E+03	0.7350E+03	0.4966E-05	0.0	0.9121E-04	0.2341E-03	0.3960E+00	0.0	0.0	0.0
65	0.2369E+03	0.0	0.3132E-04	0.1777E-03	0.1234E+03	-0.4980E+03	-0.4982E+03	-0.7350E+03	0.3130E-01	-0.1000E+01	0.2532E+03	0.0
66	0.1353E+01	0.1585E+01	-0.4982E+03	0.7350E+03	0.4966E-05	0.0	0.9121E-04	0.2341E-03	0.3960E+00	0.0	0.0	0.0
67	0.2369E+03	0.0	0.3132E-04	0.1777E-03	0.1234E+03	-0.4980E+03	-0.4982E+03	-0.7350E+03	0.3130E-01	-0.1000E+01	0.2532E+03	0.0
68	0.1353E+01	0.1585E+01	-0.4982E+03	0.7350E+03	0.4966E-05	0.0	0.9121E-04	0.2341E-03	0.3960E+00	0.0	0.0	0.0
69	0.2369E+03	0.0	0.3132E-04	0.1777E-03	0.1234E+03	-0.4980E+03	-0.4982E+03	-0.7350E+03	0.3130E-01	-0.1000E+01	0.2532E+03	0.0
70	0.1353E+01	0.1585E+01	-0.4982E+03	0.7350E+03	0.4966E-05	0.0	0.9121E-04	0.2341E-03	0.3960E+00	0.0	0.0	0.0
71	0.2369E+03	0.0	0.3132E-04	0.1777E-03	0.1234E+03	-0.4980E+03	-0.4982E+03	-0.7350E+03	0.3130E-01	-0.1000E+01	0.2532E+03	0.0
72	0.1353E+01	0.1585E+01	-0.4982E+03	0.7350E+03	0.4966E-05	0.0	0.9121E-04	0.2341E-03	0.3960E+00	0.0	0.0	0.0
73	0.2369E+03	0.0	0.3132E-04	0.1777E-03	0.1234E+03	-0.4980E+03	-0.4982E+03	-0.7350E+03	0.3130E-01	-0.1000E+01	0.2532E+03	0.0
74	0.1353E+01	0.1585E+01	-0.4982E+03	0.7350E+03	0.4966E-05	0.0	0.9121E-04	0.2341E-03	0.3960E+00	0.0	0.0	0.0
75	0.2369E+03	0.0	0.3132E-04	0.1777E-03	0.1234E+03	-0.4980E+03	-0.4982E+03	-0.7350E+03	0.3130E-01	-0.1000E+01	0.2532E+03	0.0
76	0.1353E+01	0.1585E+01	-0.4982E+03	0.7350E+03	0.4966E-05	0.0	0.9121E-04	0.2341E-03	0.3960E+00	0.0	0.0	0.0
77	0.2369E+03	0.0	0.3132E-04	0.1777E-03	0.1234E+03	-0.4980E+03	-0.4982E+03	-0.7350E+03	0.3130E-01	-0.1000E+01	0.2532E+03	0.0
78	0.1353E+01	0.1585E+01	-0.4982E+03	0.7350E+03	0.4966E-05	0.0	0.9121E-04	0.2341E-03	0.3960E+00	0.0	0.0	0.0
79	0.2369E+03	0.0	0.3132E-04	0.1777E-03	0.1234E+03	-0.4980E+03	-0.4982E+03	-0.7350E+03	0.3130E-01	-0.1000E+01	0.2532E+03	0.0
80	0.1353E+01	0.1585E+01	-0.4982E+03	0.7350E+03	0.4966E-05	0.0	0.9121E-04	0.2341E-03	0.3960E+00	0.0	0.0	0.0
81	0.2369E+03	0.0	0.3132E-04	0.1777E-03	0.1234E+03	-0.4980E+03	-0.4982E+03	-0.7350E+03	0.3130E-01	-0.1000E+01	0.2532E+03	0.0
82	0.1353E+01	0.1585E+01	-0.4982E+03	0.7350E+03	0.4966E-05	0.0	0.9121E-04	0.2341E-03	0.3960E+00	0.0	0.0	0.0
83	0.2369E+03	0.0	0.3132E-04	0.1777E-03	0.1234E+03	-0.4980E+03	-0.4982E+03	-0.7350E+03	0.3130E-01	-0.1000E+01	0.2532E+03	0.0
84	0.1353E+01	0.1585E+01	-0.4982E+03	0.7350E+03	0.4966E-05	0.0	0.9121E-04	0.2341E-03	0.3960E+00	0.0	0.0	0.0
85	0.2369E+03	0.0	0.3132E-04	0.1777E-03	0.1234E+03	-0.4980E+03	-0.4982E+03	-0.7350E+03	0.3130E-01	-0.1000E+01	0.2532E+03	0.0
86	0.1353E+01	0.1585E+01	-0.4982E+03	0.7350E+03	0.4966E-05	0.0	0.9121E-04	0.2341E-03	0.3960E+00	0.0	0.0	0.0
87	0.2369E+03	0.0	0.3132E-04	0.1777E-03	0.1234E+03	-0.4980E+03	-0.4982E+03	-0.7350E+03	0.3130E-01	-0.1000E+01	0.2532E+03	0.0
88	0.1353E+01	0.1585E+01	-0.4982E+03	0.7350E+03	0.4966E-05	0.0	0.9121E-04	0.2341E-03	0.3960E+00	0.0	0.0	0.0
89	0.2369E+03	0.0	0.3132E-04	0.1777E-03	0.1234E+03	-0.4980E+03	-0.4982E+03	-0.7350E+03	0.3130E-01	-0.1000E+01	0.2532E+03	0.0
90	0.1353E+01	0.1585E+01	-									

```

O.O      O.O      O.O      O.9469E-03 -O.6968E-03 -O.1935E-04 O.O      O.O
***** STRESSES AND STRAINS IN ELEMENT NUMBER 300*****
11 O.2580E+02 O.3941E+02 O.6599E+01 -O.7773E+01 -O.4244E+00 -O.4695E+00 O.1690E+01 -O.7785E+01 O.1690E+01 -O.1000E+01 O.O
O.O      O.O      O.6597E-03 -O.6817E-03 -O.7921E-04 O.O      O.O      O.6609E-03 -O.6828E-03 O.1690E+01 O.O
12 O.2580E+02 O.3984E+02 O.1074E+02 -O.2007E+01 -O.1224E+00 O.3492E+01 O.1074E+02 -O.2008E+01 O.5503E+00 -O.1000E+01 O.O
O.O      O.O      O.6762E-03 -O.5132E-03 -O.2285E-04 O.O      O.O      O.6763E-03 -O.5133E-03 O.5503E+00 O.O
21 O.3620E+02 O.3941E+02 O.1438E+01 -O.7684E+01 -O.1705E+00 -O.2498E+01 O.1441E+01 -O.7687E+01 O.1071E+01 -O.1000E+01 O.O
O.O      O.O      O.3674E-03 -O.4840E-03 -O.3183E-04 O.O      O.O      O.3677E-03 -O.4843E-03 O.1071E+01 O.O
22 O.3620E+02 O.3984E+02 O.5275E+01 -O.2082E+01 -O.6193E-01 O.1277E+01 O.5275E+01 -O.2082E+01 O.4823E+00 -O.1000E+01 O.O
O.O      O.O      O.3731E-03 -O.3135E-03 -O.1156E-04 O.O      O.O      O.3731E-03 -O.3135E-03 O.4823E+00 O.O

```

SUMMARY OF COMPUTER TIME

```

ITERATION  STIFF REFORM.  SOLUTION TIME  STRESS CALCUL.
(MILLI SEC.) (MILLI SEC.) (MILLI SEC.)
-----
1          6493          3102          2501
2          5812          3103          2527
3          5845          3103          2559
4          5822          3099          2542
5          5849          3110          2526
-----
TOTAL      5          29821          15517          12655

TIME IN FOR THIS STEP  "
TIME OUT FOR THIS STEP  "  1361 MILLI SEC.
TIME ELAPSED FOR THIS STEP  "  65651 MILLI SEC.
                             64290 MILLI SEC.

```

```

END OF STEP NUMBER 13
*****

```